



Advanced scanning electron microscopy in materials science

Marek Faryna

Institute of Metallurgy and Materials Science

Polish Academy of Sciences

Reymonta 25

30-059 Kraków, Poland

m.faryna@imim.pl

Project WND-POWR.03.02.00-00-1043/16

International interdisciplinary PhD Studies in Materials Science with English as the language of instruction

Project co-financed by the European Union within the European Social Funds



Project WND-POWR.03.02.00-00-1043/16

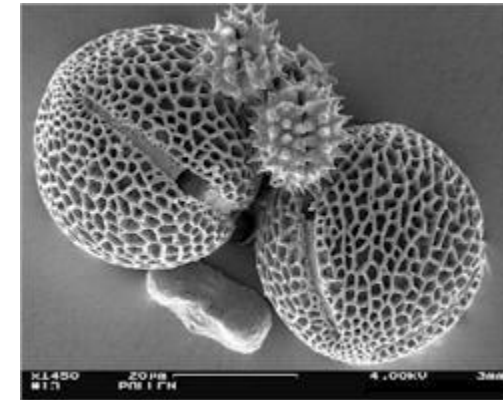
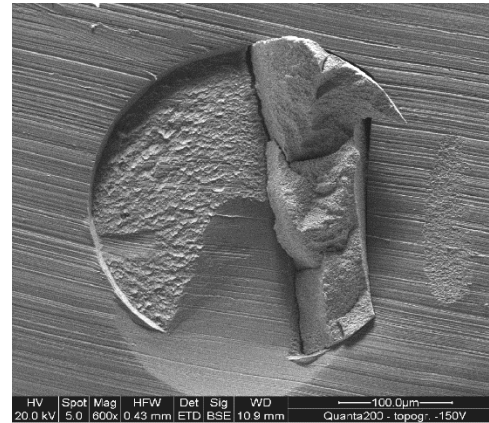
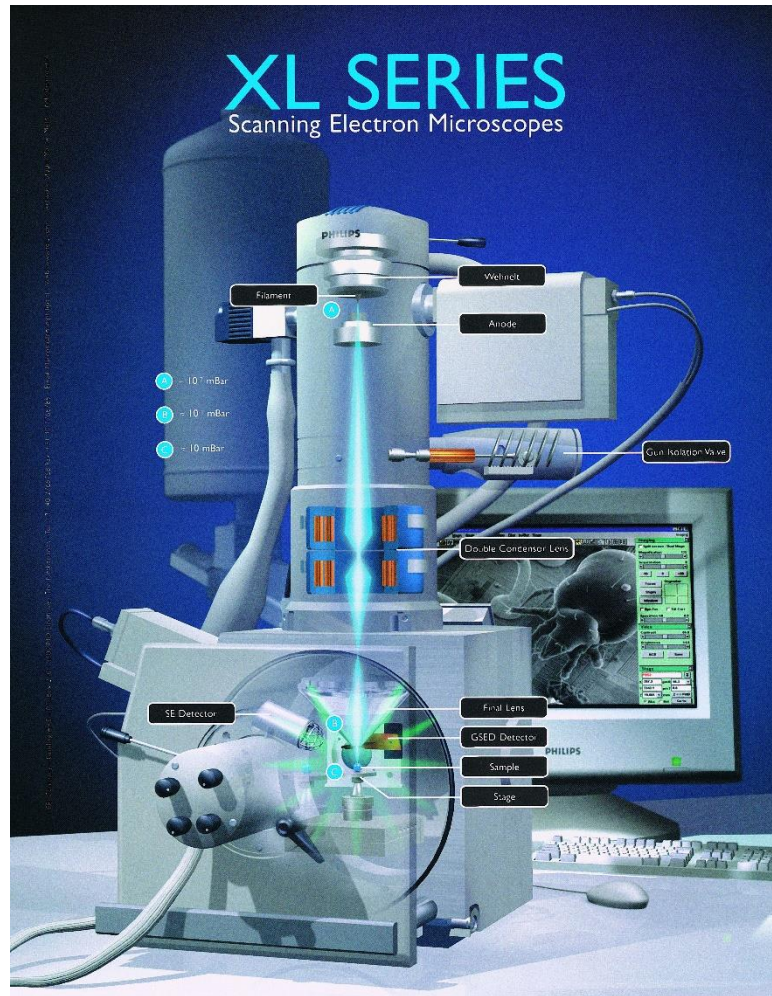
International interdisciplinary PhD Studies in Materials Science with English as the language of instruction

Project co-financed by the European Union within the European Social Funds



Literature

- 1. *Scanning Electron Microscopy and X-ray Microanalysis (Third Edition)*, Joseph Goldstein, Dale Newbury, David Joy, Charles Lyman, Patrick Echlin, Eric Lifshin, Linda Sawyer and Joseph Michael, Kluwer Academics/Plenum Publishers, 2003**
- 2. *Electron Microscopy and Analysis (Third Edition)*, Peter Goodhew, John Humphries, Richard Beanland, Taylor & Francis, London, 2001**
- 3. *Electron Microprobe Analysis (Second Edition)*, S.J.B. Reed, Cambridge University Press, 1993**
- 4. *Principles and Practice of Variable Pressure/Environmental Scanning Electron Microscopy (VP-ESEM)*, Debbie J Stokes, John Wiley&Sons 2008**
- 5. *Transmission Electron Microscopy*, David B.Williams, C.Barry Carter, Plenum Press, New York, 1996**





Electron Beam – Specimen Interaction

Def.:

Scattering – interaction between beam electrons and atoms/electrons of the specimen resulting in „elastic scattering” and „inelastic scattering”

Elastic scattering

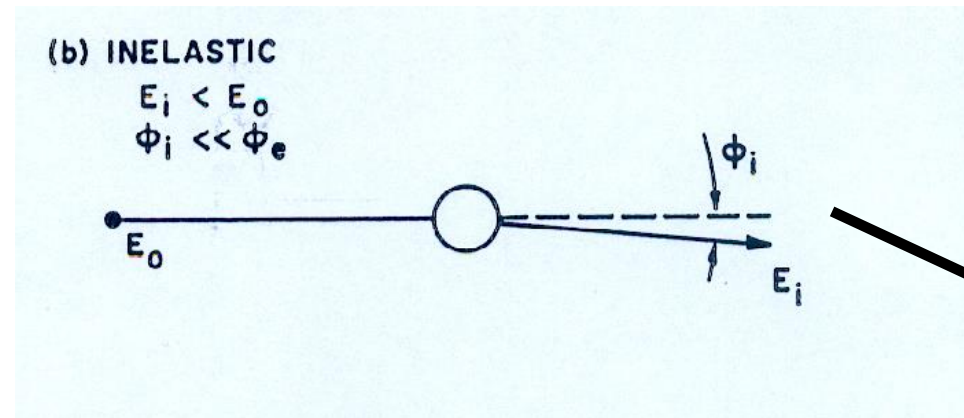
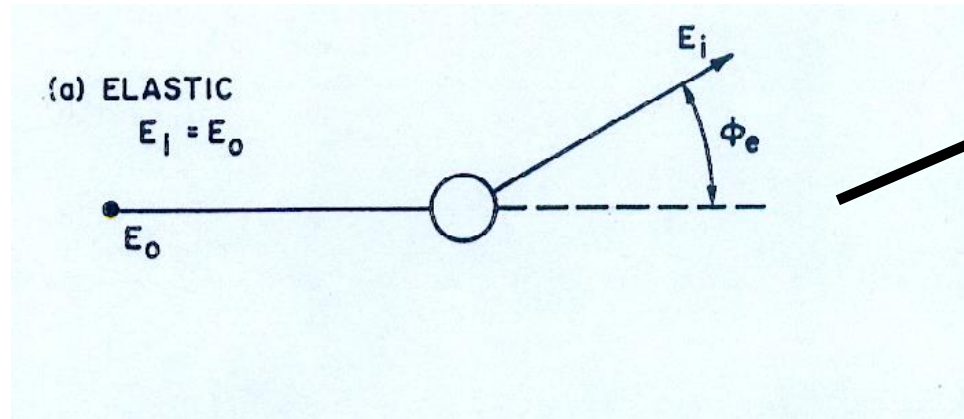
- **A new trajectory**
- **No kinetic energy loss**

Inelastic scattering

- **The beam electrons lose energy and transfer it in various ways to the specimen atoms – this transfer takes place gradually, so that the beam electrons propagate through many atom layers into the specimen before losing all their energy**



Elastic scattering



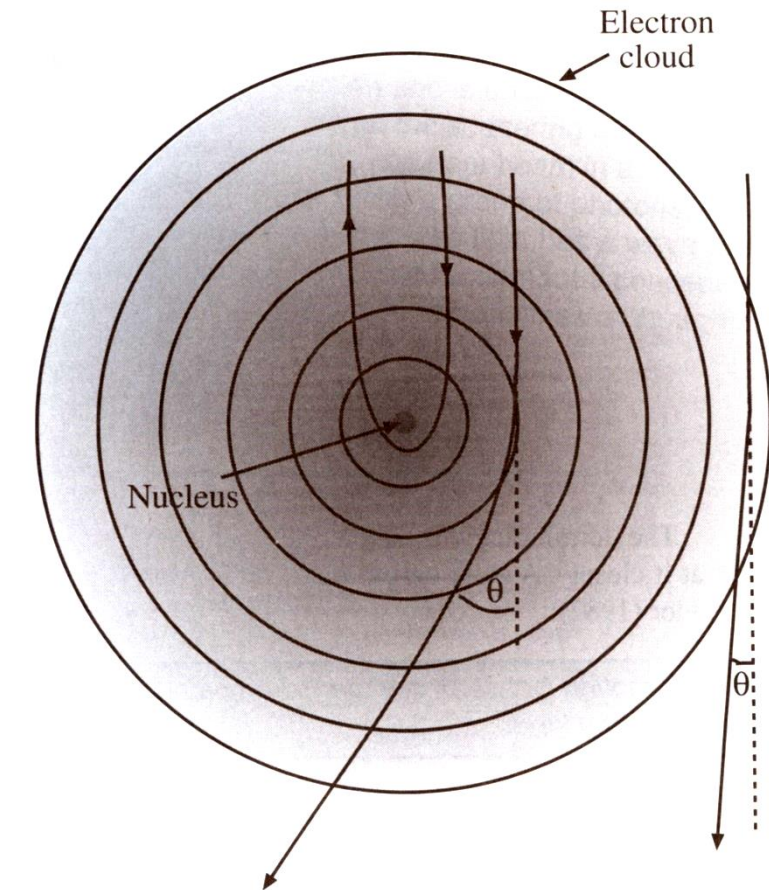
Inelastic scattering



Two mechanisms by which a high-energy electron is scatter by isolated atom:

- Coulombic interaction within the electron cloud results in low-angle (θ) scatter
- Coulombic attraction by the nucleus results in high-angle (θ) scatter and complete backscatter.

The potential within the electron cloud is always positive



$0 < \theta_e < 180^\circ$
typically $\theta_e = 5^\circ$
 $1 \text{ eV} \ll 10 \text{ keV}$ (the
energy of electron
beam)

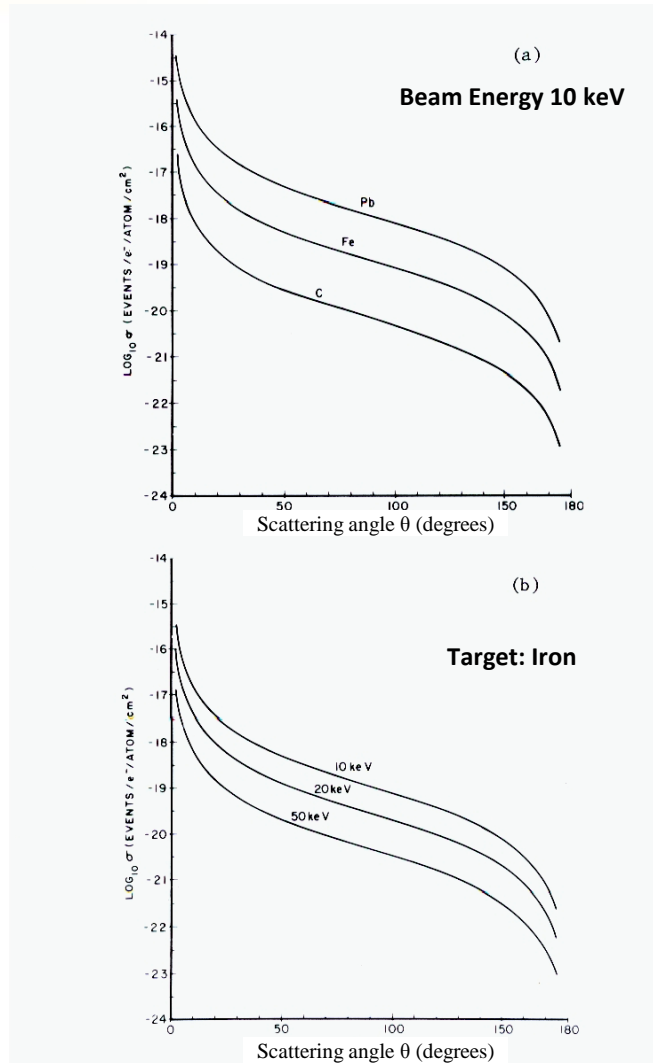


A mathematical description of elastic scattering

$$Q_e(>\theta) = 1.62 \times 10^{-20} \frac{Z^2}{E^2} \cot^2 \frac{\theta}{2} \quad \frac{\text{events} > \theta}{[\text{electron}(\text{atom}/\text{cm}^2)]}$$

where: $Q(>\theta_e)$ – cross section (cm^2) for elastic scattering (i.e. probability of elastic scattering)
 Z – atomic number
 E – electron energy in keV

- $Q_e(>\theta)$ reaches ∞ , when θ approaches 0°**
(smaller scattering angle θ , higher elastic cross section – less electron change their trajectories at 160° then at 5°)
- The probability of elastic scattering increases strongly with atomic number $Q_e(>\theta) \uparrow \propto Z^2$** (because heavier atoms have much stronger positive charge on the atomic nucleus)
- The probability of elastic scattering decreases as the electron energy decreases $Q_e(>\theta) \downarrow \propto E^2$**



$$Q_e(> \theta) = 1.62 \times 10^{-20} \frac{Z^2}{E^2} \cot^2 \frac{\theta}{2}$$



Mean Free Path MFP

the distance between scattering events designated as λ and is calculated from the cross section and density of the atoms along the path

$$\lambda = \frac{A}{N_o \rho Q} \quad (cm)$$

A – Atomic weight (g/mol)

N_o – Avogadro's number (6.02×10^{23} atoms/mol)

ρ – density (g/cm³)

Q – cross section (cm²)

$$Q \approx \frac{1}{\lambda}$$

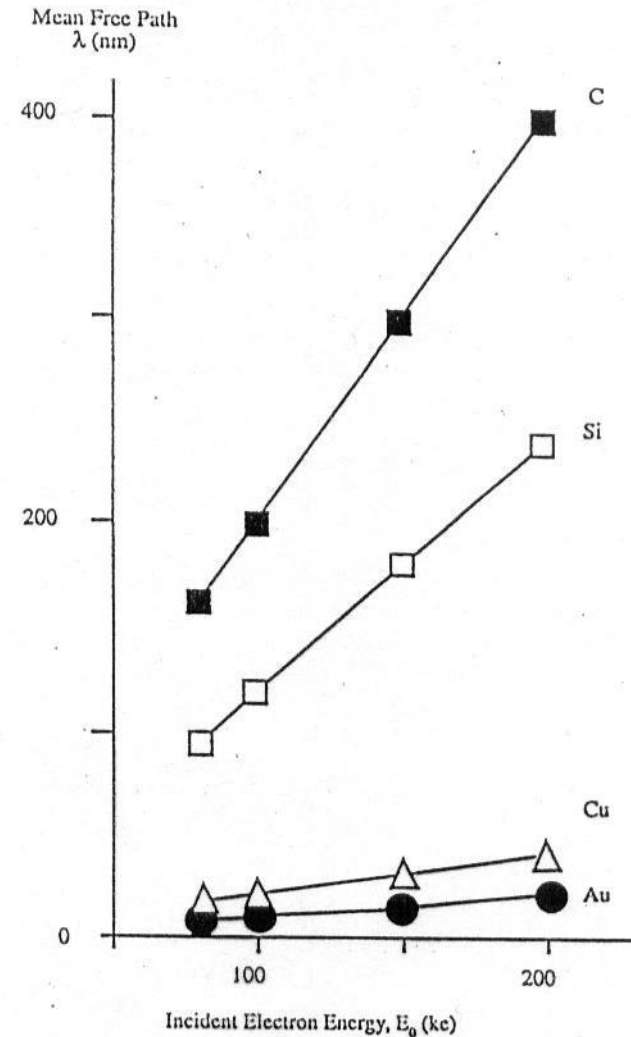
Cross section is inversely proportional to Mean Free Path!!!



The variation of the mean free path of elastic scatter for four different elements

Table 3.1. Elastic Mean Free Path, in Nanometers
(Scattering Events Greater than 2°)

Element	10 keV	20 keV	30 keV	40 keV	50 keV
C	5.5	22	49	89	140
Al	1.8	7.4	17	29	46
Fe	0.3	1.3	2.9	5.2	8.2
Ag	0.15	0.6	1.3	2.3	3.6
Pb	0.08	0.34	0.76	1.4	2.1
U	0.05	0.19	0.42	0.75	1.2



Electron energy $E_0 \uparrow - \lambda \text{ (nm)} \uparrow$

Atomic number $Z \uparrow - \lambda \text{ (nm)} \downarrow$



Elastic scattering

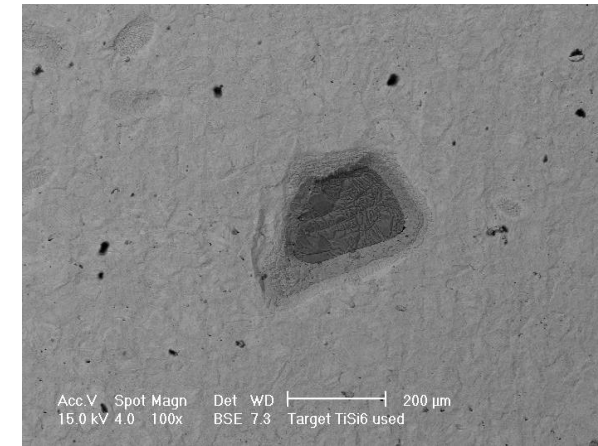
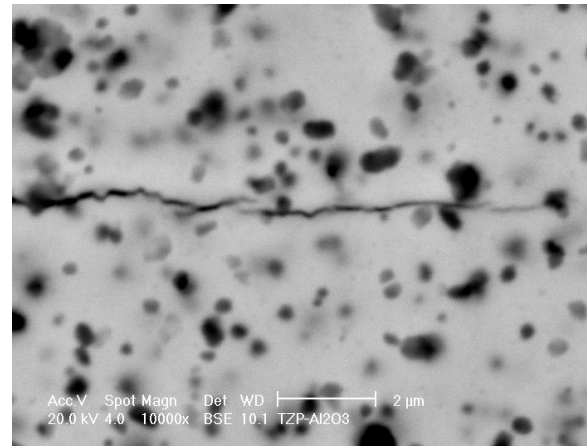
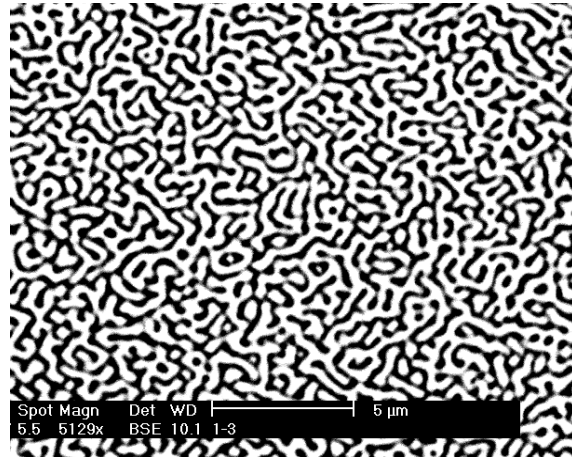
The result: *BackScatter Electrons BSE*

Generally, these electrons have undergone numerous elastic scattering events to accumulate enough deviation from the incident beam path to return to the surface

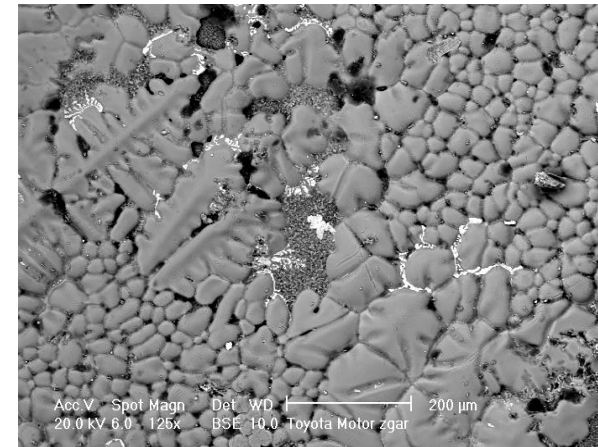
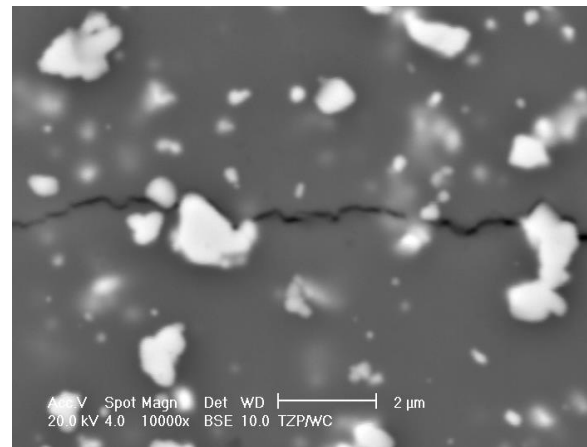


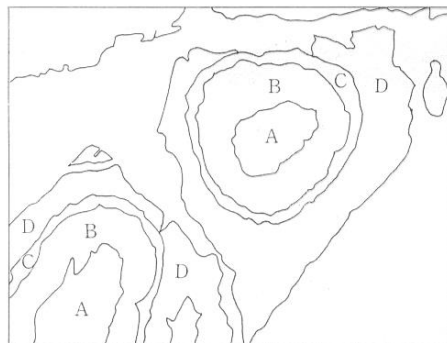
Backscatter electrons – a result of elastic scattering

Examples of BSE images

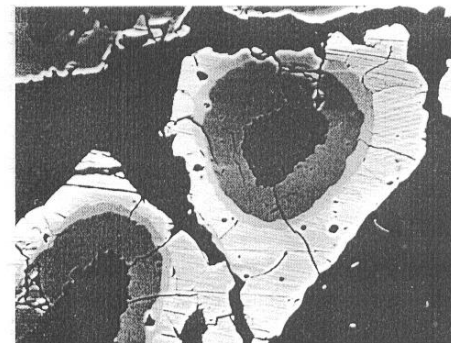


**A strong correlation
with atomic number Z**

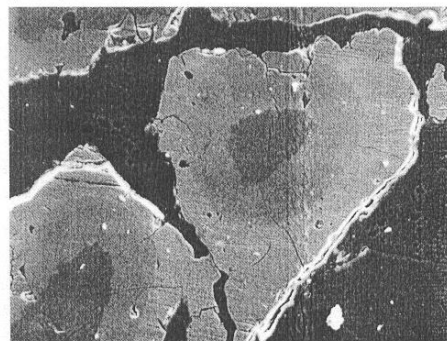




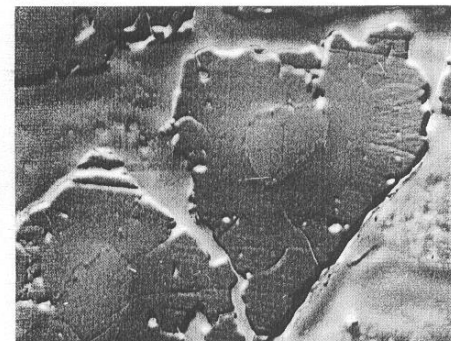
a) Composition distribution



c) Backscattered electron composition image



b) Secondary electron image



d) Backscattered electron topographic image

	A	B	C	D
Chemical composition	SiO₂	CaSiO₃	Ca₃Si₂O₇	Ca₂SiO₄
Mean atomic number	10.76	13.45	14.02	14.40



$$\eta = -0.0254 + 0.016Z - 1.886 \times 10^{-4} Z^2 + 8.3 \times 10^{-7} Z^3 \quad \text{Reuter (1972)}$$

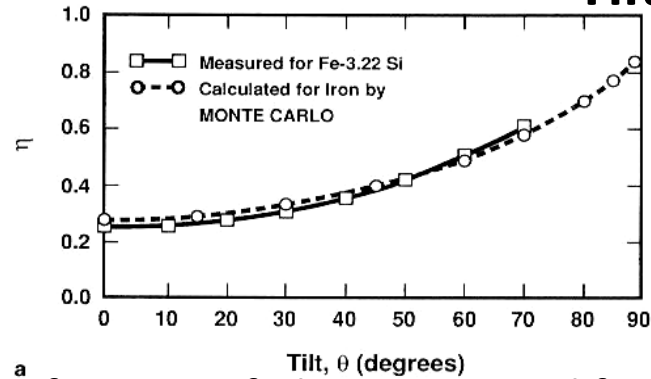
$$\eta = \sum_i C_i \eta_i$$

When a target is a mixture of elements that is homogeneous on an atomic scale (e.g. solid solution), the BC follows the simple rule of mixtures based on weight (mass) concentrations C_i of the individual constituents

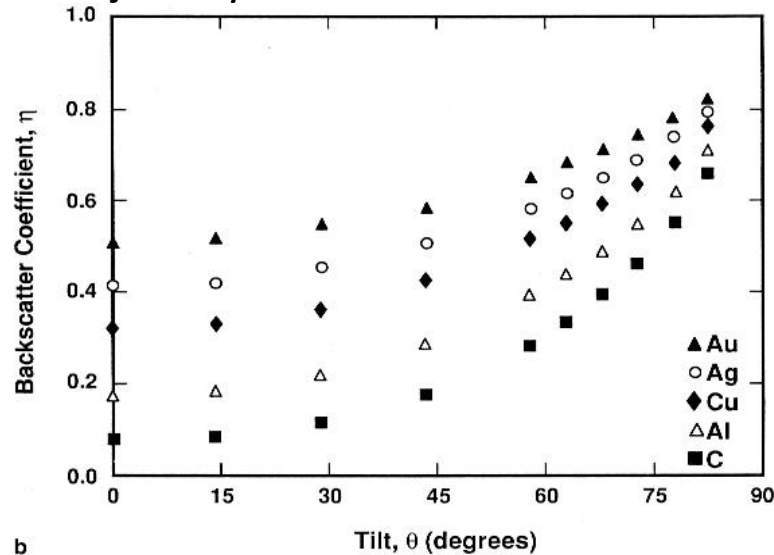
where: i denotes each constituent, η is the pure element BC for element i , and the summation is taken over all constituents



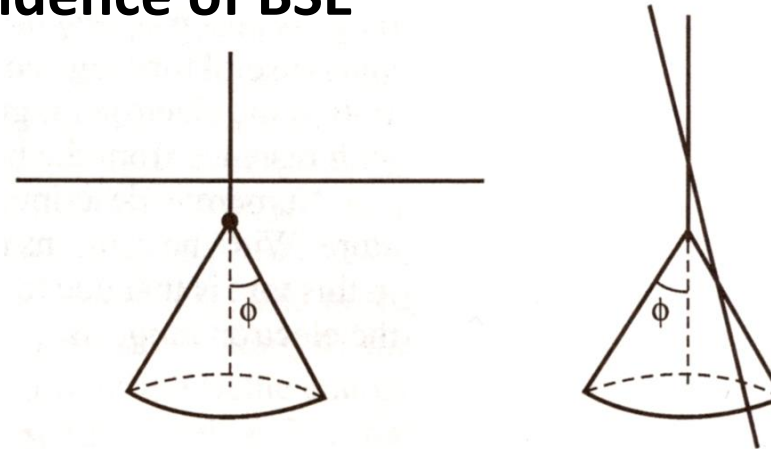
Tilt dependence of BSE



a
BC as a function of tilt as measured for iron and calculated by Monte Carlo electron trajectory simulation for Fe-3.22Si



b



$$\eta(\theta) = \frac{1}{(1 + \cos \theta)^p}$$

$$\text{where: } p = \frac{9}{\sqrt{Z}}$$

BC as a function of tilt as measured for iron as calculated for several elements by Monte Carlo electron trajectory simulation



Inelastic Scattering

**Inelastic processes can be separate into
three components**

- 1. Processes that result from collective interactions with many atoms**
- 2. Processes that generate other (secondary) electrons**
- 3. Processes that generate X-rays**



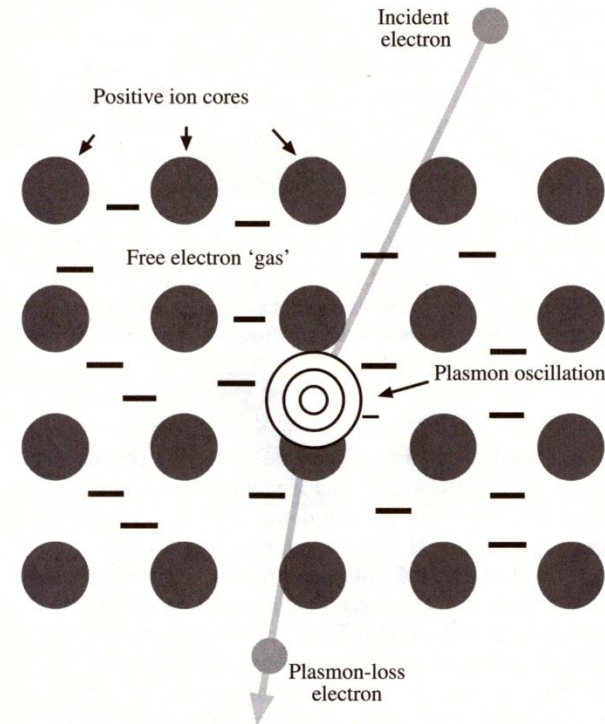
- 1. Processes that results from collective interactions with many atoms**
 - **Plasmons**
 - **Phonons**



Inelastic scattering

Collective oscillations

Plasmons are collective oscillations of free electrons that occur when the beam electron passes through the free electron „gas”



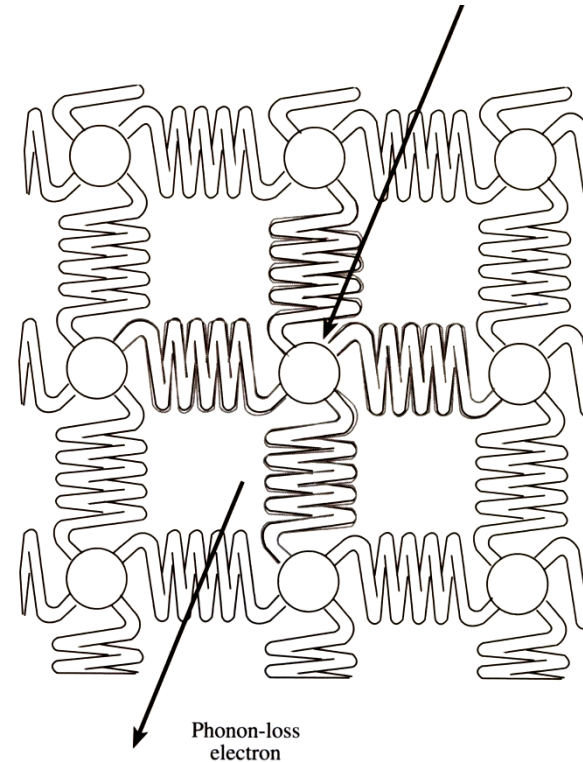
Schematic diagram of a high-energy beam exciting plasmon oscillation in a free electron gas that permeates the ion core in a metal



Inelastic scattering

Collective oscillations

Phonons are oscillations where all the atoms in the crystal lattice vibrate collectively. Such vibrations of the atoms are equivalent to specimen heating. You can reduce the number of phonons by cooling the specimen



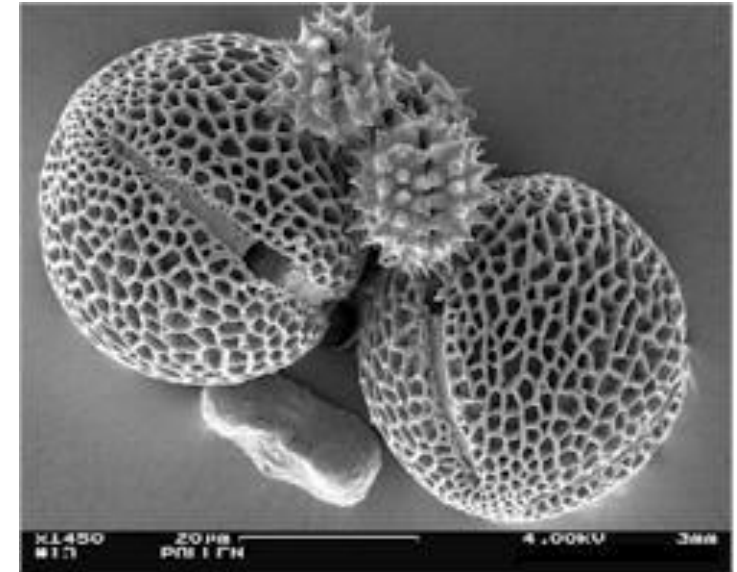
An illustration of the crystal lattice as a group of atoms linked elastically by springs. The bonds vibrate when struck by high-energy electron creating lattice oscillations or phonons. The lattice absorbs heat by creating phonons, so phonon excitation is equivalent to heating the specimen



2. Processes that generate other (secondary) electrons

- **Secondary Electrons SE**
- **Fast Secondary Electrons FSE**

High-energy electron which are generated in the specimen; they are high-energy because they receive a large fraction of the beam energy. At low beam energies we use in a SEM, FSEs are not a problem, so nobody bothers about them (however in TEM FSEs are generally both unavoidable and undesirable, they degrade spectroscopic data)



Project WND-POWR.03.02.00-00-1043/16

International interdisciplinary PhD Studies in Materials Science with English as the language of instruction

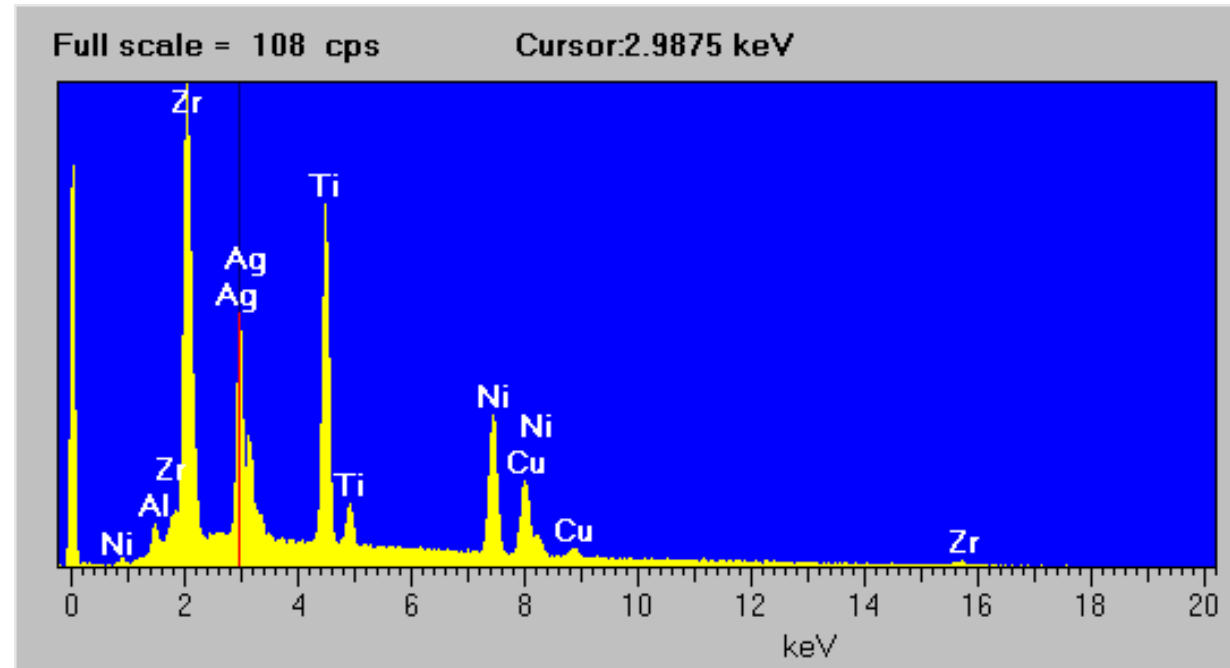
Project co-financed by the European Union within the European Social Funds



3. Processes that generate X-rays

X ray emission:

- Characteristic X-rays
- Bremsstrahlung X-rays



Project WND-POWR.03.02.00-00-1043/16

International interdisciplinary PhD Studies in Materials Science with English as the language of instruction

Project co-financed by the European Union within the European Social Funds



Signals from Inelastic Scattering

- 1. Secondary electrons with a continuous energy distribution**
- 2. Auger electrons with characteristic energy**
- 3. Brehmsstrahlung X-ray formed with a continuous energy distribution**
- 4. Characteristic X-rays**
- 5. Cathodoluminescence radiation which is the emission of ultraviolet, visible or infrared radiation**
- 6. Lattice vibrations (heat)**



Elastic scattering predominates for
high atomic number Z
Inelastic scattering predominates for
low atomic number Z



Beam electrons lose and transfer energy in various ways to the specimen. This transfer takes place gradually, so that the beam electrons propagate through many atom layers into the specimen before losing all their energy
Bethe (1930) described the rate of energy loss dE with distance traveled ds as:

$$\frac{dE}{ds} = -2\pi e^4 N_0 \frac{Z\rho}{AE_i} \log_e \left(\frac{1.166E_i}{J} \right) = -7.85 \times 10^4 \frac{Z\rho}{AE_i} \log_e \left(\frac{1.166E_i}{J} \right)$$

where:

e – electron charge ($2\pi e^4 = 1.304 \times 10^{-19}$ for E in KeV)

E – electron energy

N_0 – Avogadro's number

Z – atomic number

A – atomic weight (g/mol)

ρ – density (g/cm³)

E_i – average energy along the path segment s (keV)

J – mean ionization potential

Negative sign indicates the loss of energy





J – mean ionization potential – the average energy loss per inelastic interaction considering all the energy loss processes

$$\mathbf{J = (9.76Z + 58.5Z^{-0.19})10^{-3} \quad [kev]}$$

Table 3.1. Energy Loss Due to Inelastic Scattering

Element	Z	A	$\rho(\text{g/cm}^3)$	J (keV)	dE/ds (keV/cm)	dE/ds (eV/nm)
Carbon	6	12.01	2.1	0.100	2.24×10^4	2.24
Iron	26	55.85	7.87	0.285	6.32×10^4	6.32
Silver	47	107.9	10.5	0.487	6.94×10^4	6.94
Uranium	92	238.03	18.95	0.923	9.27×10^4	9.27



Simulation of interaction volume

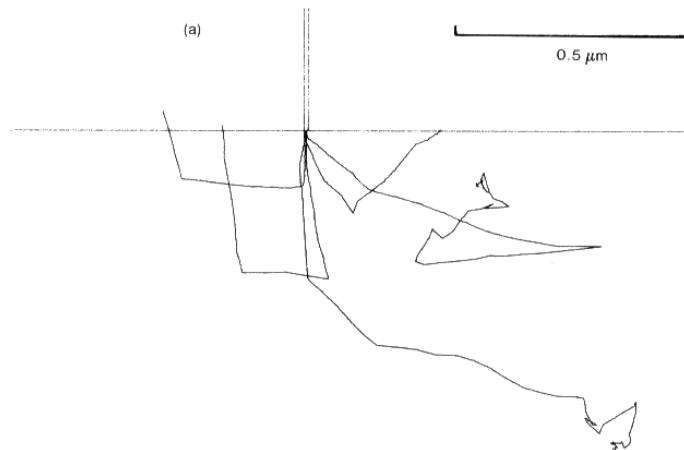
To construct an electron trajectory simulation, the effects of elastic and inelastic scattering are calculated to determine:

- scattering angles
- distance between scattering sites (MPF)
- the rate of energy loss

From these parameters the electron trajectories can be simulated in a stepwise fashion from the location at which it enters the specimen to its final fate.

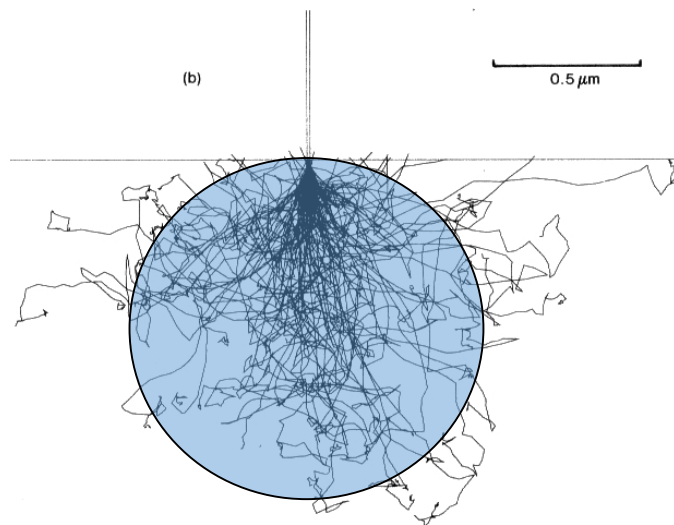
Random numbers are used with a weighting factor to produce the appropriate statistical distribution of the physical events. The use of random numbers give rise to the name of „Monte Carlo”

The electron location in the specimen (coordinates: x, y, z) the electron velocity vector (v_x, v_y, v_z) and kinetic energy ($mv^2/2$) are constantly updated.



**Monte Carlo electron
trajectory simulation of
the beam interaction in Fe
 $E_0 = 20$ kV, tilt = 0°**

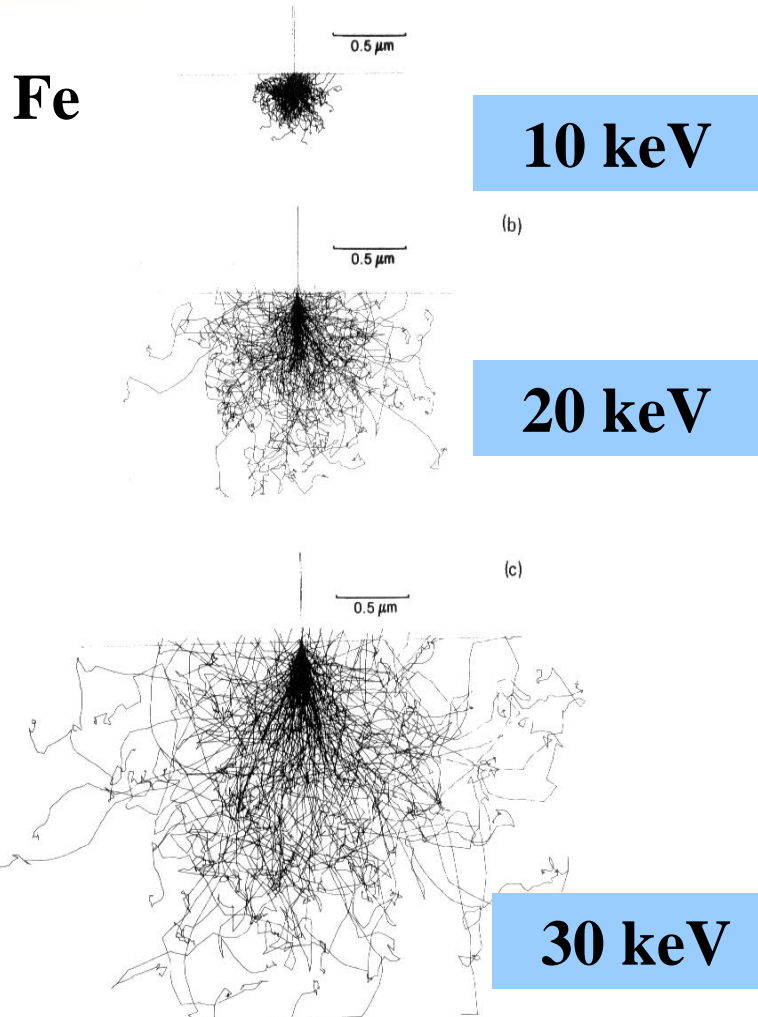
**Plot of 5 trajectories showing
random variation**



**Plot of 1000 trajectories
projected on the plane
perpendicular to the surface,
giving a visual impression of
interaction volume**

**The penetration range is not
precisely defined!!!**

Good statistics 10^3 - 10^4 trajectories



Monte Carlo electron-trajectory simulation of interaction volume in iron at beam energies of 10 keV, 20 keV and 30 keV

$$Q_e \approx \frac{1}{E_0^2} \quad Q_e \approx \frac{1}{\lambda}$$

$$E_0 \uparrow \quad Q_e \downarrow \rightarrow E_0 \uparrow \quad \lambda \uparrow$$

!!!

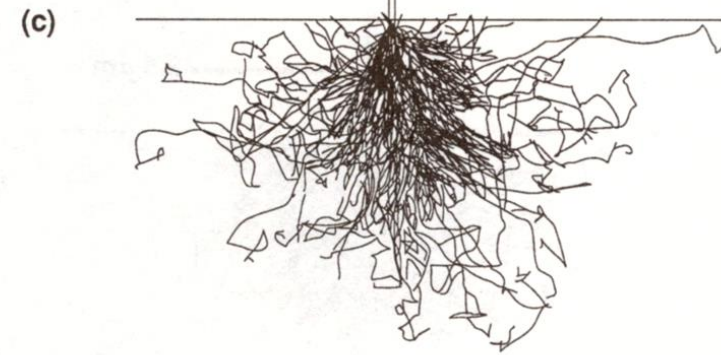
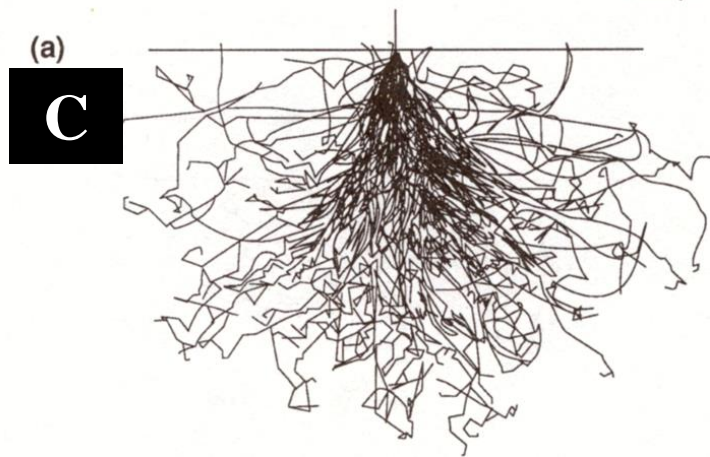
λ - electron mean free path increases with electron energy

$$\frac{dE}{dx} \approx \frac{1}{E_0} \quad \text{Bethe equation}$$

The higher electron energy, the lower rate of energy loss with distance traveled dx , i.e.

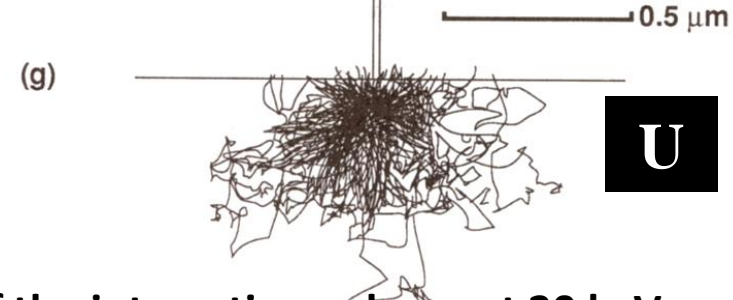
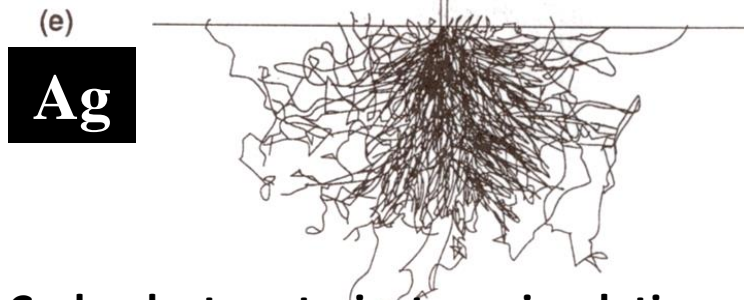
Electrons penetrate deeper into materials

20 keV



Fe

20 keV



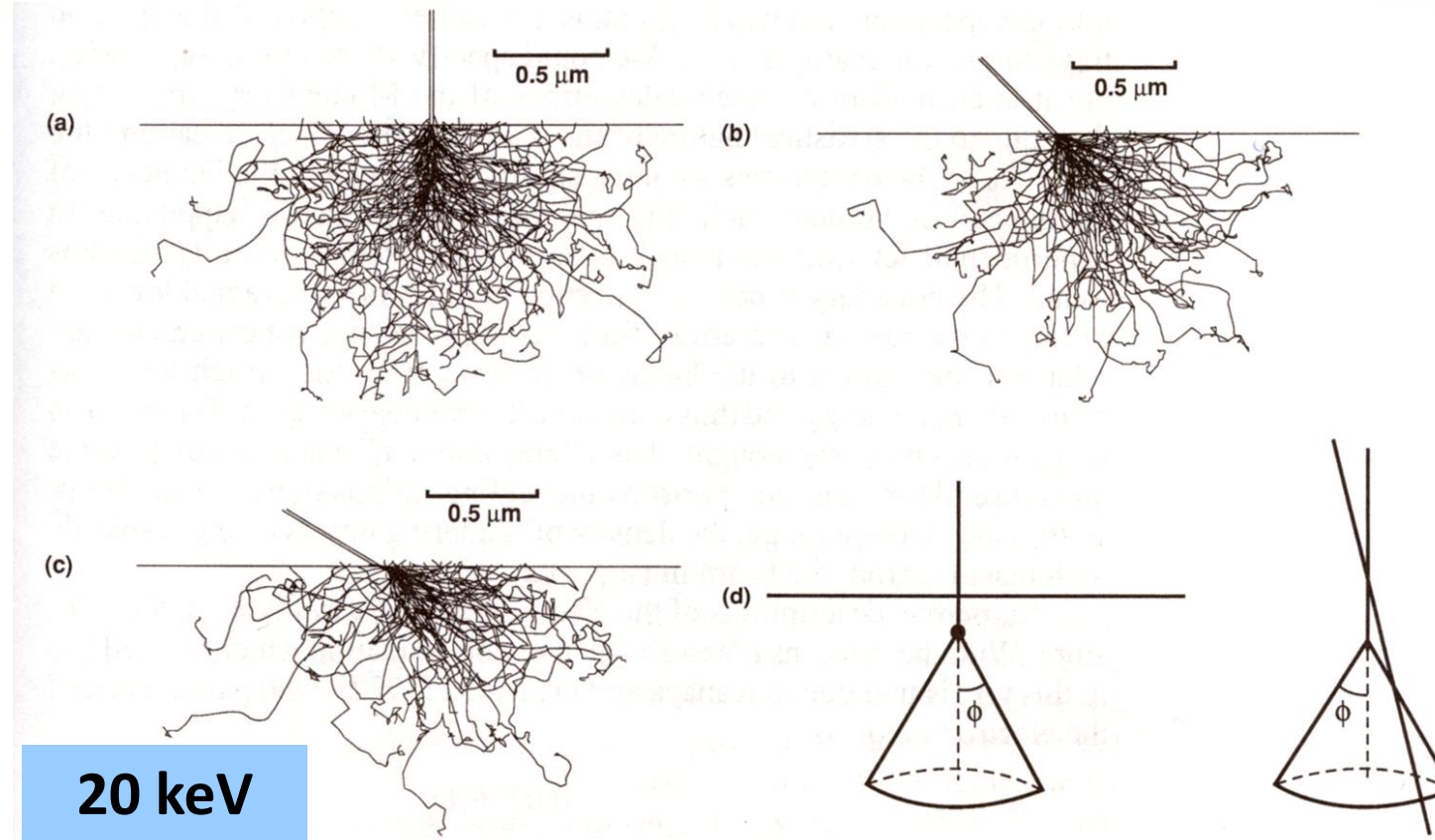
U

Monte Carlo electron trajectory simulations of the interaction volume at 20 keV and 0° tilt in various targets: carbon K-shell, iron K-shell, silver L-shell, uranium M-shell

Project WND-POWR.03.02.00-00-1043/16

International interdisciplinary PhD Studies in Materials Science with English as the language of instruction

Project co-financed by the European Union within the European Social Funds



20 keV

Monte Carlo electron-trajectory simulation in iron at $E_0 = 20 \text{ keV}$ for various tilts: a) 0° tilt, b) 45° tilt, 60° tilt

d) Schematic illustration of the origin of increased backscattering from tilted sample.

Consider a given average elastic scattering angle which produces the scattering cone. The electron may land at any point on the base of the cone with equal probability. At normal incidence, no matter where on the base of the cone the electron lands, it tends to propagate into the solid. When the specimen is tilted, some of the possible locations of the base of the scattering cone carry the electron out of the solid.

Project WND-POWR.03.02.00-00-1043/16

International interdisciplinary PhD Studies in Materials Science with English as the language of instruction

Project co-financed by the European Union within the European Social Funds



Kanaya i Okayama (1972) range equation

$$R_{K-O} = \frac{0.0276A}{Z^{0.89} \rho} E_o^{1.67} \quad \mu\text{m}$$

where:

A – atomic weight (g/mol),

Z – atomic number

ρ – density (g/cm³)

E_o – beam energy (keV)

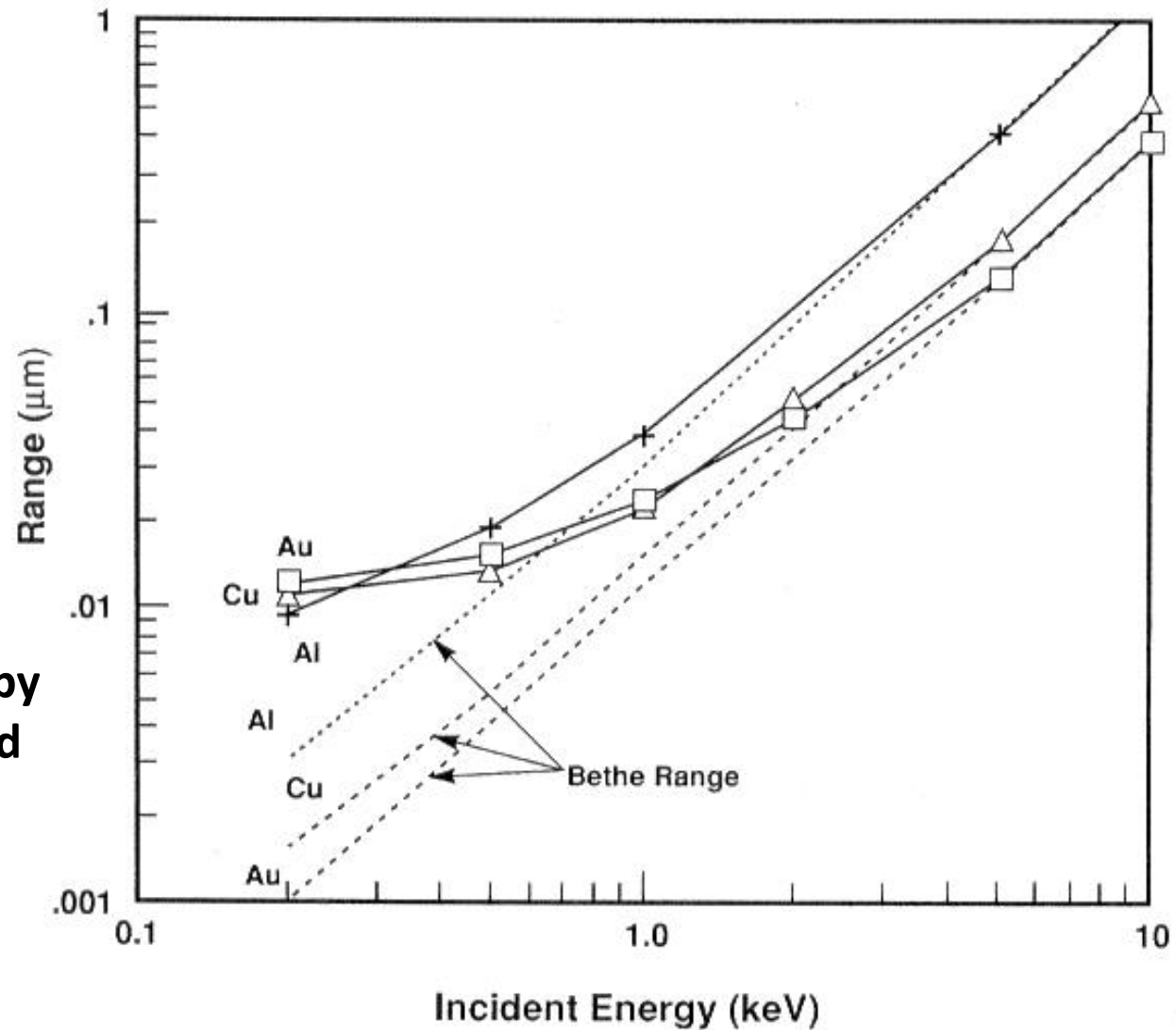
To calculate R_{K-O} in nanometers the constant becomes 27.6

Penetration range of electrons (w μm) calculated based on K-O equation

	5 keV	10 keV	20 keV	30 keV
Al	0.41	1.32	4.2	8.3
Cu	0.15	0.46	1.47	2.89
Au	<u>0.085 (!)</u>	0.27	0.86	1.70



Electron range at low incident beam energy calculated by the Bethe expression and modified by Joy and Luo for Al, Cu and Au





Joy & Luo in 1989 noted that at low beam energies the number of processes contributing to the energy loss decreases; they proposed a **modified form of the Bethe energy loss relation** which is appropriate at low beam energies

$$\frac{dE}{ds} = -7.85 \times 10^4 \frac{Z\rho}{AE_i} \left(\frac{1.166E_i}{J^*} \right) \left(\frac{\text{keV}}{\text{cm}} \right)$$

The modified mean ionization potential is given by:

$$J^* = \frac{J}{1 + \frac{kJ}{E}}$$

where:

J is the value given by the conventional expression

k – is a variable dependent on atomic number which is always close but less than unity

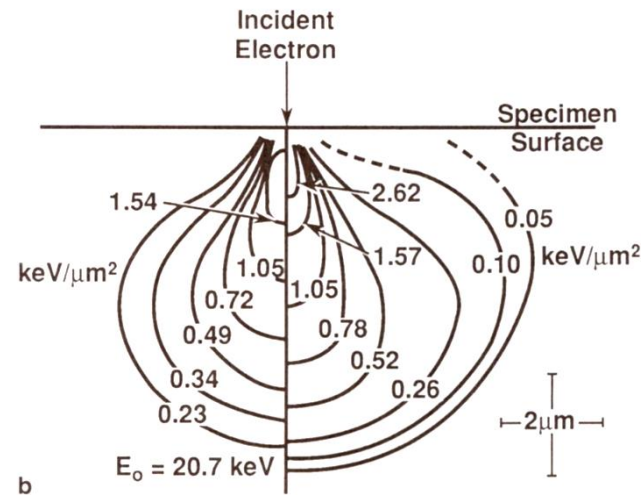
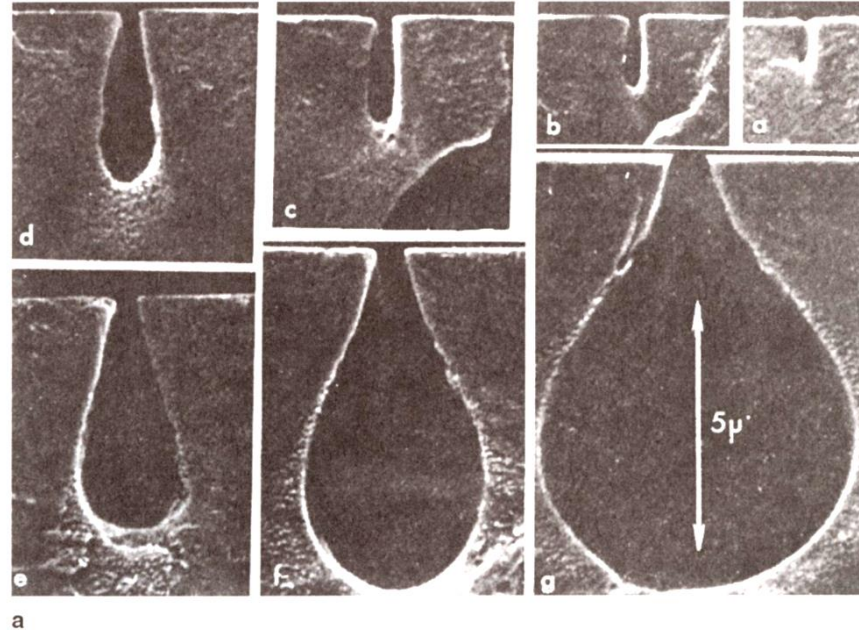
K - is the distance along the trajectory

$$k = 0.731 + 0.0688 \log_{10} Z$$

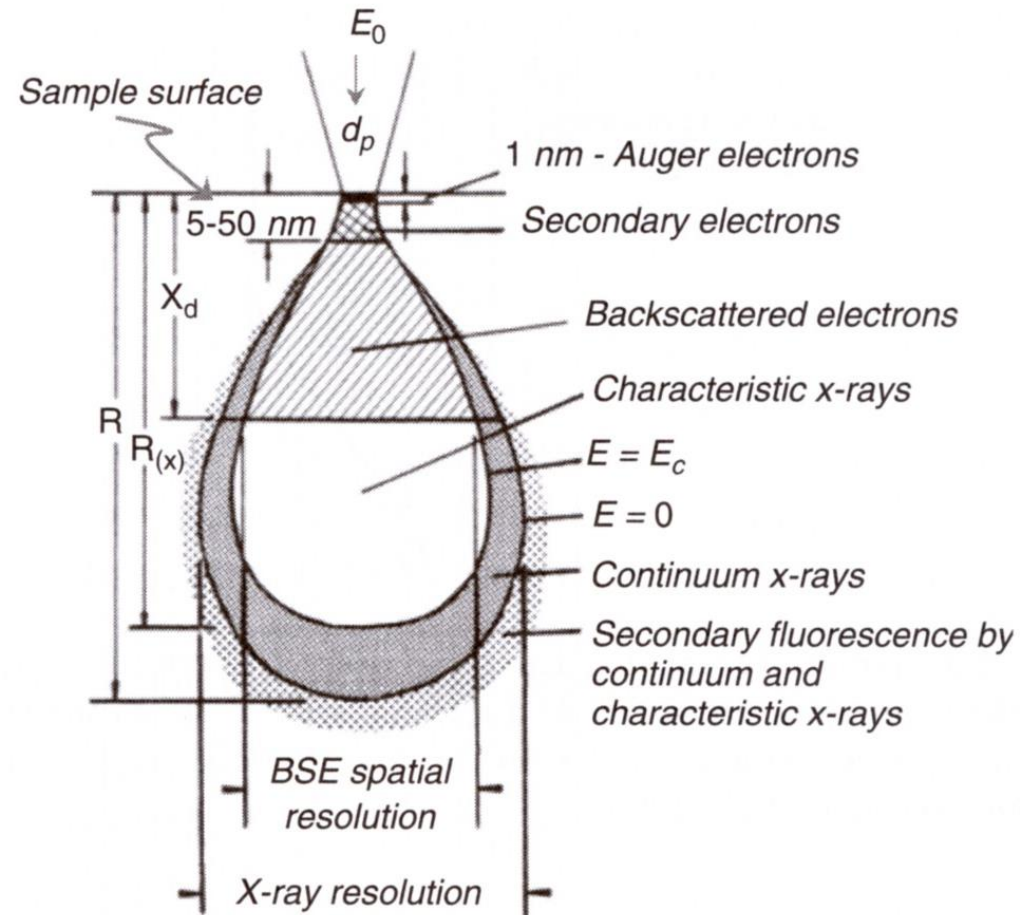


66

CHAPTER 3



a) Etching experiment performed in polymethylmethacrylate (PMMA) for an incident beam dose energy of 20 keV at fixed dose; b) Interpretation of etching experiment of a) in terms of contours of energy deposited in the specimen (left) and as calculated with Monte Carlo simulation (right)

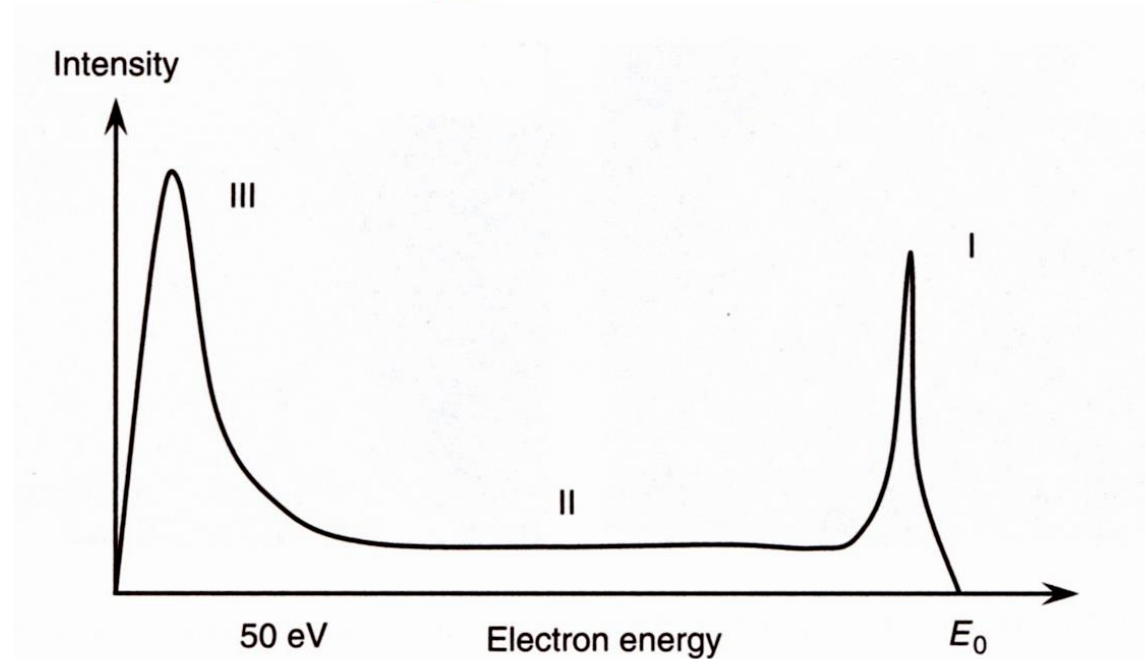


Schematic diagram to show the interaction volume of the primary electron beam

Project WND-POWR.03.02.00-00-1043/16

International interdisciplinary PhD Studies in Materials Science with English as the language of instruction

Project co-financed by the European Union within the European Social Funds



Schematic illustration of the distribution of electron signals and their approximate energies, for a given primary beam energy. Regions I and II refer to backscatter electron contributions, while Region III corresponds to secondary electron signal

$$i_{\text{Beam}} = i_{\text{BSE}} + i_{\text{SE}} + i_{\text{B}} + i_{\text{abs}}$$

where:

i_{Beam} – beam current

i_{BSE} – backscatter electron current

i_{SE} – secondary electron current

i_{B} – background current

i_{abs} – absorbed electron current



SECONDARY ELECTRONS

Produced as a result of interactions between energetic beam electrons and

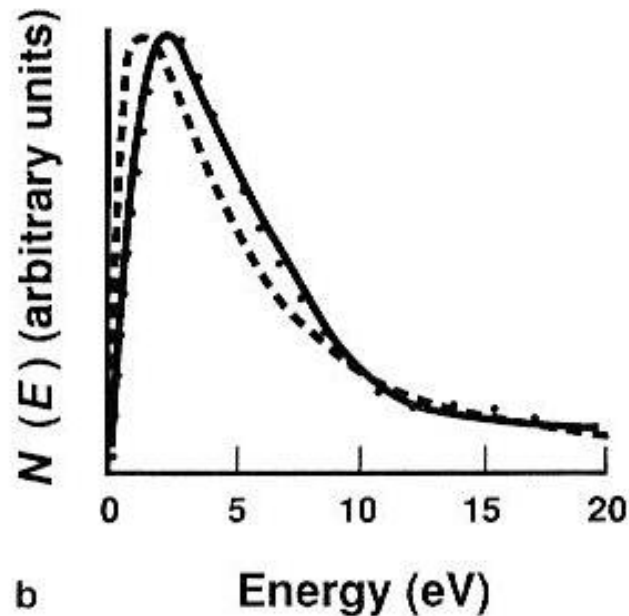
a) Weakly bound conduction band electrons in metals

b) Outer-shell valence electrons in semiconductors and insulators

Because of great difference in energies between the beam electrons and the specimen electrons only a small amount of kinetic energy can be efficiently transferred to the secondary electrons



The energy distribution of secondary electrons emitted from the specimen is narrow and peaks at very low energy, generally in the range of 2-5 eV.



$$\delta = \frac{n_{SE}}{n_B} = \frac{i_{SE}}{i_B}$$

δ – total secondary electron coefficient

n_{SE} - number of secondary electrons

i_{SE} – secondary electron current

i_{Beam} – number of beam electrons



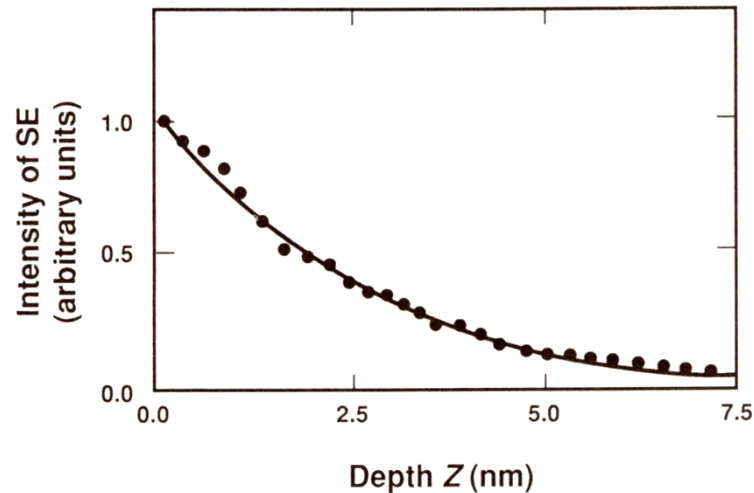
Experimental data for the secondary coefficients for Al and Au over a range of energy

	5 keV	20 keV	50 keV
Al	0.4	0.1	0.05
Au	0.7	0.2	0.10

The secondary electron coefficient δ generally increases as the beam energy is lowered

Why?

Because the escape depth of secondary electrons is small (in the order of a few nanometers) so all secondaries created by the beam electrons at depths greater than a few nanometers are lost!



As a consequence of strong attenuation of the SE due to inelastic scattering, the probability of escape decreases exponentially with depth

$$p \approx \exp\left(-\frac{Z}{\lambda}\right)$$

Maximum depth of emission is about 5λ

λ – Mean Free Path ca 1 nm for metals

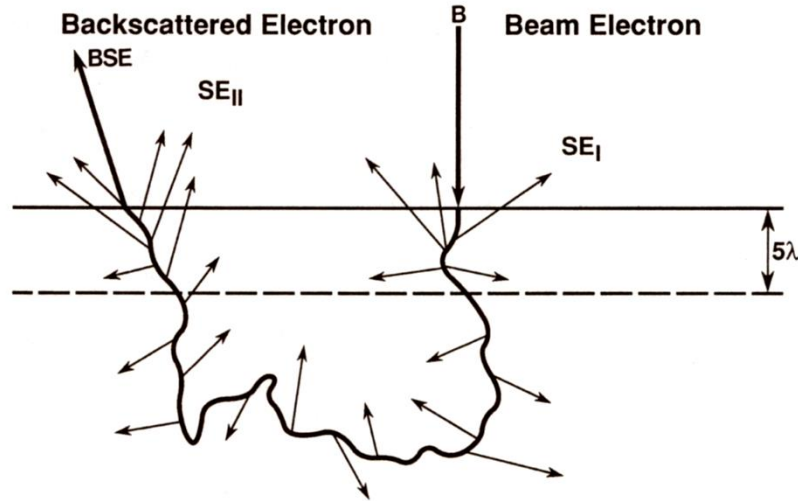
λ – Mean Free Path ca 10 nm for insulators

$5\text{ nm} < \lambda < 50\text{ nm}$

p – probability

Z – depth below the surface where the SE is generated secondaries are generated

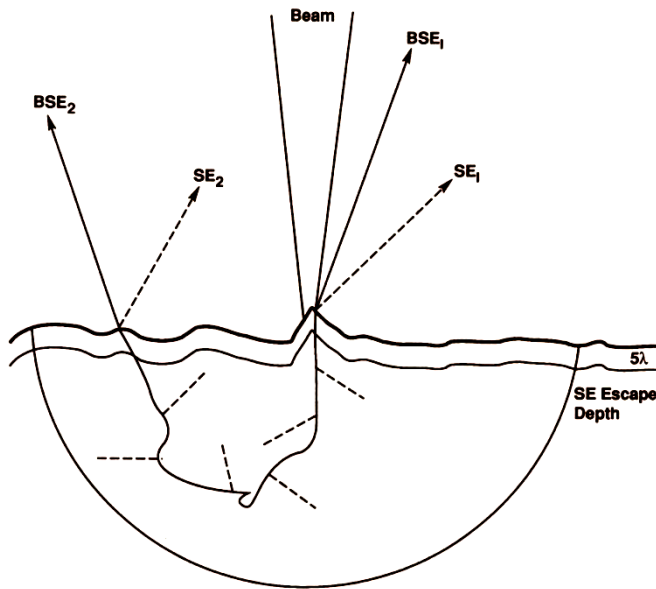
λ – Mean Free Path of SE



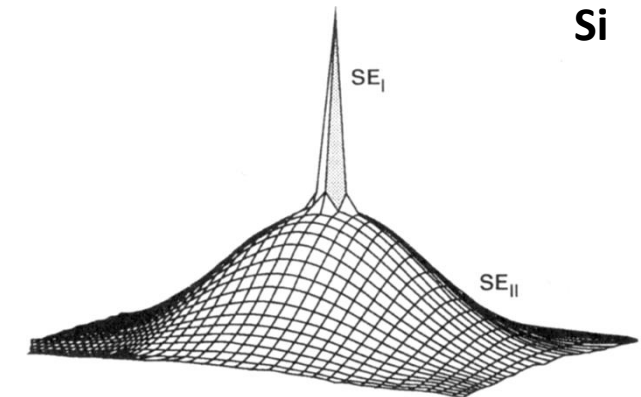
	δ_{Total}	η	SE_2/SE_1
C	0.05	0.06	0.18
Al	0.1	0.16	0.48
Cu	0.1	0.30	0.9
Au	0.2	0.50	1.5

$$\delta_{\text{Total}} = \delta_1 + \delta_2 \eta$$

- SE_1 prevails for C and Al (backscattering is low)
- For mean atomic number Z (e.g. Cu): $\text{SE}_1 = \text{SE}_2$
- SE_2 prevails for high atomic number (backscattering is high)



Limits of Interaction Volume (scale = 0.1)



Si



Total emitted-electron coefficient $\eta + \delta$ as a function of energy

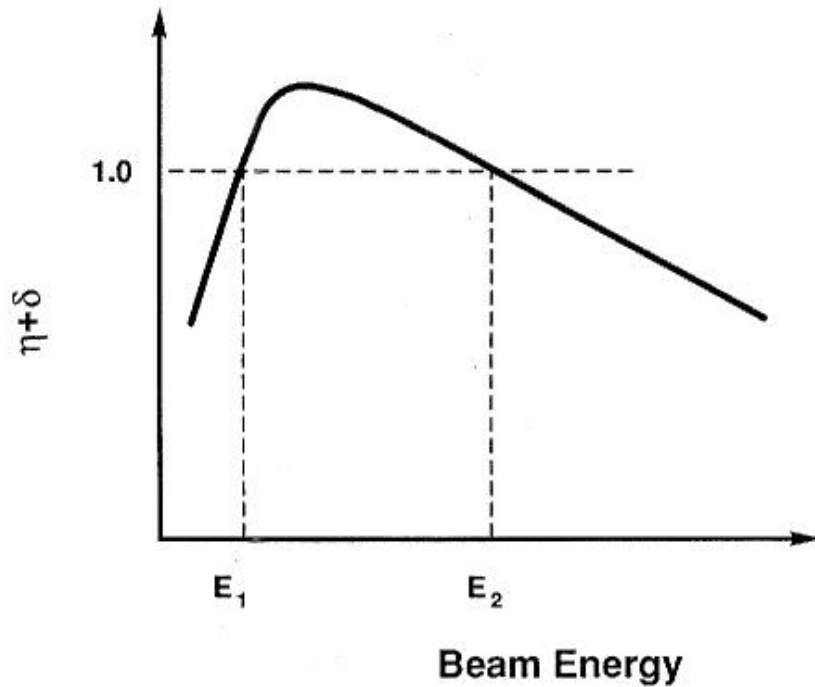


Table 3.6. Upper Crossover Energy for Various Materials (Normal Beam Incidence)

Material	E_2 (keV)	Reference
Kapton	0.4	Joy (unpublished)
Electron resist	0.55–0.70	Joy(1987)
Nylon	1.18	Joy (unpublished)
5% PB7/nylon	1.40	Krause <i>et al.</i> (1987)
Acetal	1.65	Vaz (1986)
Polyvinyl chloride	1.65	Vaz (1986)
Teflon	1.82	Vaz and Krause (1986)
Glass passivation	2.0	Joy (1987)
GaAs	2.6	Joy (1987)
Quartz	3.0	Joy (1987)
Alumina	4.2	Joy (unpublished)

When the primary electron beam energy is reduced below 3 keV, the primary range becomes so shallow that a much greater fraction of secondaries occurs within escape depth and δ increases

As δ increases, there comes a point, denoted as E_2 and called the *upper (or second) crossover point*, where $\eta + \delta$ reaches a value of unity. As the beam energy is lowered further, $\eta + \delta$ increases above unity: **more electrons are emitted from the surface than are supplied by the beam!!!**

As the beam energy is further reduced, the value $\eta + \delta$ decreases until the *lower (or first) crossover point* E_1 is reached. Below E_1 , $\eta + \delta$ decreases with decreasing energy.

High-vacuum evaporation is one of the more popular ways of applying thin-metal and carbon films as coating layers on specimens. The noble metals and their alloys are highly conductive and are suitable as a coating for most samples to be images using secondary electrons.

Carbon, though a relatively poor conductor, is one of the best coating materials for studies involving X-ray microanalysis, provided one of the elements of interest is not carbon.



Project WND-POWR.03.02.00-00-1043/16

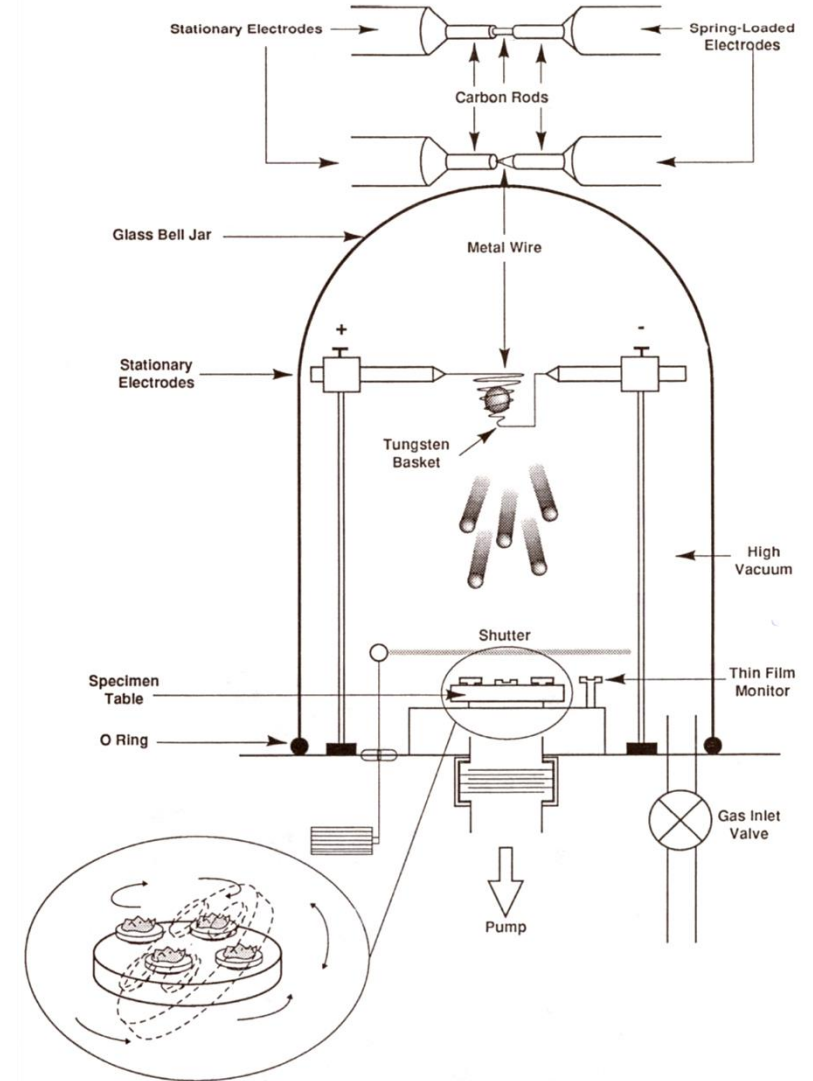
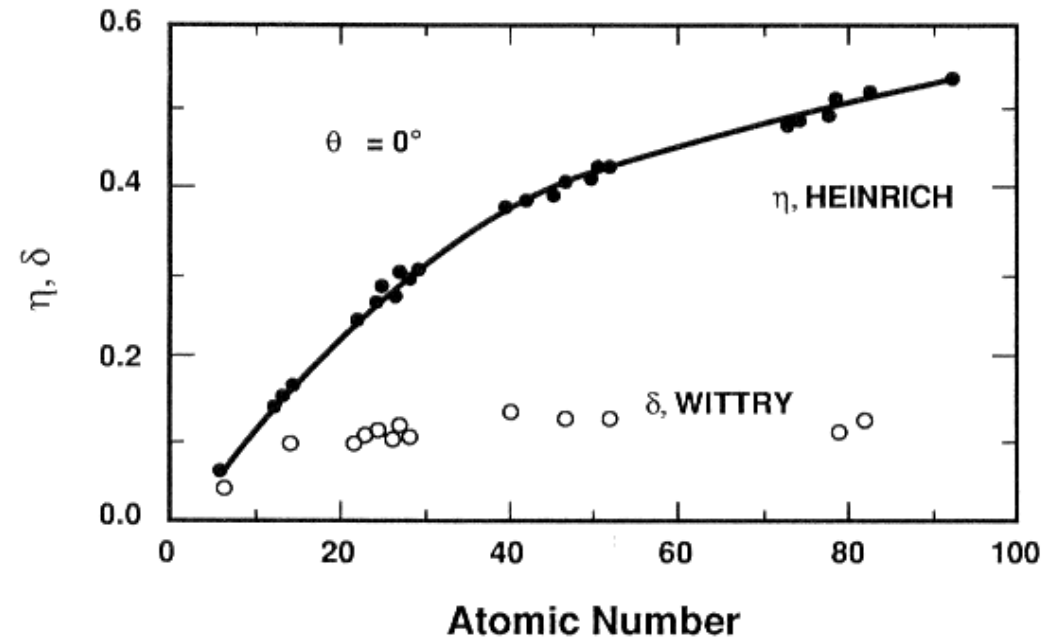


Diagram of a high vacuum evaporative coater

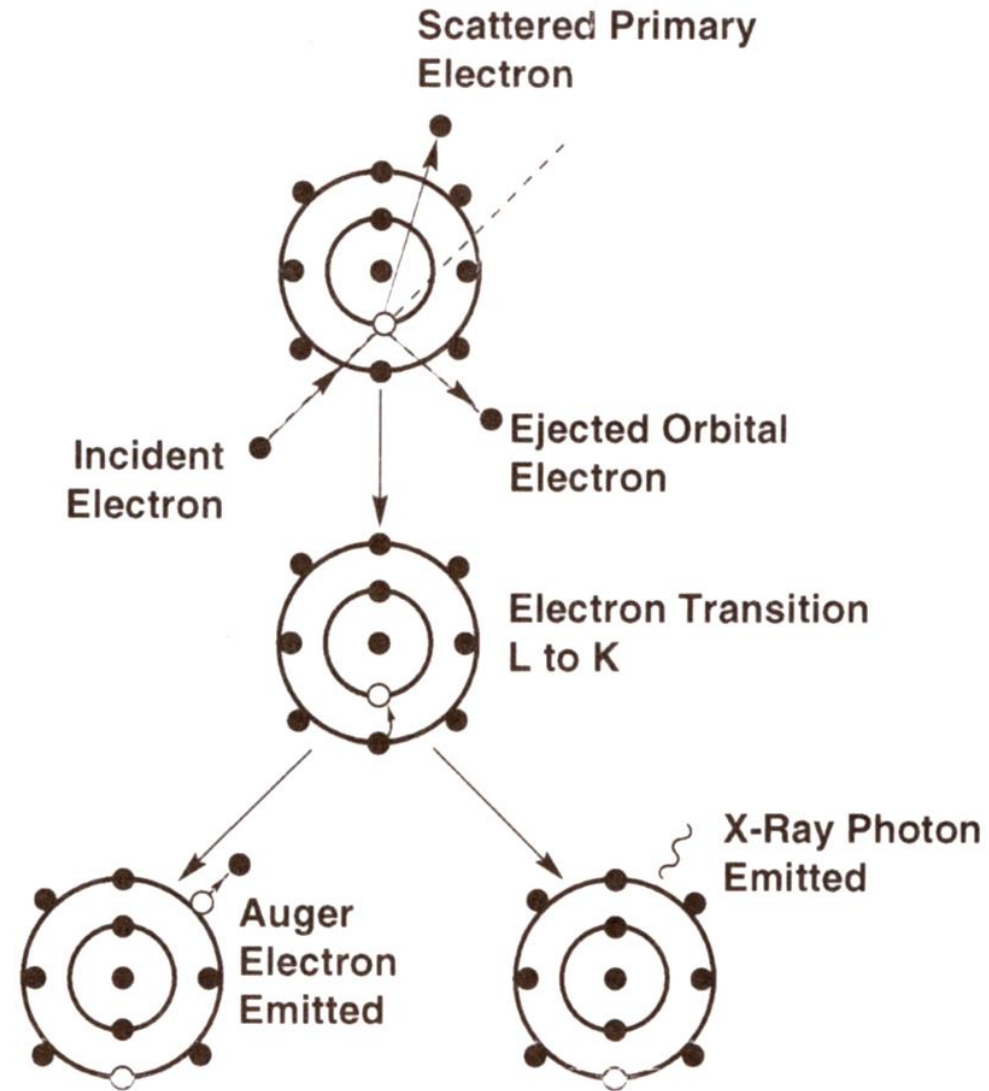


η – strongly increases with atomic number Z !!!

δ – dependence with Z is not so strong!!!



Pierre Auger and Niels Bohr



Project WND-POWR.03.02.00-00-1043/16

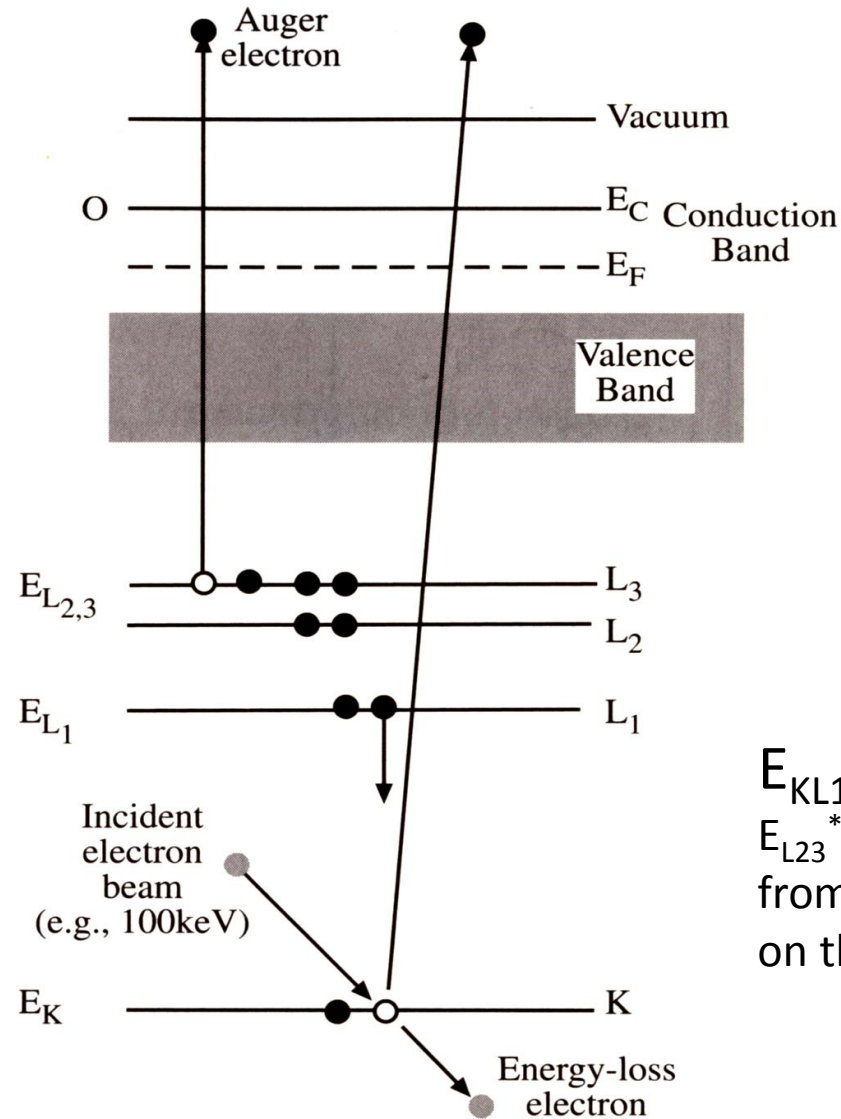
International interdisciplinary PhD Studies in Materials Science with English as the language of instruction

Project co-financed by the European Union within the European Social Funds



The process of inner (K) shell ionization and subsequent Auger electron emission.

The energy released when L_1 electron fills the hole in the K shell is transferred to an electron $L_{2,3}$ shell which is ejected as electron $K_{L_1L_{2,3}}$



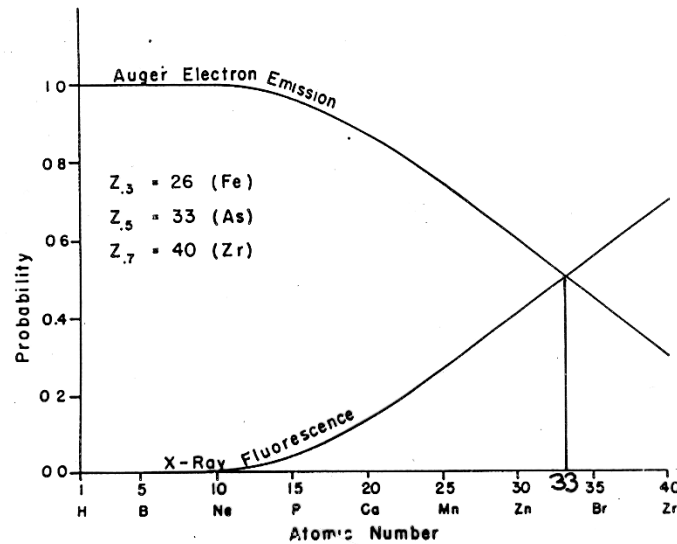
$$E_{KL_1L_{2,3}} = E_K - E_{L_1} - E_{L_{2,3}}^*$$

$E_{L_{2,3}}^*$ binding energy different from $E_{L_{2,3}}$ due to the presence on the hole in the L_1 shell



Fluorescence yield

$$\omega_K = \frac{\text{production of photons } K}{K \text{ shell ionization}}$$



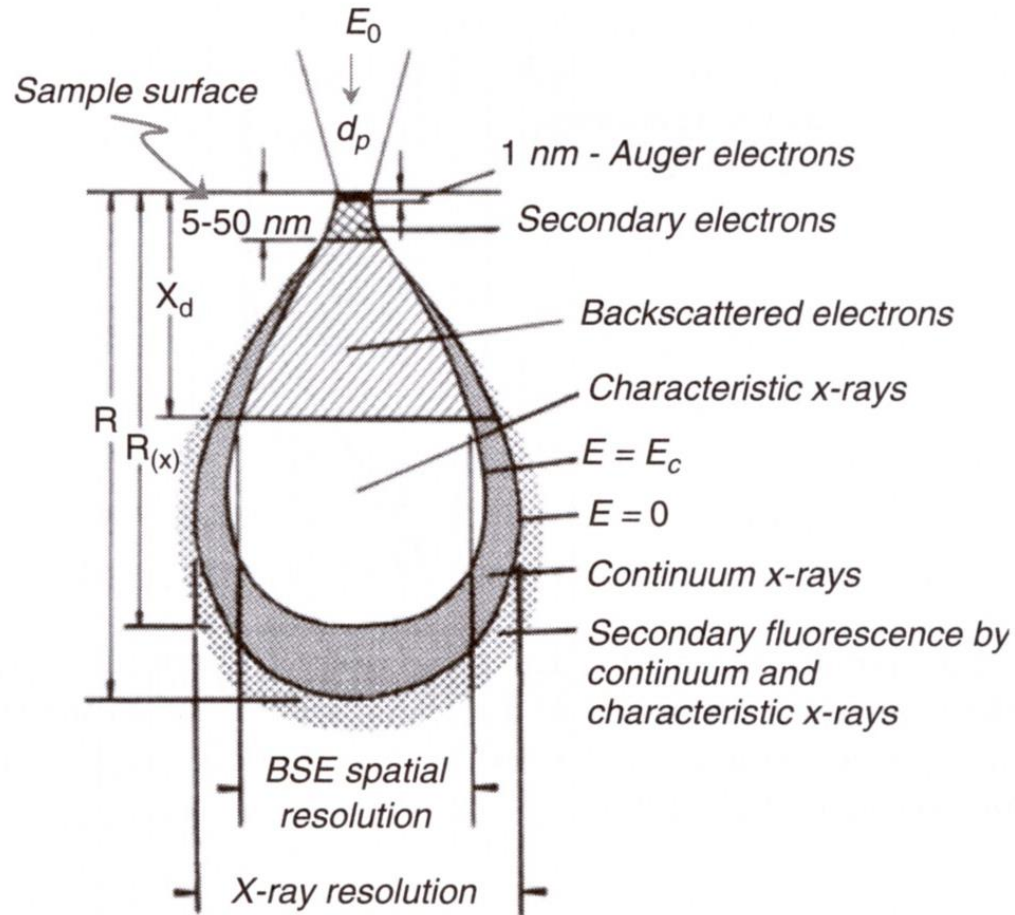
$$\omega = \frac{Z^4}{a + Z^4}$$

$a = 10^6$ for K shell

for C $\omega_K \sim 0.005$

for Ge $\omega_K \sim 0.5$

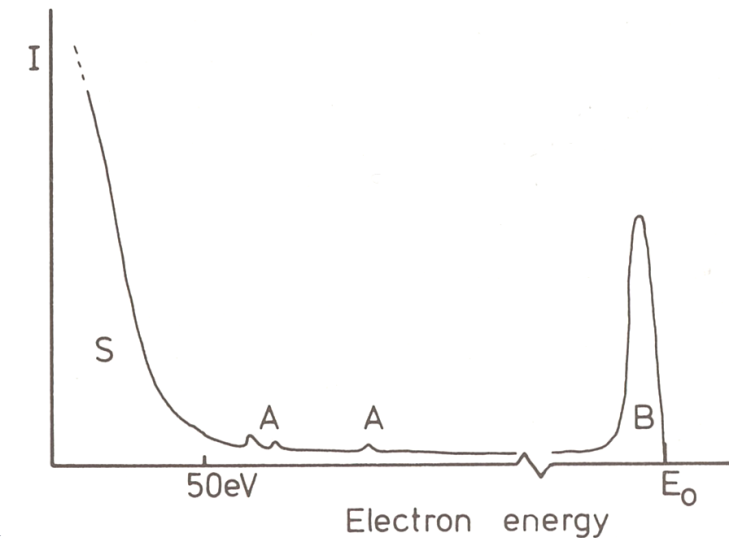
Auger electron emission predominates for light elements

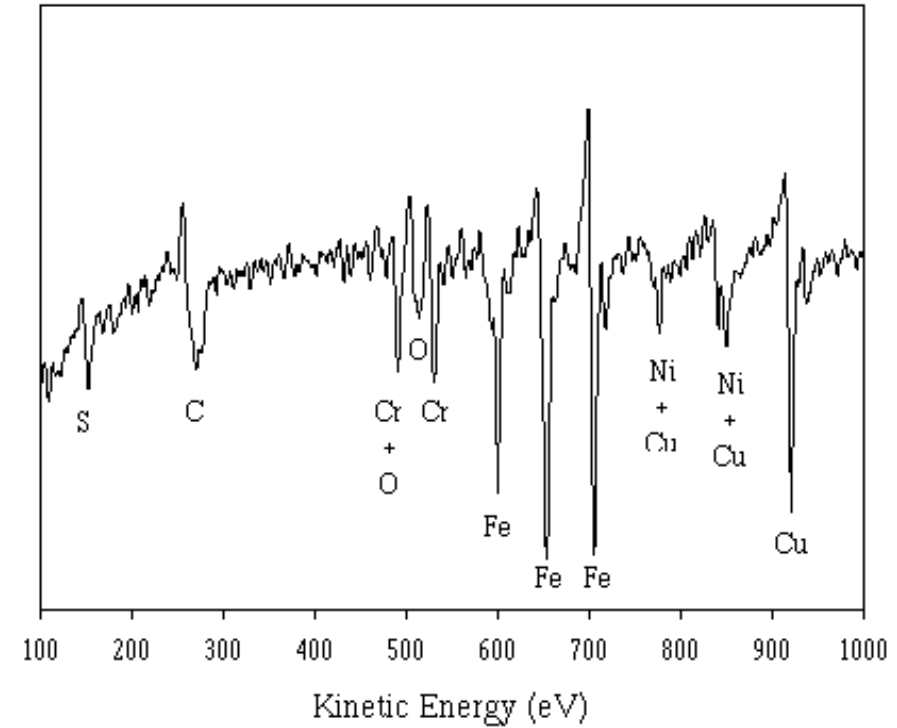
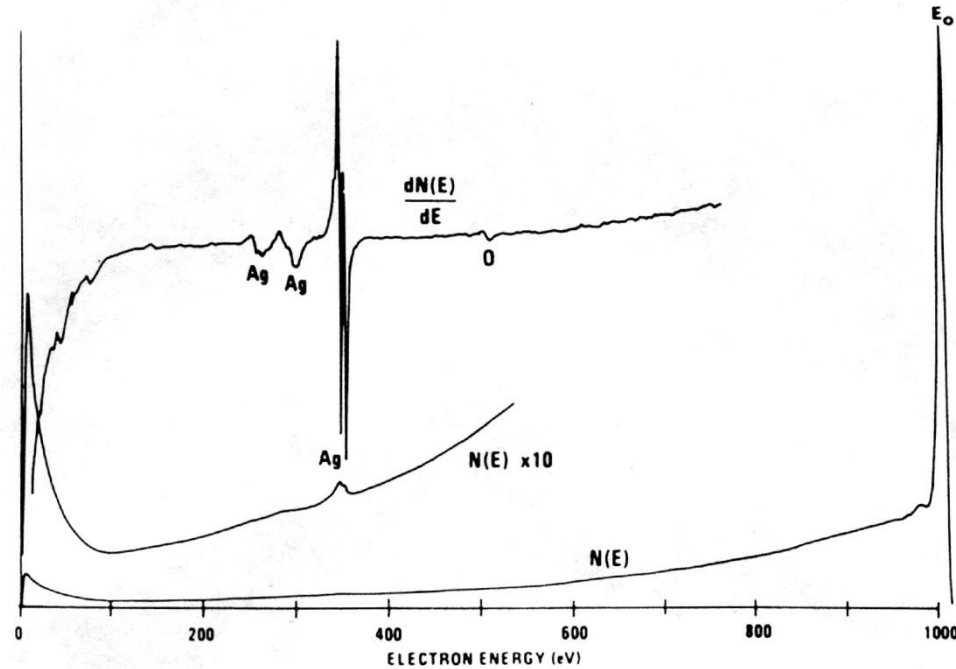


Energy range of Auger electrons: from a few hundreds eV to several keV

Signal is emitted from a few monolayers

**Ideal technique for surface analysis
Scanning Auger Microscopy - SAM**





Auger electron spectrum of silver excited with an incident electron beam energy of 1 keV. Integral (shown with two different vertical expansions) and derivative representations are shown





X-ray emission

$$E = h\nu = \frac{hc}{\lambda} \quad \text{keV}$$

$$\lambda = \frac{1.2398}{E} \quad \text{nm}$$

where:

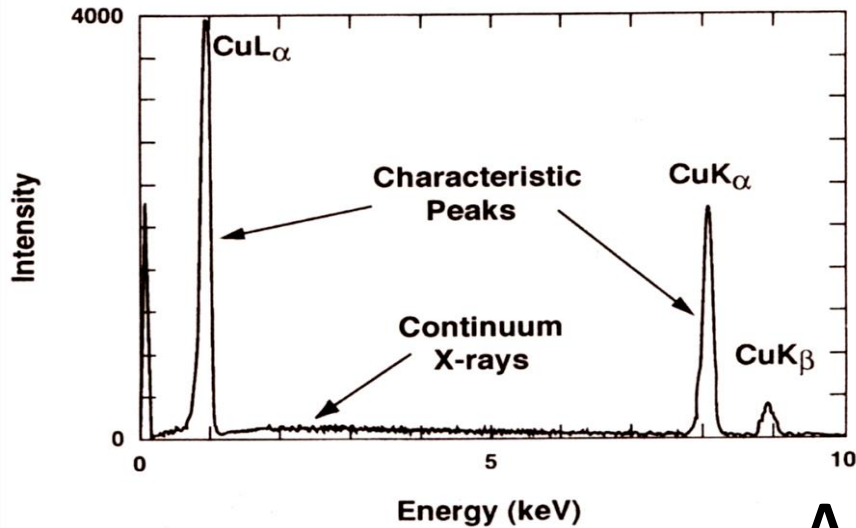
h – Planck's constant

ν – frequency

c – velocity of light

λ – X-ray wavelength (nm)

E – energy of photon (keV)



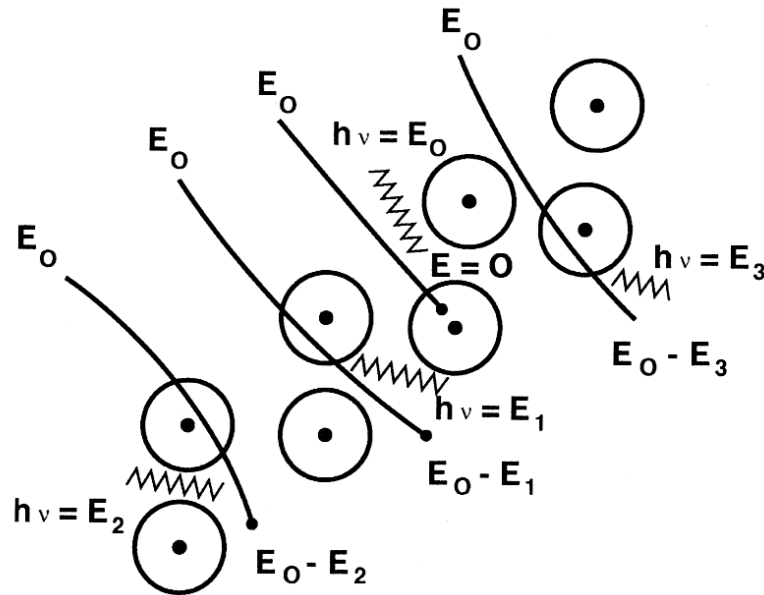
X-Ray spectrum of copper showing K-series and L-series of X-ray peaks and the continuous X-ray spectrum obtained with a Si(Li) EDS detector with an ultrathin X-ray window. Natural widths of peaks are much narrower. A noise peak is measured at very low energies.

A typical X-ray spectrum includes major spectral peaks superimposed on a broad background.

Each element produces characteristic spectral peaks therefore qualitative information can be extracted.

Extracting quantitative information is also possible but more complicated.

Continuum X-ray production (Bremsstrahlung)



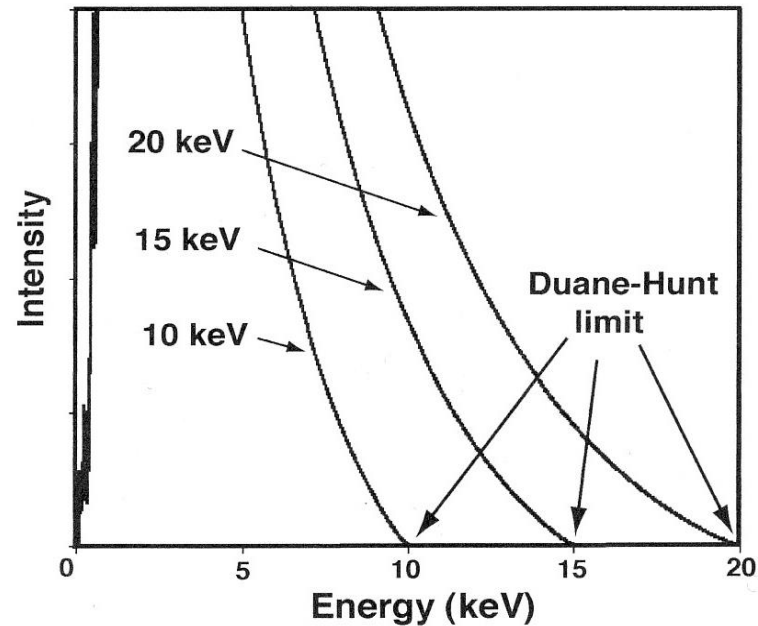
Schematic illustration of the origin of the X-ray continuum which results from the deceleration of beam electrons in the Coulombic field of the atoms

The maximum X-ray energy observed in the spectrum corresponds to beam electrons that have lost all of their incident energy in a single event.

Since X-ray wavelengths is inversely proportional to energy, the most energetic X-rays will have a minimum wavelength λ_{\min} or λ_{SWL} , called the short-wavelength limit or Duane-Hunt limit which can be related to the incident energy E_0



Continuum X-ray production (Bremsstrahlung)



Duane-Hunt limit for simulated spectra from a carbon specimen at beam energies of 10, 15 and 20 keV. Duane-Hunt limit is the energy where the continuum background intensity goes to zero.



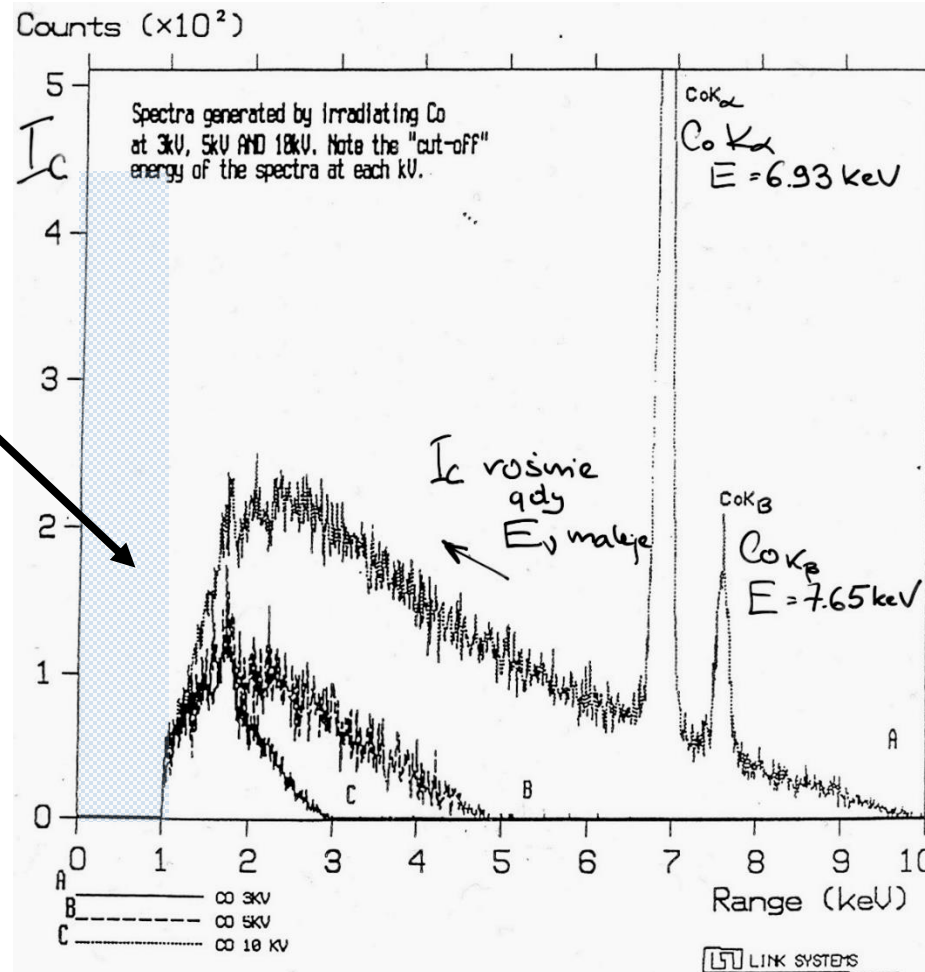
Continuum X-ray production (Bremsstrahlung) Kramer, 1923

$$I_{\text{cm}} \approx i_p \bar{Z} \frac{E_0 - E_v}{E_v}$$



Continuum X-ray production (Bremsstrahlung)

Absorption of
the X-ray by
Beryllium
window



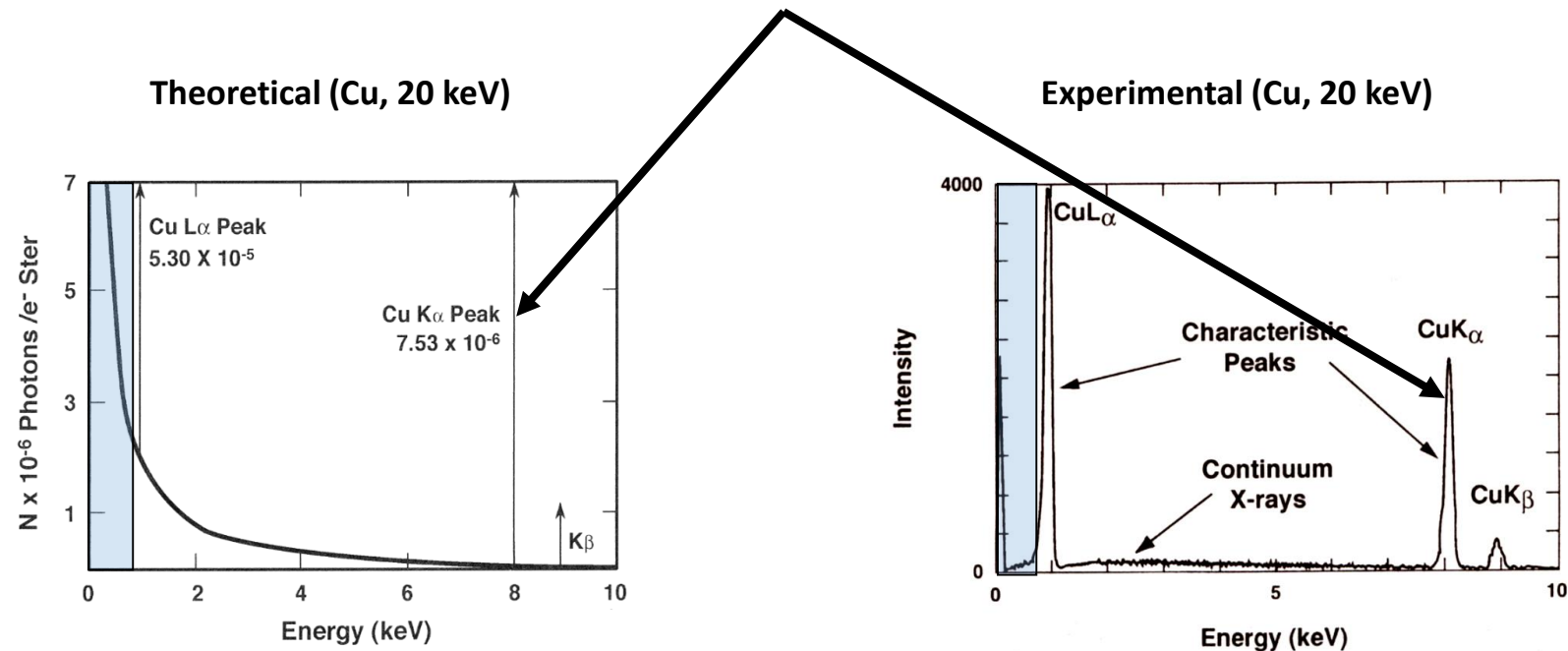
A = 10 keV

B = 5 keV

C = 3 keV



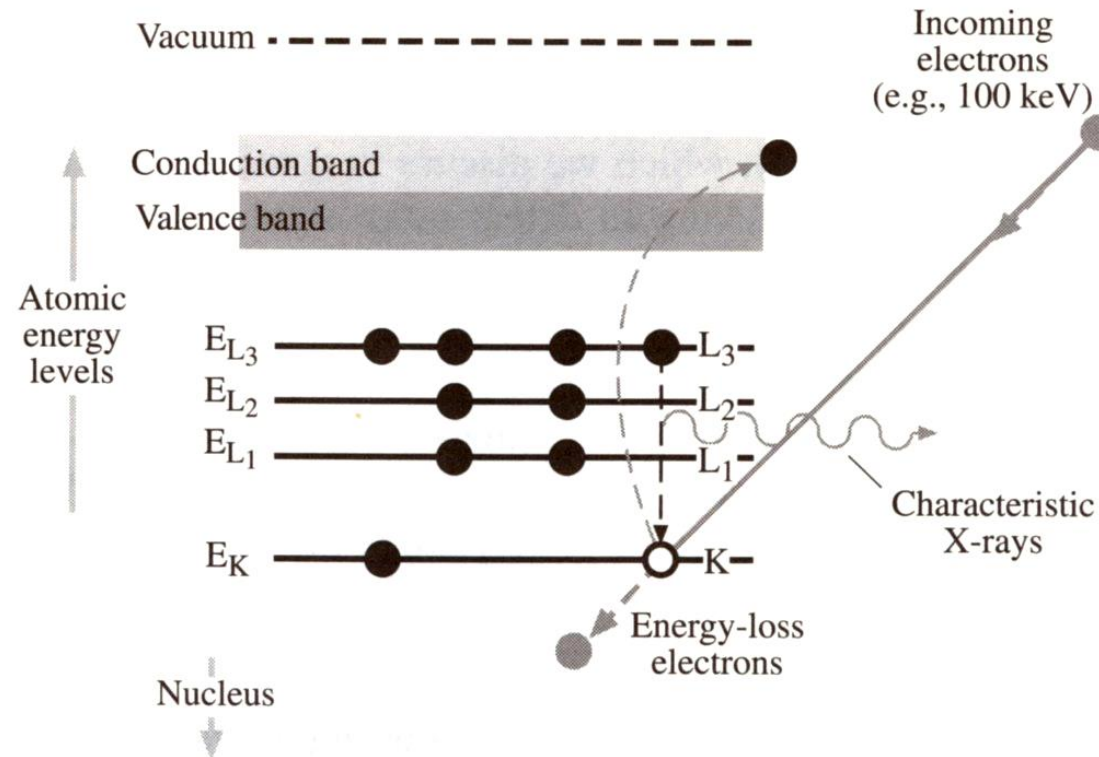
Continuum X-ray production (Bremsstrahlung)



Bremsstrahlung – a big problem during analysis



Characteristic X-ray – The ionization process



An inner K=(K) shell electrons is ejected from the atom by a high-energy electron. When the hole in the K shell is filled by an electron from the L shell, characteristic $K\alpha$ X-ray emission occurs. The beam electron loses energy but continues on through the sample.



Critical ionization inergy

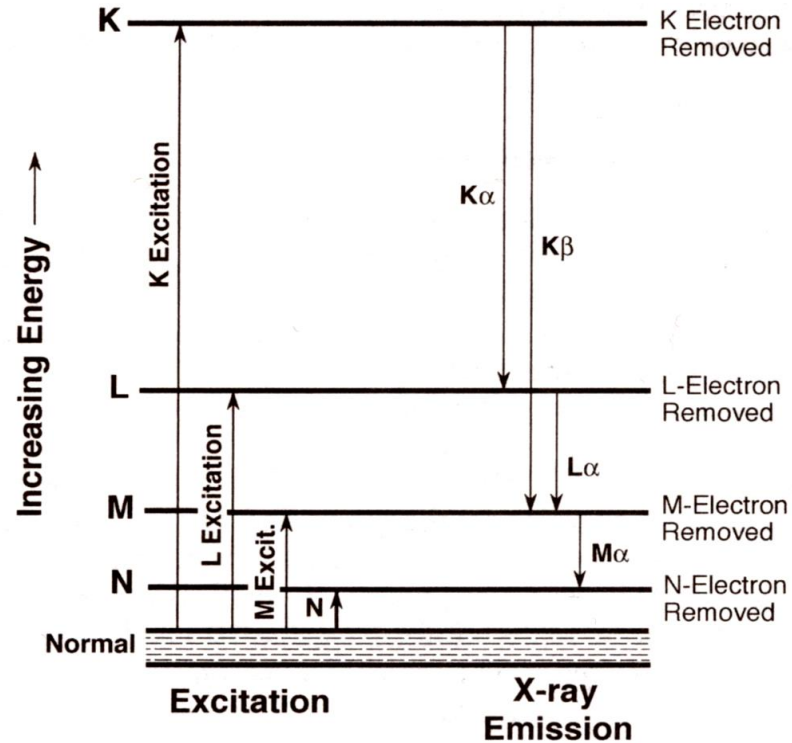


Table 6.2. Critical Ionization Energies for Pt, Nb, and Si

Shell	E_c for Pt (keV)	E_c for Nb (keV)	E_c for Si (keV)
K	78.39	18.99	1.839
L_I	13.88	2.697	0.149
L_{II}	13.27	2.464	0.099
L_{III}	11.56	2.370	0.099
M_I	3.296	0.468	
M_{II}	3.026	0.378	
M_{III}	2.645	0.363	
M_{IV}	2.202	0.207	
M_V	2.122	0.204	

The rule in SEM

We work with beam energies 3 times higher than Critical Ionization Energy

Primary ionization involves removing an electron from a bound state in a shell to an effective infinity outside atom. However, characteristic Si: $E_{K\alpha} (E_K - E_L) = 1.740 \text{ keV} < E_c = 1.839 \text{ keV}$



Moseley's Law(1914)

The energies of the electron shells vary in a discrete fashion with atomic number.

Thus, the emitted X-rays have energies characteristic of that atomic number.

The difference in energy between shells changes in regular step when the atomic number changes by one unit.



$$E = A(Z - C)^2$$

A, C – constants

e.g.

$$\lambda = \frac{A}{(Z - C)^2}$$

C = 1.13 for the K series

C = 7 for the L series

The equation may be used to find energy of any element K or L line
Moseley's law forms the basis for qualitative X-ray analysis, i.e. the identification of elemental constituents



Electron range expression

$$\rho R = k E_0^n \quad \mu m$$

k – depends on material parameter = $0.0276 A/Z^{0.89}$

E_0 – is the incident electron beam energy (keV)

P – in the density

n – is a constant between 1.2 and 1.7

Depth of X-ray production (X-ray range)

$$\rho R = k (E_0^n - E_c^n) \quad \mu m$$

E_c – Critical ionisation energy (keV) of the shell

n – is a constant between 1.2 and 1.7

**X-ray excitation depth is
ALWAYS smaller than electron
excitation depth.**



Anderson-Hasler X-ray Range

$$R_{A-H} = \frac{0.064}{\rho} (E_0^{1.68} - E_c^{1.68}) \quad \mu\text{m}$$

$$E_c = 0 \text{ keV}$$

$$R = \frac{0.064}{8.93} 20^{1.68} = 1.10 \mu\text{m}$$

$$\text{Cu} - \text{L}\alpha (E_c = 0.933 \text{ keV})$$

$$R = \frac{0.064}{8.93} (20^{1.68} - 0.933^{1.68}) = 1.09 \mu\text{m}$$

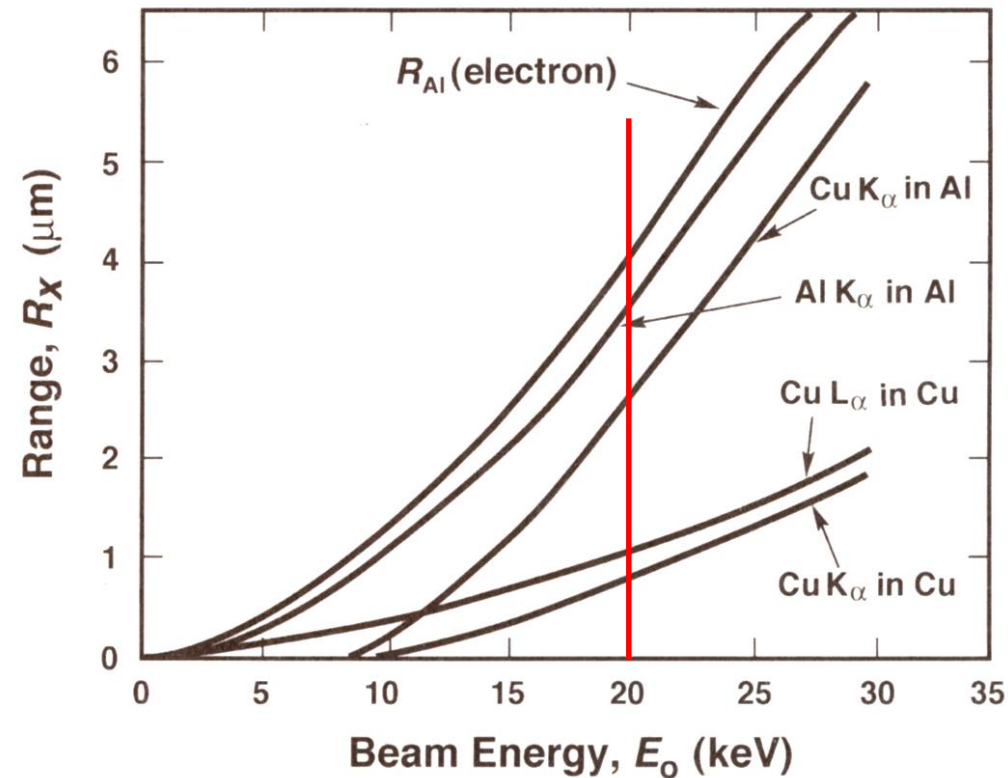
$$\text{Cu} - \text{K}\alpha (E_c = 8.980 \text{ keV})$$

$$R = \frac{0.064}{8.93} (20^{1.68} - 8.980^{1.68}) = 0.81 \mu\text{m}$$

R_x has unit in μm , E is in keV
and ρ is in g/cm^3

$$\text{Cu}, \rho_{\text{Cu}} = 8.93 \text{ g}/\text{cm}^3,$$

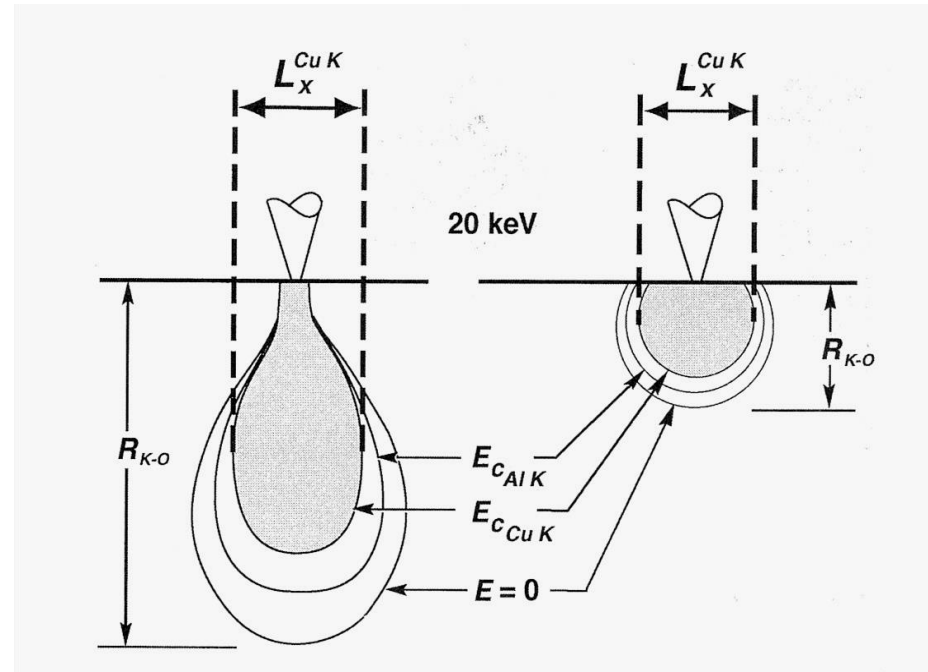
$$E_0 = 20 \text{ kV}$$



X-ray generation range (Anderson-Hasler) for Al K_{α} and Cu K_{α} generated in Al specimen and Cu K_{α} and Cu L_{α} in a Cu specimen as a function of beam energy. Note that electron range for aluminum R_{Al} is larger than the X-ray range of the X-ray line generated by the electron beam.



X-ray spatial resolution



Al, $\rho \sim 3 \text{ g/cm}^3$

Cu, $\rho \sim 10 \text{ g/cm}^3$

Comparison of X-ray production regions from the specimen with densities of 3 g/cm^3 (left) and $\rho \sim 10 \text{ g/cm}^3$ (right) at the beam energy of 20 keV.

The X-ray spatial distribution L_x is found by projecting the maximum diameter of the X-ray distribution to the surface of the specimen

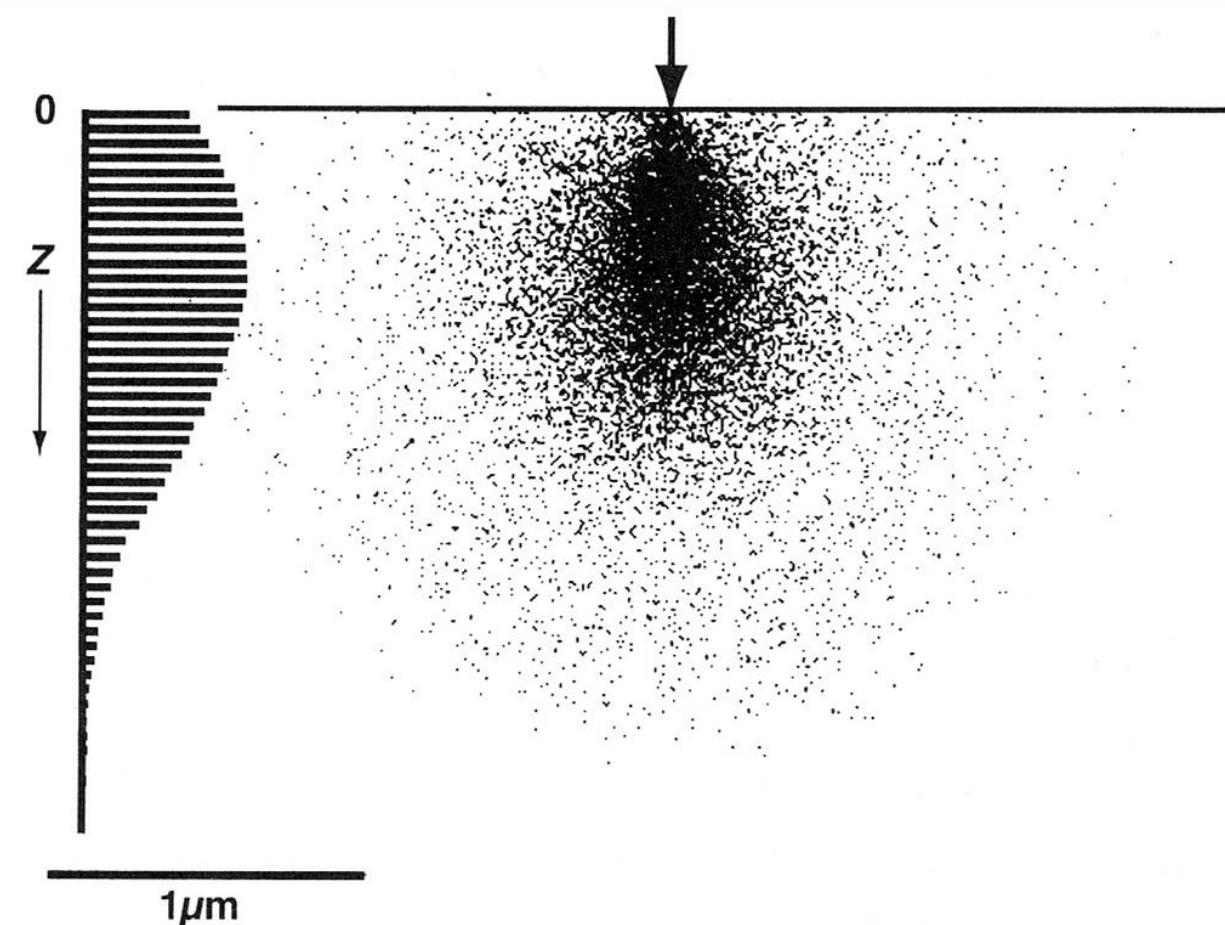


Monte Carlo simulation of the generation of Al K α X-rays in pure Al.

At 30 keV the electron beam enters the specimen at the surface, 0, and progresses into the specimen as a function of distance Z.

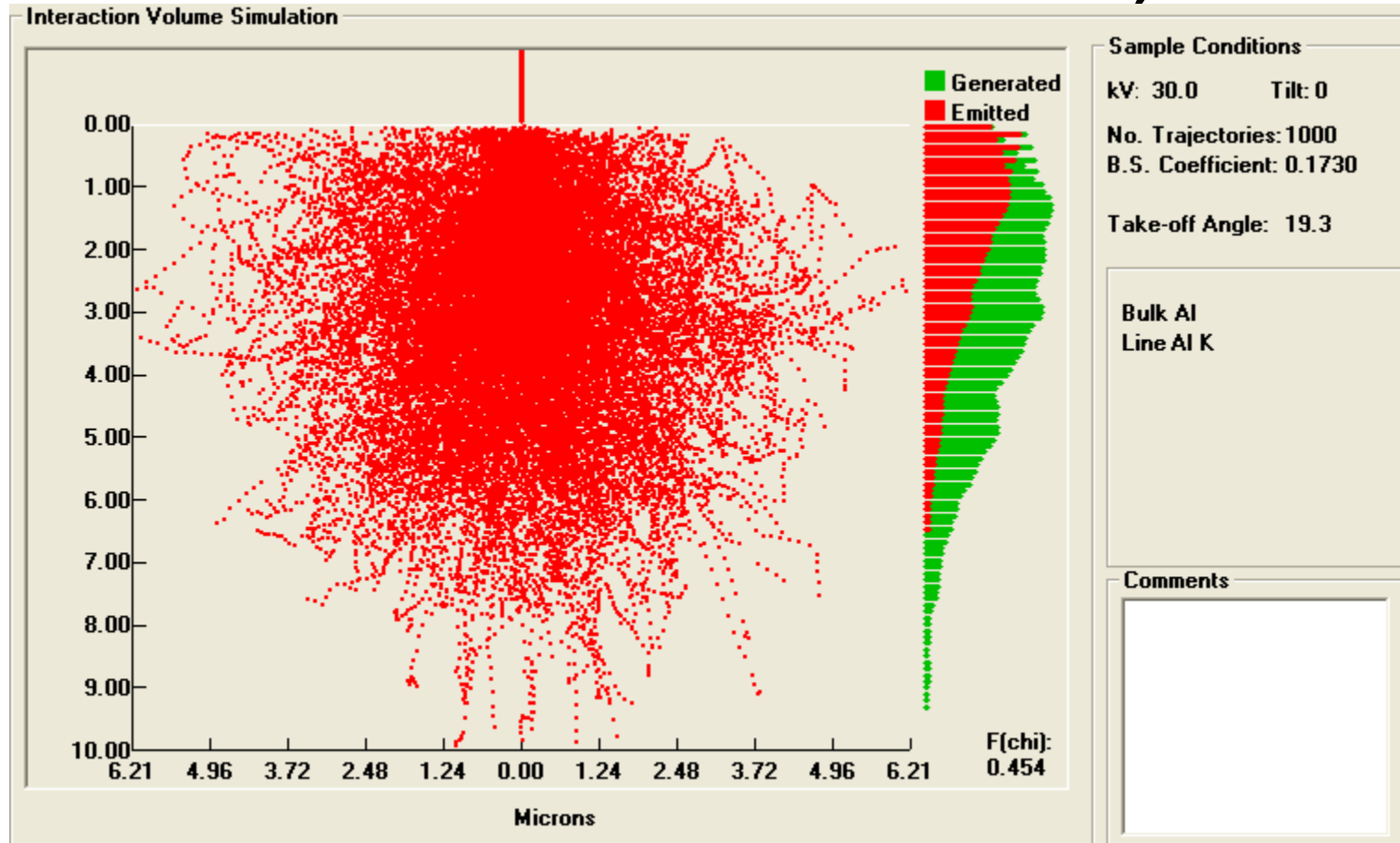
(Left A) - histogram of the X-ray generation function with depth, $\phi(\rho Z)$.

X-ray generation increases to a maximum just below the surface and then decreases as fewer X-ray are generated within the specimen.



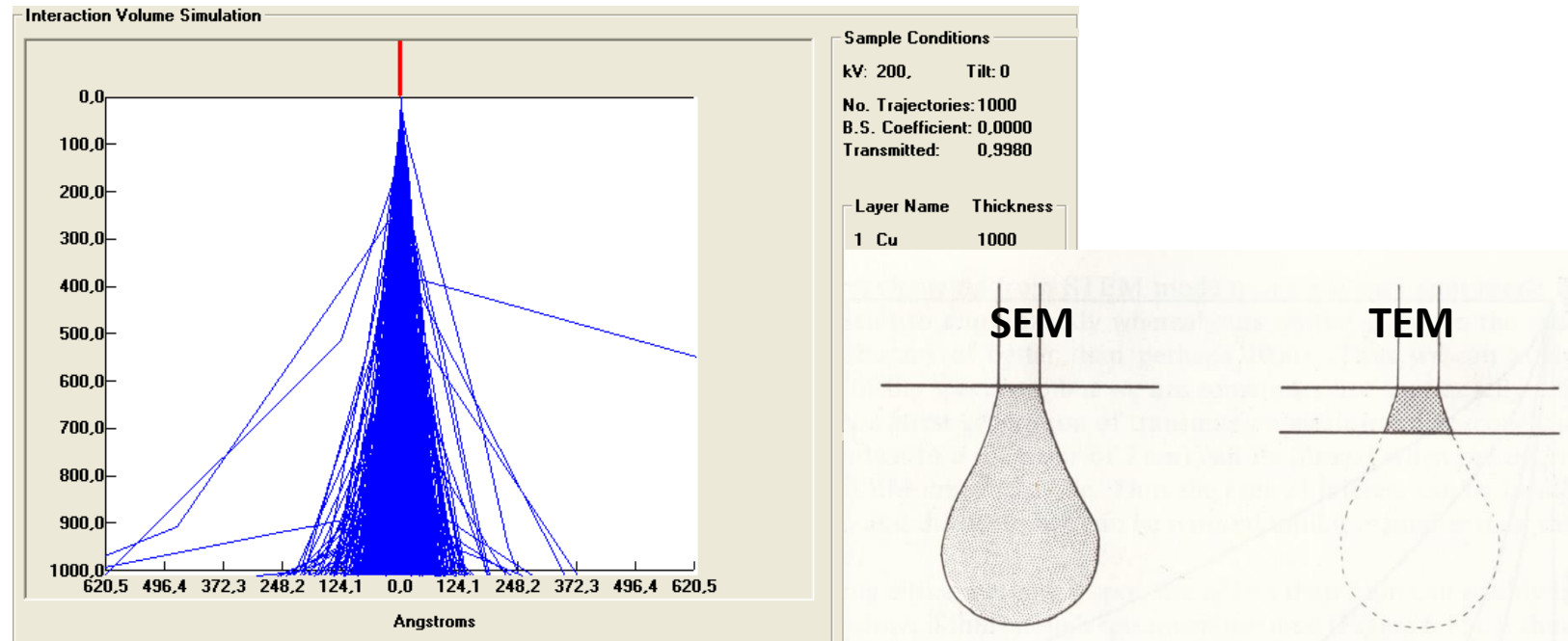


Monte Carlo simulation for Al K α line, 30 keV





Spatial resolution of X-ray analysis in TEM



Cu, $\rho \sim 10 \text{ g/cm}^3$

In TEM a spatial resolution is dependent on beam broadening



Cross section (probability) for inner shell ionization

$$Q = 6.51 \times 10^{-20} \frac{n_s b_s}{U E_c^2} \log_e (c_s U)$$

The basic form derived by Bethe (1930)

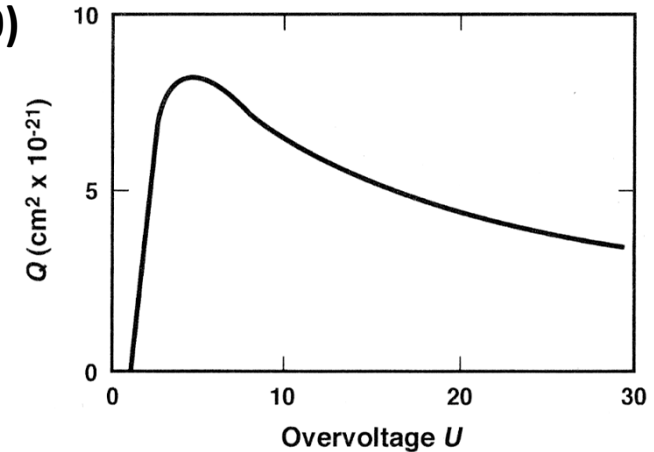
n_s number of electrons in a shell or subshell (e.g., np, $n_s=2$ for a K shell)

b_s, c_s constants for a particular shell

E_c critical ionisation energy (keV) of the shell

U „overvoltage”

E_0 beam energy



Plot of the cross section for inner shell ionization of the silicon K shell as a function of overvoltage $U=E/E_0$

$$U = \frac{E_0}{E_c}$$

The cross section increases rapidly from an overvoltage of 1 to a maximum of about $U \approx 3$

E.g. for E_c Si K = 1.839 keV, maximum K shell ionization is for $E_0 \approx 5.5$ keV



X-ray production in thick targets

(Green 1963, Lifshin 1980)

$$I_{\text{ch}} = i_p a \left(\frac{E_o - E_c}{E_c} \right)^n = i_p a (U - 1)^n$$

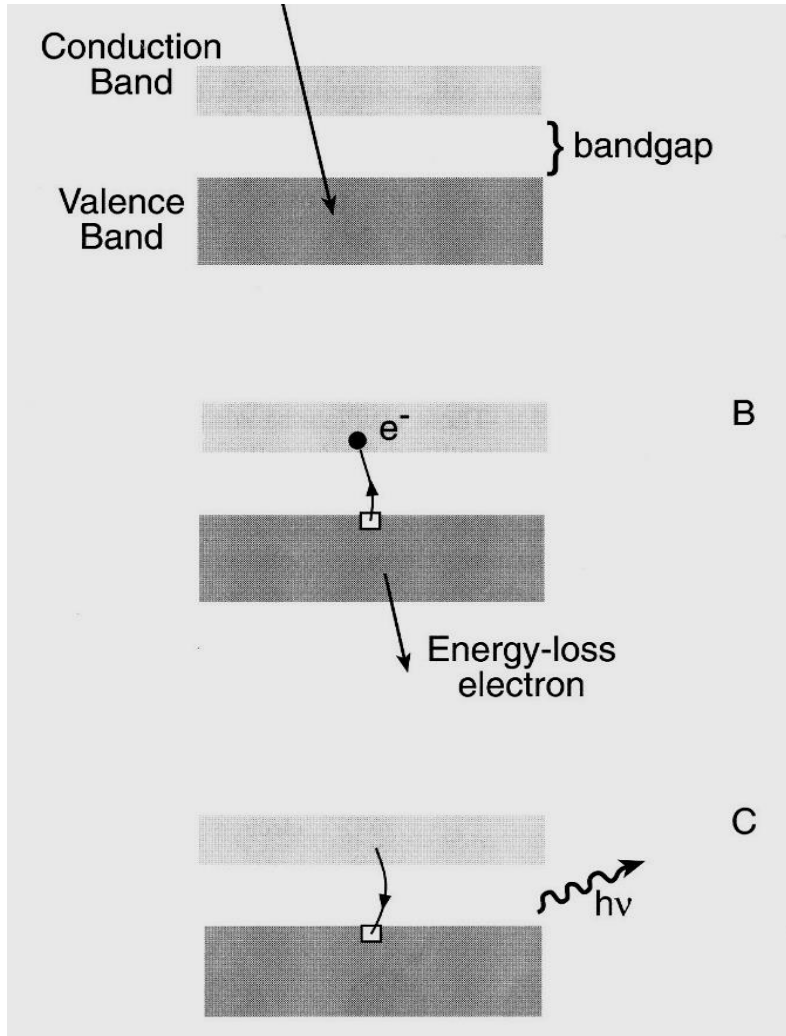
This is an intensity produced in the specimen prior to its absorption as the radiation propagated through the specimen

i_p the electron beam current

a, n - are constants for particular element and shell. The value of n is normally in the range of 1.5-2.0



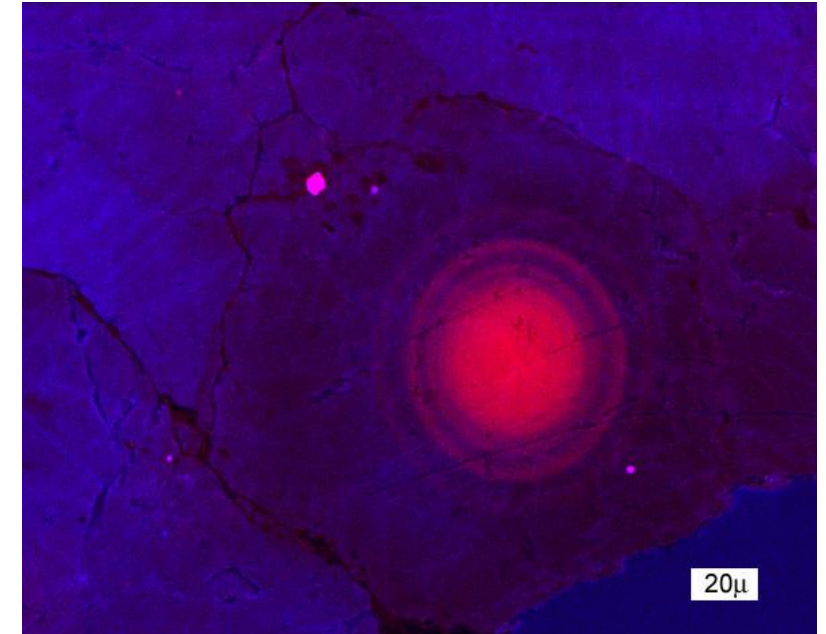
Cathodoluminescence (CL)



An initial state before a beam electron interacts with valence-band electrons

B: A valence-band electron is excited across the gap into the conduction band, leaving a hole in the valence band

C: The hole is filled by a conduction-band electron falling back into the valence-band hole. Upon recombination a photon of light is emitted, with a frequency determined by the band gap $h\nu = E_{\text{GAP}}$



$$E_{\text{GAP}} = 2.4 \text{ eV (CdS)}$$

$$E_{\text{GAP}} = 1.1 \text{ eV (Si)}$$

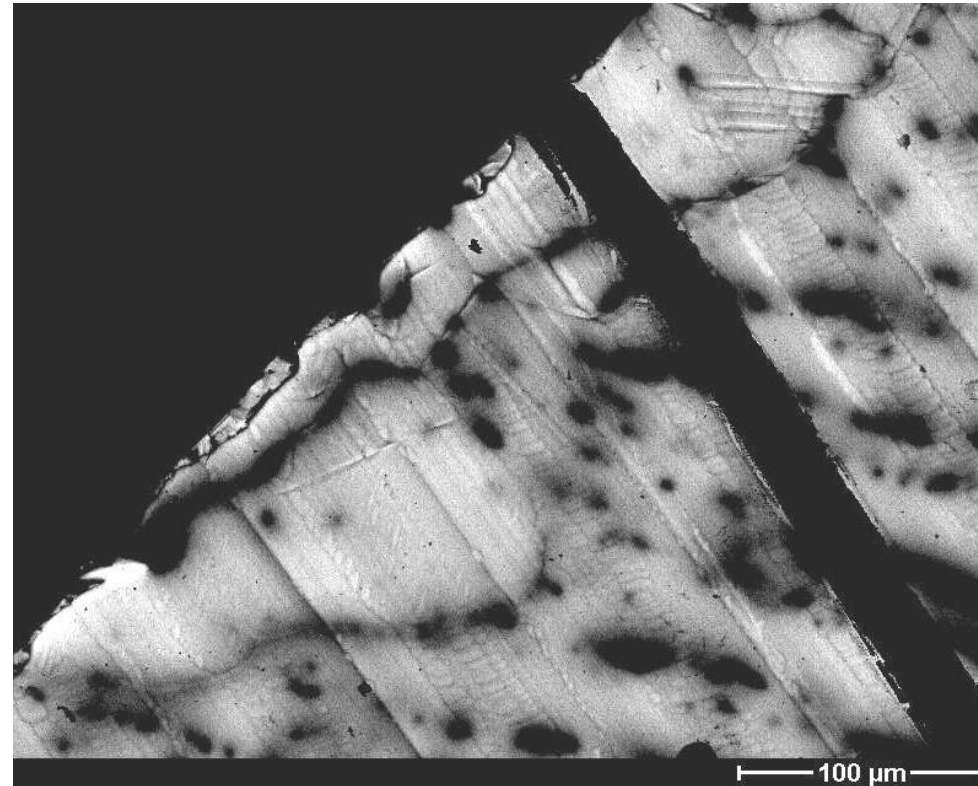


If you do not anything, the electron and holes will recombine, and in doing so give off light!!!

If, however, you apply bias to your specimen then the electron and holes can be separated under the internal bias.

You can pick up the signal if you ground the specimen through a picoammeter. In this situation the specimen is acting as its own detector!

The current you detect is called „electron beam induced current” or EBIC and if you detect it and use it to form an image then you are doing „charge-collection microscopy” or CCM.



The EBIC image of a silicon solar shows dark contrast due to recombination centers within the material.



Fundamental Constants and Definitions

Charge (e)	$(-)\mathbf{1.602 \times 10^{-19}C}$
1 eV	$\mathbf{1.602 \times 10^{-19}J}$
Rest mass m_0	$\mathbf{9.1099 \times 10^{-31} \text{ kg}}$
Kinetic energy (charge x voltage)	$\mathbf{1.602 \times 10^{-19} \text{ Nm}}$ (for 1 volt potential 1V)
Planck' constant	$\mathbf{6.626 \times 10^{-34} \text{ Js}}$
Speed of light in vacuum	$\mathbf{2.998 \times 10^8 \text{ m/s}}$



λ - wavelength

h – Planck's constant

p – particle momentum

$$\lambda = \frac{h}{p} \quad (1)$$

We impart momentum to the electron by accelerating it through a potential drop, V , giving it a kinetic energy eV . This potential energy must be equal the kinetic energy

$$eV = \frac{m_0 v^2}{2} \quad (2)$$

Now we can equate the momentum p to the electron mass (m_0) times velocity (v) and substituting for v from equation (2) we obtain equation (3)

$$p = m_0 v = (2m_0 eV)^{1/2} \quad (3)$$

Relationship between the electron wavelength λ and the accelerating voltage of the electron microscope V

$$\lambda = \frac{h}{\sqrt{(2m_0 eV)}} \quad (4)$$



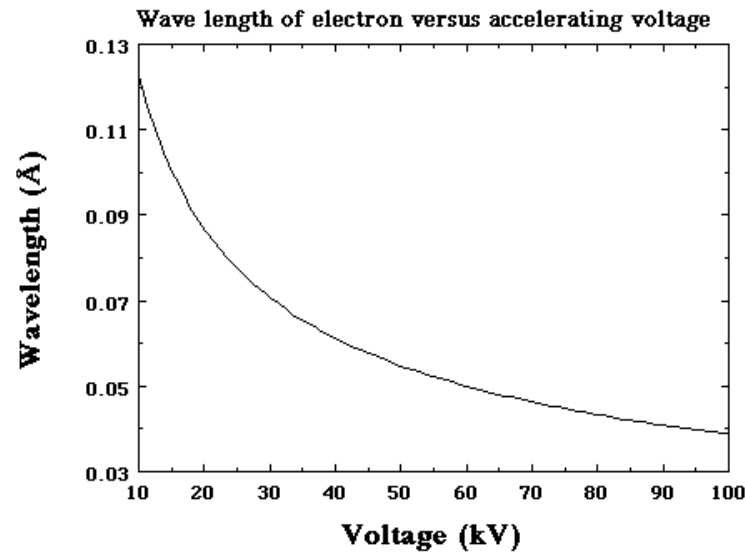
**By increasing the acceleration voltage
we decrease the wavelength of electrons**



$$\lambda = \frac{h}{\sqrt{2m_0eV \left[\frac{1 + eV}{2m_0c^2} \right]}}$$

$$\lambda = \frac{12.2630}{\sqrt{V + 0.97845 \times 10^{-6} V^2}}$$

Wavelength of electron versus accelerating voltage





Accelerating voltage V (kV)	Relativistic wavelength λ , nm
20	0.00859
30	0.00698
40	0.00602
50	0.00536
60	0.00487
70	0.00448
80	0.00418
90	0.00392
100	0.00370
200	0.00251
300	0.00197
400	0.00164
500	0.00142
600	0.00126
700	0.00113
800	0.00103
900	0.00094
1000	0.00087
2000	0.00050
4000	0.00028

Project WND-POWR.03.02.00-00-1043/16

International interdisciplinary PhD Studies in Materials Science with English as the language of instruction

Project co-financed by the European Union within the European Social Funds



Optical microscopy - Resolution

$$r = \frac{0.61\lambda}{\mu \sin \alpha}$$

r – resolution – the closest spacing of two points which can clearly be seen through the microscope

λ – is the wavelength of the light

μ – is the refractive index of the medium between the object and the objective lens

α – divergence angle

In order to obtain the best resolution (i.e. the smallest r) we decrease λ or increase μ and α

Project WND-POWR.03.02.00-00-1043/16

International interdisciplinary PhD Studies in Materials Science with English as the language of instruction

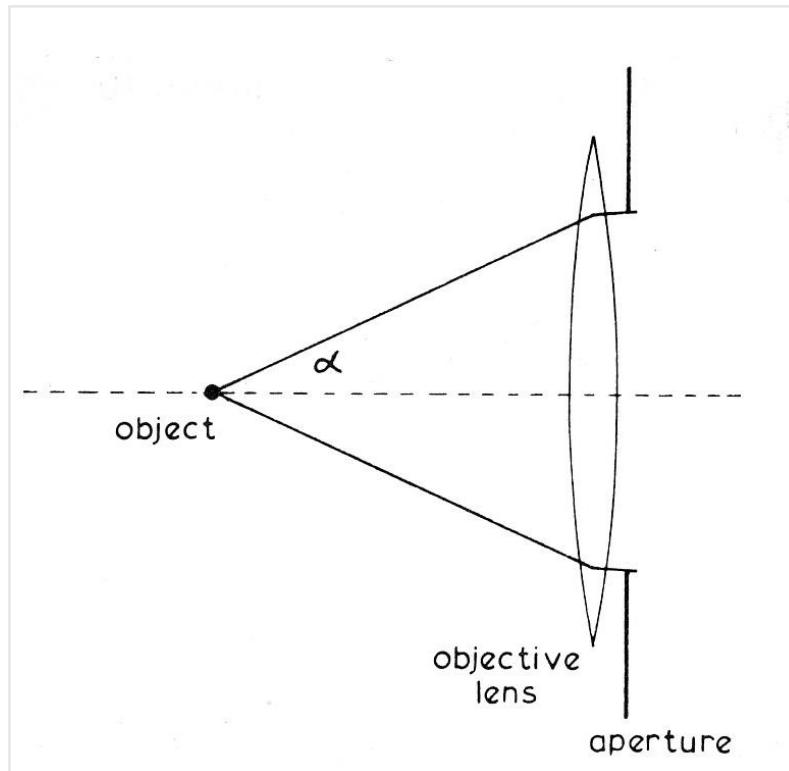
Project co-financed by the European Union within the European Social Funds



**With a light microscope λ can be decreased to 400 nm by using green light
(or to 200 nm when use ultraviolet light)**

μ – can be increased by using oil immersion objective lens

$\sin \alpha$ – can be increased towards 1 by using as large an aperture as possible



**However it is impractical to make
 $\mu \sin \alpha$ much greater than about 1.6
since $\sin \alpha$ must be less than unity,
and even very exotic materials are
limited to a refractive index of about
1.7**

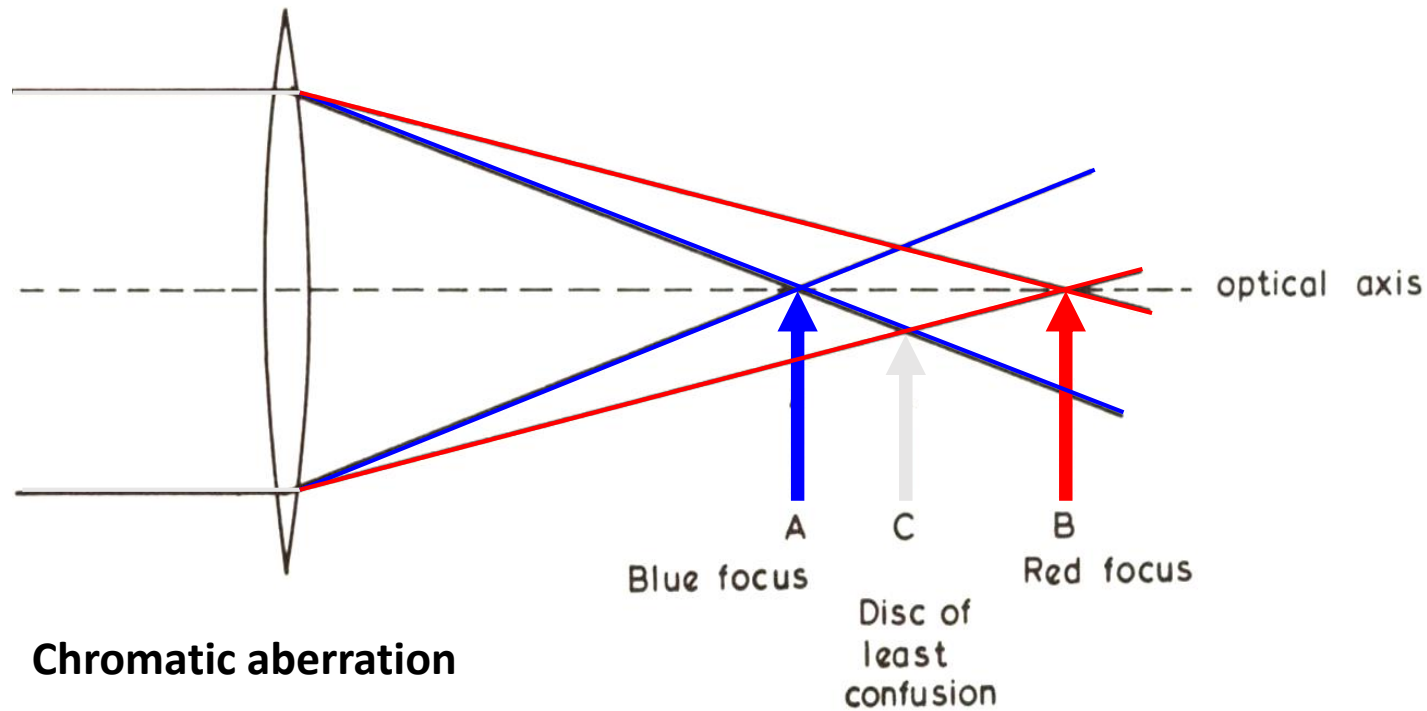
**The absolute resolution limit using
green light is therefore about 150
nm (0.15 μ m)**



Optical microscopy	Electron microscopy
$\lambda = 400 - 700 \text{ nm}$	$\lambda = 0.0005 - 0.01 \text{ nm}$
$r = \frac{0.61\lambda}{\mu \sin\alpha}$	$r_1 = \frac{0.61\lambda}{\alpha}$
$\mu \geq 1$	$\mu = 1$ (vacuum)
max. $r = 150 \text{ nm}$	for $\lambda = 0.0037 \text{ nm}$ and $\alpha = 0.1$ radians $r = 0.02 \text{ nm} = 0.2 \text{ \AA}(!?)$ Theoretically, because spherical aberration exists



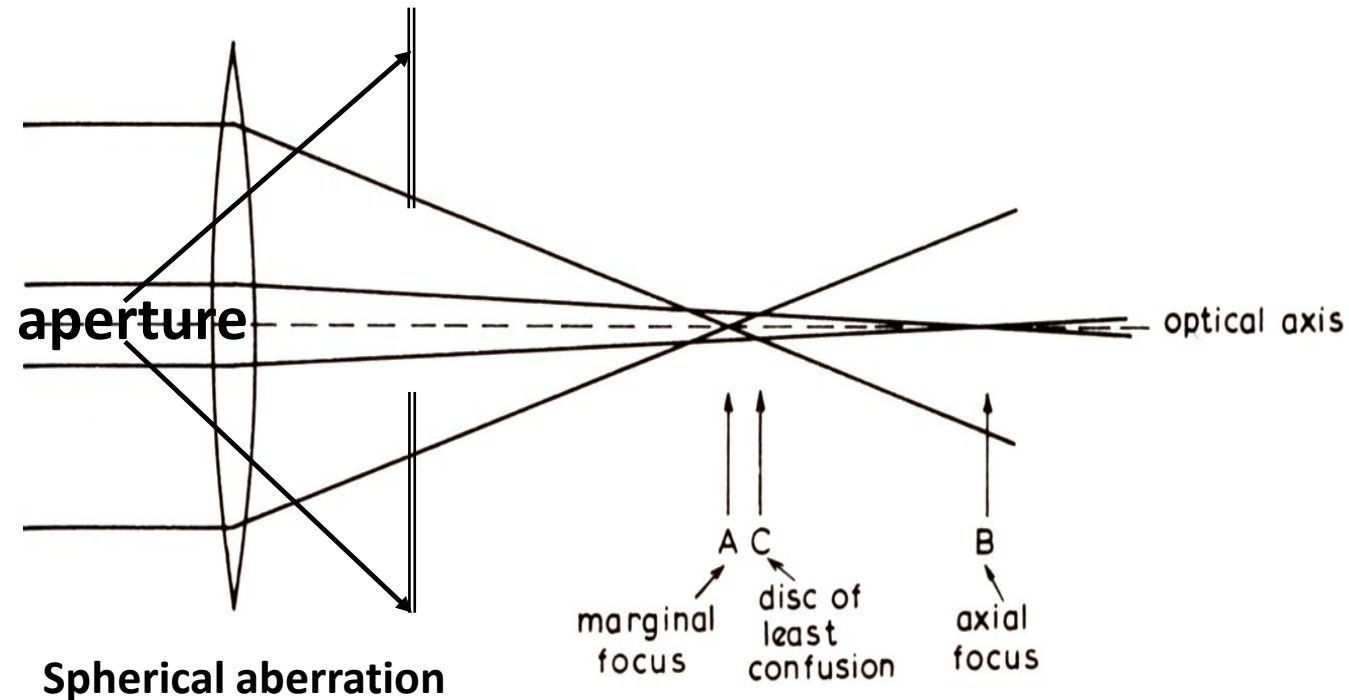
Aberrations in optical system



Ray diagram illustrating the introduction of chromatic aberration by a single lens. Light of shorter wavelength (blue) is brought to a focus nearer the lens than the longer wavelength (red) light. The smallest „focused” spot is the disc of least confusion.

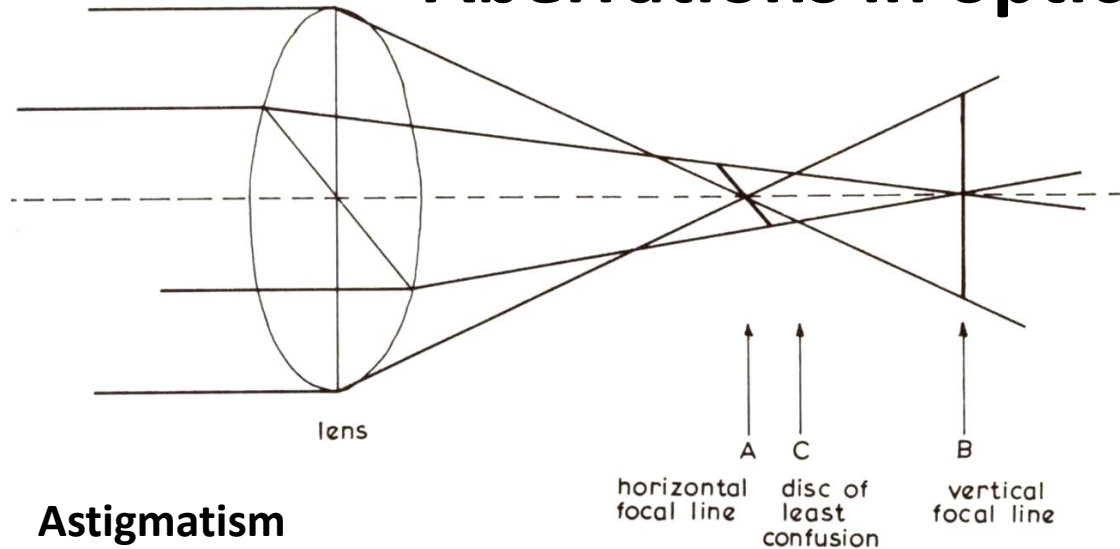


Aberrations in optical system



**Ray diagram illustrating spherical aberration by a single lens.
Marginal rays are brought to focus nearer the lens than near axis rays.
The smallest „focused” spot is the disc of least confusion.**

Aberrations in optical system

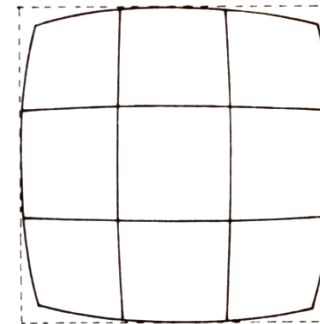


Astigmatism

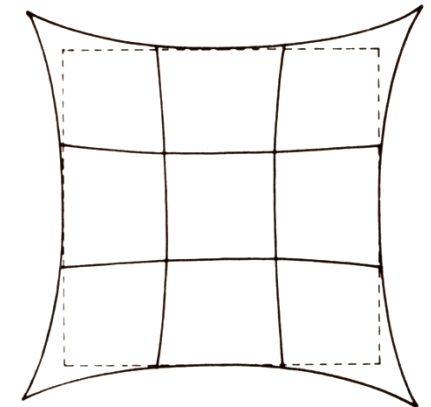
Ray diagram illustrating the formation of astigmatism for a lens with slightly different optical properties in the horizontal and vertical direction.

Here, the lens is more powerful in the vertical grid

The appearance of square grid in the presence of:



(a)
Barrel distortion



(b)
Pincusssion distortion



Chromatic aberration easily removed
Spherical aberration difficulty removed
Solution: electron beam near the electron optical
axis (use apertures of small diameters)

$$\mathbf{r}_2 = \mathbf{c}_s \alpha^3$$

C_s – spherical aberration coefficient

$$\mathbf{r}_{\text{optimum}} = \sqrt{\mathbf{r}_1^2 + \mathbf{r}_2^2}$$

$$\mathbf{r}_{\text{optimum}} = \sqrt{\left(0.61 \frac{\lambda}{\alpha}\right)^2 + \left(\mathbf{c}_s \alpha^3\right)^2}$$

Hawkes (1972)



$$\alpha_{\text{optimum}} = 0.77\lambda^{1/4} c_s^{-1/4}$$

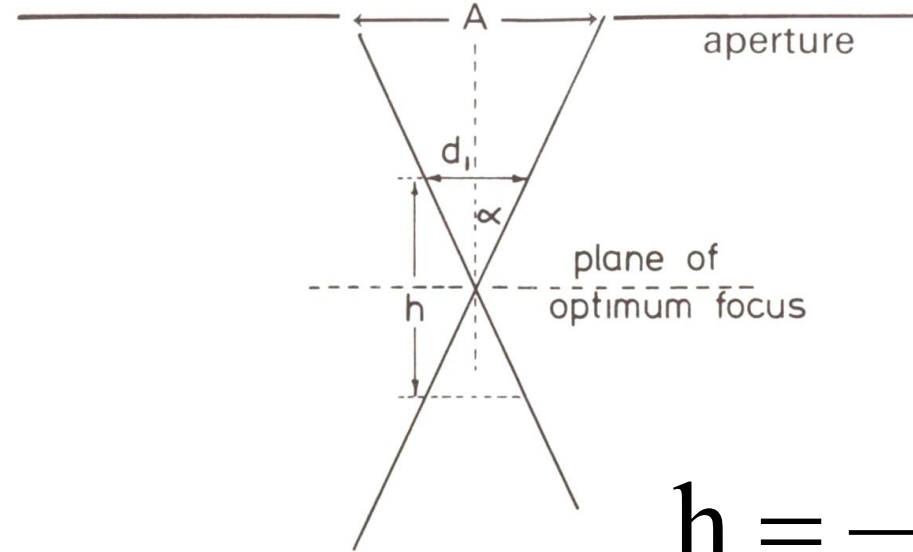
For 100 keV ($\lambda=0.0037$ nm) and $c_s=3$ mm $\rightarrow \alpha_{\text{opt}} \approx 15$ mrad = 0.86°

$$r_{\text{optimum}} = 0.91\lambda^{3/4} c_s^{1/4}$$

Ultimate point resolution TEM (HREM)
0.12 nm = 1.2 Å



Depth of Field (SEM)



$$\frac{\frac{d_1}{2}}{\frac{h}{2}} = \operatorname{tg} \alpha$$

$$\frac{d_1}{h} = \operatorname{tg} \alpha$$

$$h = \frac{d_1}{\operatorname{tg} \alpha}$$

$$d_1 = r_1 = \frac{0.61\lambda}{\mu \sin \alpha}$$

$$h = \frac{0.61\lambda}{\mu \sin \alpha \operatorname{tg} \alpha}$$

For optical microscopy:

For $\alpha = 45^\circ$ resolution the same as the depth of field

However, for a divergence angle $\alpha = 5^\circ$ resolution is $d = 5 \mu\text{m}$ and depth of focus is equal $h = 40 \mu\text{m}$!



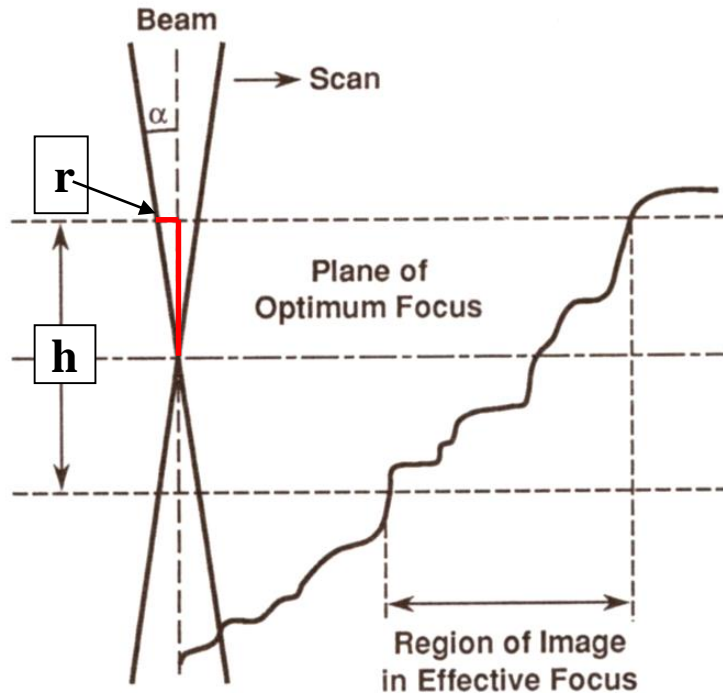
$$\mathbf{h} = \frac{\mathbf{0.61\lambda}}{\alpha^2}$$

**Strong dependence of depth of
field from divergence angle!**

Theoretical dependence



Depth of Field (SEM)



Schematic illustration of depth of focus (filed) in the SEM image. Any portion of the specimen that lies within the range defined by the planes located at $\pm h/2$ from the plane of optimum focus will appear to be in focus

On a high resolution CRT display where the spot size is = 0.1 mm (100mm) most observers will find the defocusing becomes detectable when two pixels are fully overlapped, that is $r = 1$ pixel

The pixel size referred to the specimen space is given by:

$$r = \frac{0.1\text{mm}}{M}$$

where: M – is the magnification

Substituting $r = 0.1/M$ in the equation below we obtain a practical expression for depth of focus:

$$h = \frac{2r}{\alpha} = \frac{0.2\text{mm}}{\alpha M}$$



Table 4.3. Depth of Field at 10-mm Working Distance

Magnification	100- μm aperture ($\alpha = 5 \times 10^{-3}$ rad) 0.29°	200- μm aperture ($\alpha = 10^{-2}$ rad) 0.57°	600- μm aperture ($\alpha = 3 \times 10^{-2}$ rad) 1.72°
10 \times	4 mm	2 mm	670 μm
50 \times	800 μm	400 μm	133 μm
100 \times	400 μm	200 μm	67 μm
500 \times	80 μm	40 μm	13 μm
1 000 \times	40 μm	20 μm	6.7 μm
10 000 \times	4 μm	2 μm	0.67 μm
100 000 \times	0.4 μm	0.2 μm	0.067 μm

To increase the depth of focus D , the microscopist can choose two ways:

- either to reduce the magnification M
- or to reduce divergence angle α



Changing the magnification is not an option, because we choose the magnification to fill the image with the specimen feature of interest!!

Only the divergence as the adjustable parameter must be decreased to obtain greater depth of field!

The divergence is adjusted by the selection of final-beam defining aperture.

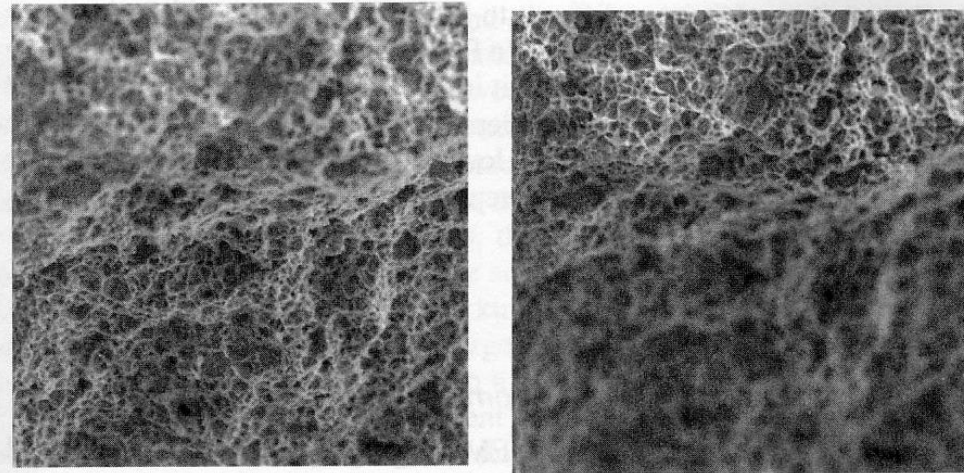
For the aperture of radius R_{Ap} located at the scan crossover in the exit of objective lens and working distance D_w , we find:

$$\alpha = \frac{R_{Ap}}{D_w}$$

Decreasing R_{Ap} and increasing D_w both increase the depth of field



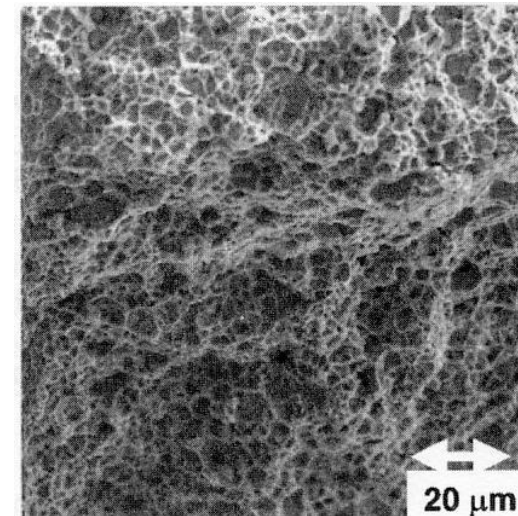
Small depth of focus; the lens weakly excited to give focus at the bottom of the field; 130 μm aperture



Small depth of focus; the lens strengthened to raise the focus by 160 μm ; 130 μm aperture

Appearance of a surface with extreme topography (metal fracture surface) with different depths of focus obtained by varying the aperture size

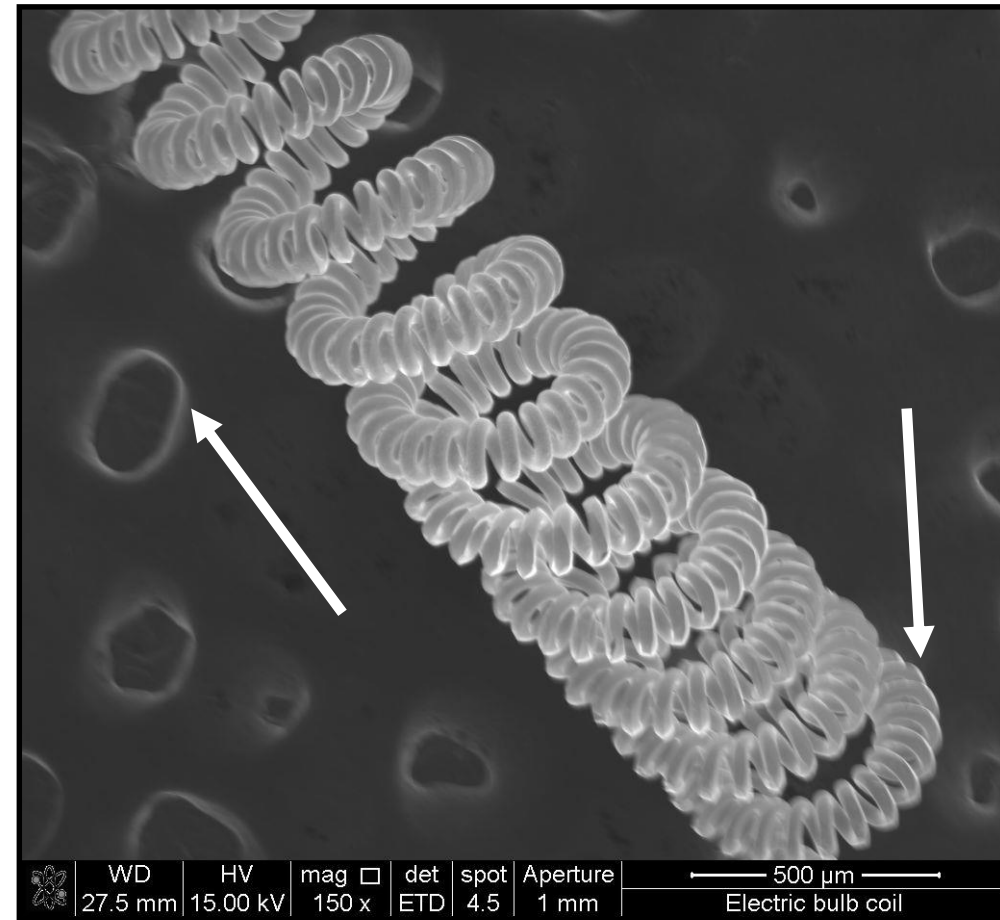
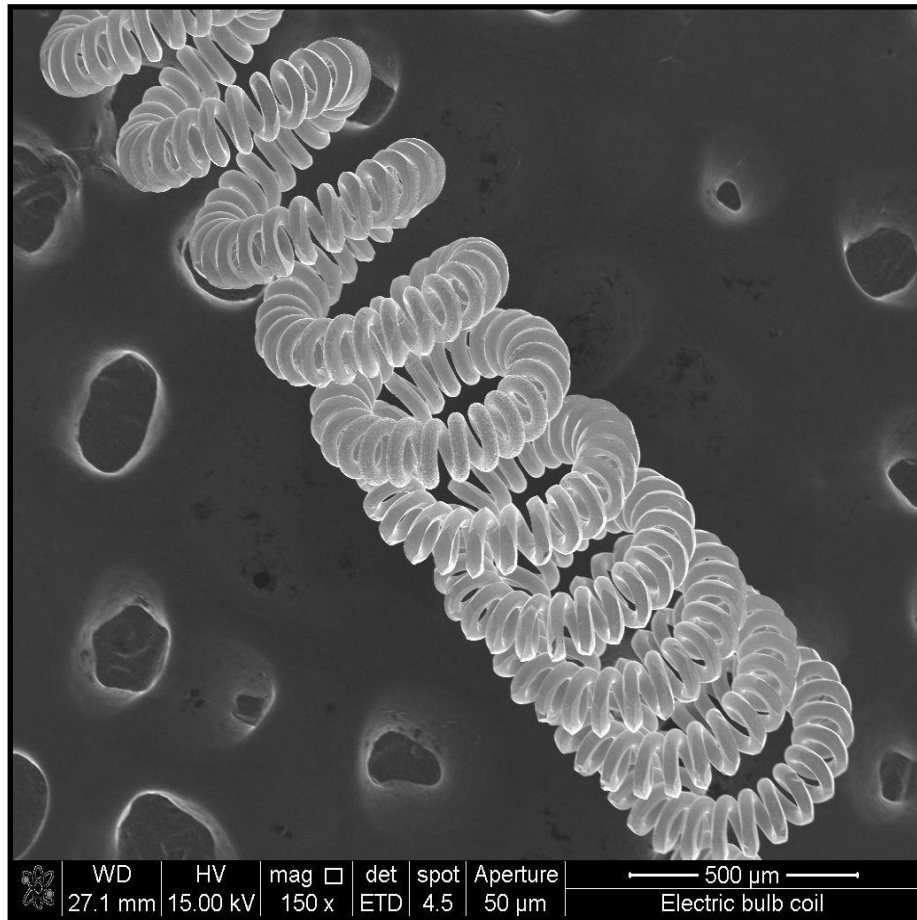
Beam energy 20 kV, 15 mm WD



Large depth of focus entire field in focus; 70 μm aperture



Depth of field



Aperture diameter 50 µm

WD ca 27 mm

Aperture diameter 1000 µm

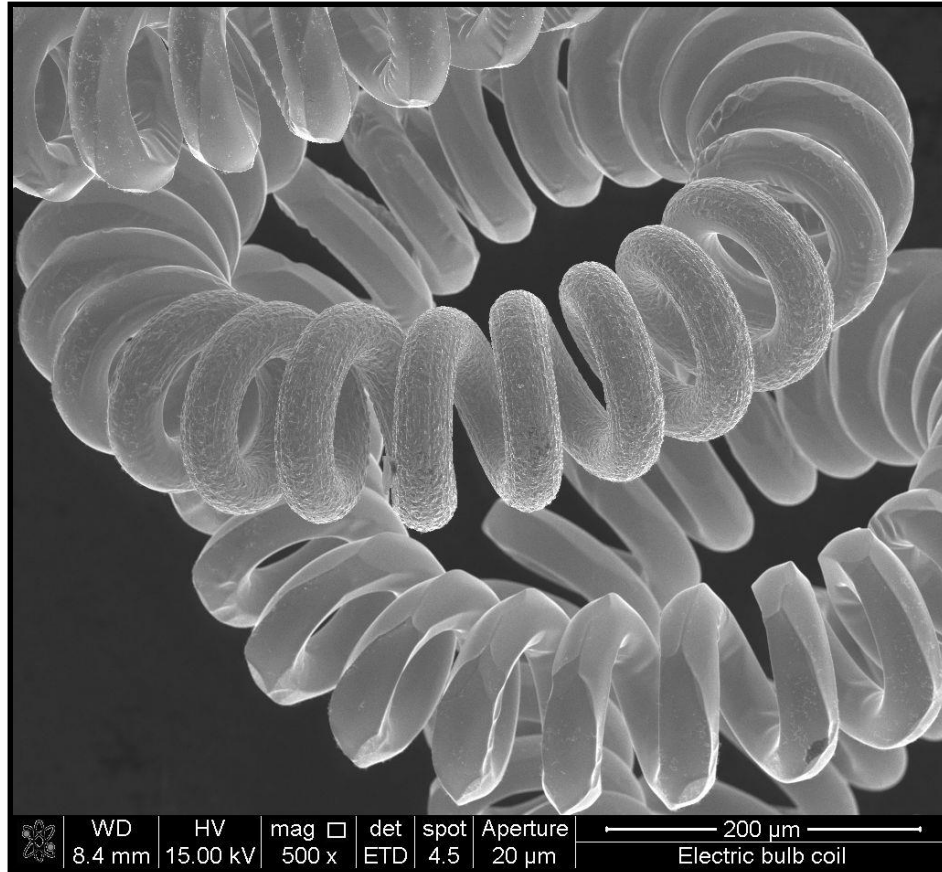
Project WND-POWR.03.02.00-00-1043/16

International interdisciplinary PhD Studies in Materials Science with English as the language of instruction

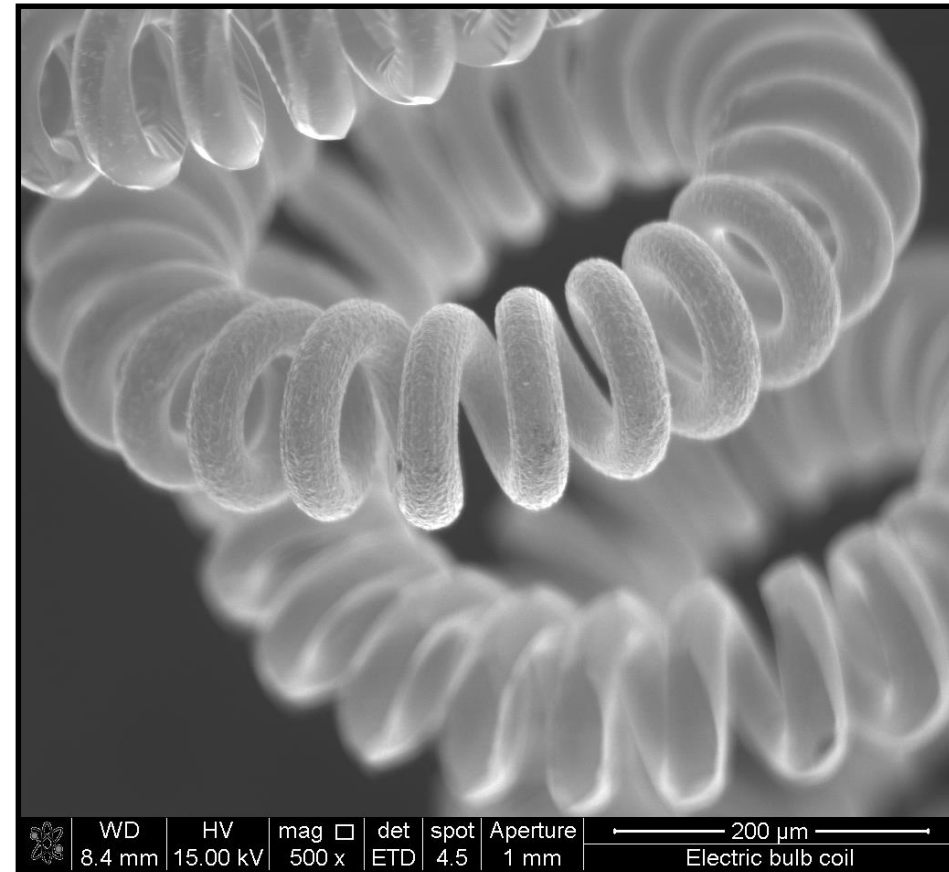
Project co-financed by the European Union within the European Social Funds



Depth of field



Aperture diameter 20 µm

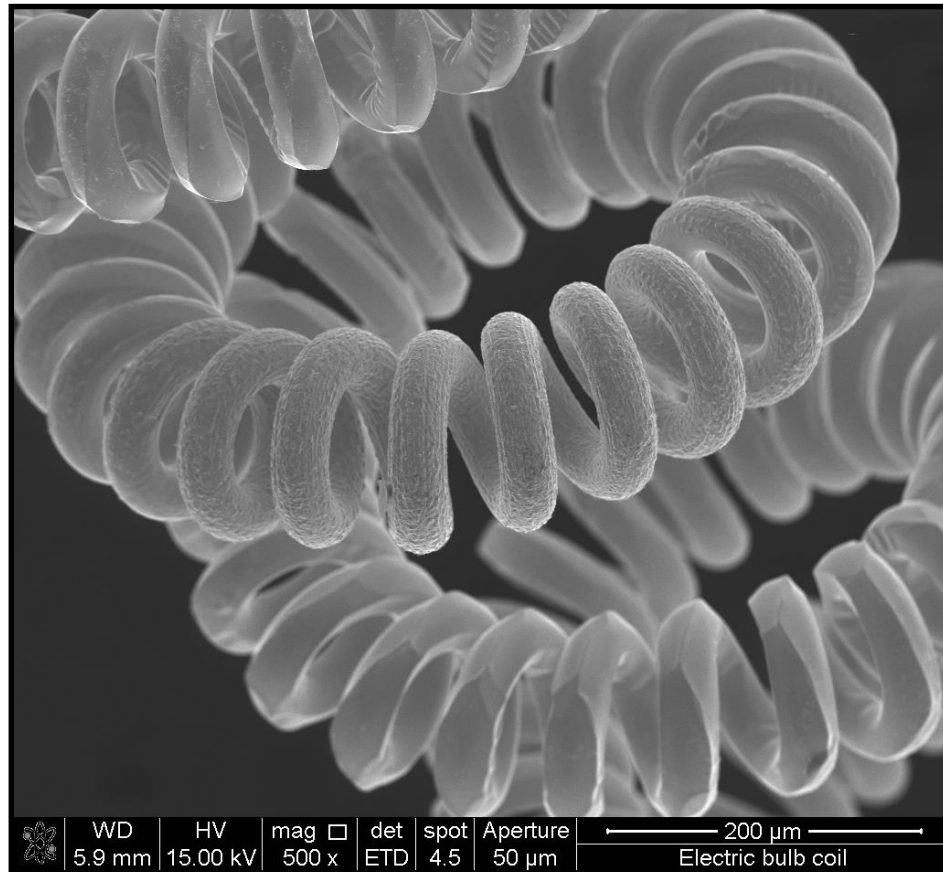


WD 8.4 mm

Aperture diameter 1000 µm

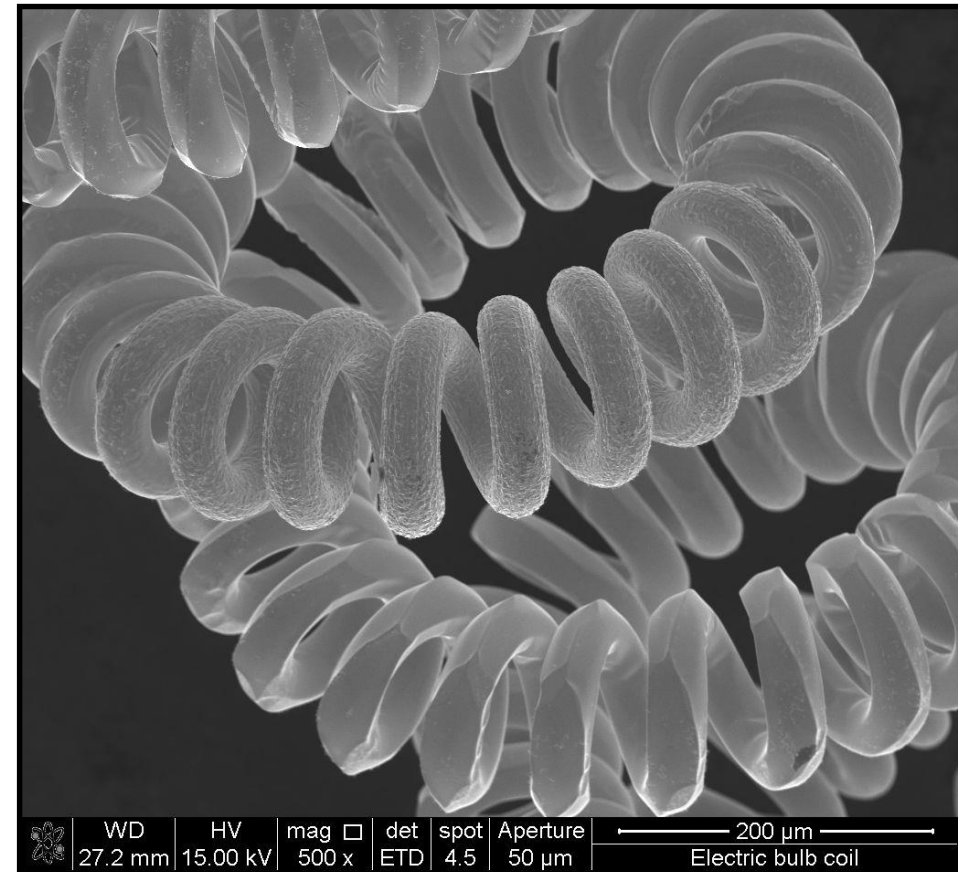


Depth of field



WD 5.9 mm

Aperture diameter 50 μm



WD 27.2 mm

The higher WD, the lower divergence angle and, consequently, the increased depth of field.

Project WND-POWR.03.02.00-00-1043/16

International interdisciplinary PhD Studies in Materials Science with English as the language of instruction

Project co-financed by the European Union within the European Social Funds

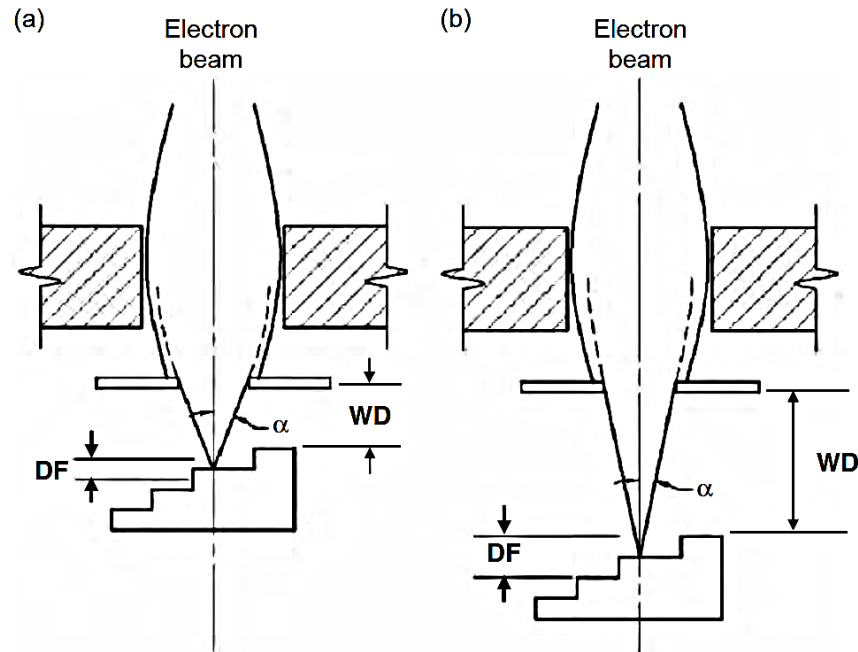


FIGURE 1.19. Beam diagram showing enhancement of depth of field (DF) by increasing working distance (WD). (a) Short working distance and (b) long working distance.

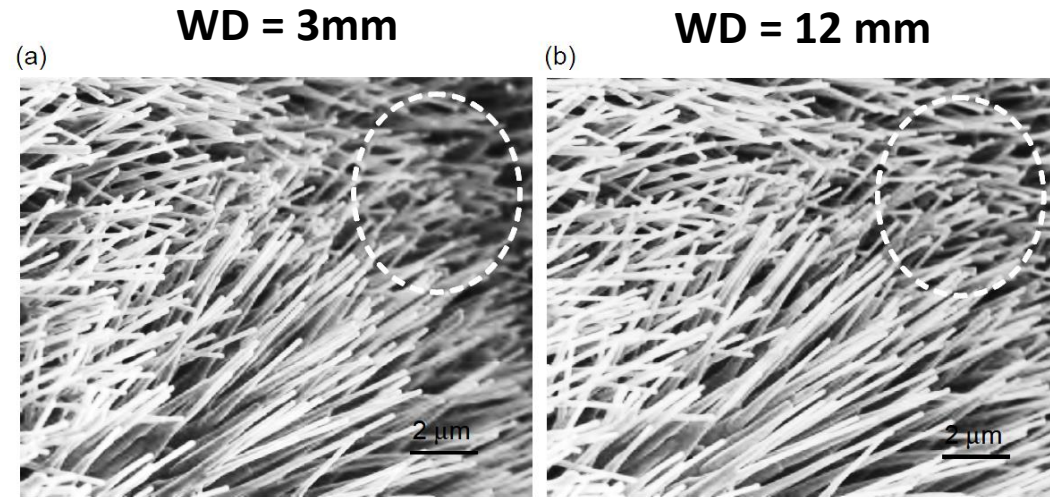
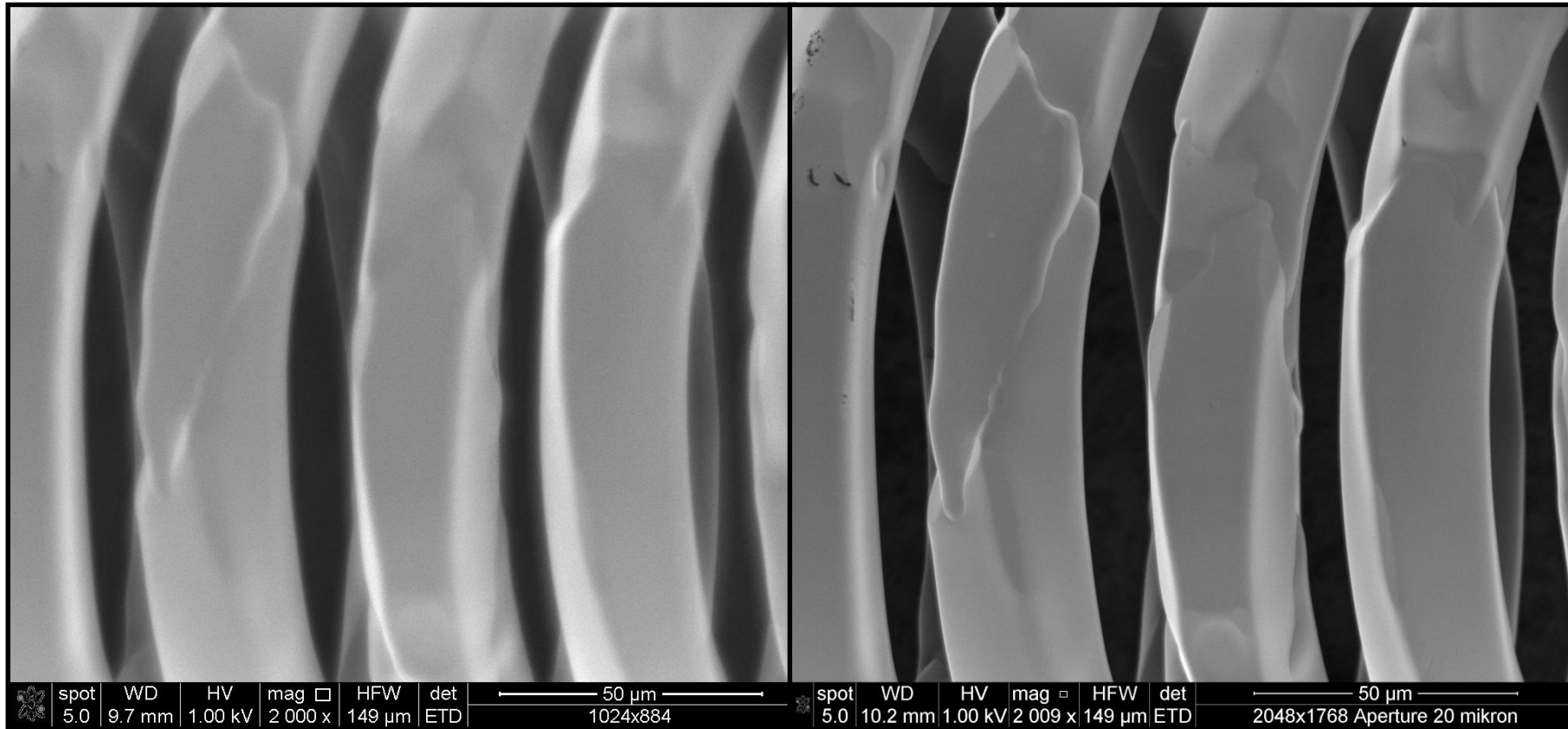


FIGURE 1.20. Well aligned Co-doped ZnO nanowires array fabricated by chemical vapor deposition, showing the enhancement of depth of field by increasing the working distance from (a) 3 mm to (b) 12 mm, which is emphasized by circles.



Image resolution and aperture diameter



spot	WD	HV	mag	HFV	det	50 µm
5.0	9.7 mm	1.00 kV	2 000 x	149 µm	ETD	1024x884

WD 9.7 mm

HV 1 kV

1024x884

Aperture diameter 50 µm

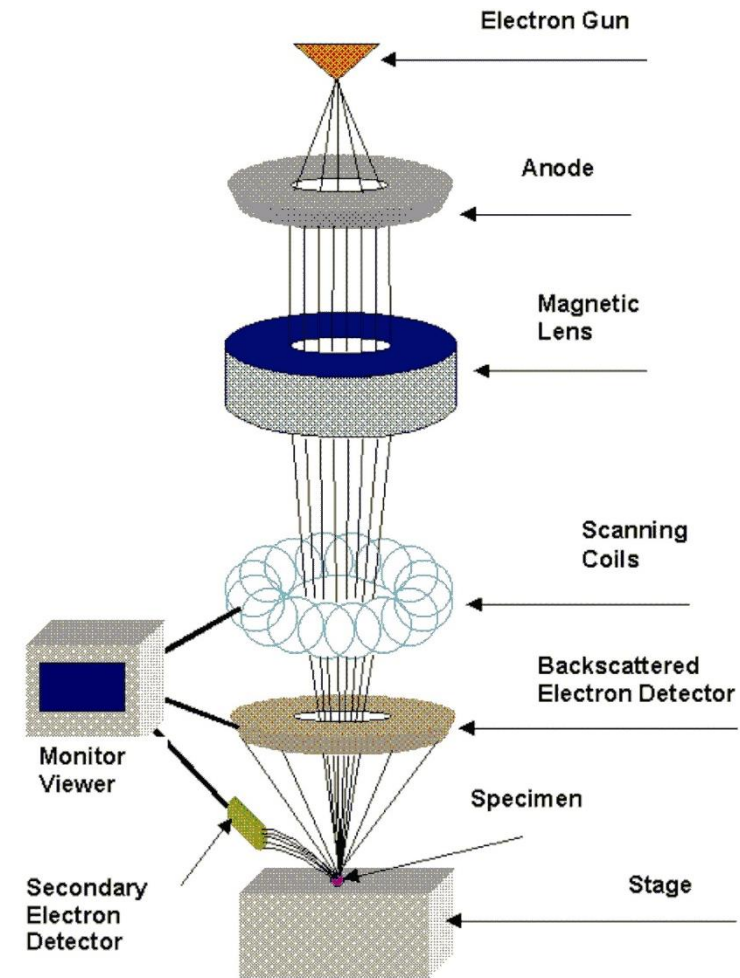
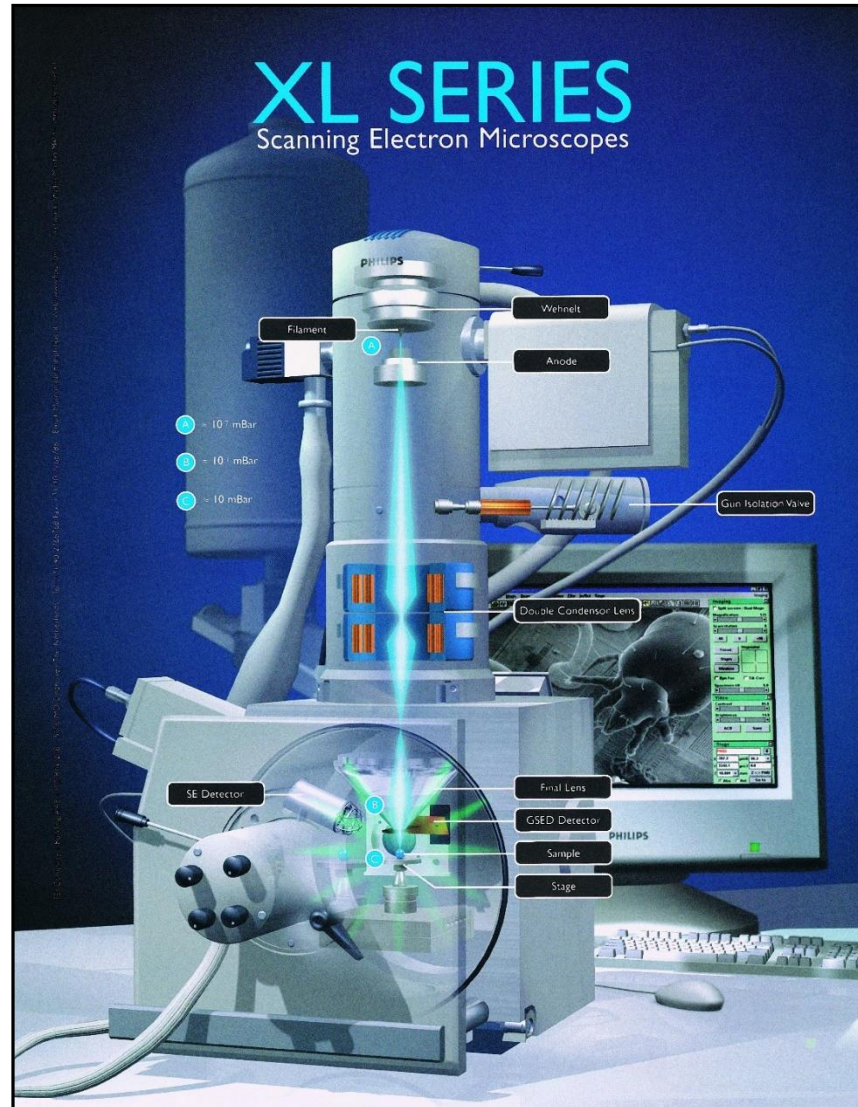
spot	WD	HV	mag	HFV	det	50 µm
5.0	10.2 mm	1.00 kV	2 009 x	149 µm	ETD	2048x1768 Aperture 20 mikron

WD 10.2 mm

HV 1 kV

2048x1768

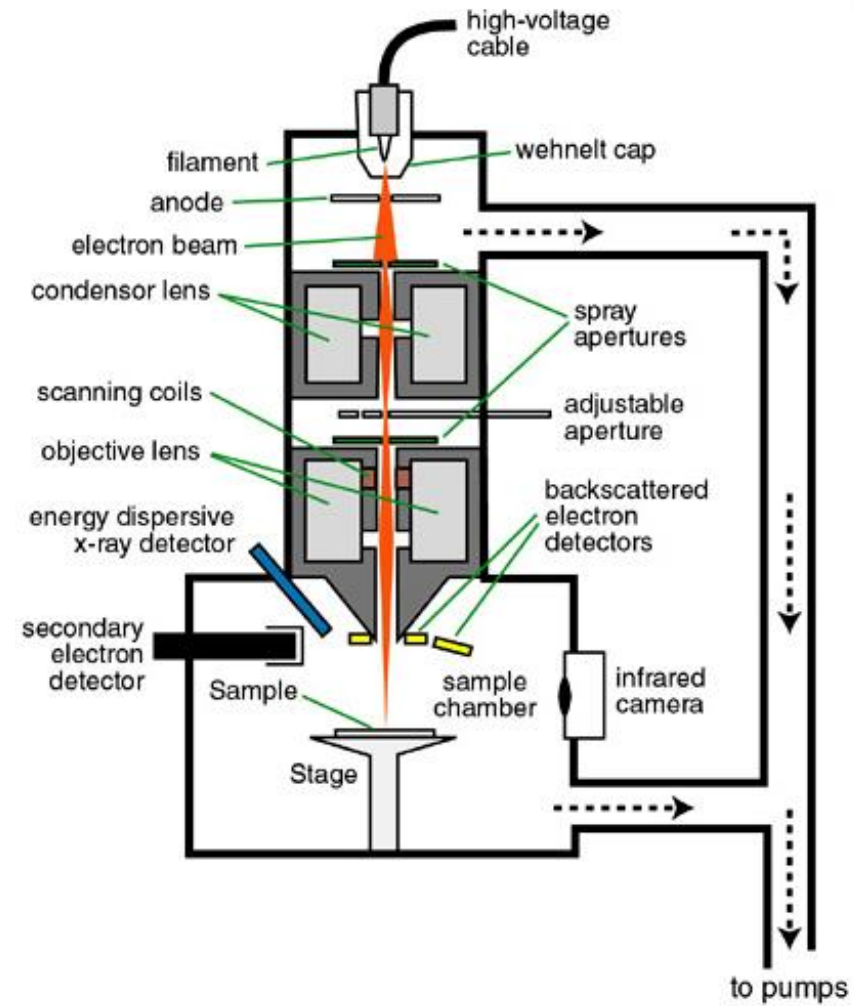
Aperture diameter 20 µm



Project WND-POWR.03.02.00-00-1043/16

International interdisciplinary PhD Studies in Materials Science with English as the language of instruction

Project co-financed by the European Union within the European Social Funds

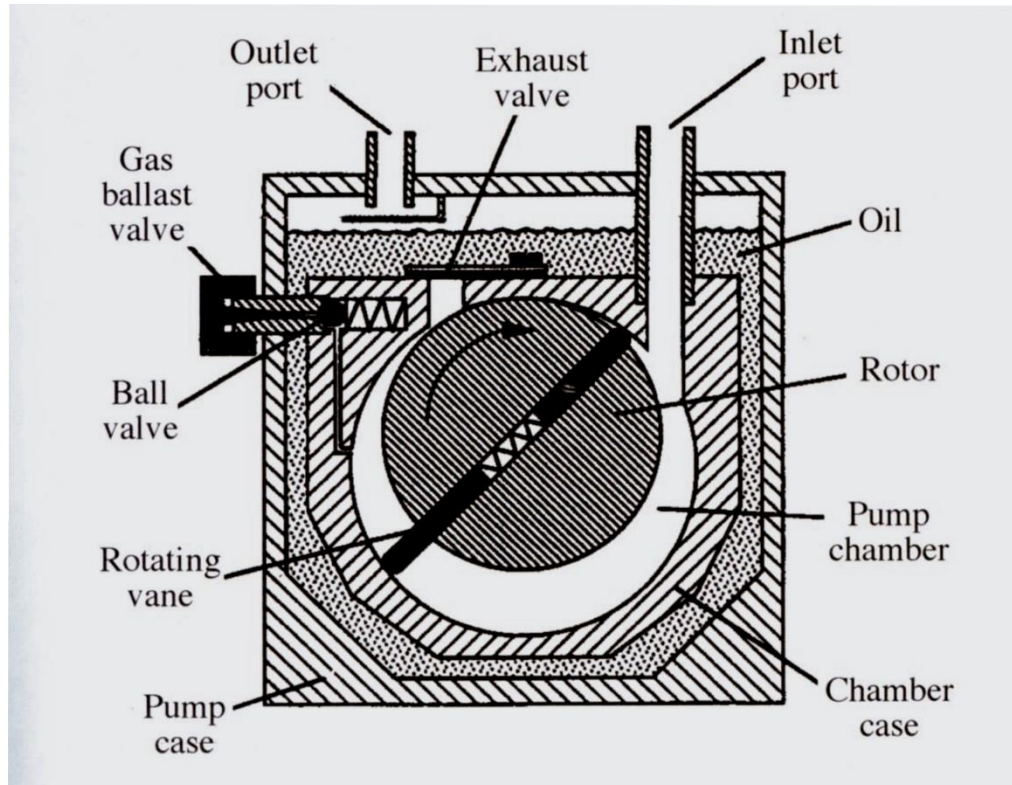




Roughing pump

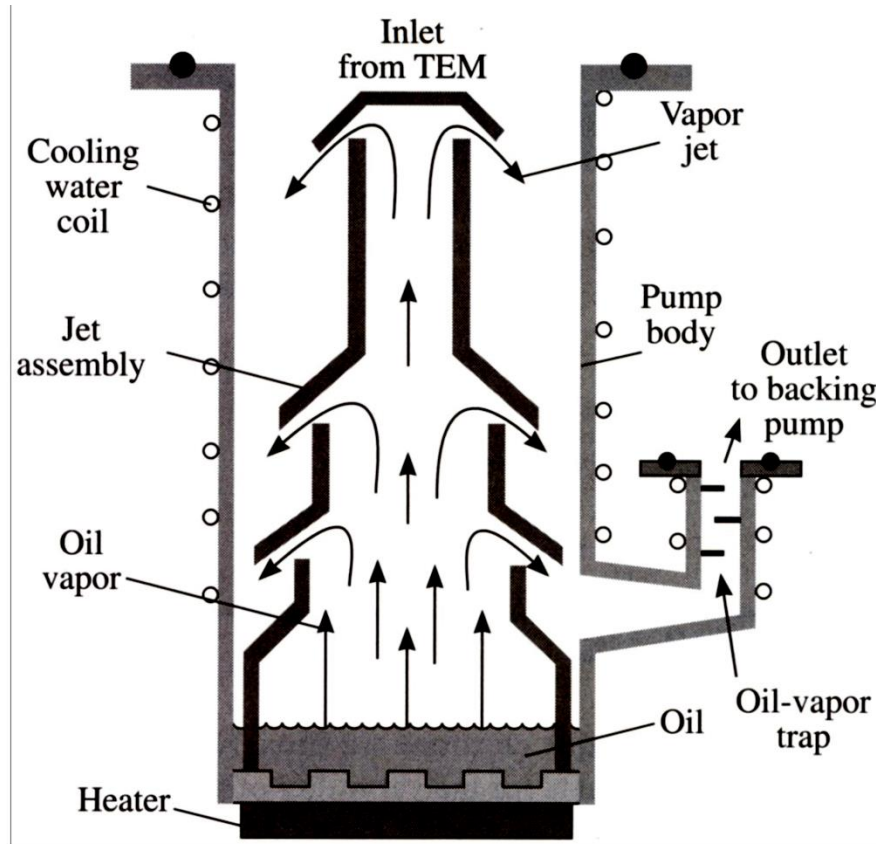
A mechanical pump for roughing vacuum

The eccentric motion of the pump creates a vacuum in the RH side when it rotates and the vacuum sucks air into the inlet valve. As a cylinder rotates further, it cuts off the inlet and forces the air on the LH side, creating a vacuum again on the inlet side. Because the constant contact between the rotating cylinder and the inside of the pump oil is needed to reduce frictional heating.





Diffusion pump

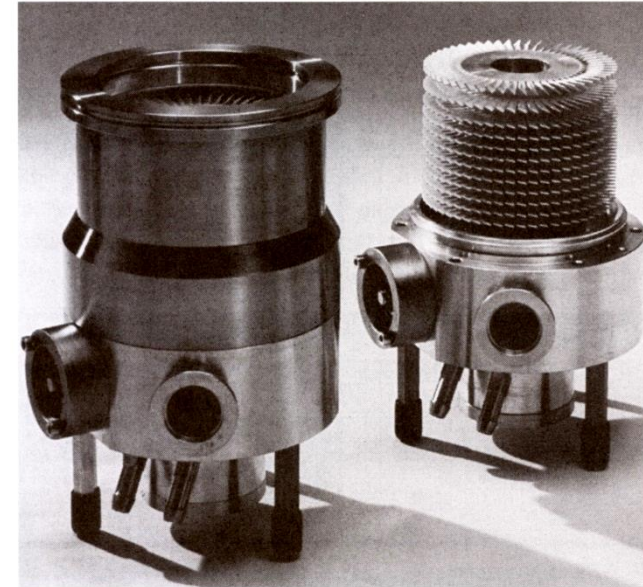
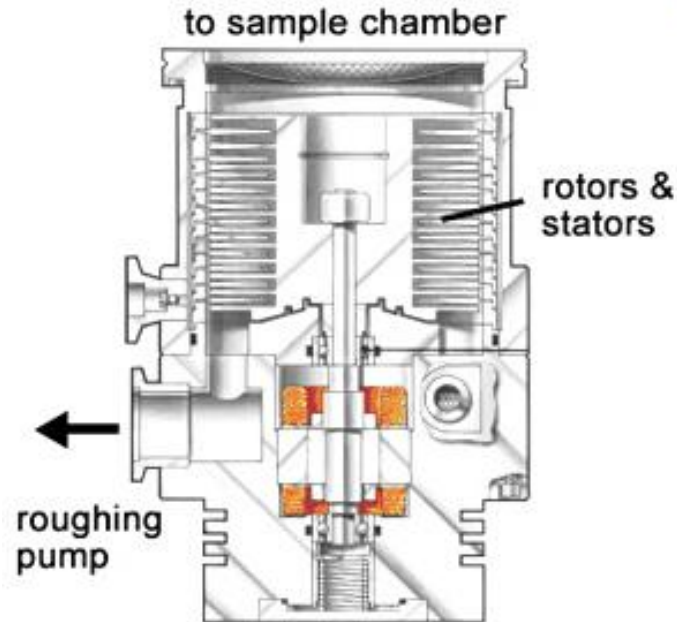


Principles of diffusion pump operation.

A heater plate at the base of the pump boils a synthetic oil. The expansion of oil vapor on boiling creates a pressure, which forces the vapor up the central column and out of several holes. The stream of oil vapor pulls gas molecules out of the top of the pump down to the base, where the oil condenses and the air is pumped out of the base by a mechanical backing pump.



Turbomolecular pump



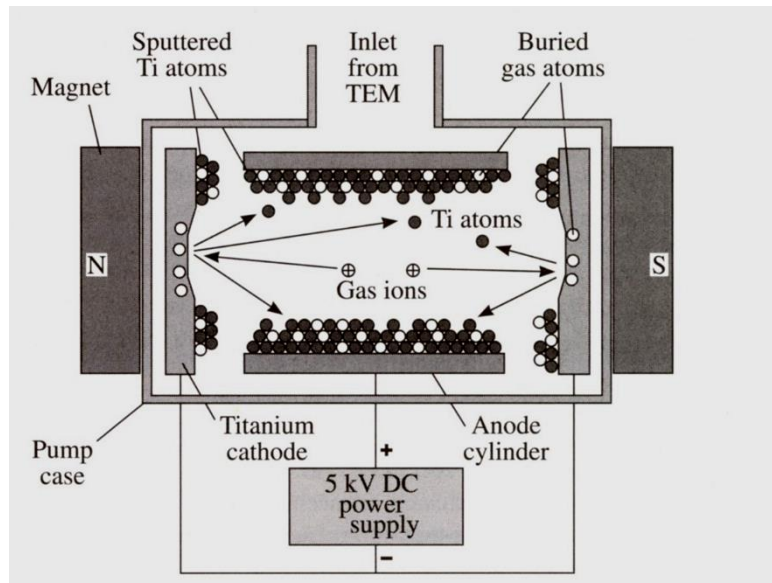
A turbopump is nothing more than a small turbine that rotates at high speed. Like a jet turbine it pulls air in at the front end and forces it out of the back. The blades are designed like airfoils to enhance the flow of the gas through the system



Mechanical, diffusion and turbopumps are all exhausted pumps

They pull in air from one end and expel it from the other

Ion pump



Schematic diagram showing how ion pump traps ionized gas atoms by layer of Ti atom as electrodes.

Once trapped, the ions cannot escape until the pumps is turned off

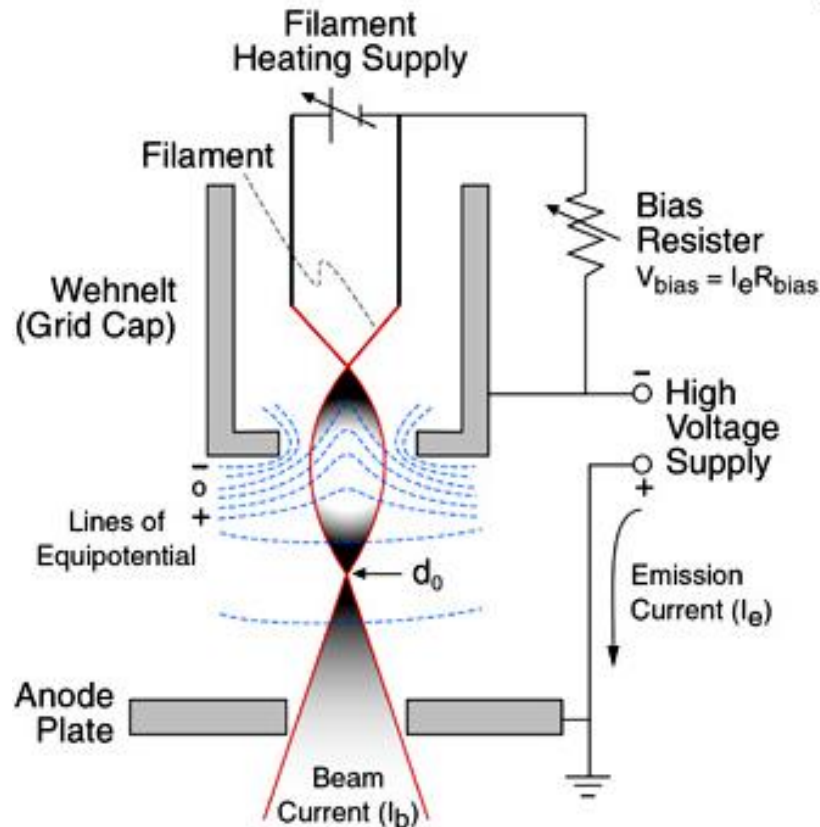


Electron Guns (SEM & TEM)

- **Tungsten Hairpin Electron Gun**
- **Lanthanum Hexaboride LaB_6 Electron Gun**
- **Field Emission Guns**
 - **Cold Field Emission**
 - **Thermal Field Emission (Schottky Field Emission)**



Tungsten hairpin electron gun



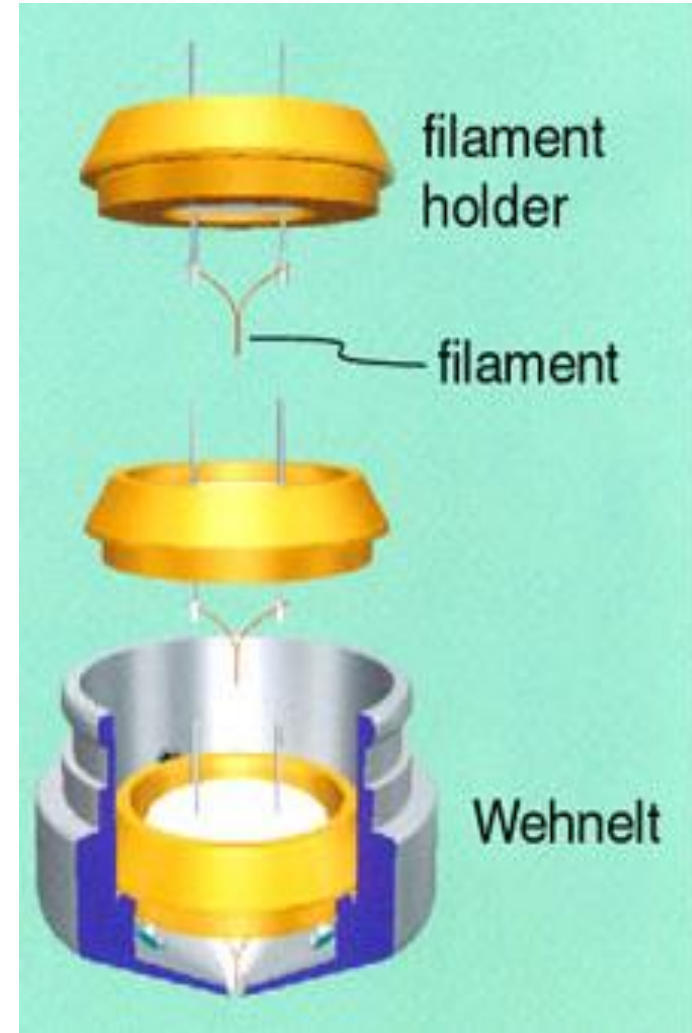
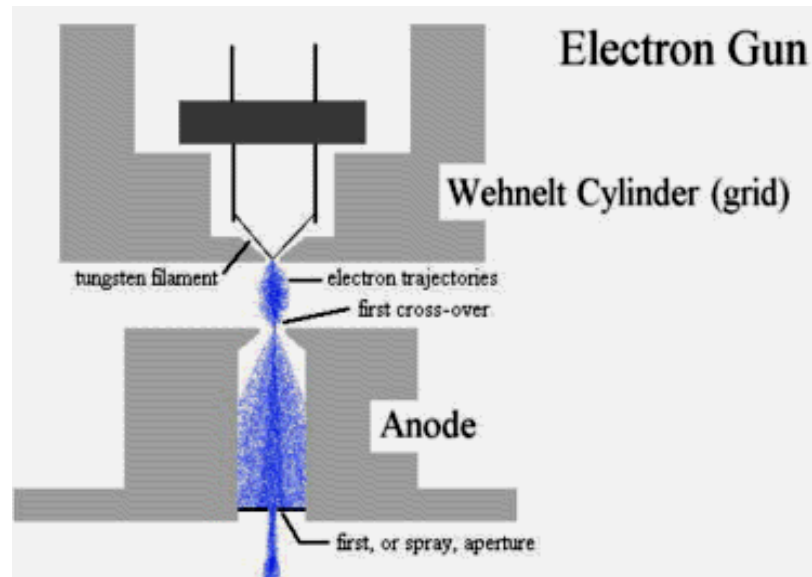
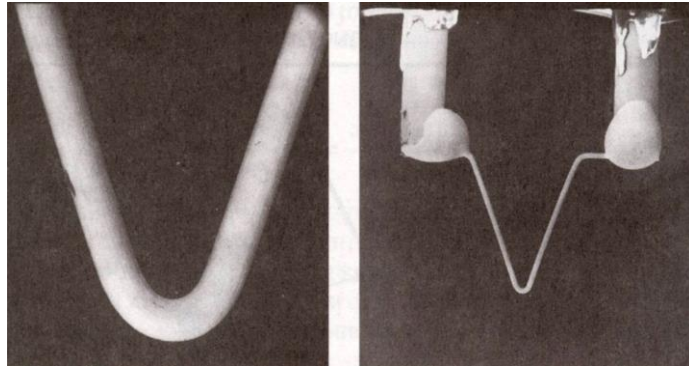
The most common filament is the Tungsten hairpin gun. This filament is a loop of tungsten which functions as the cathode. A voltage is applied to the loop, causing it to heat up. The anode, which is positive with respect to the filament, forms powerful attractive forces for electrons. This causes electrons to accelerate toward the anode.

melting temperature for tungsten: 3653 K, W - work function $\phi = 4.5 \text{ eV}$,
 $d_0 = 50 \text{ }\mu\text{m}$ (cross-over)

Work function of the material is the energy barrier than must be exceeded for electrons to escape into the vacuum

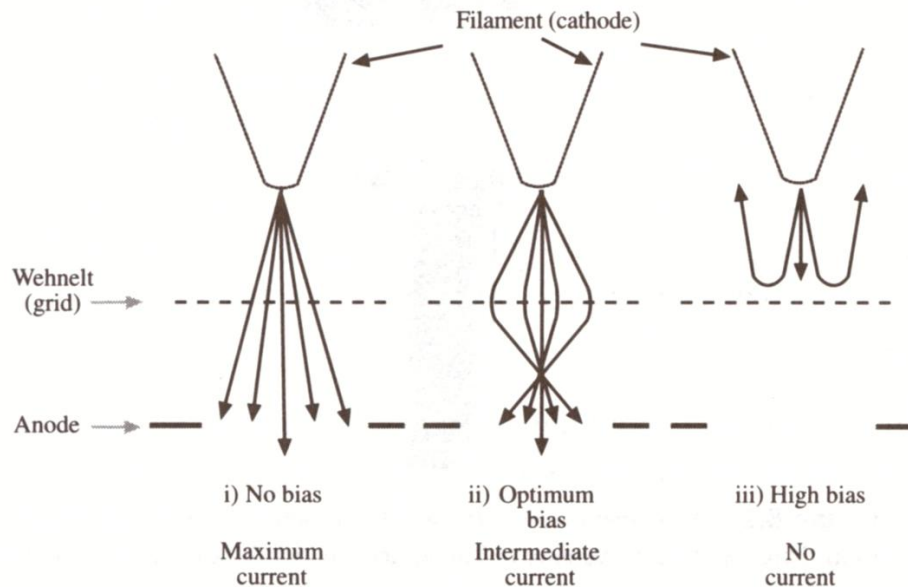


Tungsten hairpin electron gun

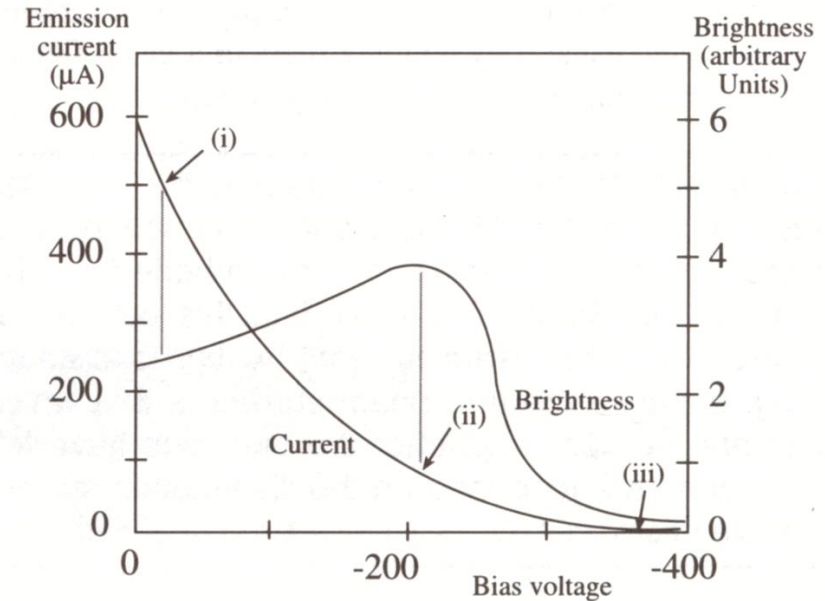




Grid cap (Wehnelt cylinder)



The effect of increasing Wehnelt bias (i-iii) on the distribution of electrons coming through the anode



The relationship between the biasd and the emission current/gun brightness. Maximum brightness is achieved at an intermediate Wehnelt bias and an intermediate emission current condition (ii)



$$\beta = \frac{\text{current}}{\text{area} \cdot \text{solid angle}} \frac{i_p}{\left(\frac{\Pi d^2}{4}\right) \Pi \alpha^2} = \frac{4i_p}{\Pi^2 d \alpha^2}$$

β – brightness

i – beam current

d – cross sectional area of the beam

α – angular spread of electrons at various points in the column

$$\beta = 2 \times 10^5 T V \exp\left(-\frac{\Phi}{kT}\right) \left[\frac{\text{A}}{\text{m}^2 \text{srkV}}\right]$$

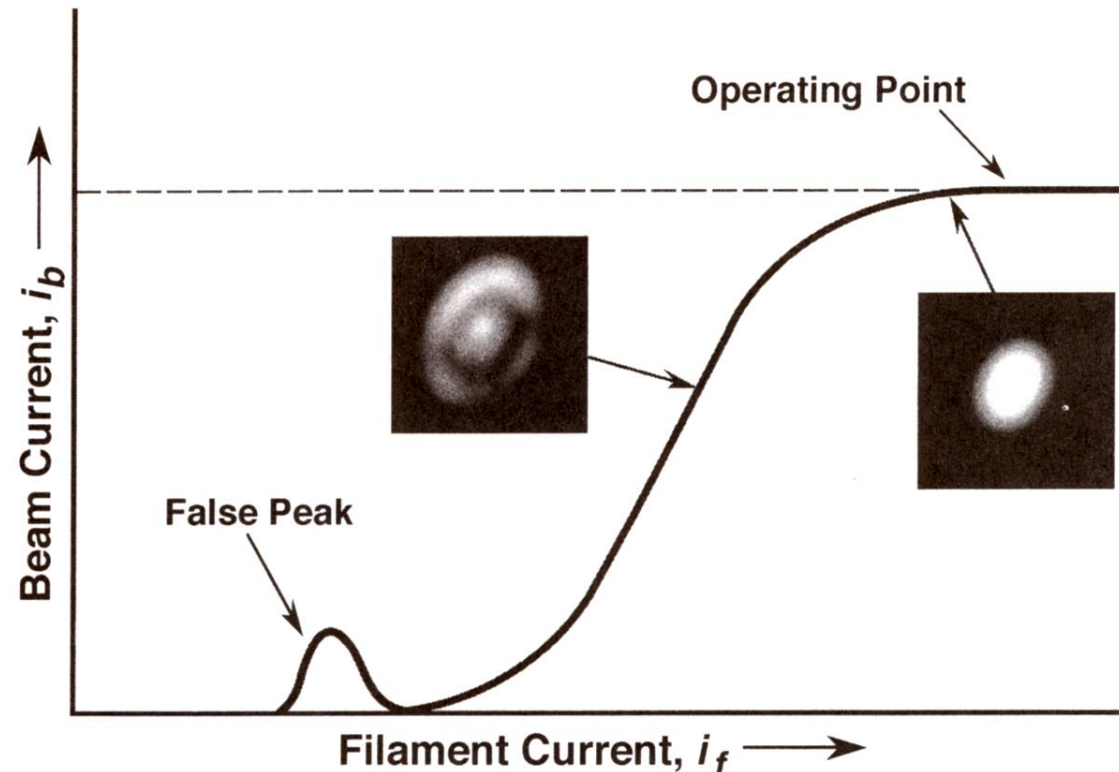
T – temp [K],

V – accelerating voltage

Φ – work function [eV]

$\beta \uparrow T \uparrow$ (we can not heat the filament without consequences)

$\beta \uparrow \Phi \downarrow !!!$



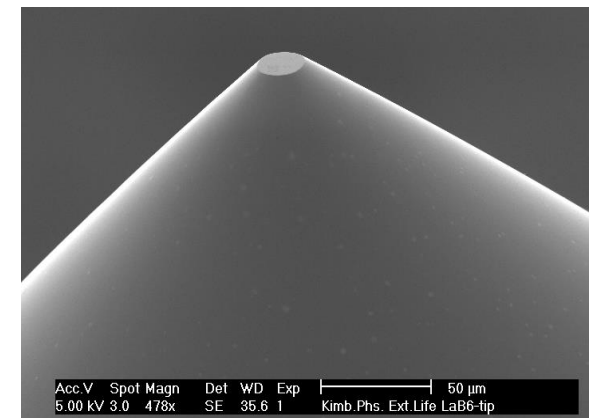
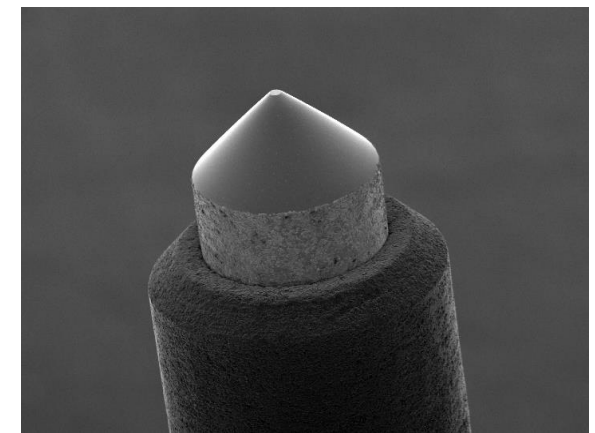
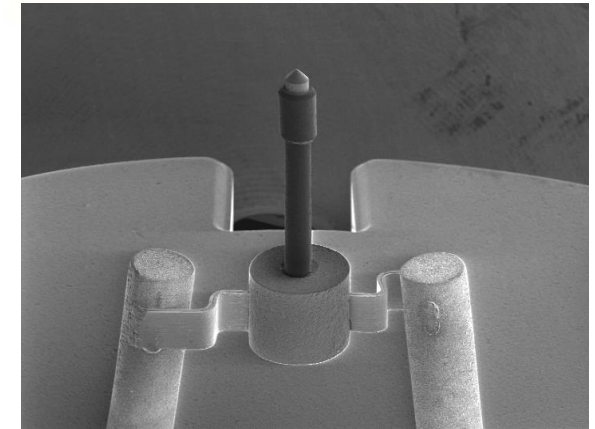
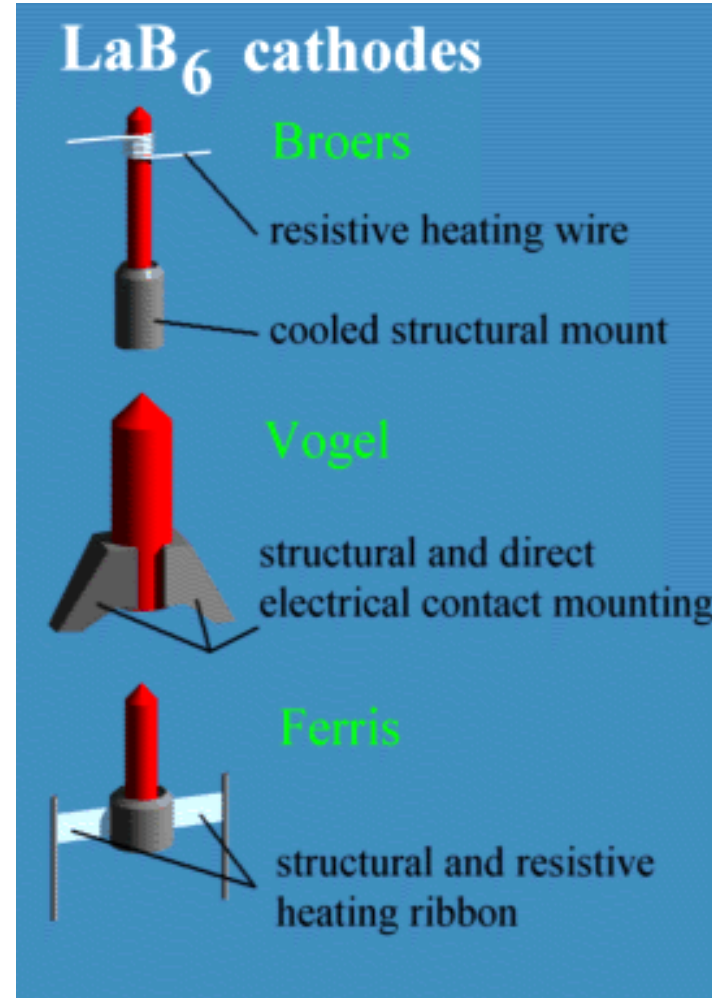
Saturation of a tungsten hairpin electron gun.

At low filament heating some electrons are emitted into various directions from the undersaturated filament (*left filament image*). At higher filament heating, near saturation, electrons are concentrated into a tight bundle (*right filament image*). Further filament heating provides little increase in beam current. The gun should be operated just at the saturation point.



Lanthanum Hexaboride (LaB_6)
electron guns provide 5-10 times greater
brightness and longer life time compared to
tungsten

LaB_6 work function $\phi =$
3.0 eV
 $\beta_{\text{LaB}_6} \approx 10 \beta_{\text{W}}$
 $d_o = 10 \mu\text{m}$



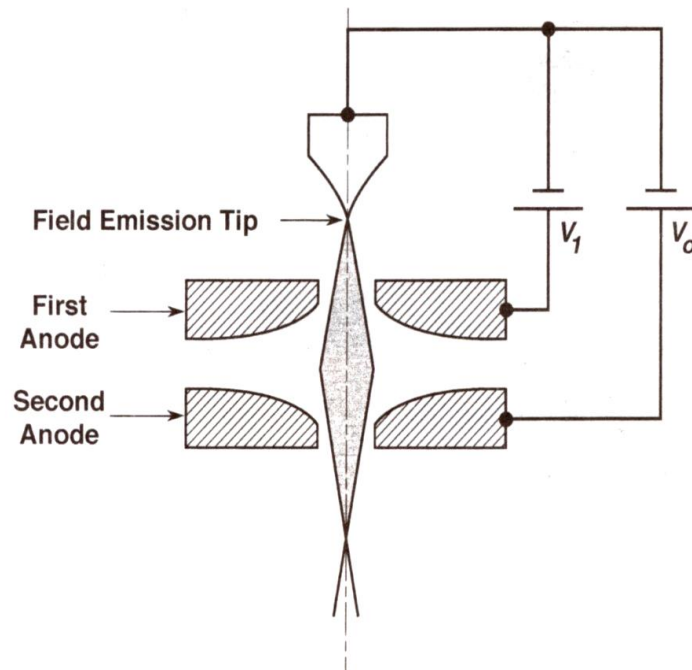


FEG (Field Emission Gun)

- **CFE (Cold Field Emission)**
- **TFE (Thermal Field Emission)**



CFE (Cold Field Emission)



Schematic diagram of the Butler triode field emission source. V_i is the extraction voltage of a few kilovolts and V_o is the accelerating voltage

Cold filed emission source requires that the cathode surface must be atomically clean

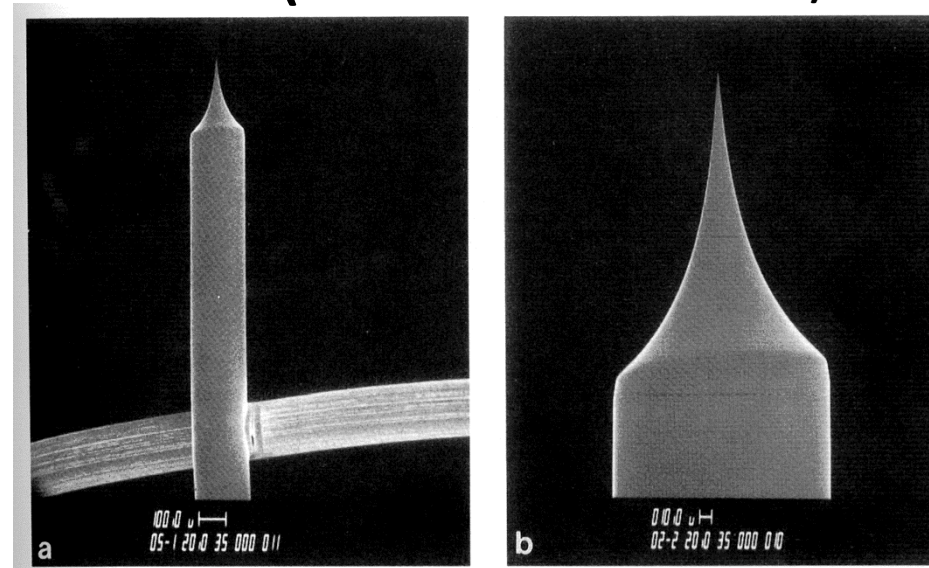
At the vacuum of 10^{-5} Pa a monolayer of the gas is deposited every second

At the vacuum of 10^{-10} Pa – a monolayer of the gas is deposited every 7 hours

Operation for sustained periods requires a vacuum level of 10^{-8} – 10^{-9} Pa



CFE (Cold Field Emission)



Cold field emission tip of (310) single crystal wire spot welded to a tungsten wire - diameter of the tip 100 nm

When a negative potential is applied to the cathode the electric field is concentrated by the tip. When the field on the tip reaches a magnitude of about 10V/nm, the potential barrier is lowered in height and also becomes so narrow the electrons can „tunnel” directly through it and leave the cathode

Tungsten is usually used as a cathode materials because it is strong enough to withstand the high mechanical stress produced on the tip by electron field

A cathode current density of as high as 10^5 A/cm² may be obtained from a field emitter as compared with about 3 A/cm² from thermionic source



CFE (Cold Field Emission)

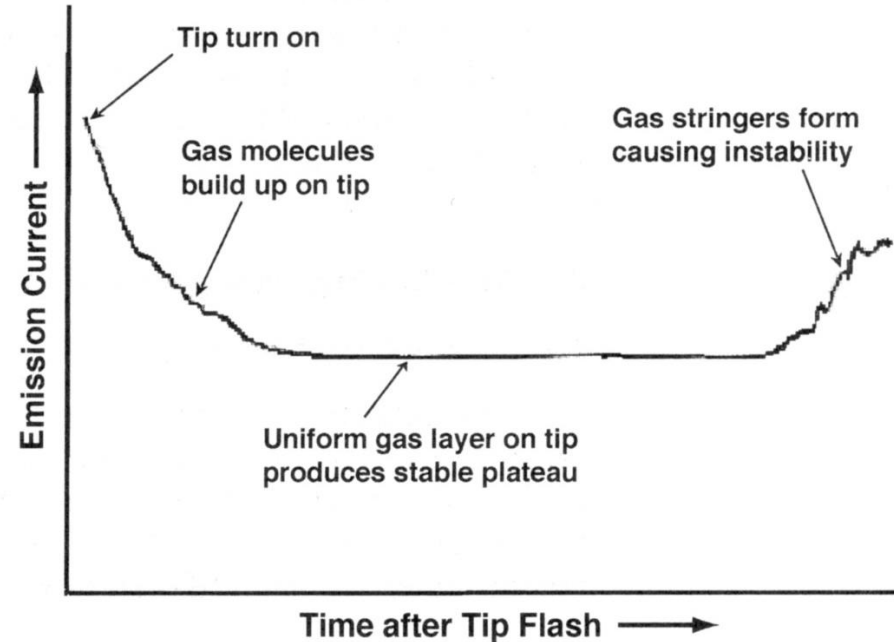
Emission current intensity versus time after a cold field emission tip has been flashed (rapidly heated) to remove absorbed gas atoms

Advantages of CFE:

1. cross-over $d_o = 2-3 \text{ nm}$
2. 2. monochromatic electron beam (0.3 eV spread)

Disadvantage of CFE:

instability (catastrophic during X-ray microanalysis)





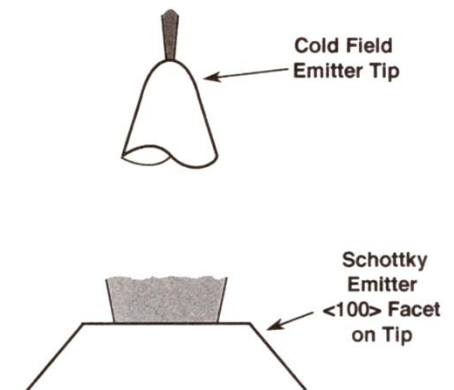
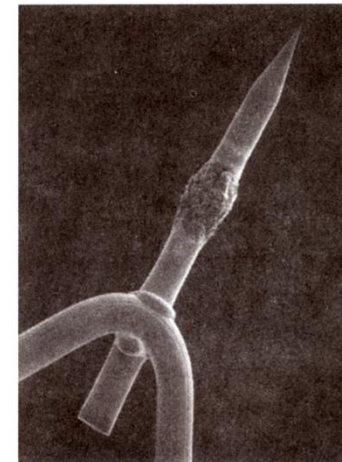
SFE - Schottky Field Emission

TFE (Thermal Field Emission) – has the same properties as a CFE but is operated at an elevated temperature (1800°C). This helps to keep the tip clean.

SFE (Schottky Field Emission) In the Schottky emitter the field at the tip is mostly used to reduce the work function barrier. ZrO_2 is deposited on the flatted tip from a small dispenser – $\phi = 2.6 \text{ eV} \rightarrow$ the highest β among all sources.

A Schottky gun runs continuously even when no current is being drawn from it, ensuring that it stays clean and stable and no flashing is required.

Because the ZrO_2 reservoir is finite in size, the useful life time of a SFE is a bout 12-15 months, so must be replaced on regular basis.

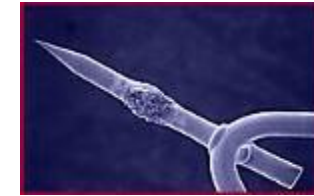
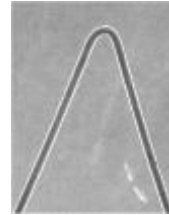


Project WND-POWR.03.02.00-00-1043/16

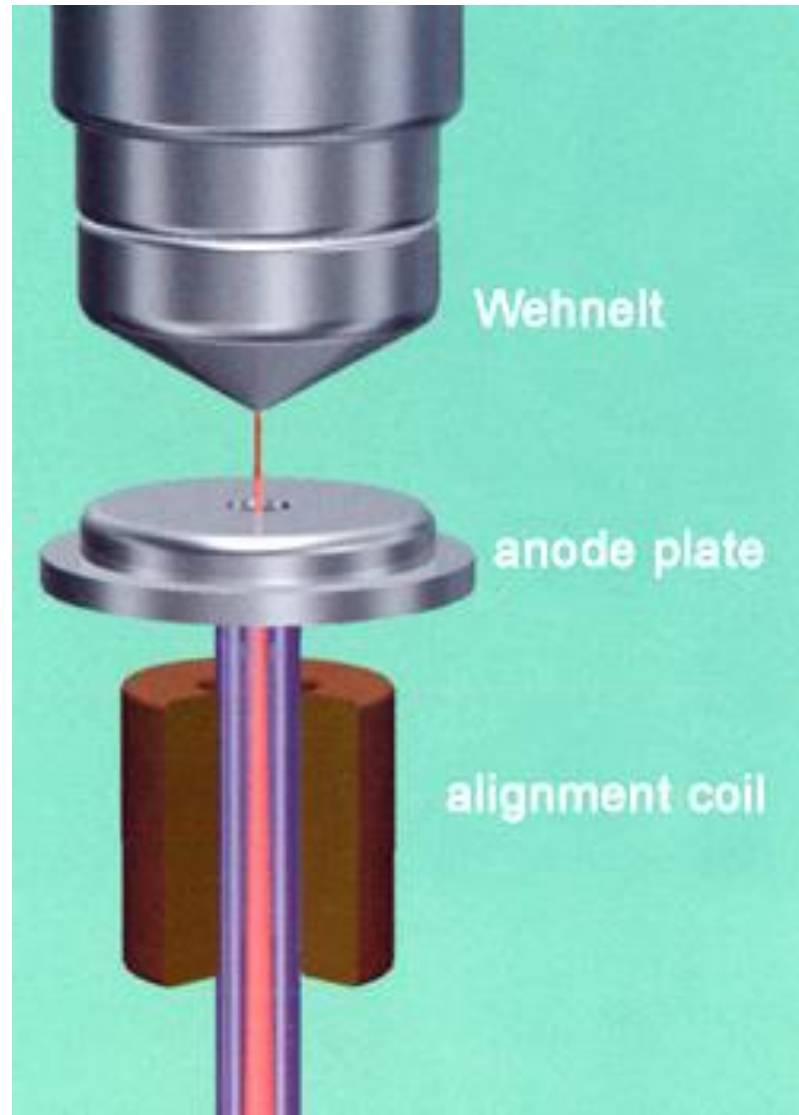
International interdisciplinary PhD Studies in Materials Science with English as the language of instruction

Project co-financed by the European Union within the European Social Funds

$d_o = 20-30 \text{ nm}$



	Tungsten	LaB₆	FEG
Normalized Brightness (-)	1	10	1000
Maximum probe current (nA)	2000	500	200
Life time (hrs)	60-200	200-1000	> 10000
Beam current stability (10 hrs)	<1%	<1%	<0.4%
Resolution 30kV (nm)	3.0	2.0	1.2
Resolution 1kV (nm)	25	15	3.0
Cost source (EUR)	40	1000	5000



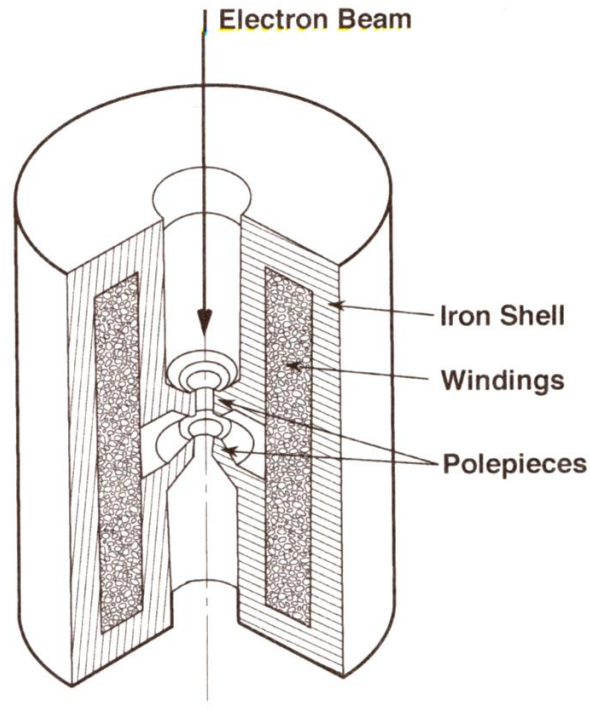
Project WND-POWR.03.02.00-00-1043/16

International interdisciplinary PhD Studies in Materials Science with English as the language of instruction

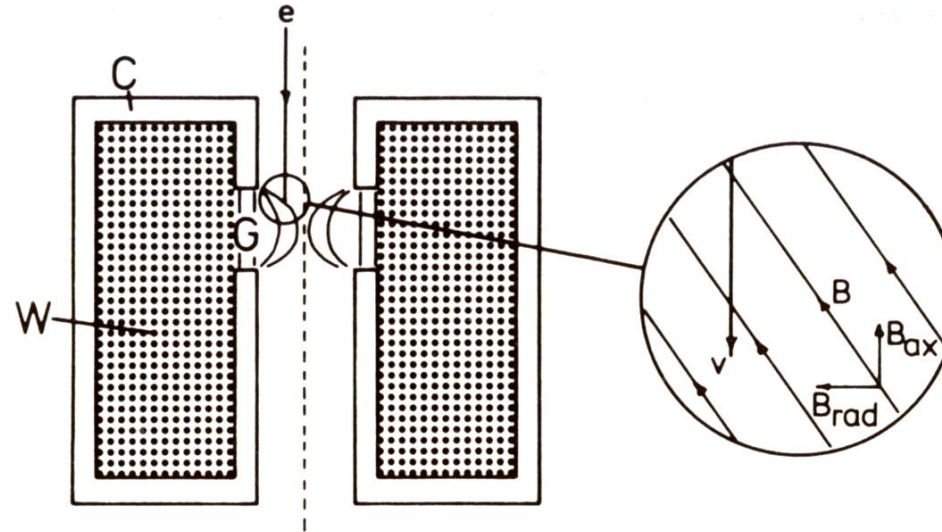
Project co-financed by the European Union within the European Social Funds



Lenses – to shape and focus electron beam lenses



Electromagnetic lens consists of many thousands of windings of copper wire inside a soft iron shell (the polepiece)



When an electric current is passed through the winding, both electric E and magnetic B fields are generated, applying on a force F to the electrons in the beam according to the Lorentz equation:

$$\mathbf{F} = e(\vec{E} + \vec{B} \otimes \vec{v})$$

v – velocity of the electrons in the beam

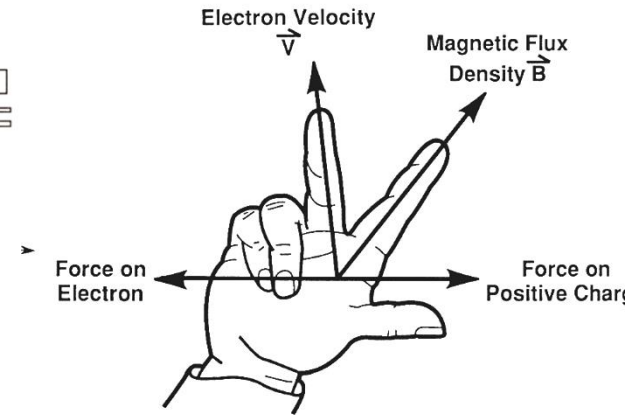
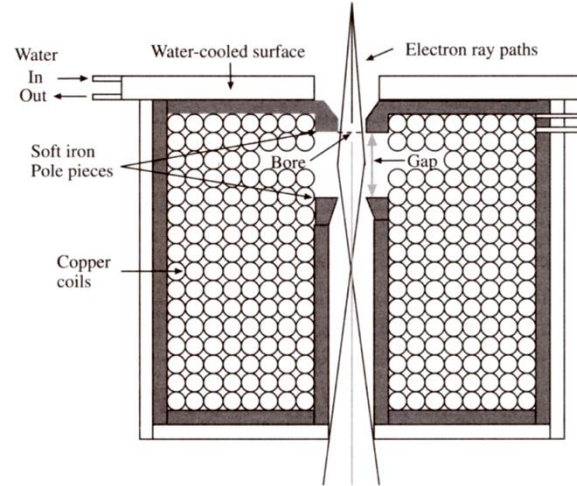
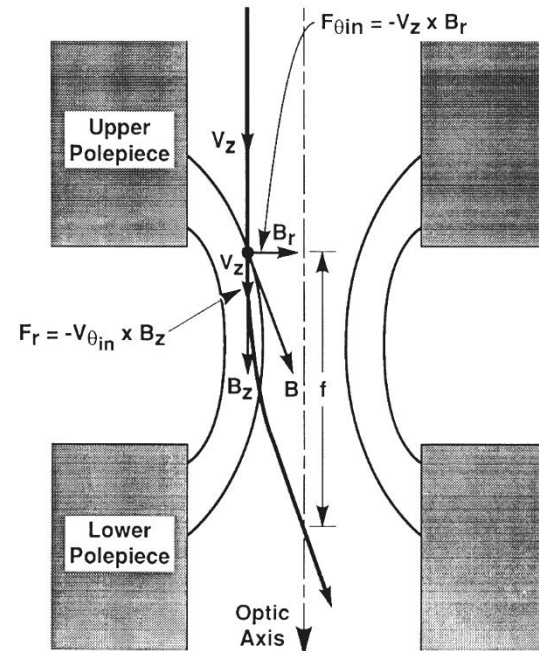


Illustration of the right-hand rule

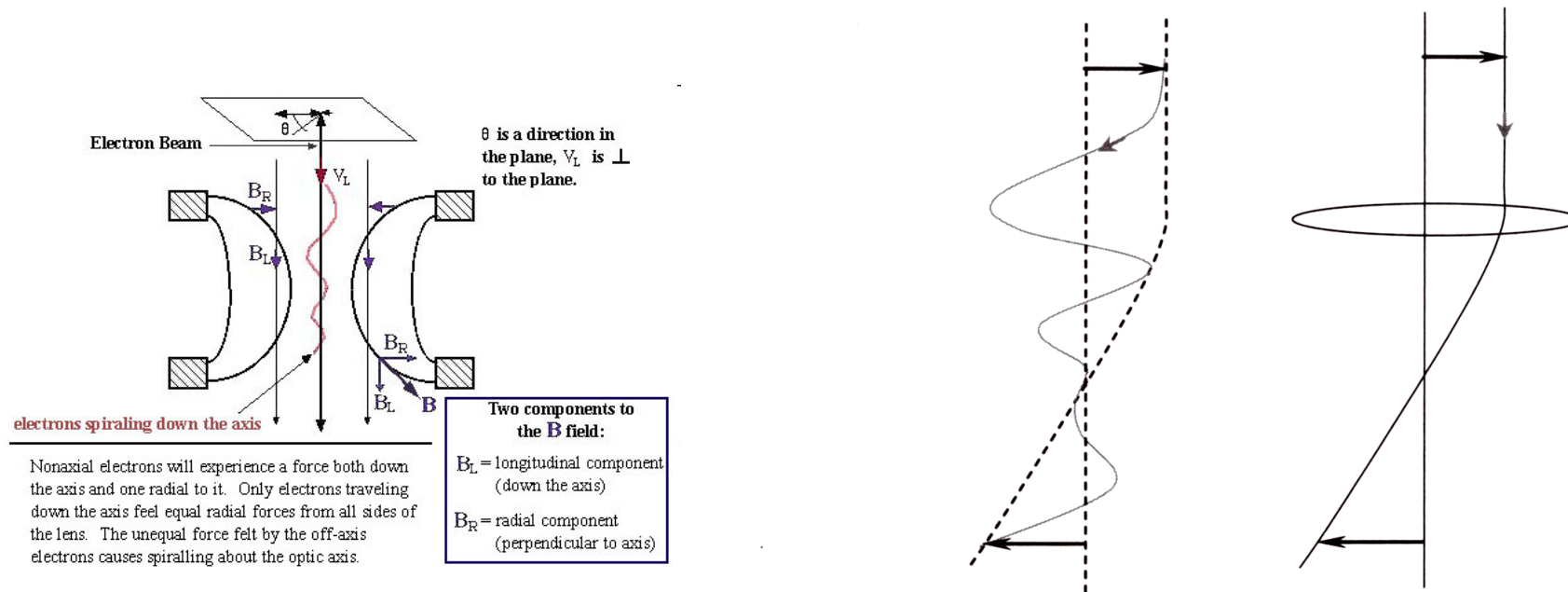
Schematic diagram of a magnetic lens. The polepieces surround the coils and when viewed in cross section the bore and the gap between the polepieces are visible. The magnetic field is weakest on axis and increases in strength toward the side of the polepiece, so the electrons are more strongly deflected as they travel off axis.



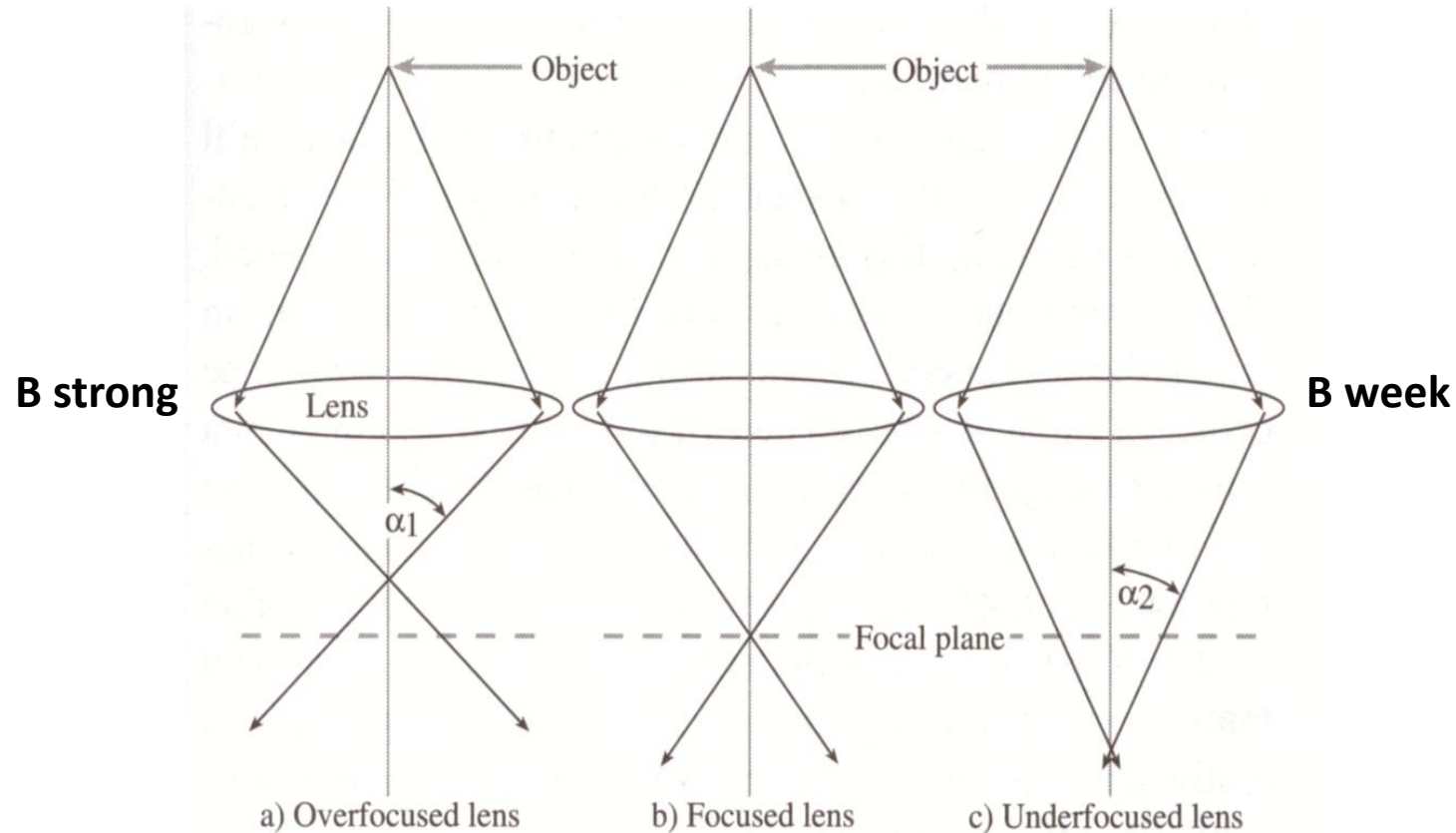
Enlarged schematic of polepiece area showing the forces on an electron that cause it to be focused



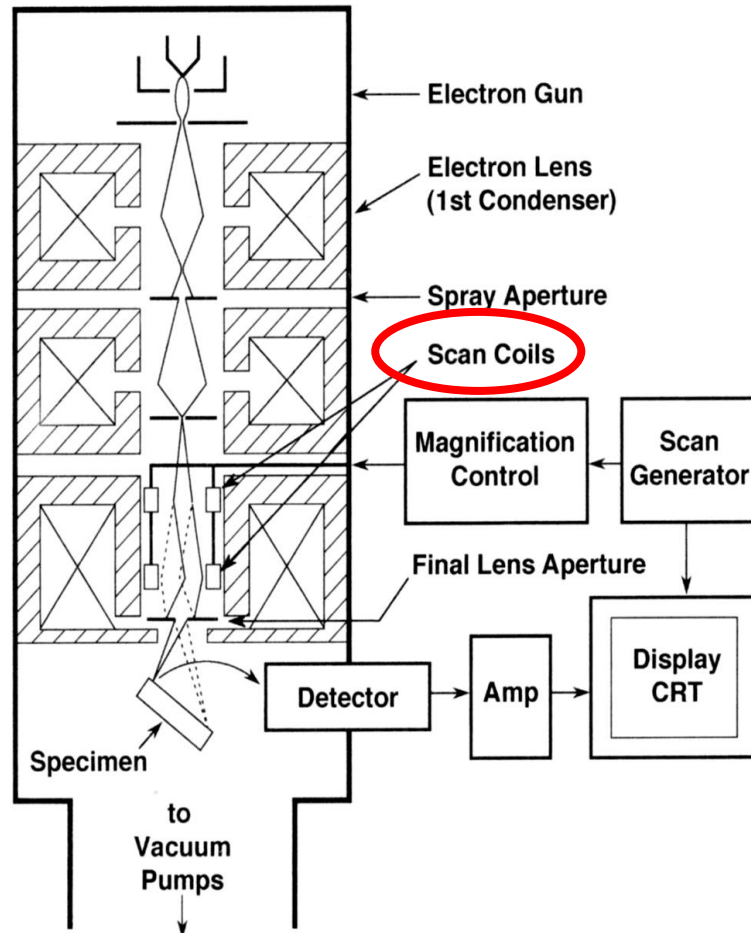
As electrons pass through the lens, they feel both radial and circumferential forces and so begin to spiral toward the centre of the lens bringing the beam to focus



The „envelope” (marked by the dashed line) around the path of the electrons resembles the ray path that would normally depict in a light ray

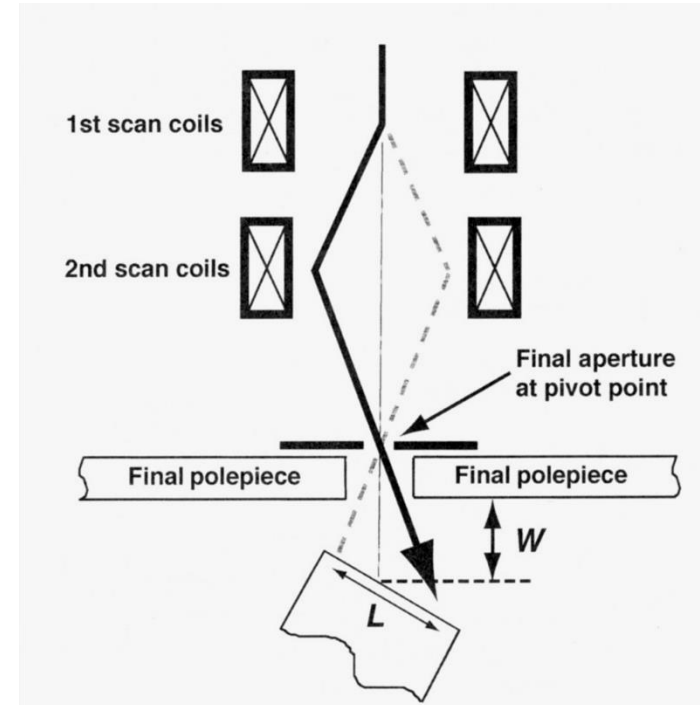


a) Ray diagram illustrating the concepts of overfocus, in which a strong lens focuses the electrons before the imagine plane, and c) underfocus, where a weaker lens focuses after the imaging plane. It is clear from the (c) that at a given underfocus electrons are more parallel that the equivalent divergent electrons at overfocus ($\alpha_2 < \alpha_1$)



Schematic diagram showing the electron column, the deflection system and the electron detectors

Scan coils



Deflection system inside the final lens

W (WD) – Working Distance – a distance between the specimen and final lens polepiece



Scan coils

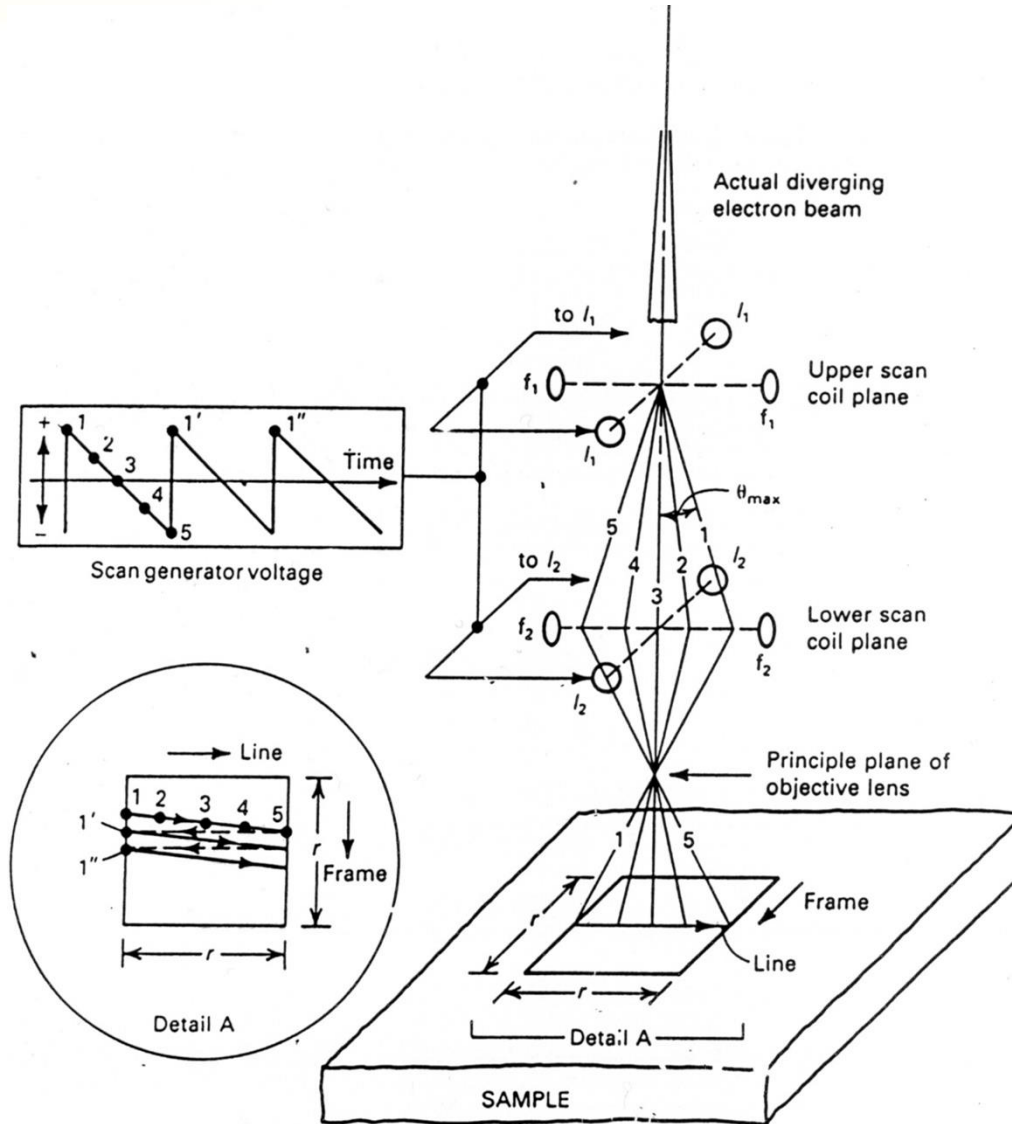
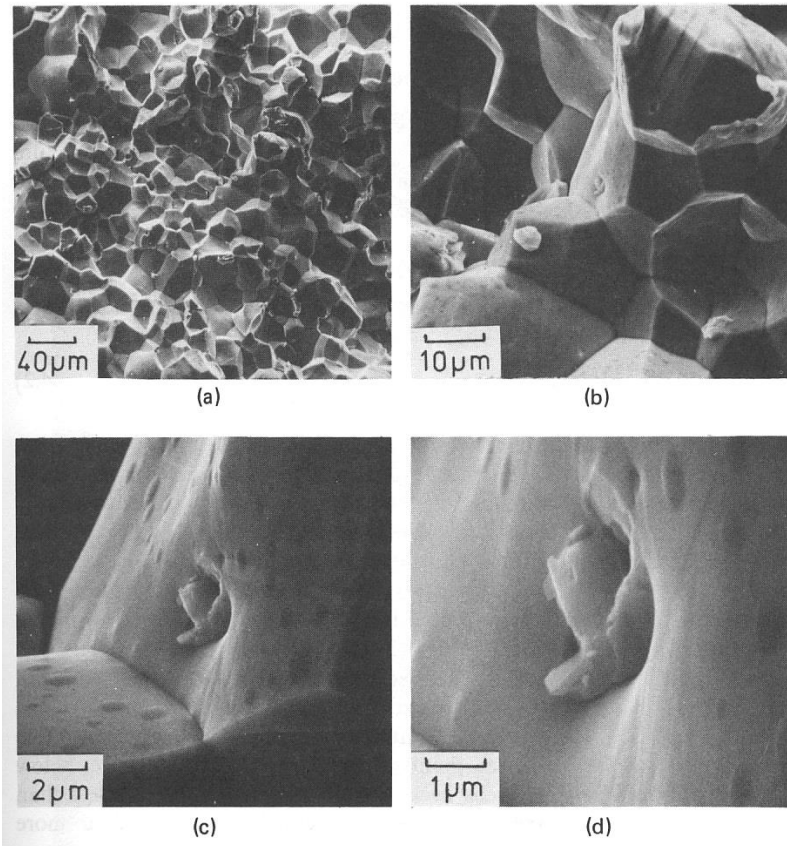


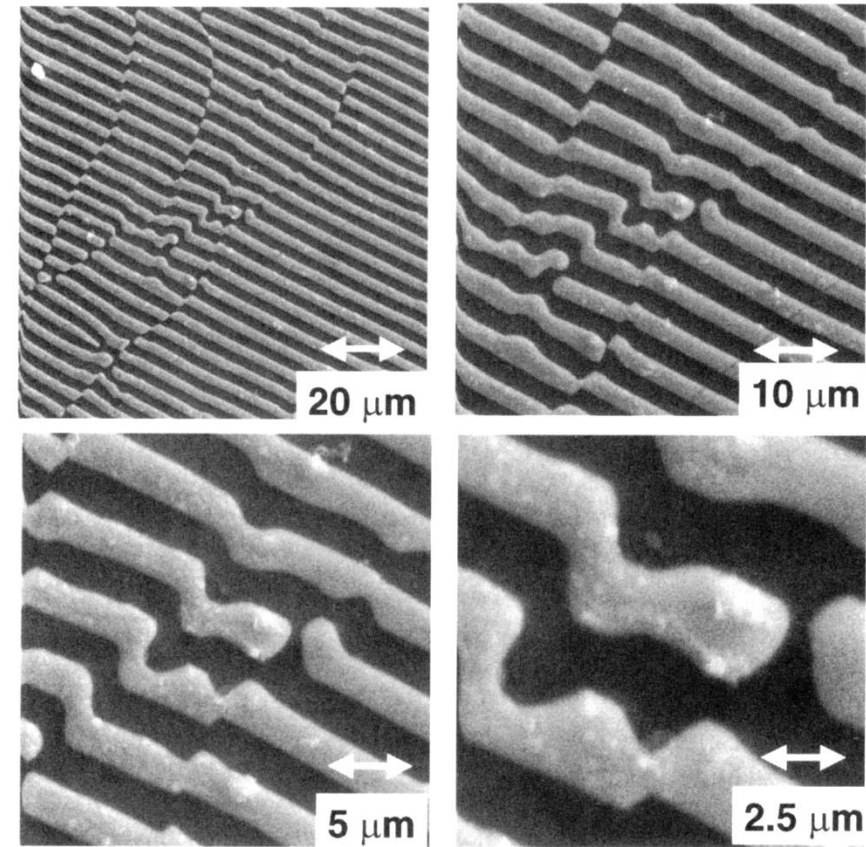
Table 4.1. Area Sampled as a Function of Magnification

Magnification ^a	Area on sample
10×	(1 cm) ² = 100 mm ²
100×	(1 mm) ² = 1 mm ²
1,000×	(100 μm) ² = 0.01 mm ²
10,000×	(10 μm) ² = 10 ⁻⁴ mm ²
100,000×	(1 μm) ² = 10 ⁻⁶ mm ²
1,000,000×	(100 nm) ² = 10 ⁻⁸ mm ²

^a Assumes magnification is relative to a CRT screen that measures 10 cm × 10 cm.



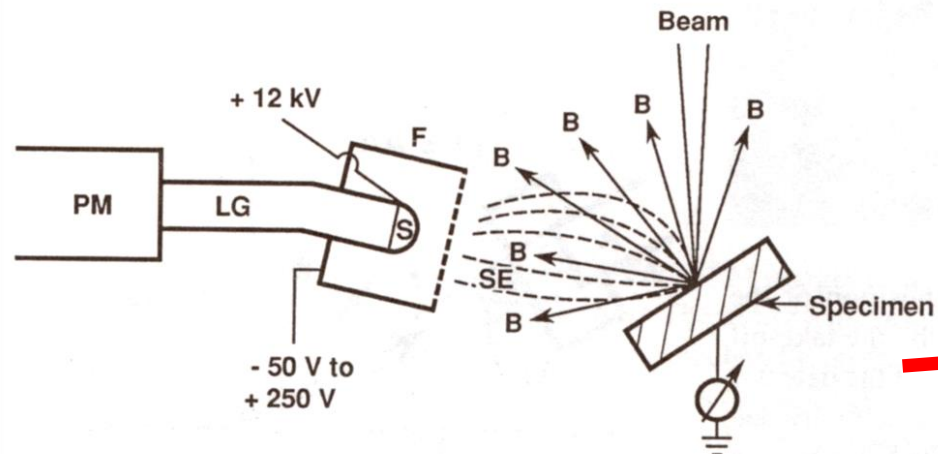
Brittle fracture of steel, MnS visible,
WD = constans, $E_0 = 20$ keV



AlCu eutectic
WD = constans, $E_0 = 20$ keV



Everhart-Thornley Detector - SE

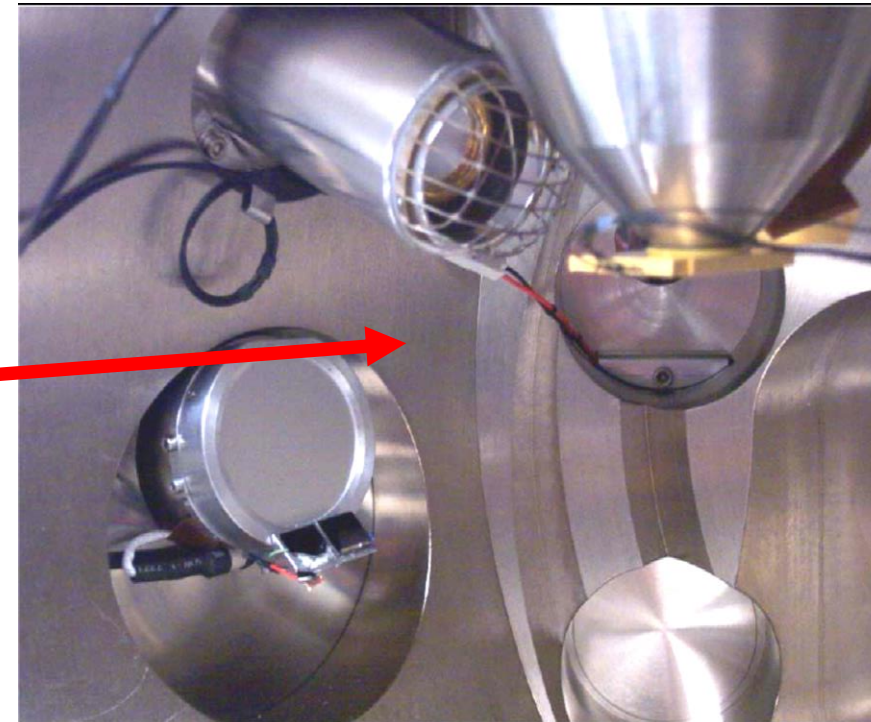


F – Faraday cage (bias range: -50V do + 250V)

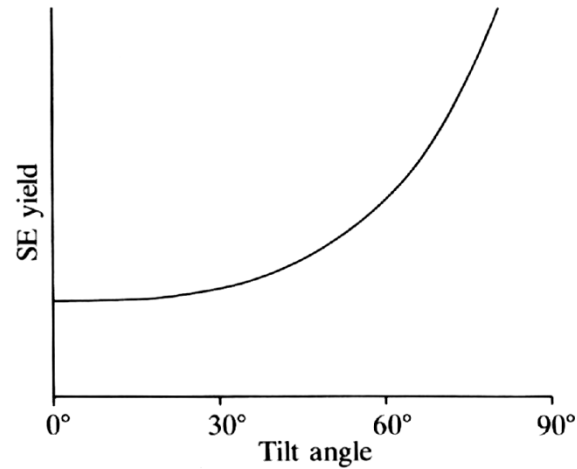
S – scintillator with thin metallic coating; high bias (+12kV) supply to the scintillator coating

LG – light guide

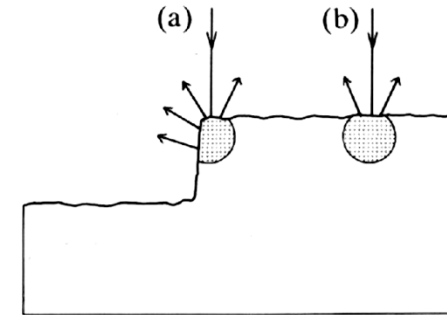
PM – photomultiplier



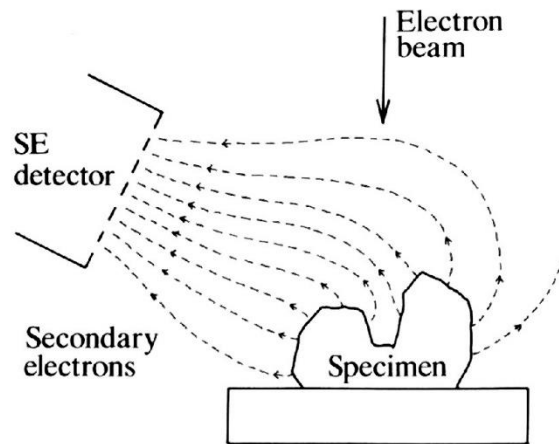
A small amount of BSE will be always detected by E-T detector



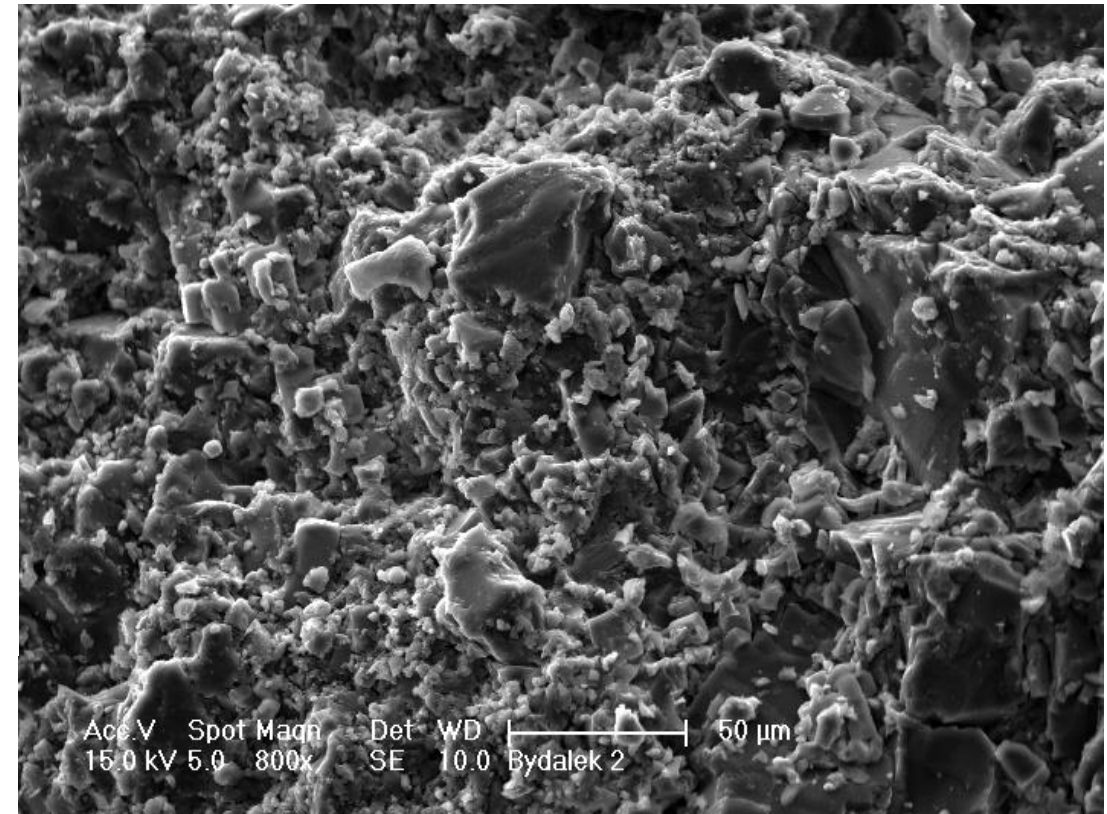
Variation in secondary electron yield angle of tilt of specimen surface relative to horizontal



Edge effect in secondary electron image: signal enhanced when beam is (a) close to edge compared to (b) away from edge

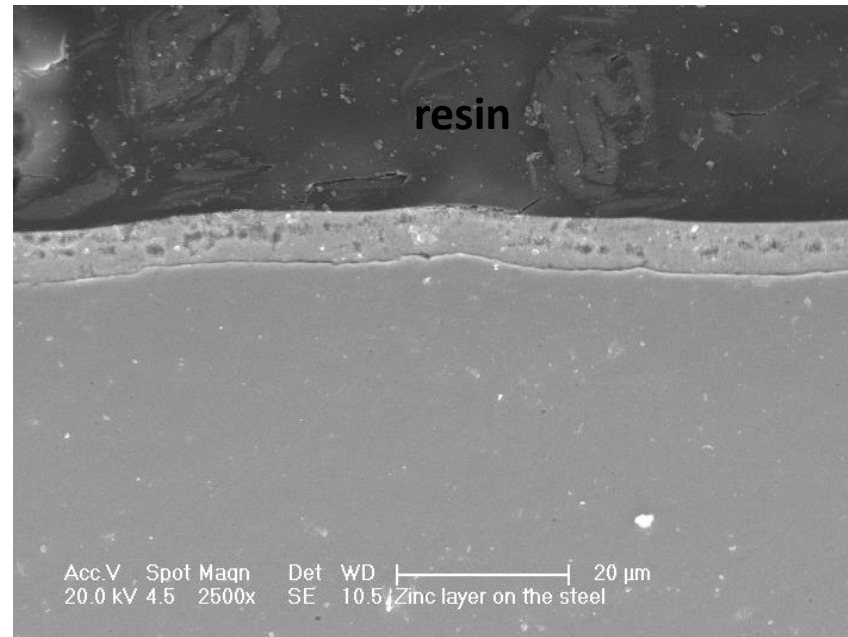


Collection of secondary electrons from three-dimensional specimen by detector with positively biased grid

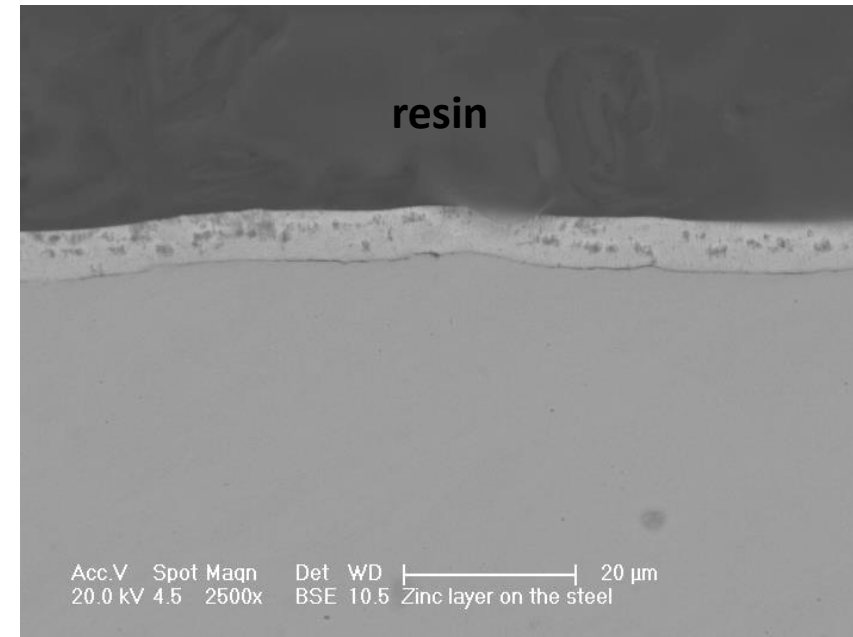




Stainless steel with Zn coating



Secondary electron image (SE)
– a contribution of backscatter
electrons is clearly visible



**Pure electron backscatter image
(BSE)**

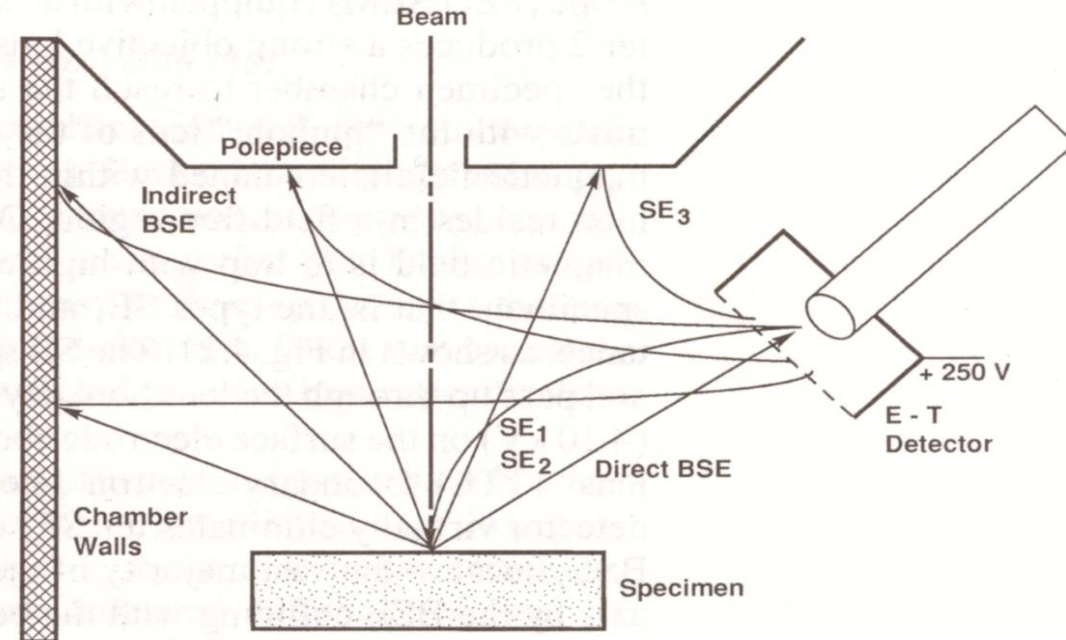
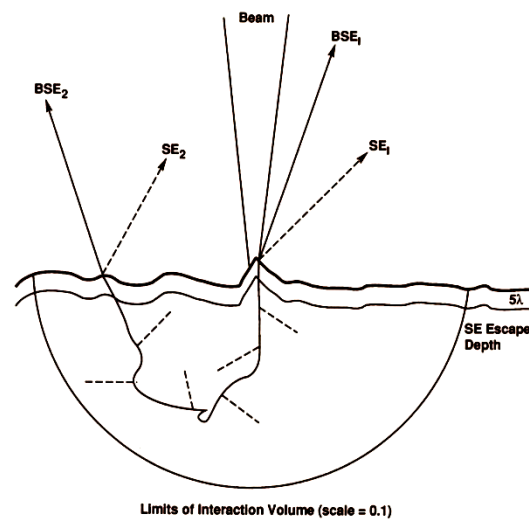
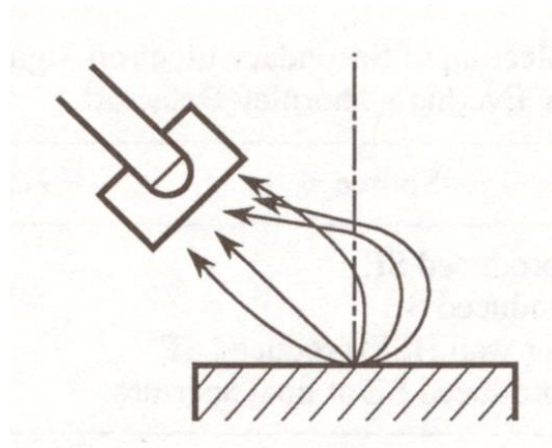


Illustration of deflection of trajectories of secondary electrons of potential on the Faraday cage

Table 4.4. Collection of Secondary Electron Signals from a Gold Specimen with the Everhart–Thornley Detector^a

Signal	Source	Percentage of total
SE ₁	Beam-produced SE	9
SE ₂	BSE-produced SE	28
SE ₃	Chamber wall BSE-produced SE	61
SE ₄	Beam-produced SE at final aperture	2

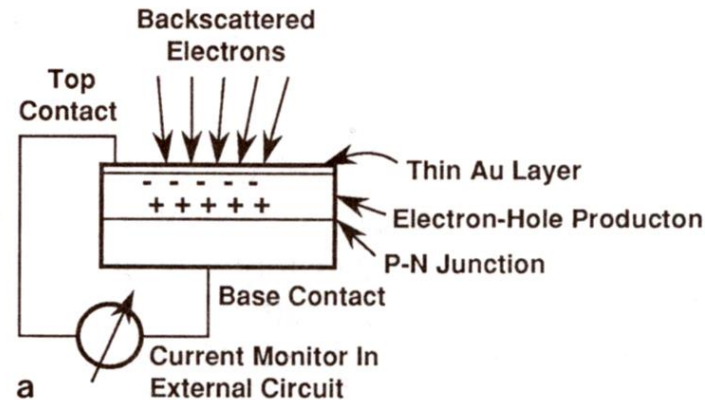
^a From Peters (1984).



Solid State Diode (SSD) Detector - BSE

For silicon energy required to create an electron-hole pair is about 3.6 eV

When a single 10 keV BS electron strikes the detector,
~ 28000 electron-hole pairs are produced



a) Schematic diagram of a solid state backscatter detector showing separation of electron-hole pairs by applied external potential

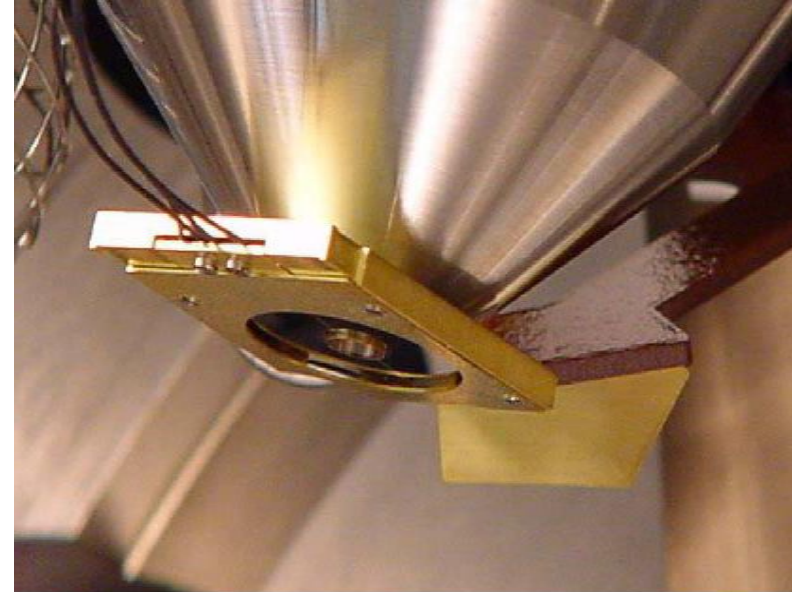
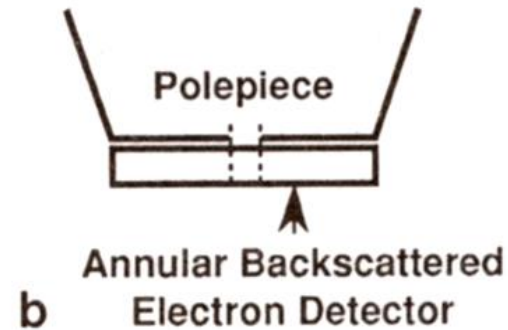
Project WND-POWR.03.02.00-00-1043/16

International interdisciplinary PhD Studies in Materials Science with English as the language of instruction

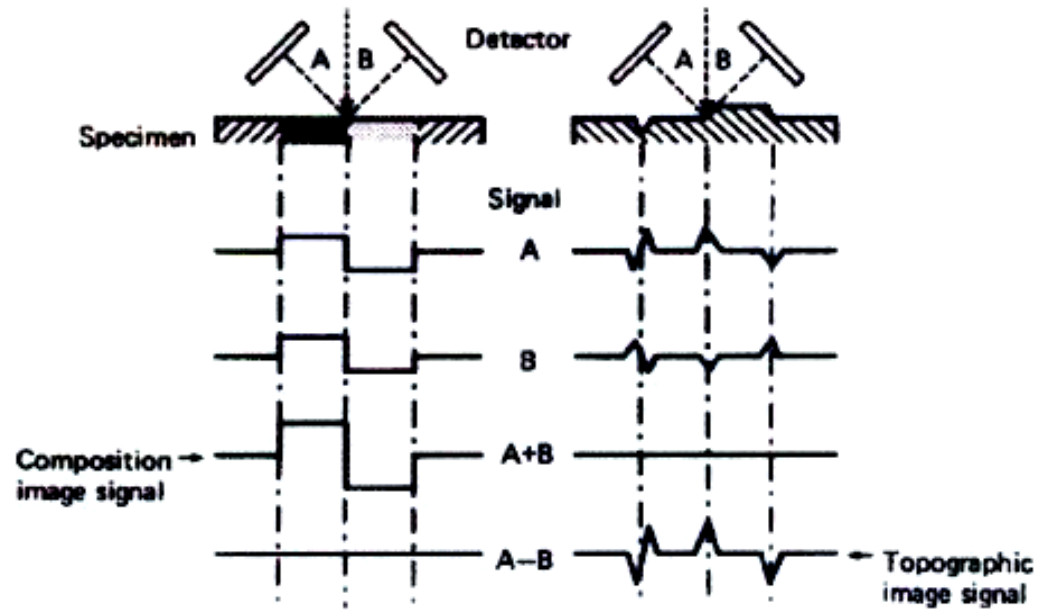
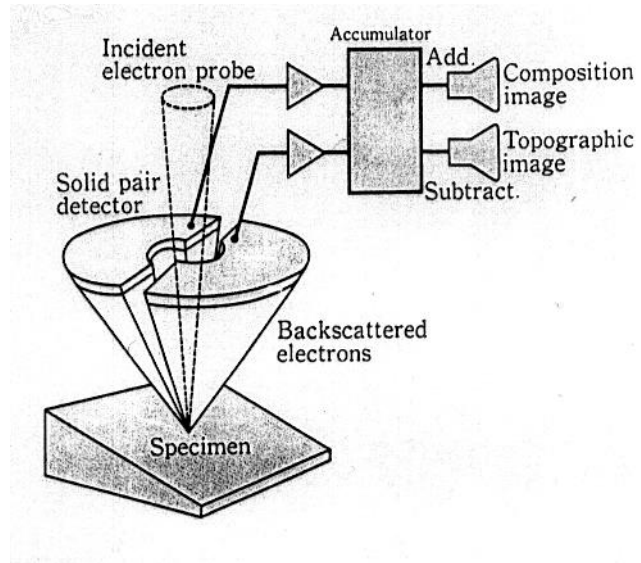
Project co-financed by the European Union within the European Social Funds

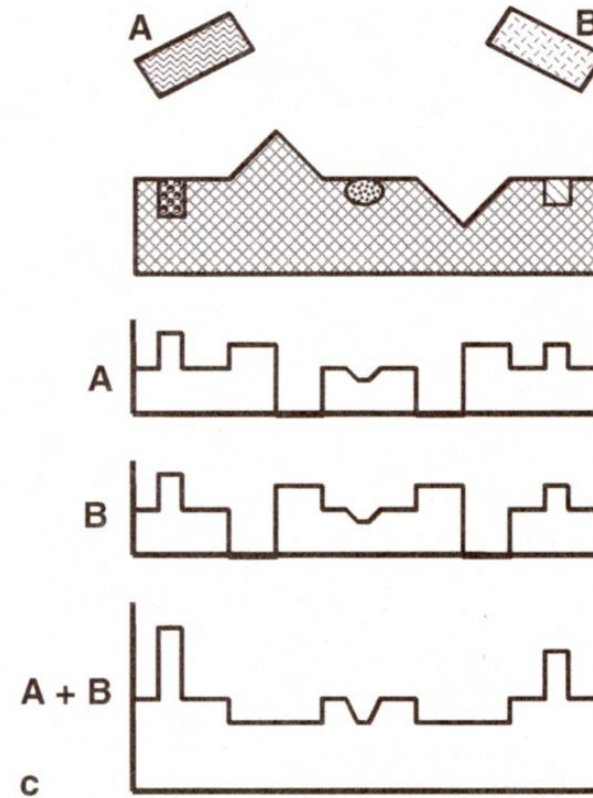
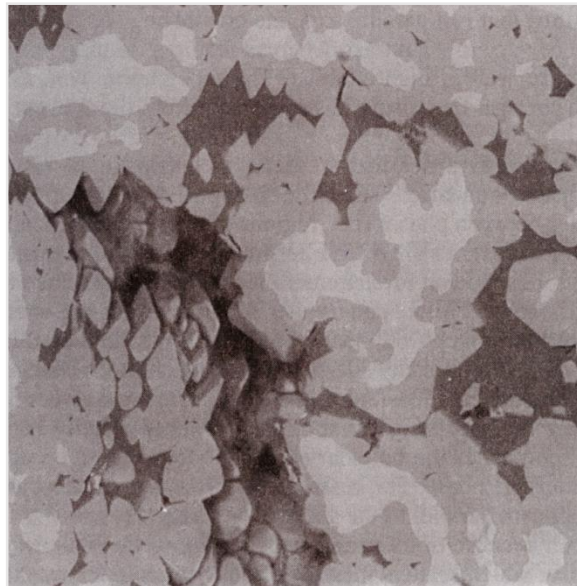
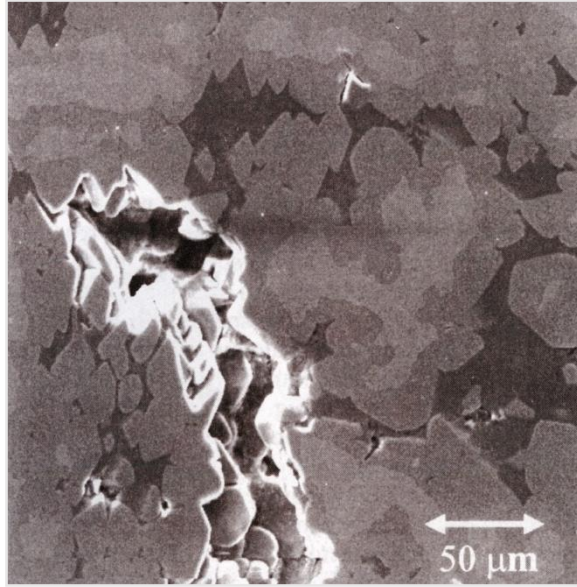


Solid State Diode (SSD) Detector



b) Typical installation of a solid state detector on the polepiece of the objective lens

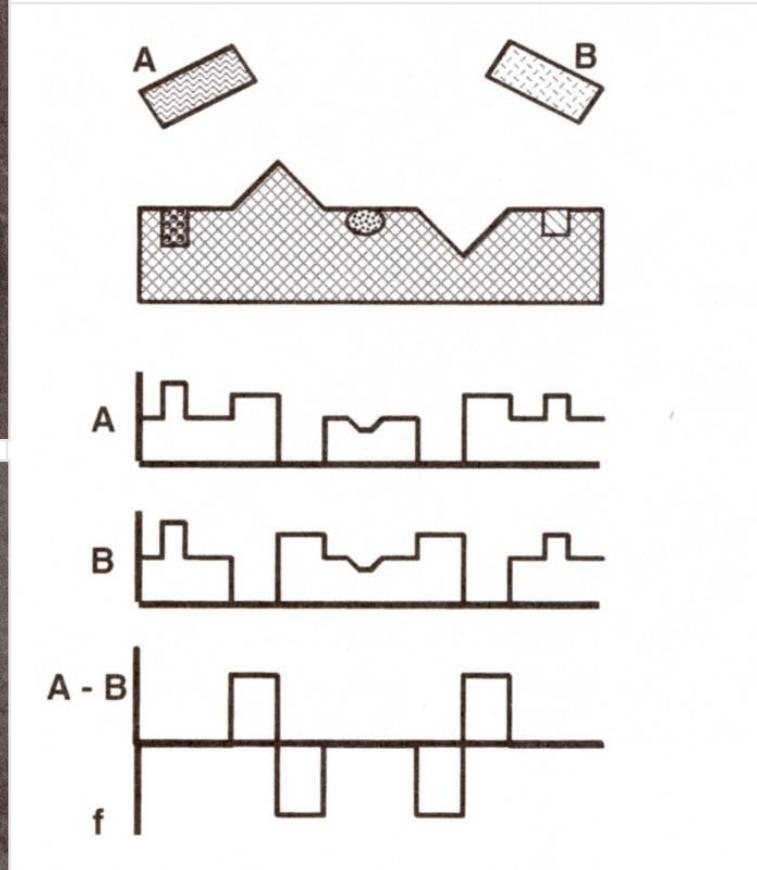
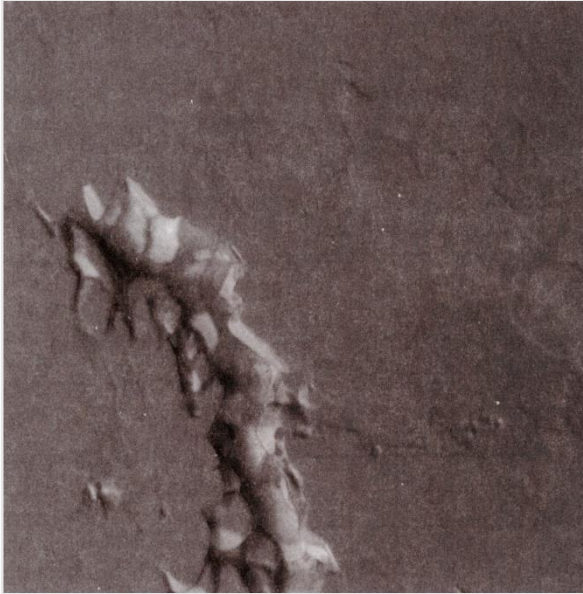




Project WND-POWR.03.02.00-00-1043/16

International interdisciplinary PhD Studies in Materials Science with English as the language of instruction

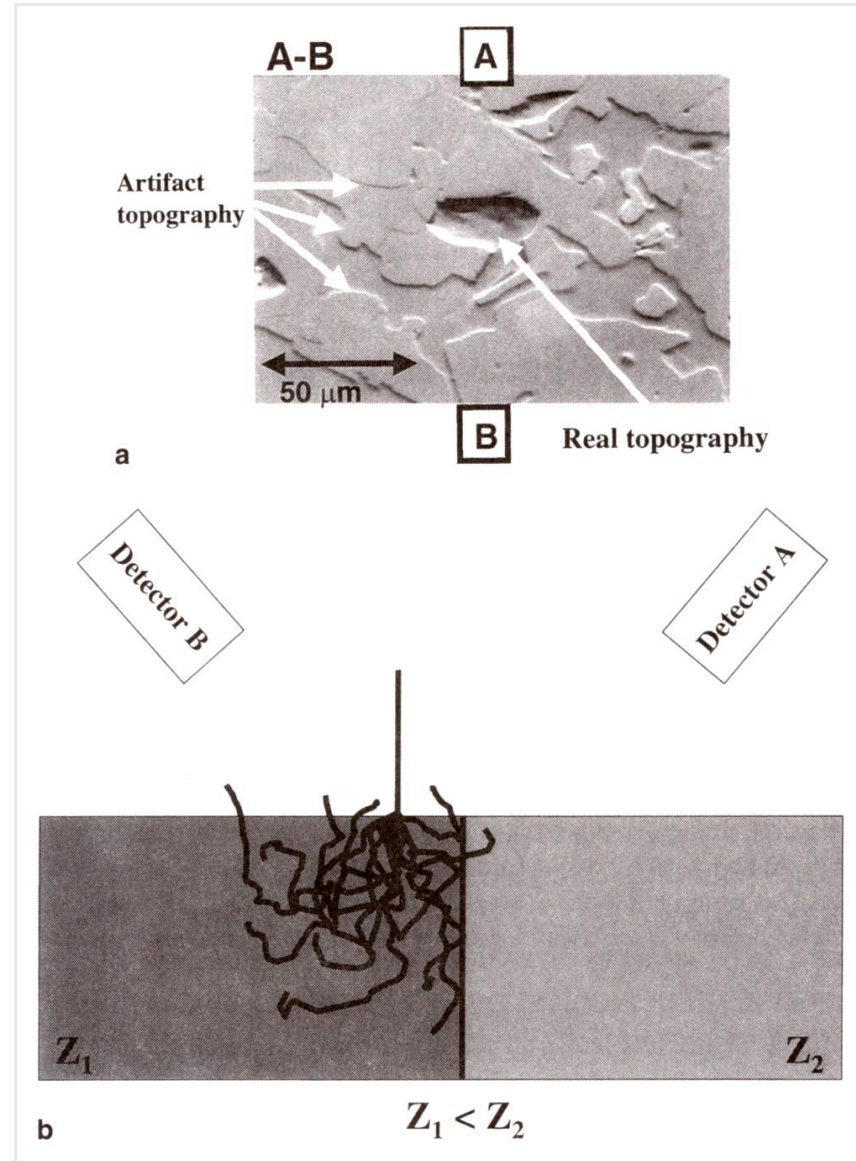
Project co-financed by the European Union within the European Social Funds



Project WND-POWR.03.02.00-00-1043/16

International interdisciplinary PhD Studies in Materials Science with English as the language of instruction

Project co-financed by the European Union within the European Social Funds



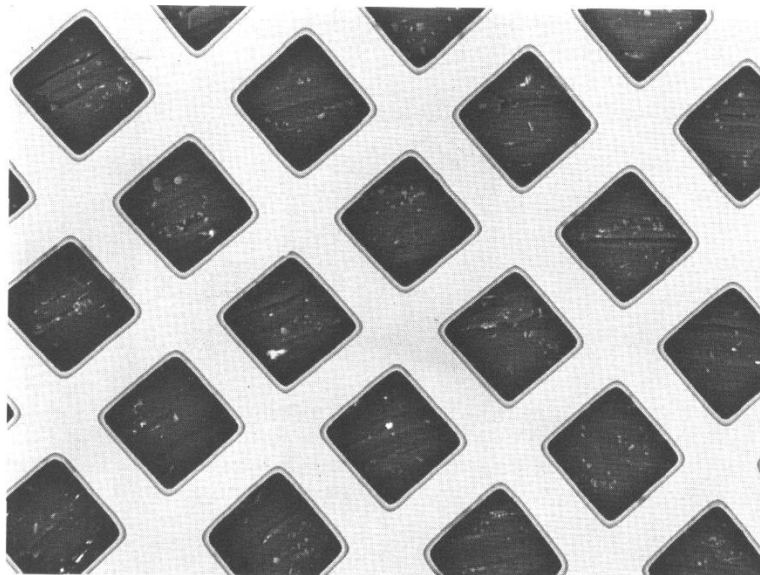
Project WND-POWR.03.02.00-00-I043/16

International interdisciplinary PhD Studies in Materials Science with English as the language of instruction

Project co-financed by the European Union within the European Social Funds

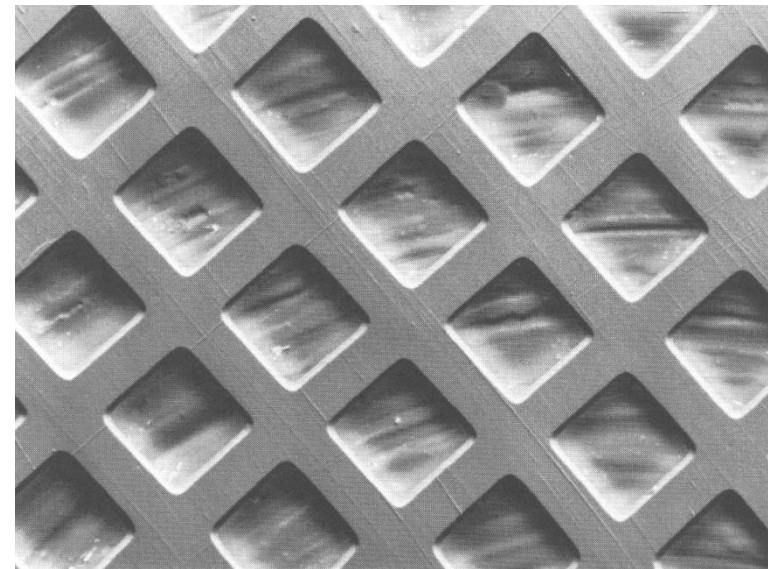


Copper grid



Compositional Image

COMPO

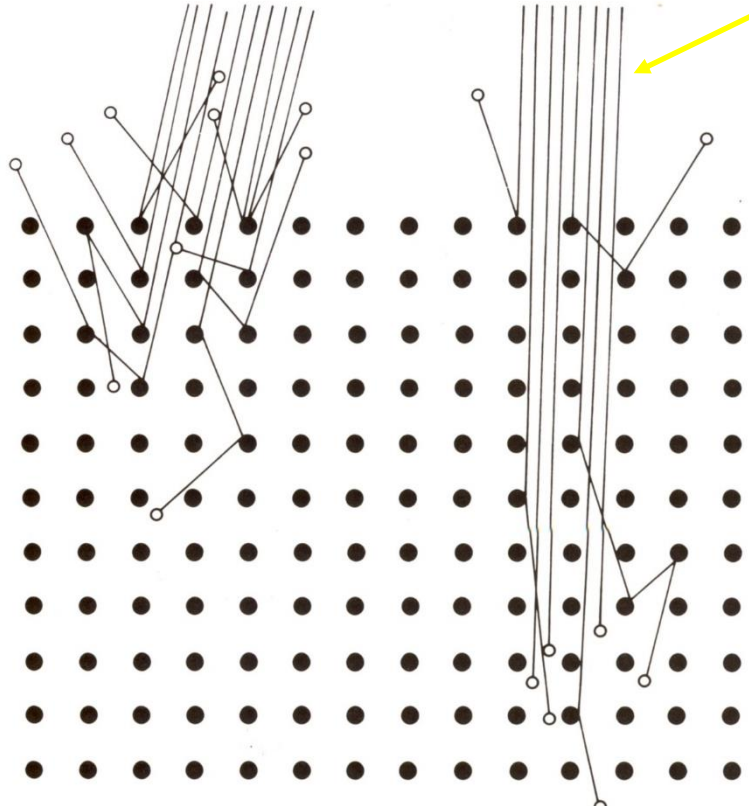


Topographical Image

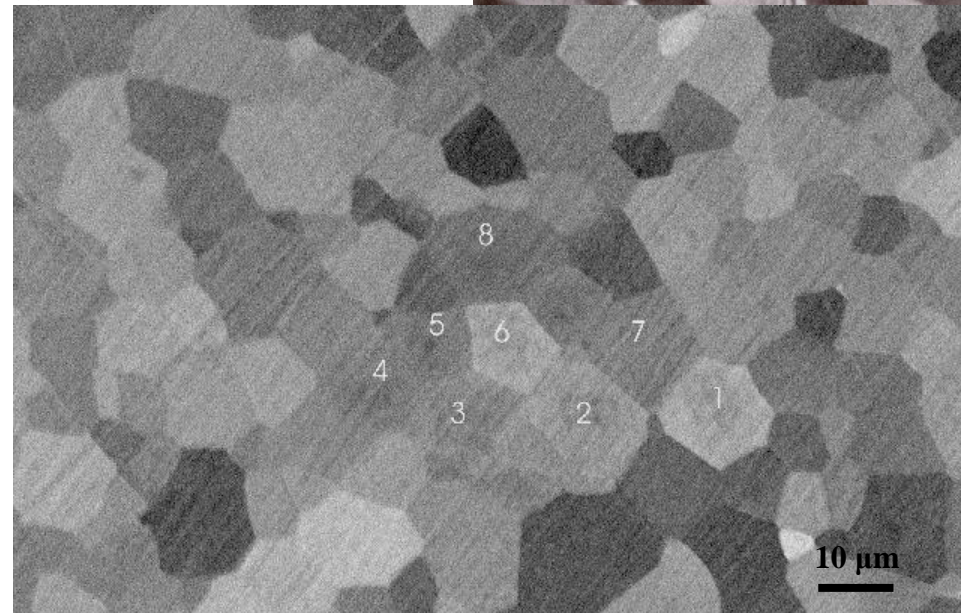
TOPO



Channeling contrast



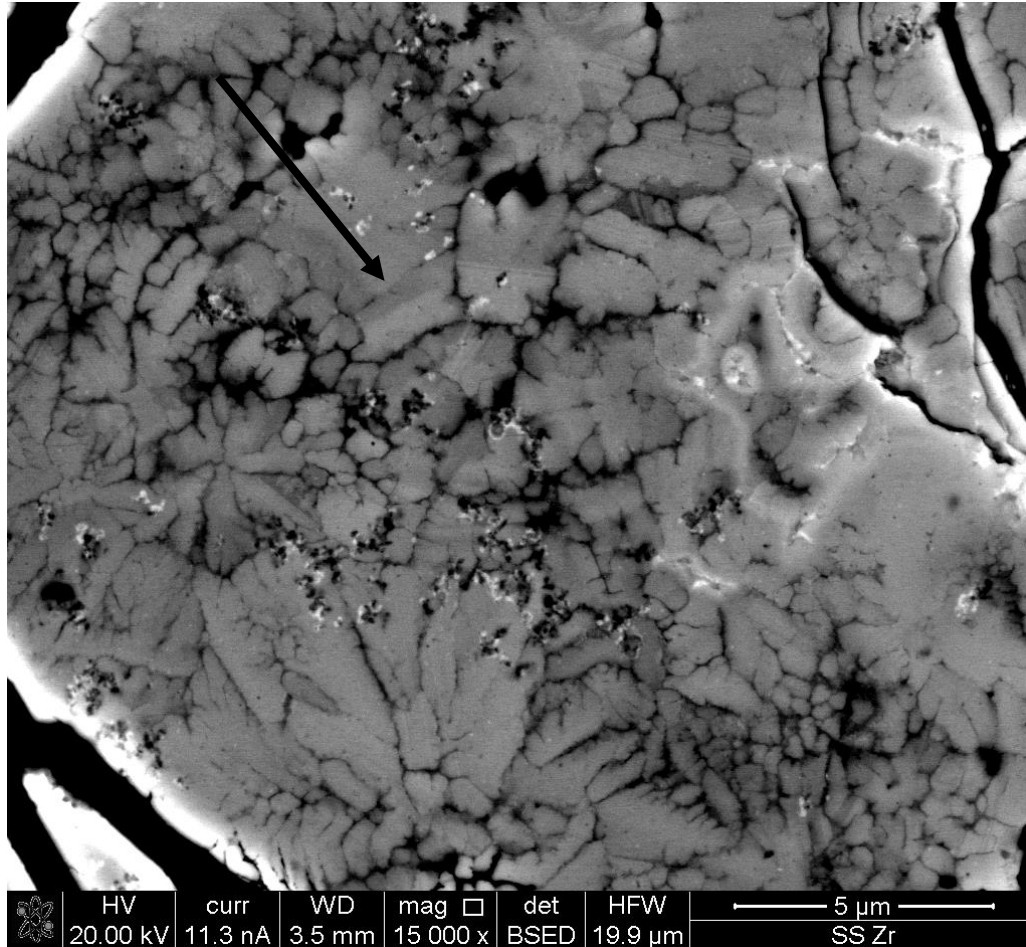
Electron beam \parallel to
crystallographic
planes



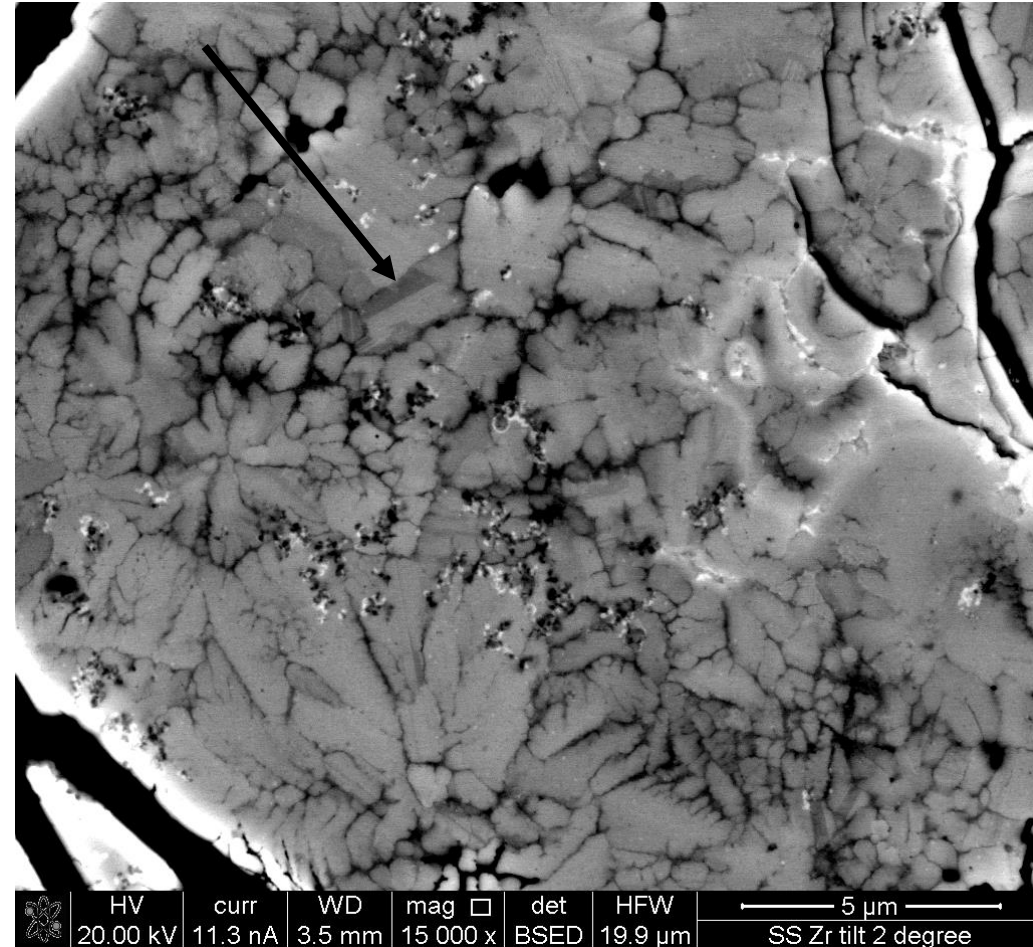
Schematic diagram showing the
origin of the channeling effect as
penetration of the beam electrons
along crystal planes

For amorphous
materials η
depends only on
Z.

For
crystallographic
materials η
**depends also on
tilt angle.**



Tilt 0°



Tilt 5°

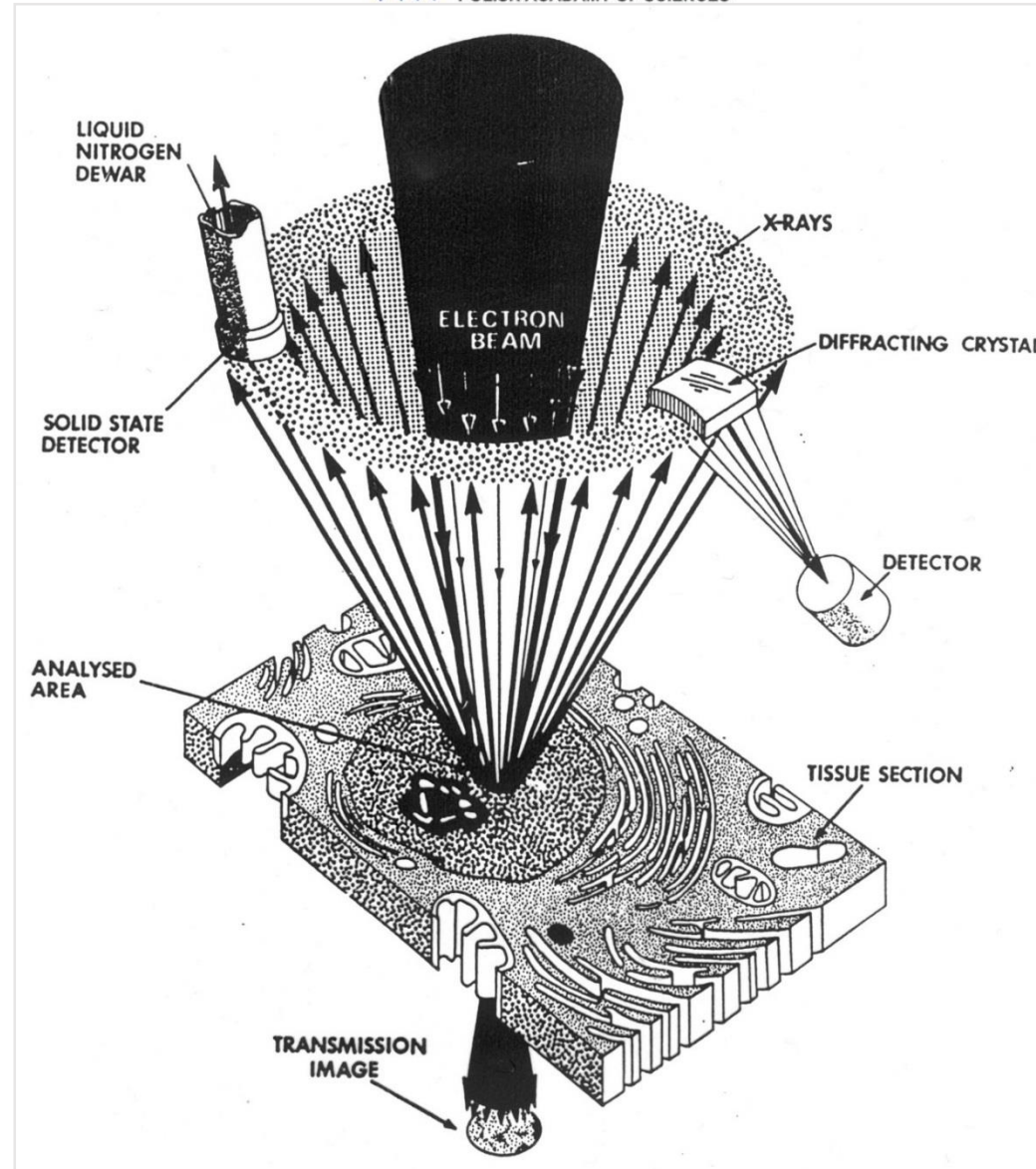


Electron Probe X-Ray Microanalysis of Bulk Materials

Courtesy of EDAX, Oxford Instruments, JEOL



EDS
(EDXS)
Energy
Dispersive
Spectrometry



WDS
(WDXS)
Wavelength
Dispersive
Spectrometry



Outline

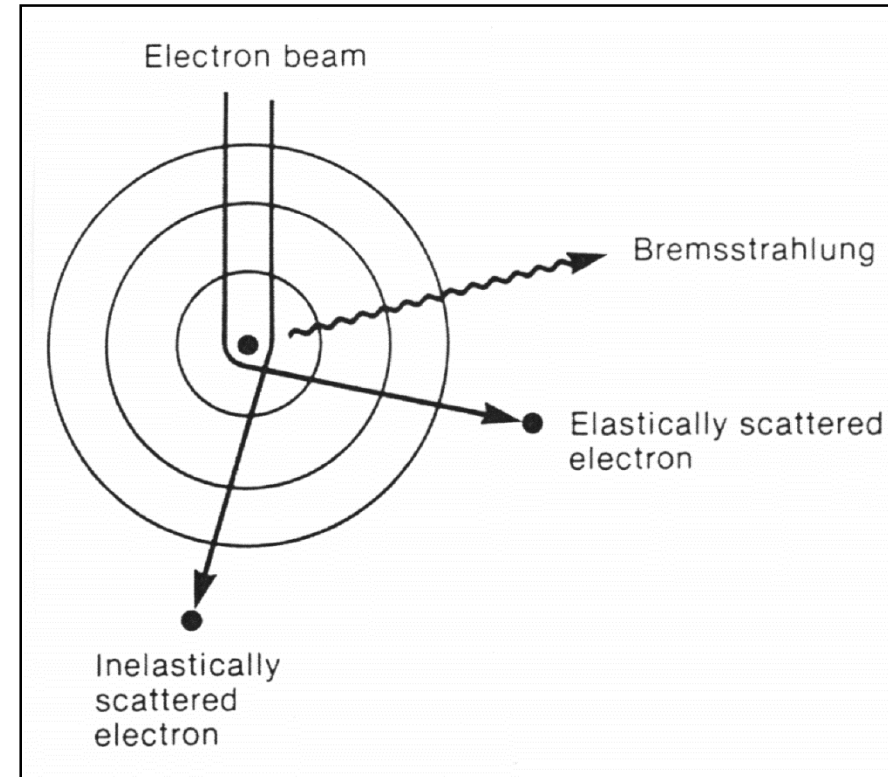
- **X-ray generation and measurement**
- **Spatial resolution**
- **Geometry**
- **Peak ID**
- **Spectral Artefacts**
- **Linescan**
- **Mapping**
- **Quantitative analysis**
- **Standards**



X-ray Generation

Inelastic and elastic scattering

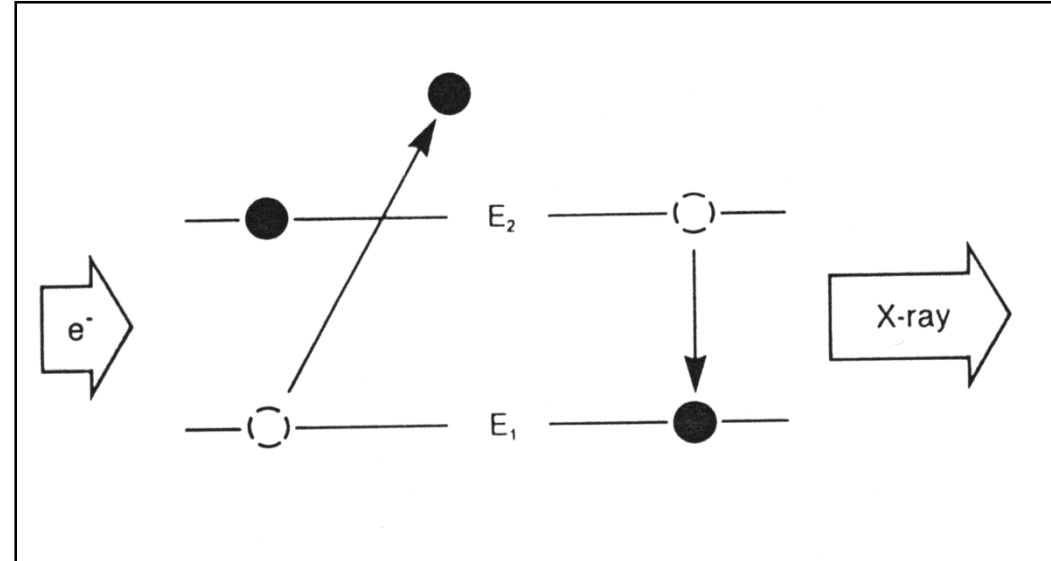
- Inelastically scattered electron loses energy depending on the type of interaction
 - „Bremsstrahlung” (braking radiation)
 - ionisation of inner shells
- Elastically scattered electron loses no energy but changes its trajectory
- Both effects results in an interaction volume





X-ray Generation

- X-ray microanalysis is based on electronic transitions between inner atomic shells (orbitals)
- An electron leaves from a shell of low energy (E_1)
- An electron of a shell of higher energy fills the vacancy losing energy in the process (E_2)
- The lost energy appears as emitted radiation of energy $E_2 - E_1$ (= X-ray radiation)





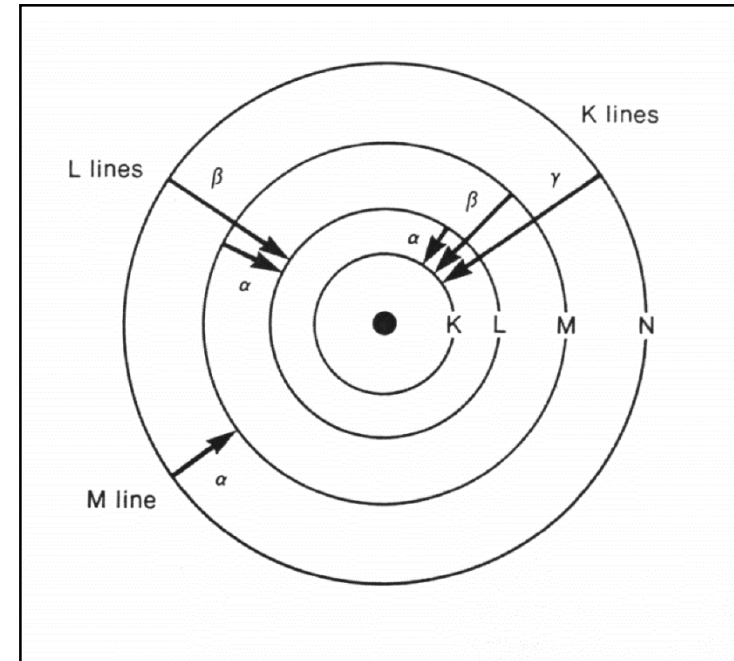
X-ray Generation - Nomenclature

- Typically transitions observed in X-ray spectra :
- K - L and M multiple lines
- Each shell comprises several energy levels
- Transitions are more numerous than shown
- Complex transition system

$$L\alpha_1 = L_3 - M_5$$

$$L\alpha_2 = L_3 - M_4$$

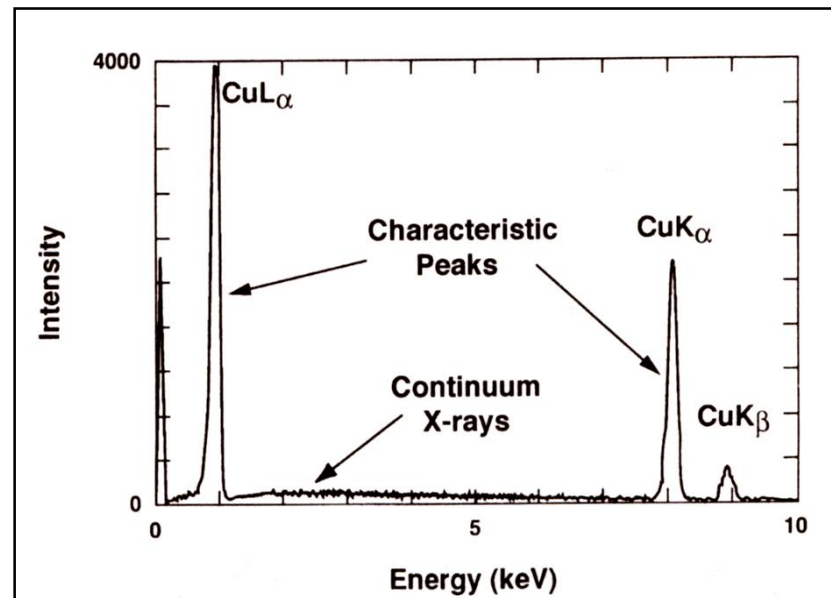
$$L\beta_1 = L_2 - M_4$$





X-ray Generation

- The accumulated counts from a sample produce an X-ray spectrum
- A typical X-ray spectrum includes major spectral peaks superimposed on a broad background
- Each element will produce characteristic spectral peaks therefore qualitative information can be extracted
- Extracting quantitative information is also possible but more complicated



Project WND-POWR.03.02.00-00-1043/16

International interdisciplinary PhD Studies in Materials Science with English as the language of instruction

Project co-financed by the European Union within the European Social Funds



- The simple model of X-ray production implies that an incoming electron must possess a minimum amount of energy to eject an inner shell electron from the atom.
- That energy is the binding energy of the particular inner shell electron (a specific, characteristic energy for each electron in the atom).
- The binding energy for a K-shell electron is greater than that of a L-shell electron, since the K-shell electron is closer to the nucleus and more tightly bound.
- Therefore, if sufficient energy exists in the incident beam to excite K X-rays then L and M X-rays will also be excited).

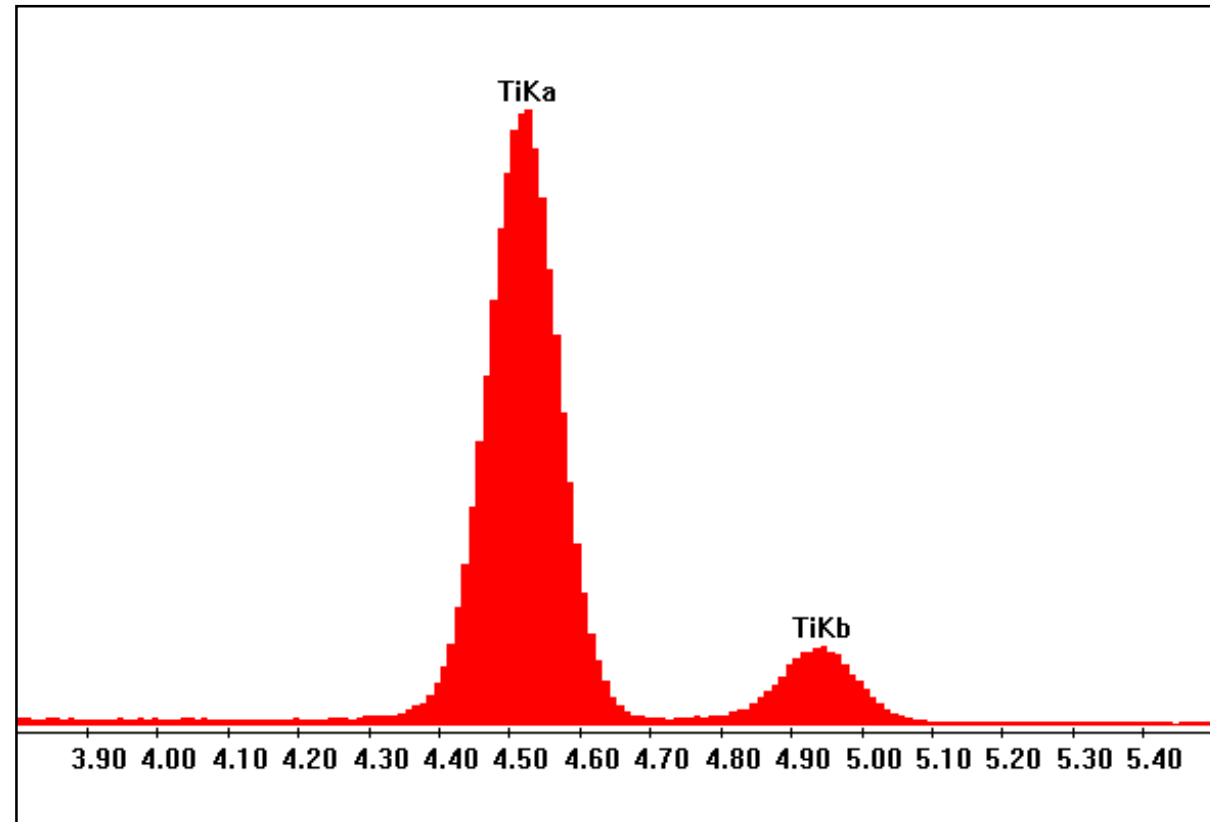
Element (atomic number)	X-ray energy (keV)		
	$K\alpha$	$K\beta$	$E_c = E_{K\text{edge}}$
Mn (25)	5.895	6.492	6.537
Fe (26)	6.400	7.059	7.111
Co (27)	6.925	7.649	7.709
Ni (28)	7.472	8.265	8.331
Cu (29)	8.041	8.907	8.980

Absorption edge energy, or critical excitation energy or ionisation energy. It is always slightly greater than the energy of corresponding X-ray emission line.



X-ray Generation

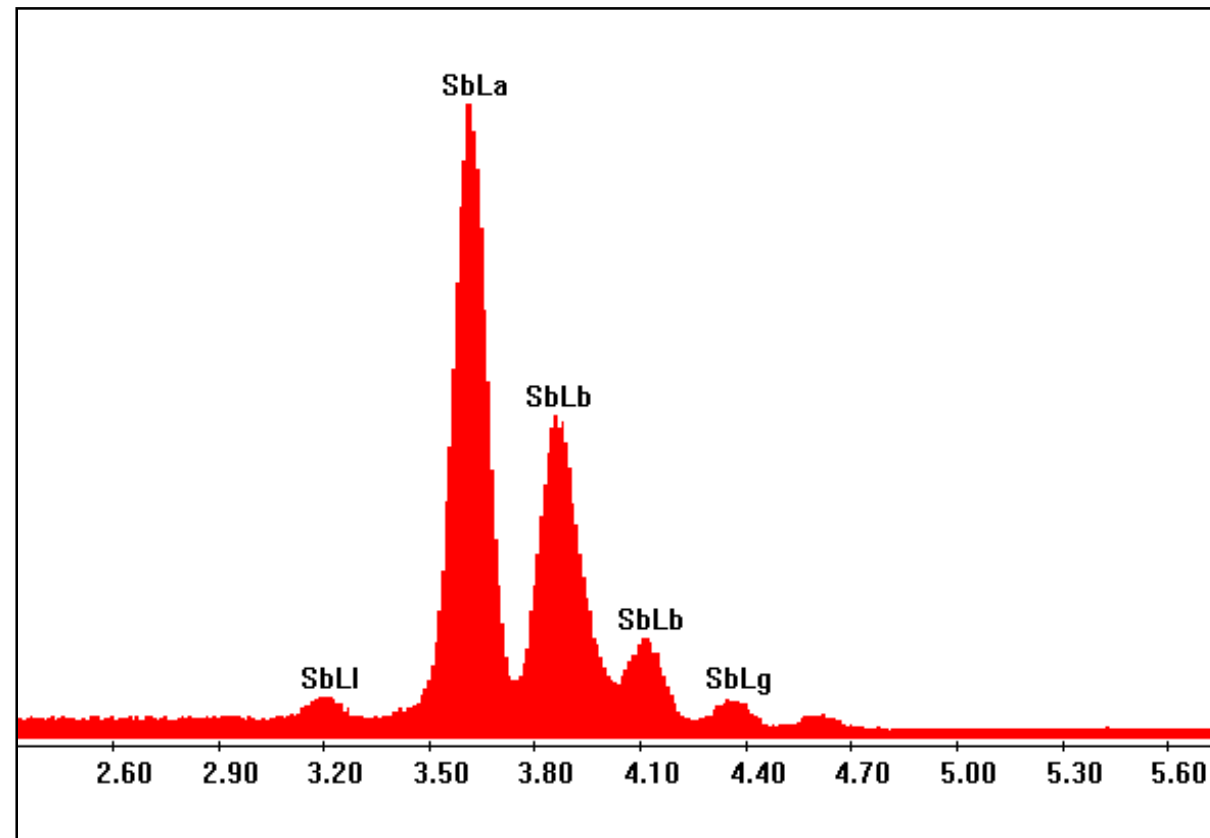
- Typical spectrum of Ti-K radiation
- K radiation normally doublet (for elements with a Z higher than Potassium, nr 19)
- K-lines : Gaussian shape
- Ratio between $K\alpha$ and $K\beta$: about 5 : 1





X-ray Generation

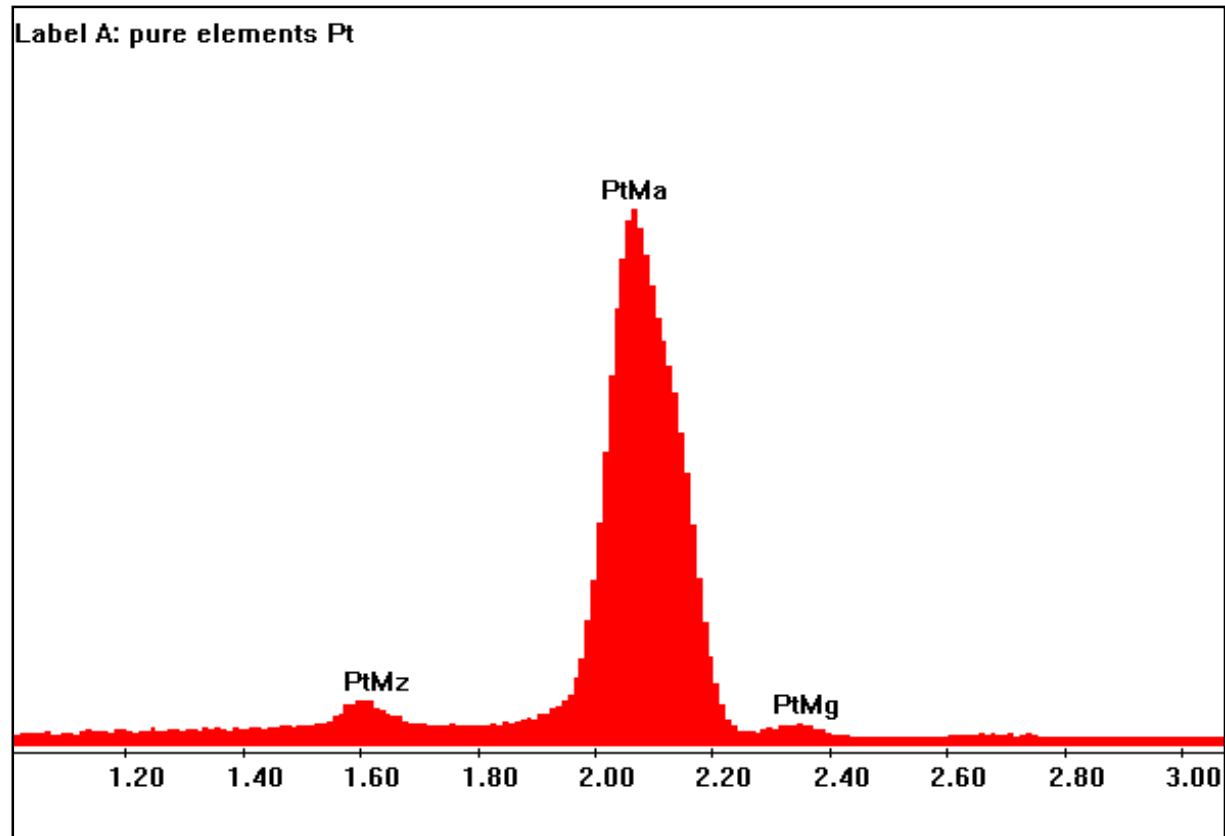
- Typical spectra of Sb-L radiation
- Multiple-lines due to many possible transitions
- Often not Gaussian, tailing towards high energy side (depending on element)
- Ratio between the L-lines slightly dependant on the accelerating voltage.





X-ray Generation

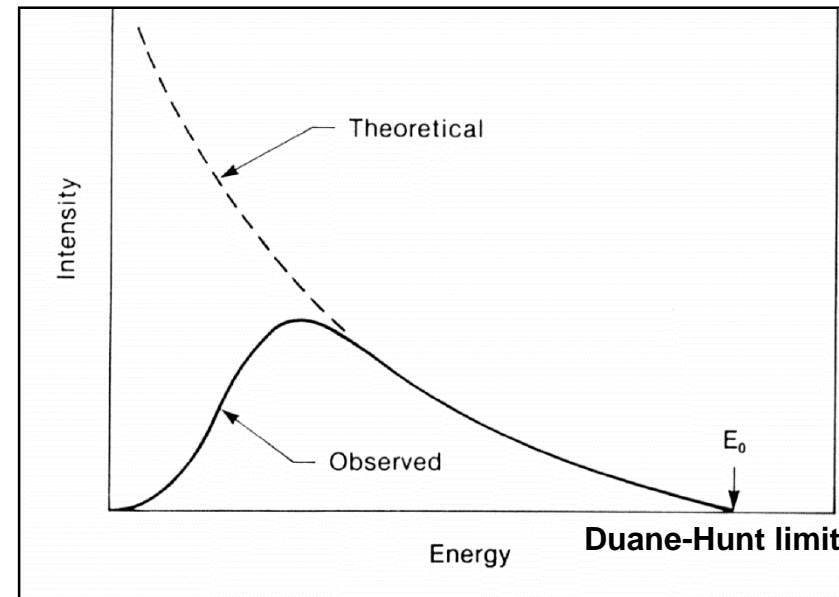
- Typical spectrum of Pt M radiation
- In theory one can expect for M lines to see dozens of peaks.
- However, most of these transitions will not be present since most orbits in the O, P and Q shell will be empty.
- Therefore even for very heavy elements we only see 2 to 4 peaks.





X-ray Generation - Continuum radiation

- Bremsstrahlung or background radiation is due to inelastically scattering
- In theory, the continuum can be expected to extend exponentially from the maximum energy of the primary beam electrons to zero keV energy.
- In reality, the background goes to zero at the low end of the energy spectrum due to absorption by the detector window and the detector dead layer.
- The intensity of the continuum is related to both the atomic number of the sample as well as the beam energy. The continuum intensity also increases with beam current.

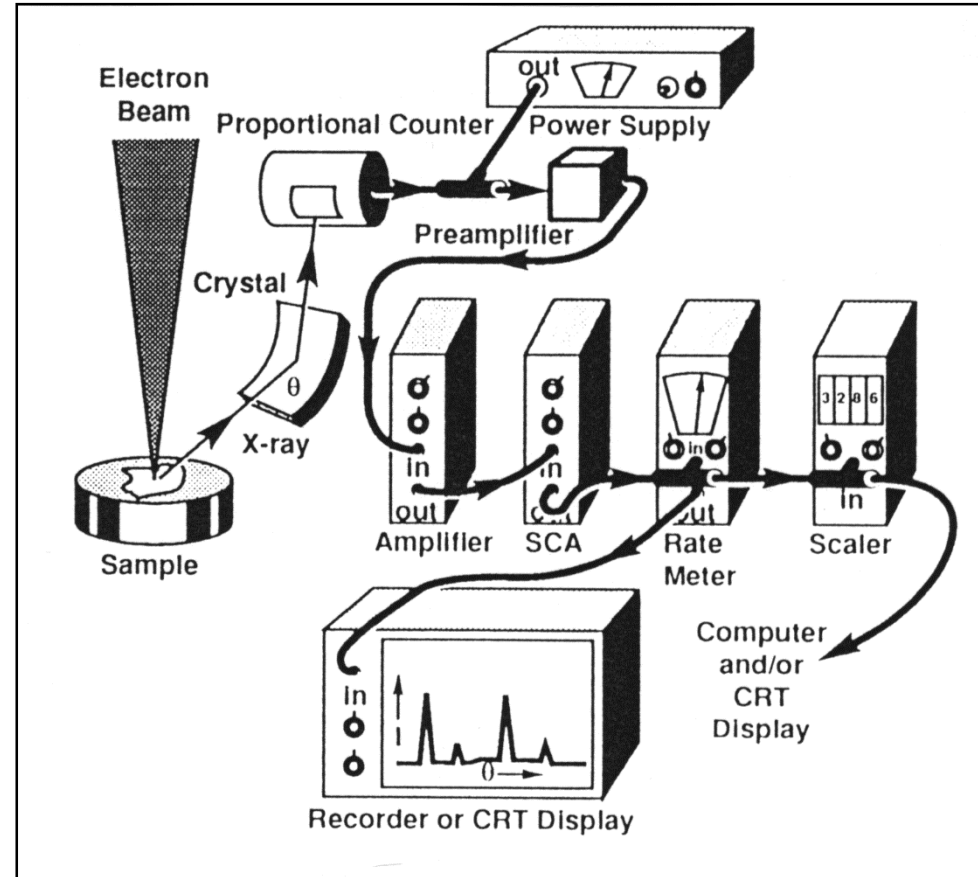


- **Background needs to be removed for quantification !!!**
- **It reduces the detectability limit in EDS !!!**



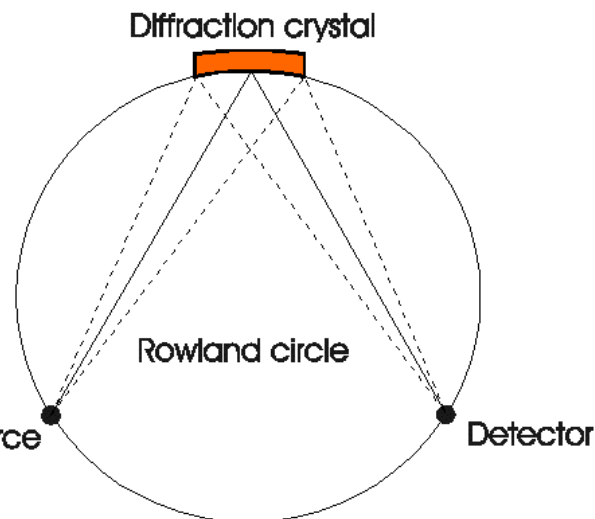
X-ray Measurement - WDS

- Based on separation of X-ray wave lengths by a monocrystal (diffraction)
- Good resolution, poor detector efficiency
- Excellent detection limit: good for finding trace elements
- SLOW; elements detected depends on number of spectrometers



WDS = Wavelength dispersive spectrometry

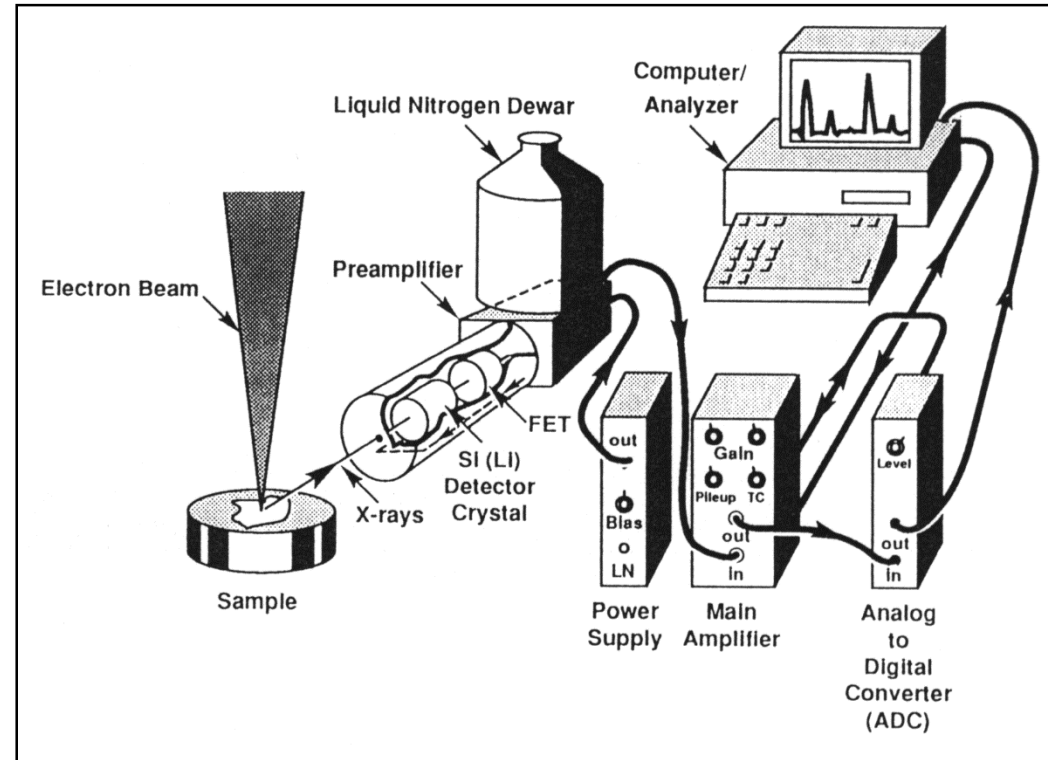
The X-rays emitted by the sample are travelling to a diffracting crystal. Most X-rays will travel straight through the crystal, but some X-rays that have a very specific wavelength will be diffracted. The diffraction condition depends on the Bragg-law





X-ray Measurement - EDS

- Based on separation of energies
- Simultaneous analysis of all energy levels
- Fast, poor resolution, high detector efficiency



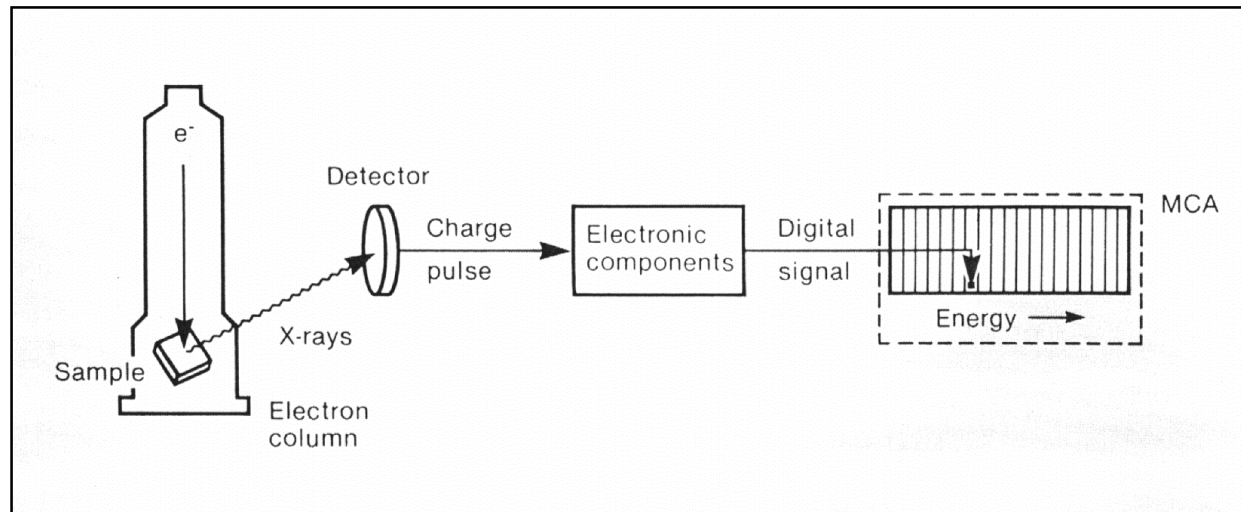
EDS = Energy dispersive spectrometry

The device consists of a detector, mounted in a tube and cooled by liquid nitrogen (the electronics are near the detector, which also requires cooling) and the multichannel analyser (MCA) that processes data.



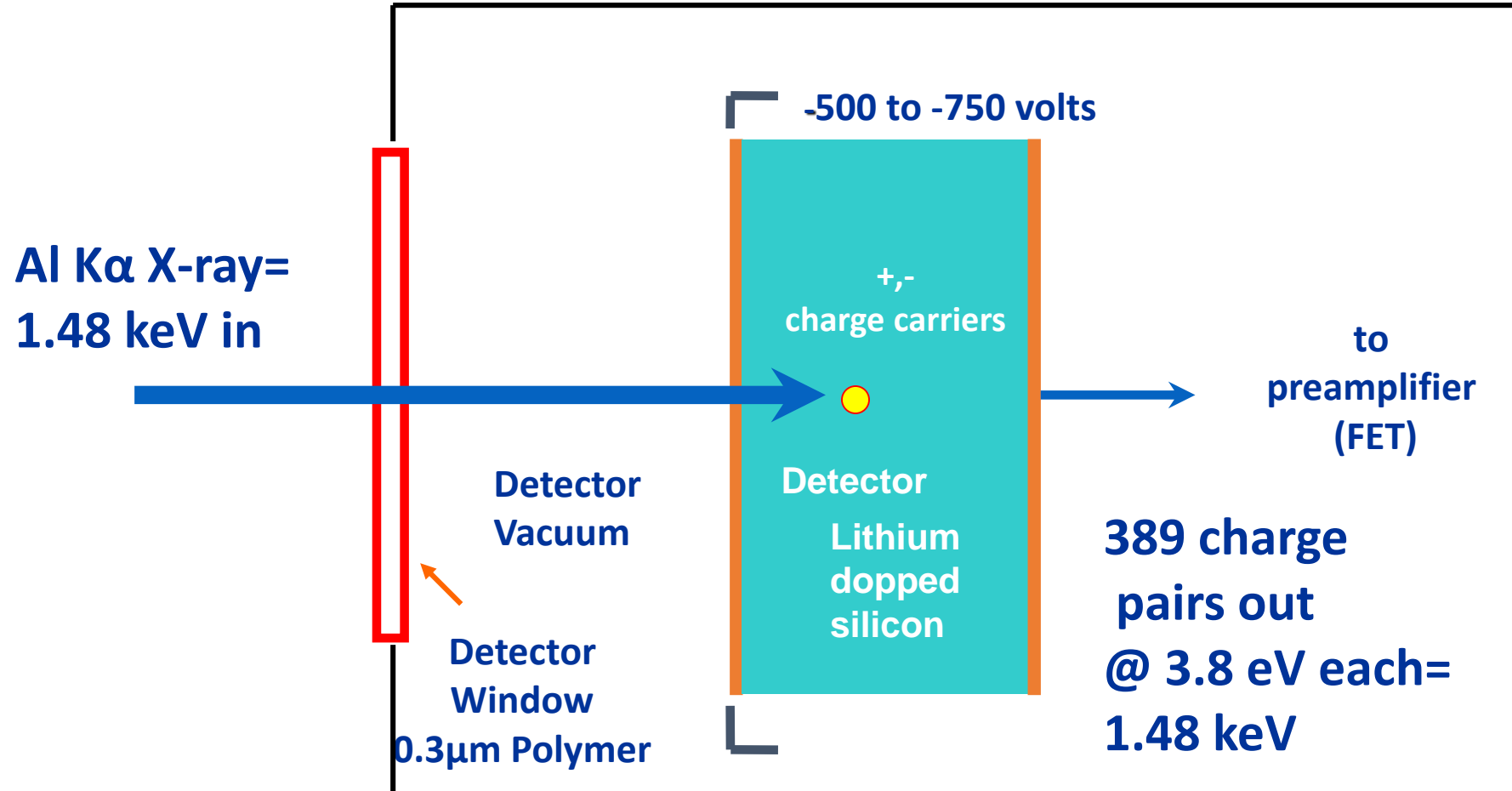
X-ray Measurement - EDS detector

- In EDS each emitted X-ray produces a charge pulse in a semiconductor detector (Si-Li detector coated at the front with a thin layer of gold)
- The small current is converted first into a voltage pulse then into a digital signal reflecting the energy of the original X-ray
- The digital signal in turn, adds a single count to the appropriate channel of a multi-channel analyzer (MCA)
- Multiple counts results in broad peaks



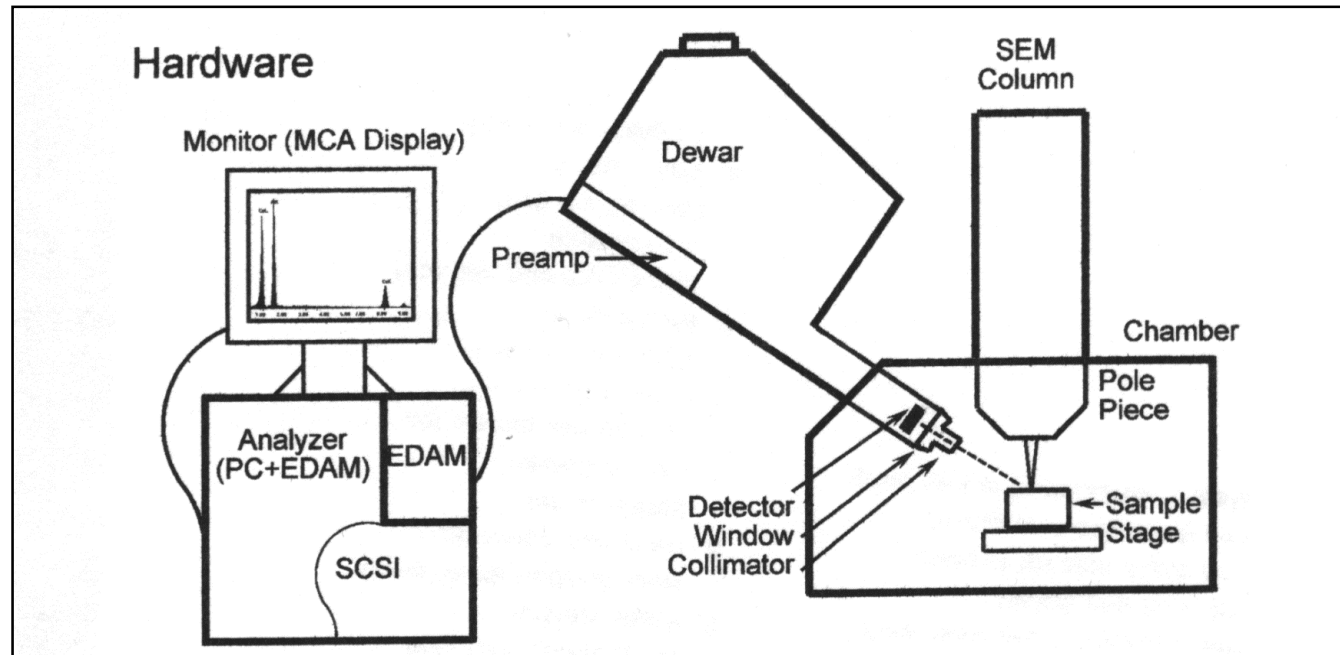


X-ray detection in EDX





X-ray Measurement - EDS System layout



EDAM - digital pulse processing electronics

SCSI- Small Computer System Interface

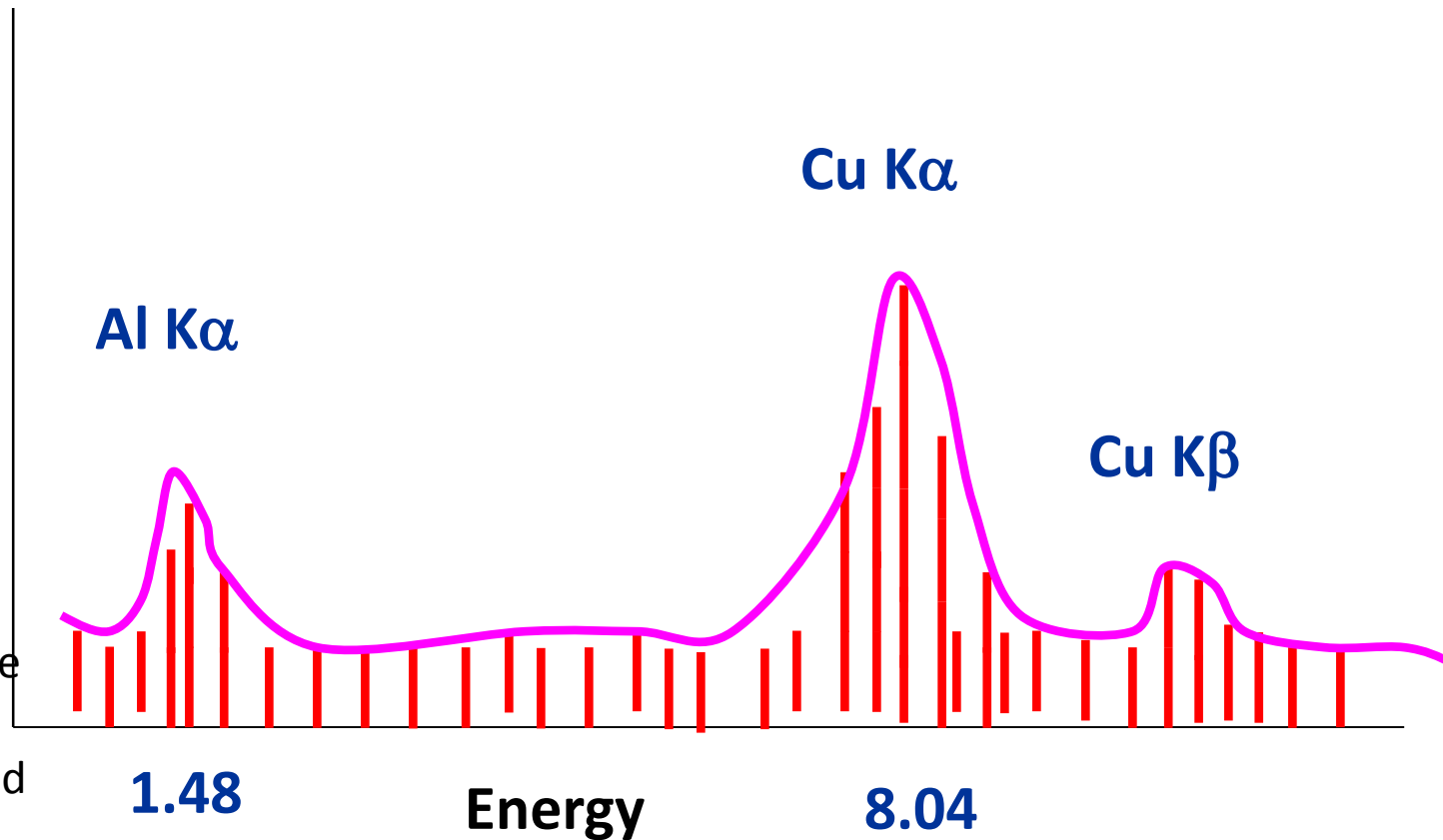
The processed pulses are digitised using an Analogue to Digital Converter. This device measures the voltage height of each event and sorts the events into a multichannel memory. This memory is organised such that each channel represents 10ev of energy. From this digitised spectrum, the X-ray intensities from each element can be obtained.



How a spectrum grows

Counts

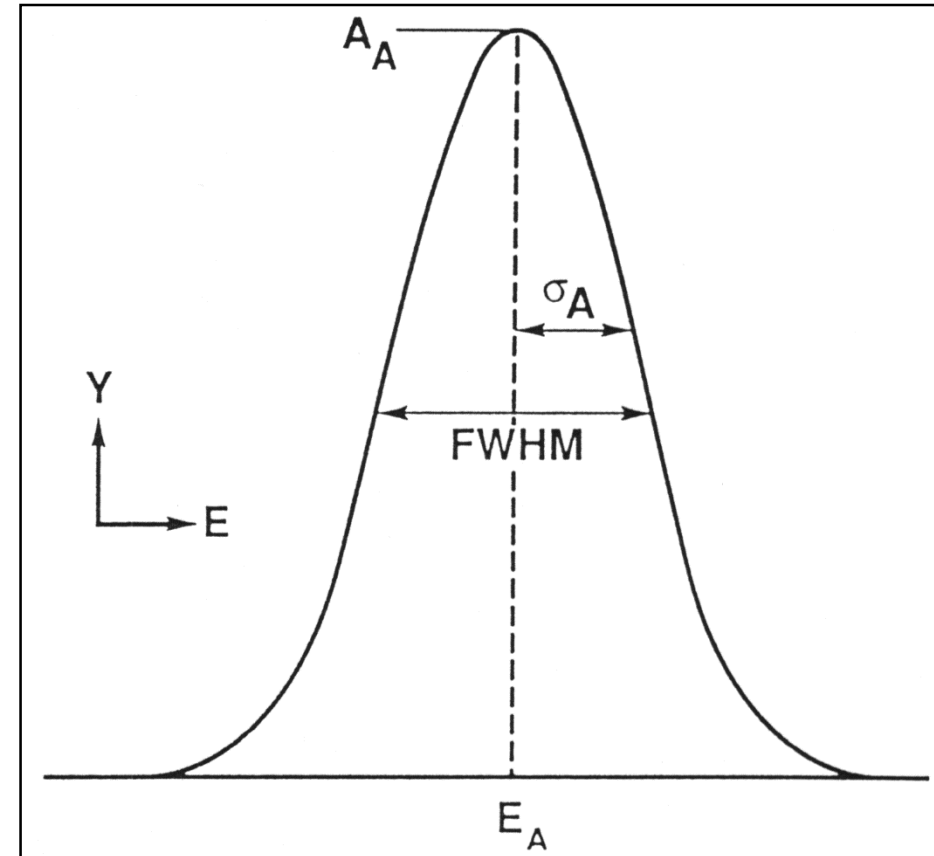
- A pulse is placed in the associated energy channel.
- As more events are counted, the spectrum becomes more pronounced and the peaks stand out over the background.





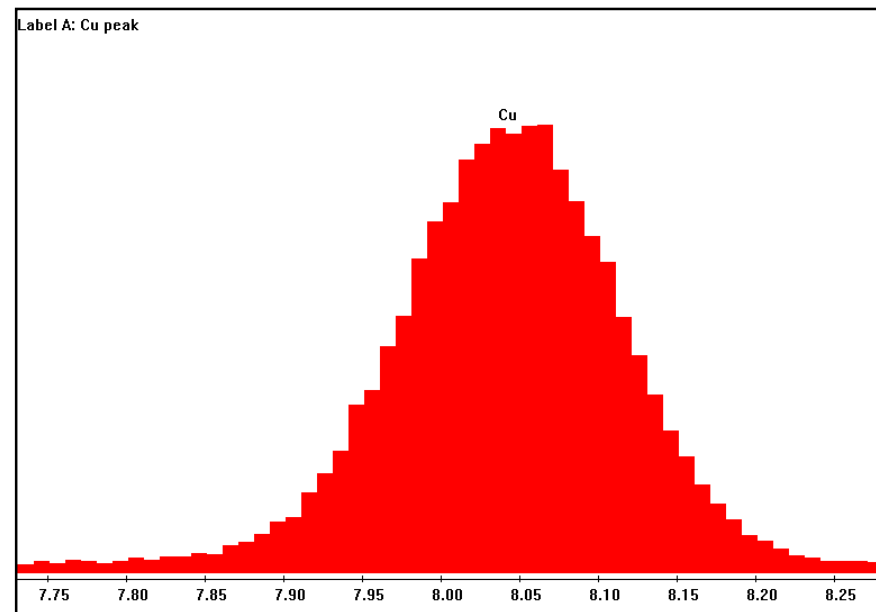
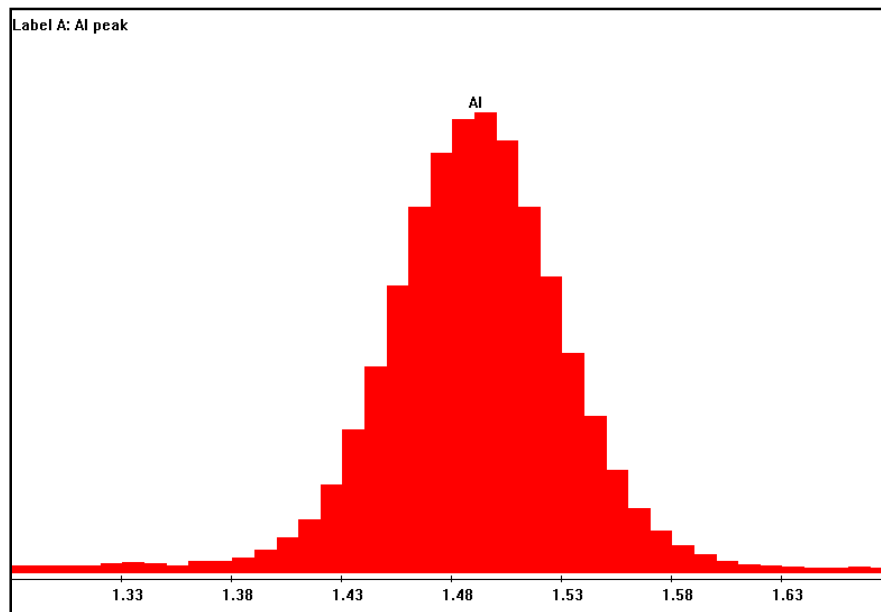
X-ray Measurement: Resolution of the X-ray line

- The original width of an X-ray peak at FWHM (Full Width at Half Maximum: the width of the peak at half the peak height), which is of the order of 2 eV (2.3 eV for Mn $K\alpha$),
- FWHM - resolving power of the detector based on Mn- $K\alpha$ line
- Peak broadening by electrical noise and statistical errors
- Today's detectors:
126 - 132 eV (Mn $K\alpha$)





X-ray Measurement: Resolution of the X-ray line



Al FWHM 95 eV

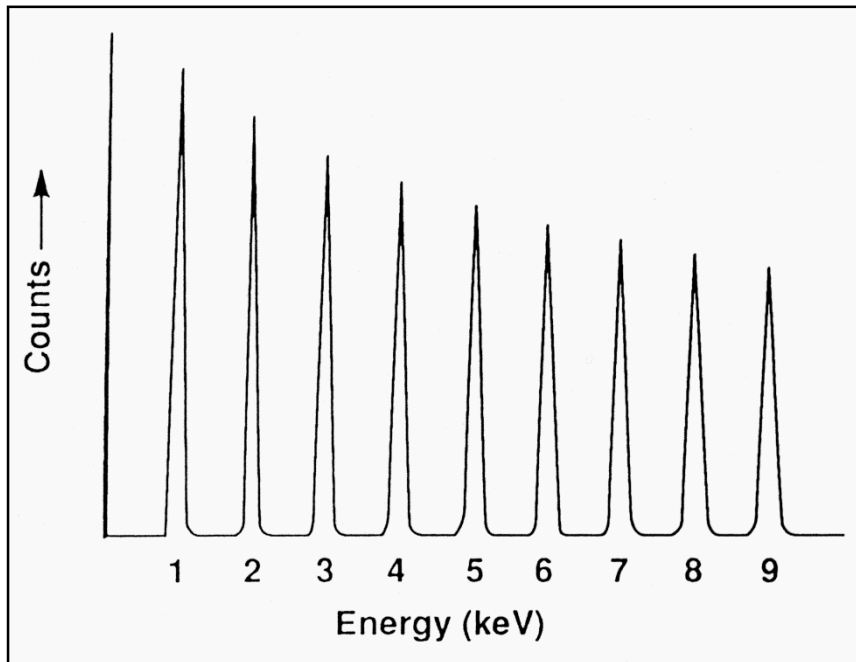
Cu FWHM 150 eV

10 eV / channel



X-ray Measurement: Resolution of the X-ray line

- Resolution depending on energy
- Approximately 3- 4 eV per element difference
- Al K FWHM = 95 eV
- Cu K FWHM = 150 eV
- Resolution depending on :
 - Count rate
 - Amplification time - time needed to process the X-ray event
 - Dead time - time when the detector or preamplifier is unable to accept a pulse because it is busy processing or rejecting an event(s)



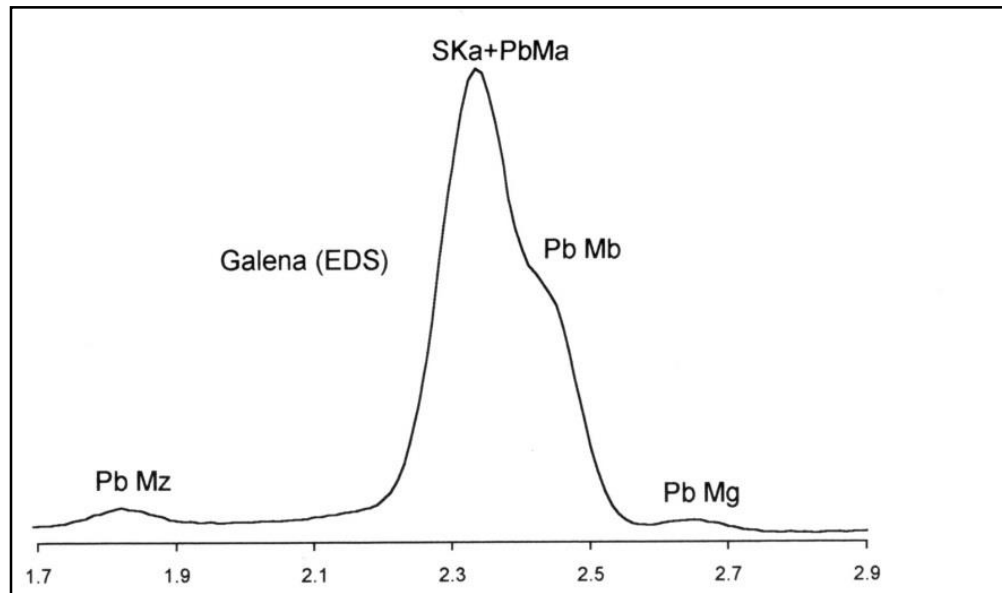
Resolution and peak intensity as a function of energy

Since the noise in the detector is uniform, the FWHM of the X-ray peaks varies with the X-ray energy. It can be seen that the FWHM increases with X-ray energy, from about 95 eV for Al (K at 1.486 keV) to about 150 eV for Cu (K at 8.040 keV). The displayed resolution is always that of the Mn $K\alpha$ line. As a rule of thumb the resolution (or FWHM of the peak) will increase approximately 3 – 4 eV per element

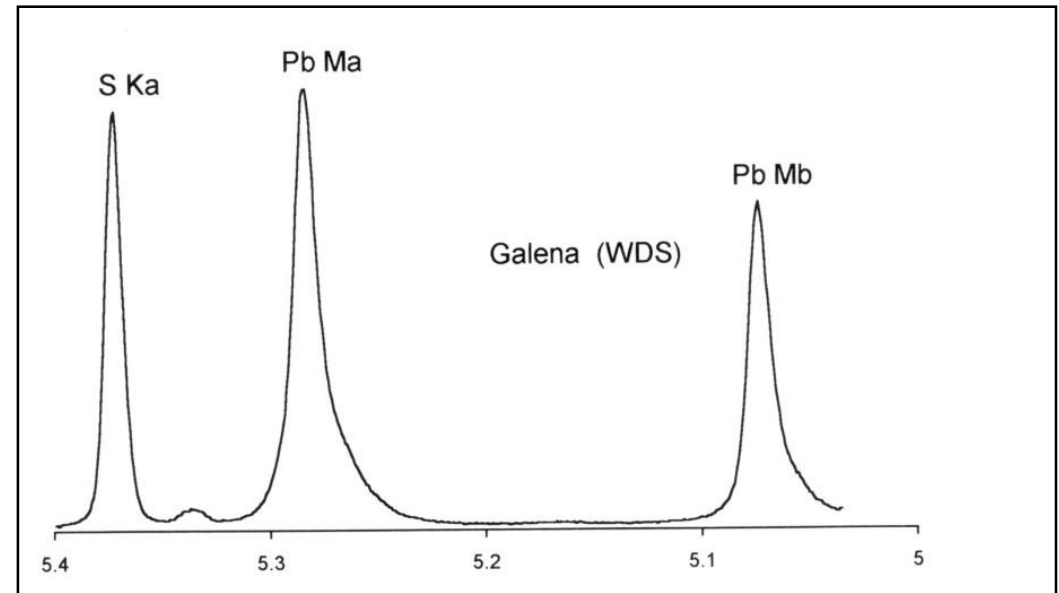


X-ray Measurement: Comparison resolution of EDS and WDS

Example of EDS and WDS : Overlap of Pb M α (2.342 keV) and S K α (2.307 keV),
difference = 35 eV



EDS

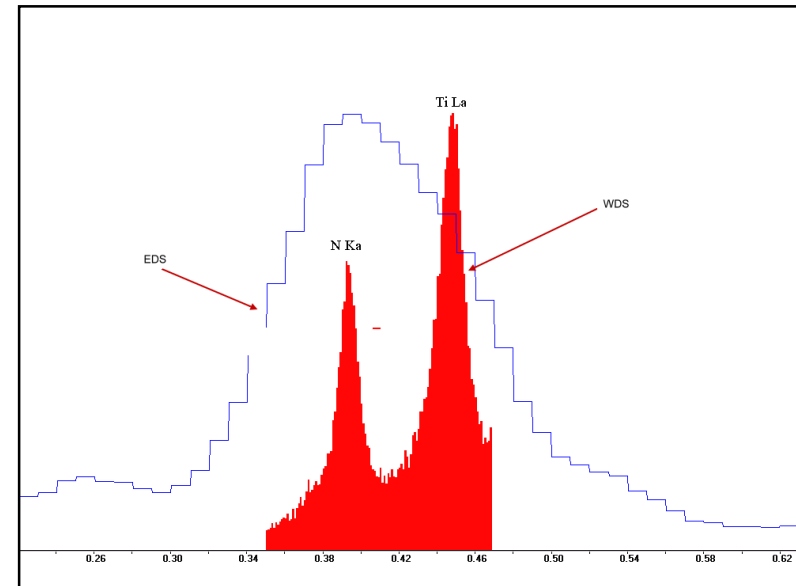
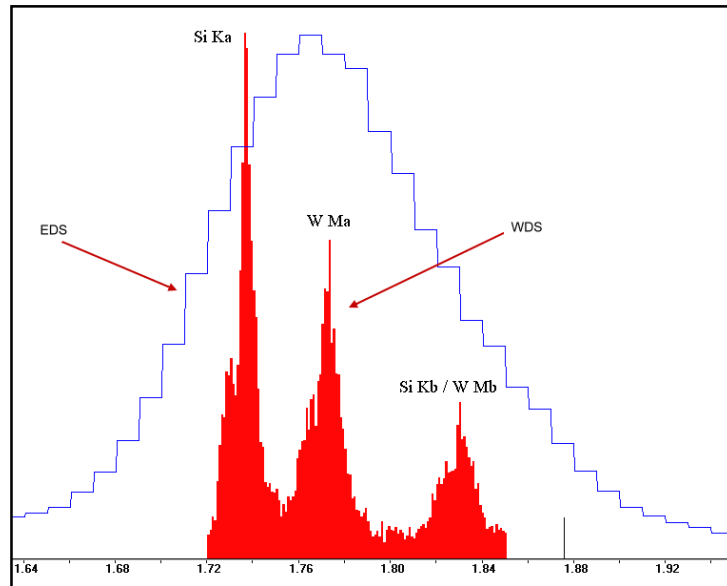


WDS

**The resolution of a WDS spectrometer is typically 5 to 20 eV (much better than at EDS).
So peaks that overlap in an EDS system are completely separated in a WDS system.**



X-ray Measurement: Comparison resolution of EDS and WDS



The much enhanced resolution in WDS also means the peak-to-background ratio is much better, and thus the detection limit will be lower.

Typically 10 to 100 ppm for WDS compared to 500 to 2000 ppm for an EDS



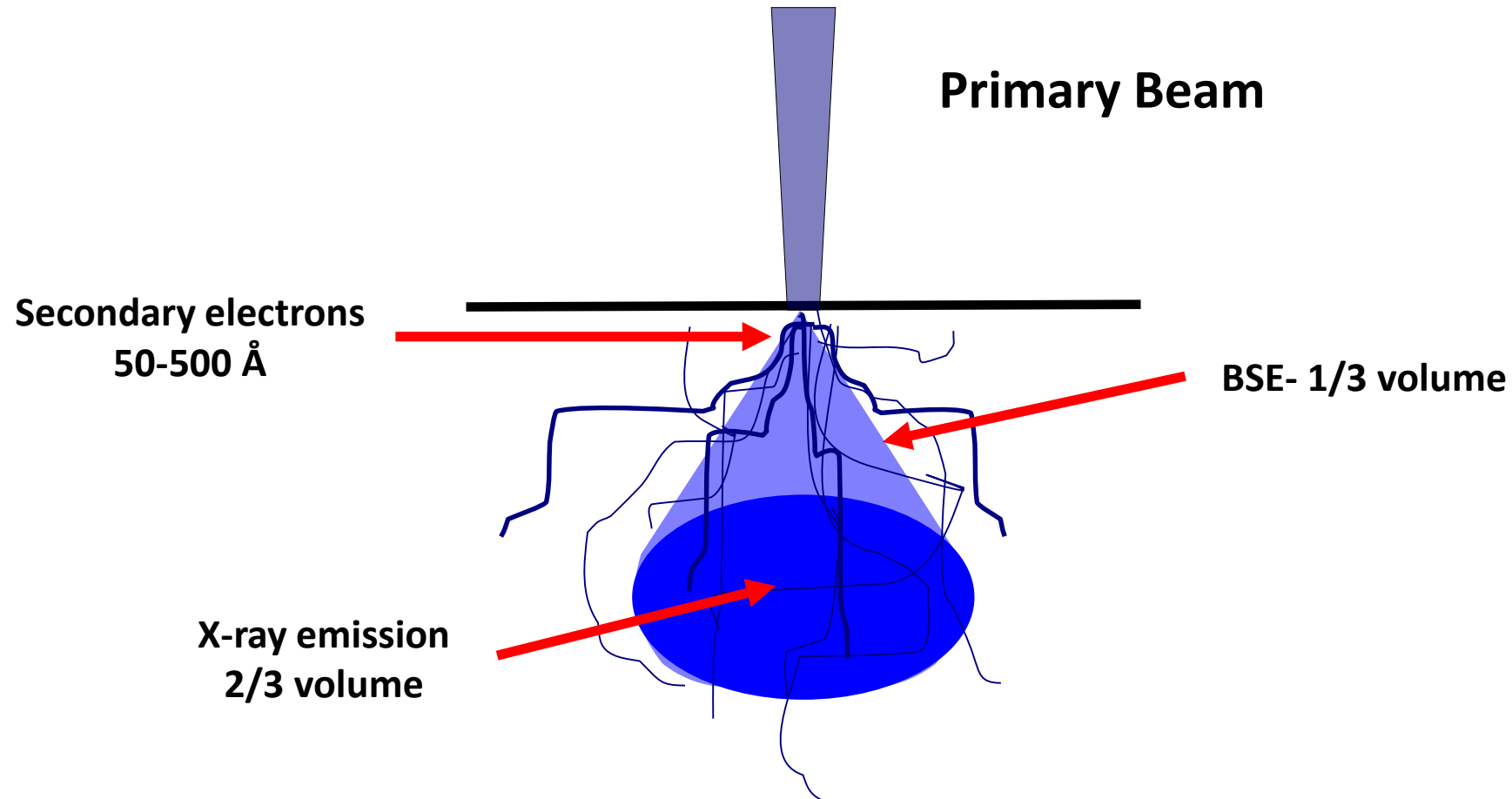
Beam - Specimen Interaction

Depth of Excitation

- Electrons lose energy in steps as they go deeper in the sample.
- The electron energy may drop below the **critical ionization energy** of the element in the sample.
- The ratio of the primary beam energy to the excitation of the element is referred to as the **overvoltage**.

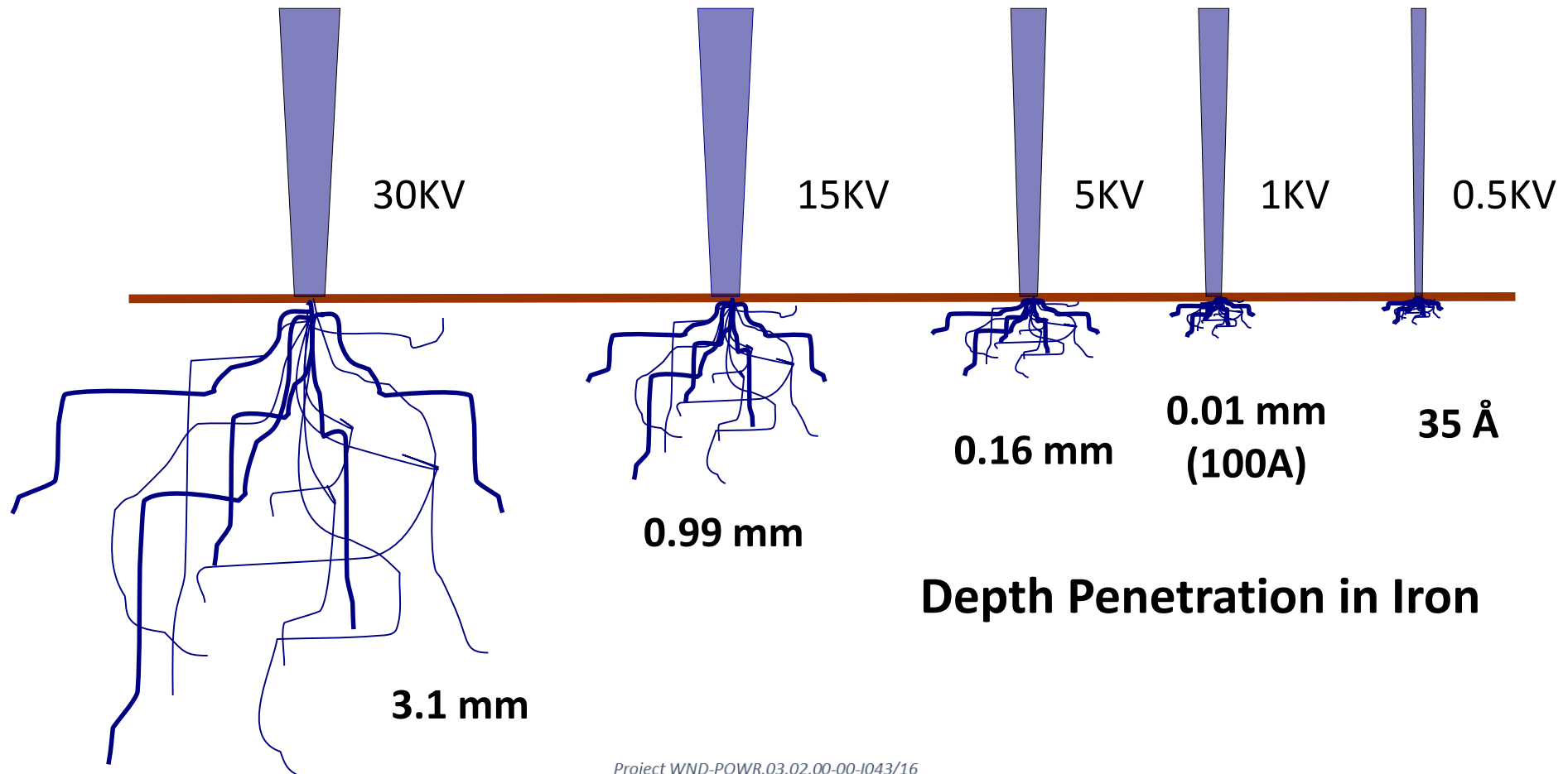


Shape of Electron Beam Penetration



Influence of Accelerating Voltage

Primary Beam



Depth Penetration in Iron

Project WND-POWR.03.02.00-00-1043/16

International interdisciplinary PhD Studies in Materials Science with English as the language of instruction

Project co-financed by the European Union within the European Social Funds

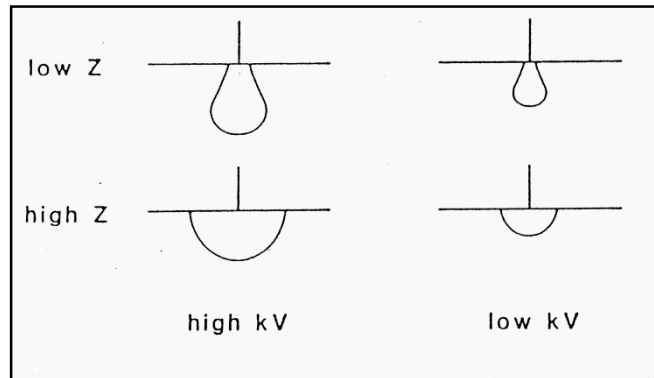


Beam - Specimen Interaction

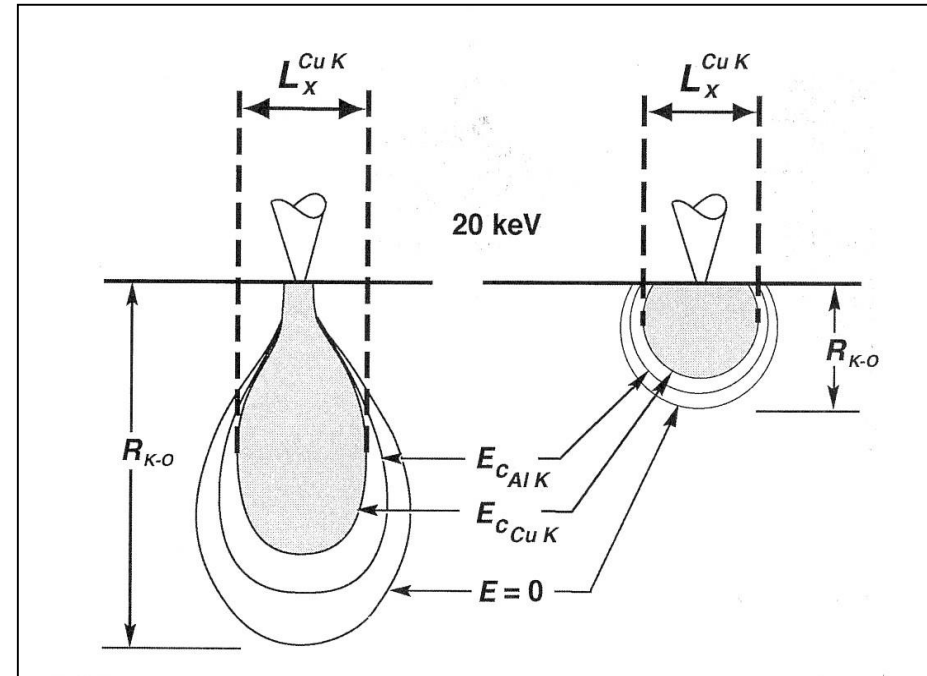
Spatial resolution

X-ray spatial resolution depends on:

- Material
- Acceleration voltage
- Specimen tilt angle



The variation of incident electron beam distributions with atomic number and voltage



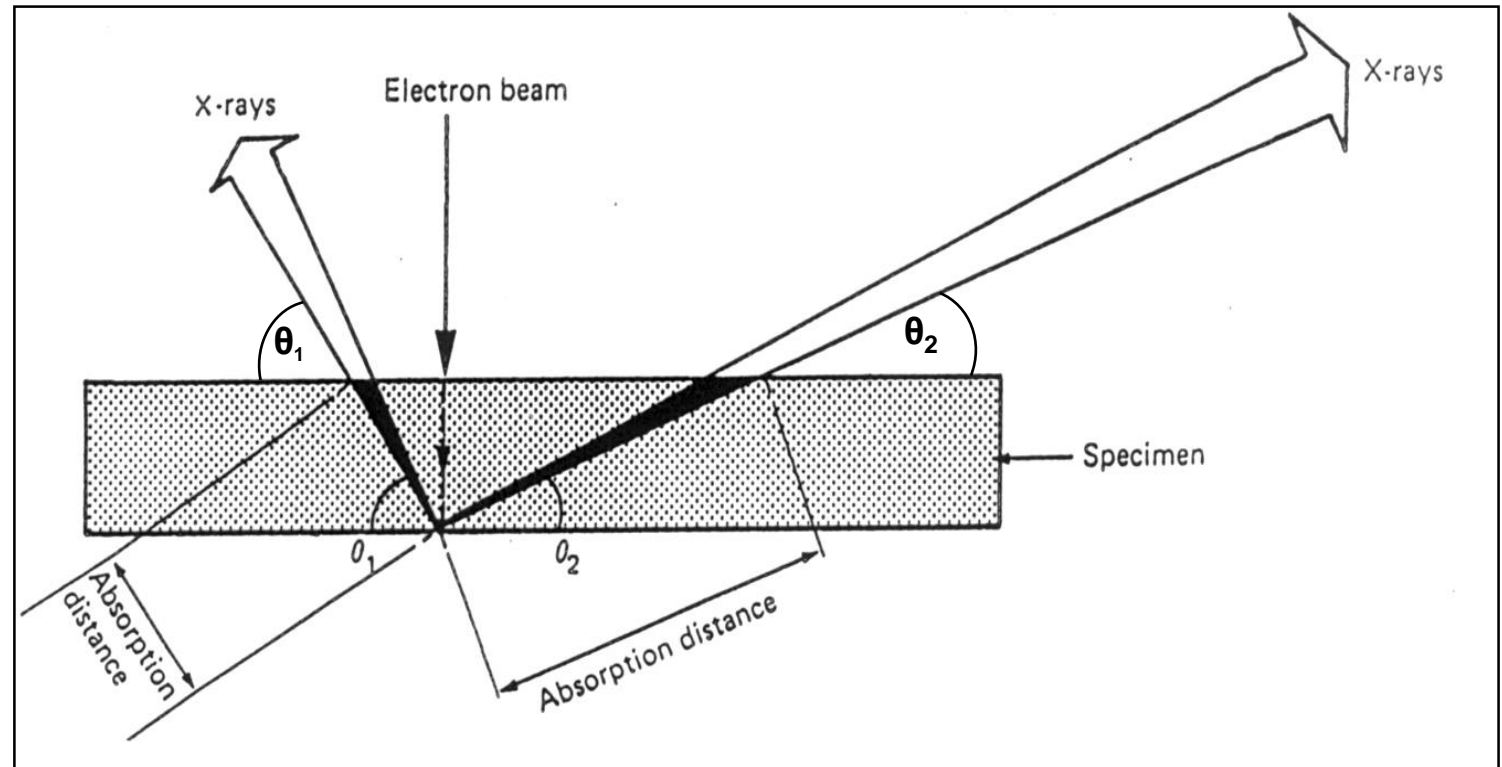
Comparison of X-ray production from specimens with densities of 3 g/cm² (Al – left) and 10 g/cm² (Cu - right) at a beam energy of 20 keV.

The X-ray spatial resolution is found by projecting the maximum diameter of the X-ray distribution on the surface of the specimen



Operation of the Analytical Microscope Geometry

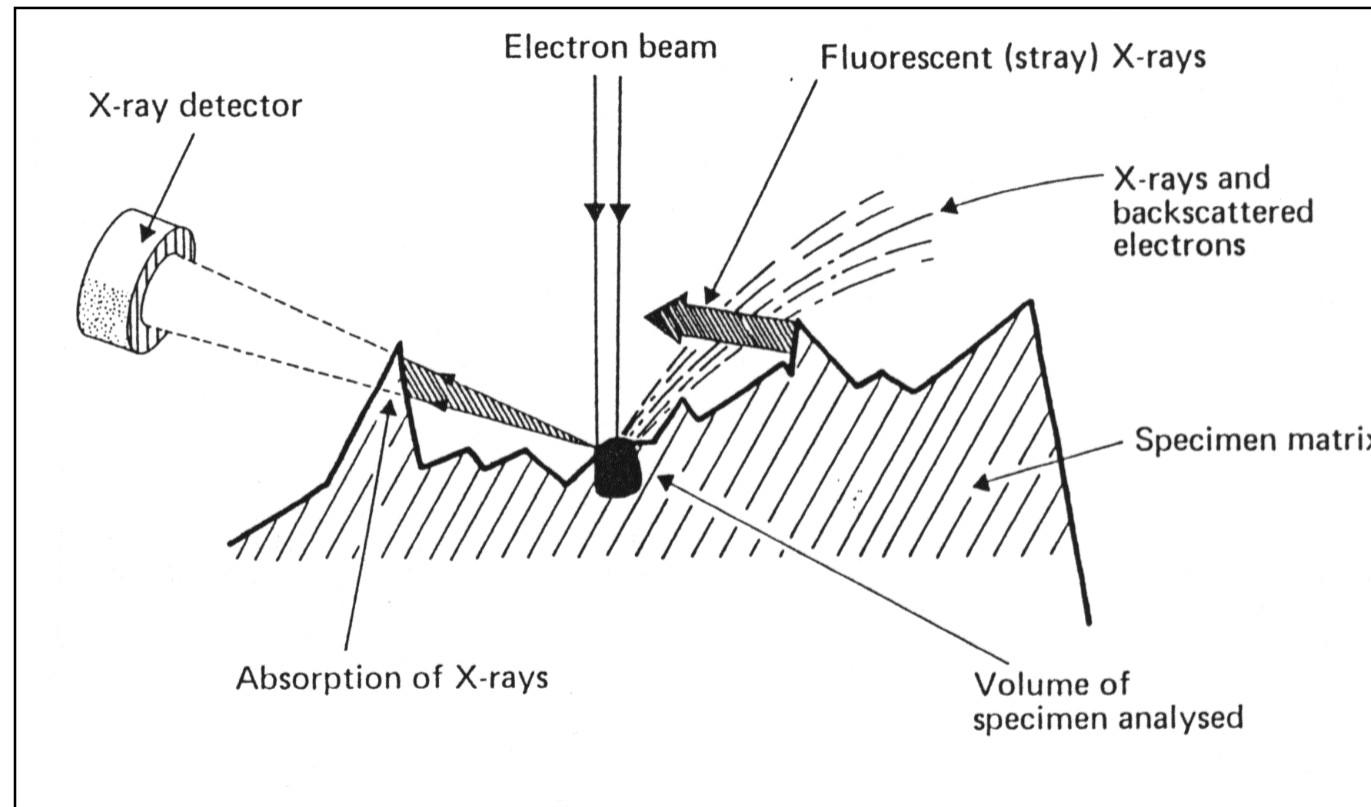
- Collection of X-rays by the detector depending on distance and angle from detector to the sample
- X-ray leaves specimen under an angle so called: Take - Off Angle (TOA)





Operation of the Analytical Microscope Topography

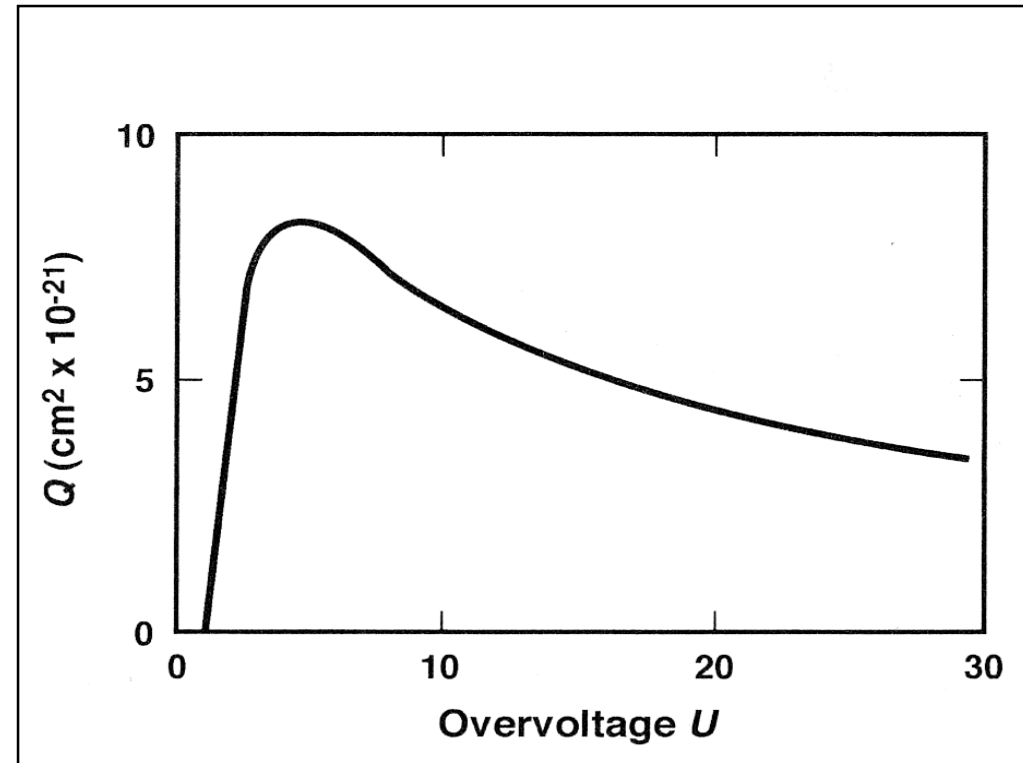
- Surface roughness has also an influence to the X-ray signal (different intensity)
- High surface roughness can lead to anomalous absorption, which the quantification software cannot take into account.





Operation of the Analytical Microscope - Overvoltage

- **Overvoltage** - a ratio of accelerating voltage used to the critical excitation energy of a given line for an element
- ↓
- Incoming electron must be higher in energy than the critical excitation energy of the element
 - Detection starts at an overvoltage of about 1.5.
 - Optimum : 2 - 5 x the energy of the emission line
 - For Fe $K\alpha = 6.4$ keV
needed voltage 20 - 25 kV

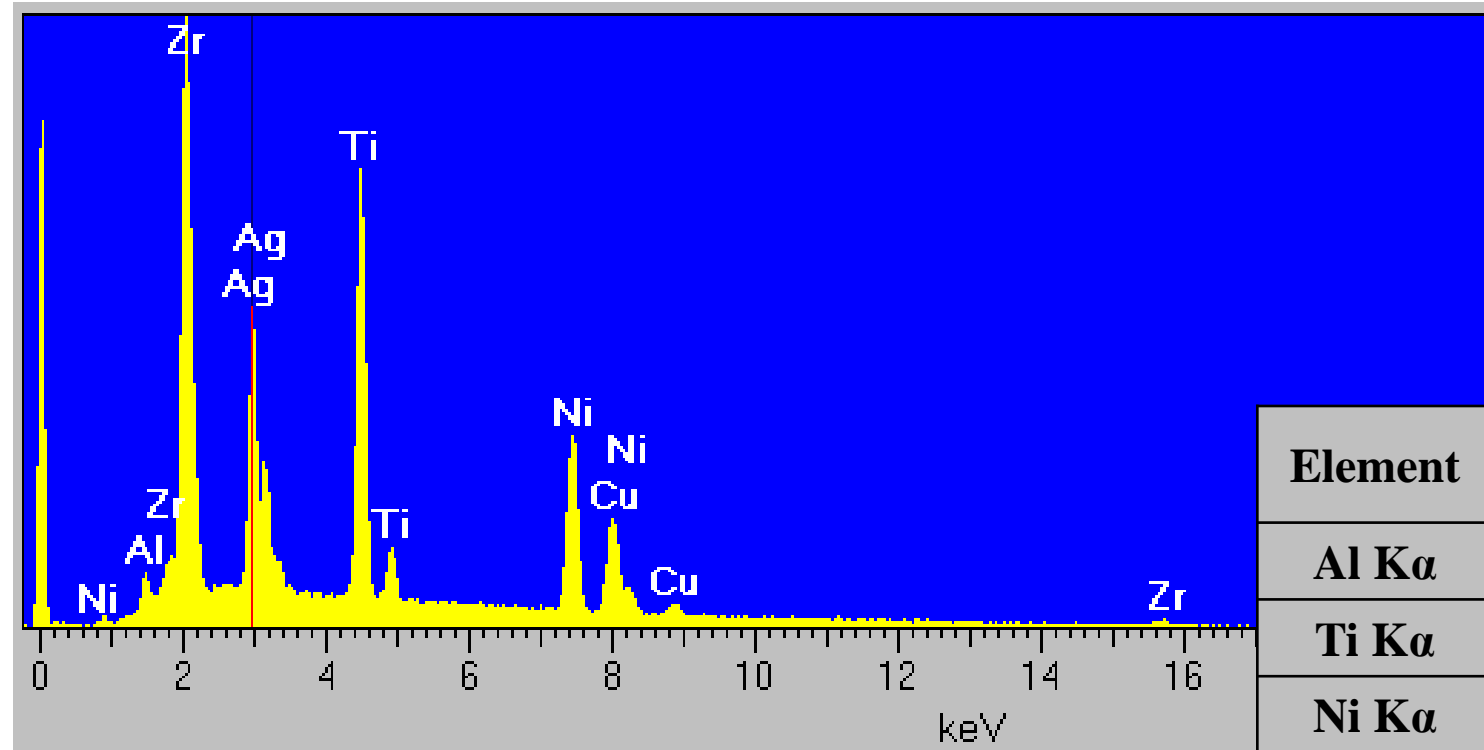


For example, if you are interested in analysis of a phase containing Fe, Mg and Si and want to use the K lines for each, then 15 kV will probably work reasonably well. If, however, you need to analyse the same three elements plus oxygen as well, then you might use 5 to 10 kV, but you might want to use the L line for the Fe.



Qualitative analysis - Peak ID

- Identification of all possible peaks
- Auto or Manual Peak ID
- Do not trust system
it is not 100% reliable
- Be aware of:
spectral artefacts
skirt effects
(low vacuum systems)



Element	%wt.	%at.
Al K α	1.05	2.75
Ti K α	17.74	25.92
Ni K α	17.79	21.21
Cu K α	11.72	12.91
Zr L α	31.17	23.92
Ag L α	20.53	13.32
Total:	100.00	100.00



Qualitative analysis - Peak ID hints

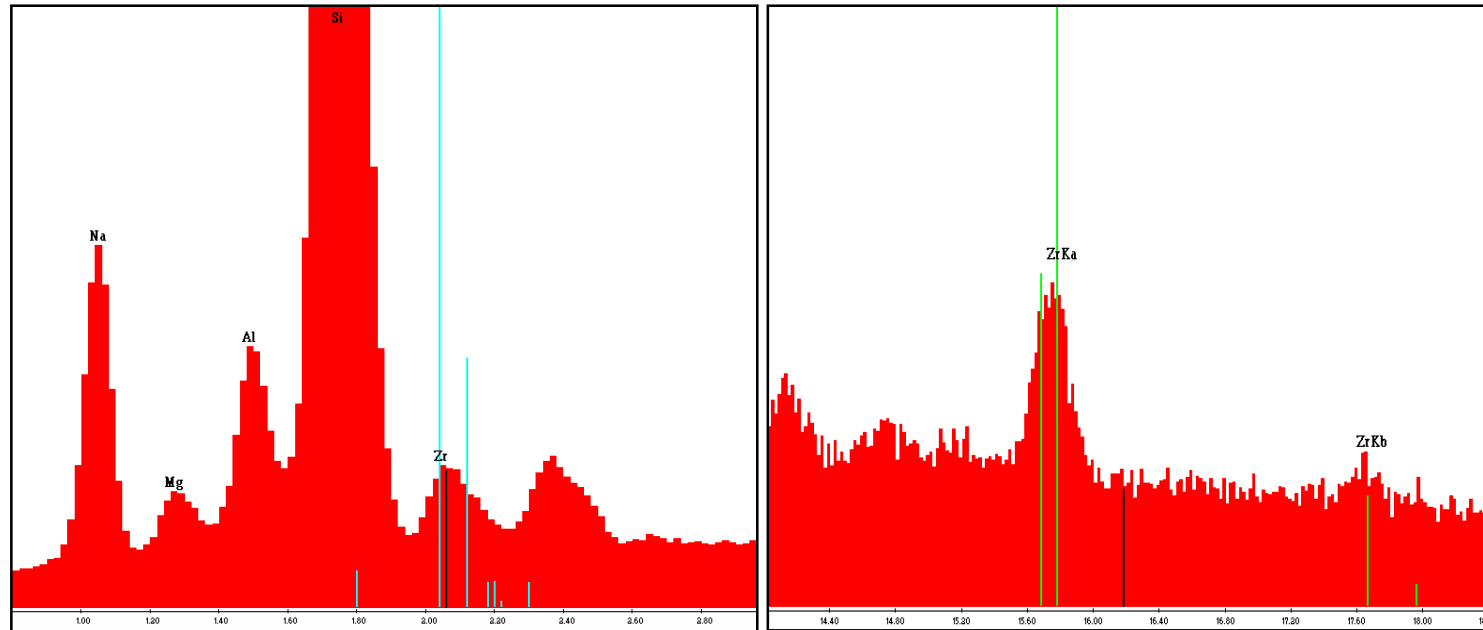
- Identification of an element
- Place cursor exact on the top of the peak (expand scale)
- L and M line can show shift due to poor separation of α/β lines
- First check main lines such as $K\alpha$, $L\alpha$ or $M\alpha$ lines
- Check the other lines of the same element
- Heavy elements will produce K and L radiation

We examine that part of the spectrum that ranges in energy between 0 and 10 keV and we quickly become aware of characteristic features of K-, L- and M-shell X-ray peaks that aid us in our peak identification. In this energy range, we can see **peaks with K-shell X-rays that correspond to atomic numbers 4 through 32, L-shell peaks that range from roughly atomic numbers 22 to 79, and M-shell X-rays ranging from 56 to the highest known and observable atomic numbers.**



Qualitative analysis - Peak ID

K-series peaks are typically fairly simple and consist of a $K\alpha$ and a $K\beta$ peak. The $K\beta$ peak occurs at a higher energy and starts to become resolvable from the $K\alpha$ for atomic numbers greater than S ($Z = 16$). The $K\beta$ peak is usually $1/8$ to $1/5$ the size of the $K\alpha$ peak



Zr L - lines and Zr K - lines (note the shift of the Zr L lines due to poor separation of α/β line)

The L-series peaks are much more complex than the K-series peak(s), and may consist of as many as 6 peaks: an $L\alpha$, $L\beta_1$, $L\beta_2$, $L\gamma_1$, $L\gamma_2$ and $L\iota$. The peaks were arranged from highest energy to lowest energy with the exception of the $L\iota$ peak which occurs before (at a lower energy than) the $L\alpha$ peak.



Operation of the Analytical Microscope

- Operation the SEM to obtain optimum X-ray results
- Main variables:
 - Spot size (current)
 - Acceleration voltage (overvoltage)
 - Sample - Detector Geometry
 - Aperture selection (FEG)
 - (Column alignment)
 - (Collimator)
 - (Working distance)
 - (Topography)

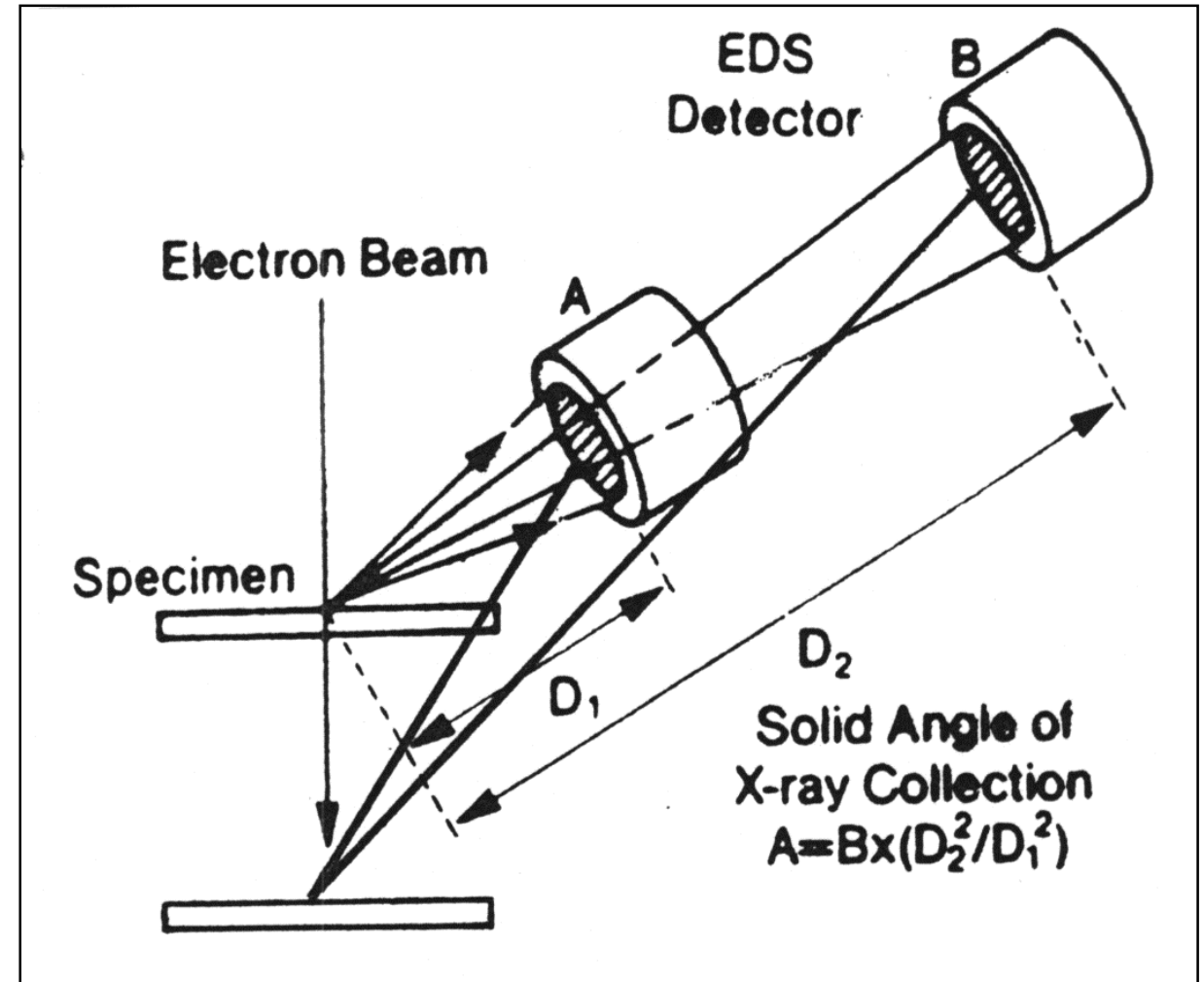


Operation of the Analytical Microscope Geometry

The efficiency of collection is controlled by the sample-to-detector geometry. The two factors that affect the number of X-ray photons that reach the detector are:

- **solid angle** (the amount of three-dimensional space around the specimen that is "seen" by the detector; the value of the solid angle depends on the specimen-detector distance and the total surface of the detector and affects the count rate)
- **take-off angle** (defined as the angle between surface of the sample and a straight line to the detector)

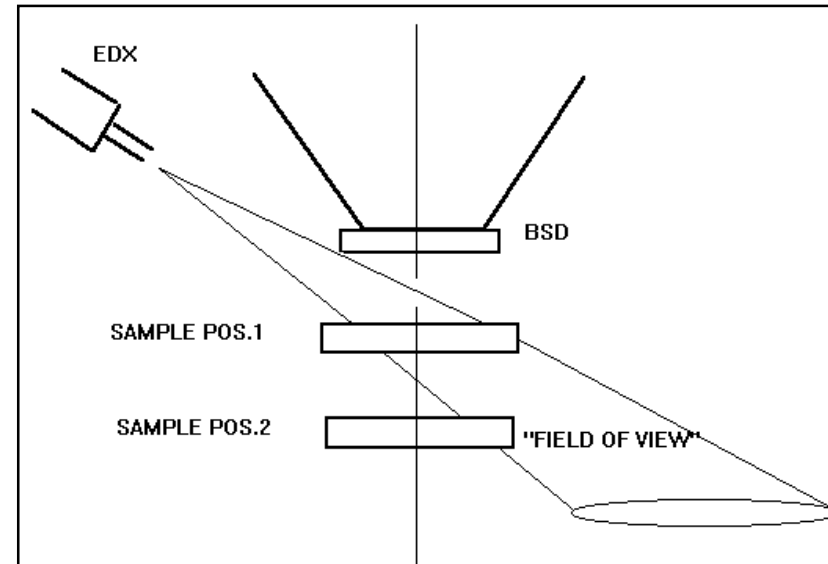
Moving the detector closer to the specimen (from D1 to D2) increases the solid angle of collection and sensitivity.





Operation of the Analytical Microscope Sample position

- Working distance is very important
- Optimum sample position
- eucentric position - 10 mm (S-FEG - 5 mm)
„eucentric” from the Latin for well-centred; it implies that tilting the specimen can be achieved without the field of view moving.
- Field of view of the EDX detector: 9 -12 mm (S-FEG: 5 - 6 mm)
- Below 12 mm: inhomogeneous “illumination” of the field at low magnification



Each SEM has its own geometry. The better the geometry, the more flexible your system will be. Always remember that the detector is focused at the eucentric point.



Operation of the Analytical Microscope - Geometry

- Fixed:

D – intersection distance (the distance in mm between the pole piece to where the electron beam intersects the detector normal)

E – elevation angle (the angle between the horizontal and the detector normal)

- Variable:

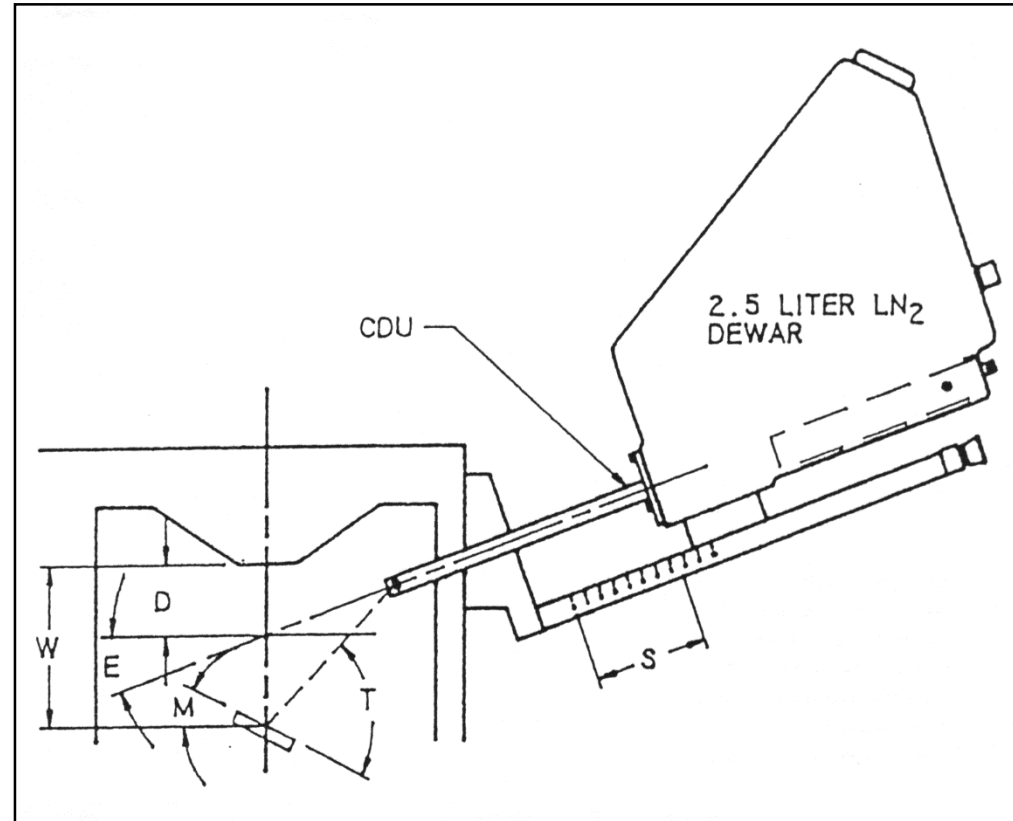
W – working distance (the distance from the pole piece to the sample surface)

S – scale setting

M – sample tilt

- Calculated:

T – take-off angle



If the sample is placed at the intersection distance and not tilted, the take-off angle will equal the elevation angle and working distance will equal intersection distance.



Spectral artefacts

Poor counting statistics

- A low count rate results in a 'noisy' spectrum => poor statistics
- 'Noisy' spectrum will introduce Peak ID errors
- System will identify noise (Auto ID)

Solution

- Long acquisition time
disadvantage: limited number of specimens per day
- High count rate in combination with appropriate amplification time disadvantage:
poor peak separation
- Find the ideal combination for your own samples
 - qualitative/quantitative work: 2500 cps (DT 40%) at Amp. Time 50 μ sec
 - acquisition time 100 live sec



Spectral artefacts - Peak overlap

- EDS has a relatively poor resolution: as a result peaks overlap
- Difference at least 60 eV to separate lines
- To improve result: use standards

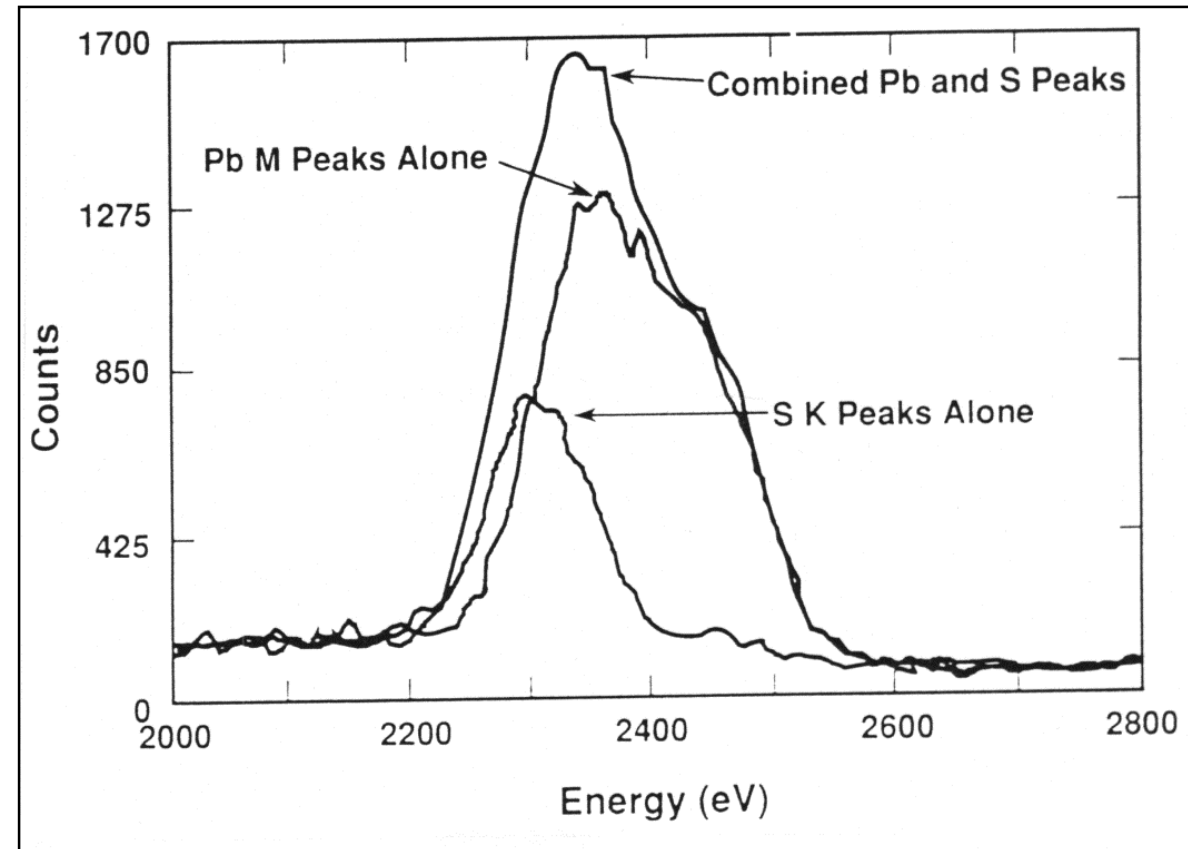
- Classical example:
Pb M α - 2.345 keV
- S K α - 2.307 keV
- difference = 38 eV

Some examples of overlap:

Cr K β - Mn K α 52 eV

Ti K α - Ba L α 41 eV

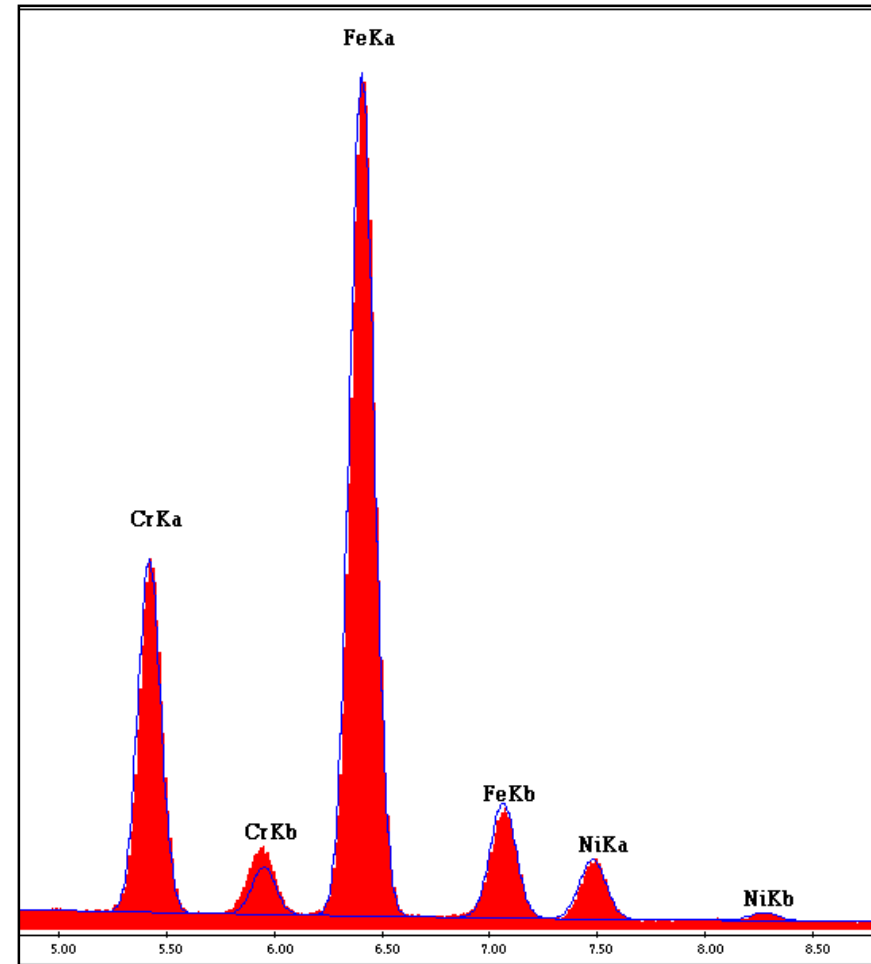
Mo L α - S K α 15 eV





Qualitative analysis - Deconvolution

- Deconvolution is used in the quantification routine to estimate the size and position of all peaks associated with each assigned element. The fit of all the peaks calculated is shown as a lined spectrum on top of the background, so that any serious gaps or misfits can be observed by the user.
- The peak-fitting routine is most accurate for the K-series peaks. The complexity of the L-series peaks does not permit as accurate of a fit, but in most cases this fit will be more than adequate to identify the peaks.





Spectral artefacts - Dead time

- Dead time means that system is busy with pulse shaping
- Dead time - relationship of input and output count rate
- Dead time depending on amplifier process time (APT)
- **Reasonable dead time 30 - 40 %**
- **High dead time: system is slow**
- **Result: sum peaks and peak broadening**

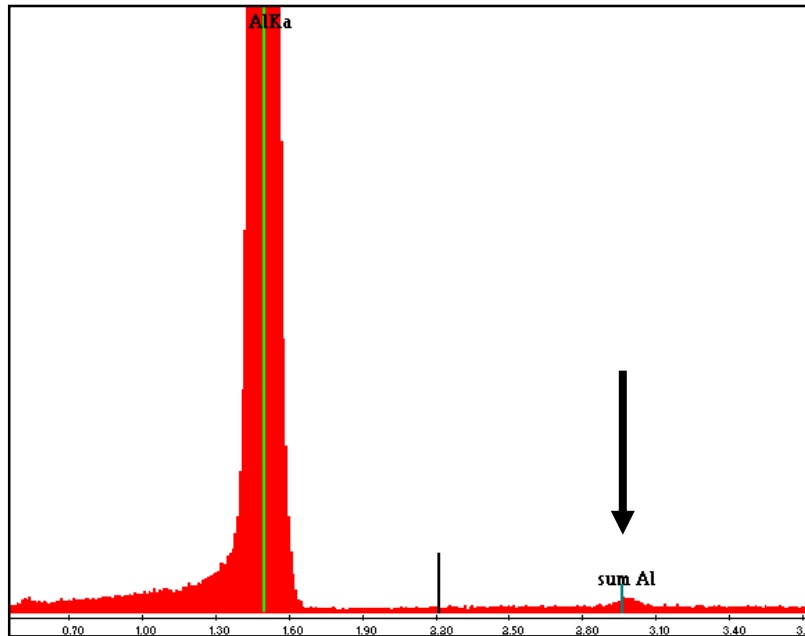


Spectral artefacts - Sum peaks

- Sum peaks due to pulse pile-up effects
- Two X-rays are entering detector at the same time
- Sum of the energies is seen as one energy
- Sum peaks depending on too high count rates
- Not only pure elements: combinations possible
- Prevent sum peaks by keeping dead time at the level 25% - 35%

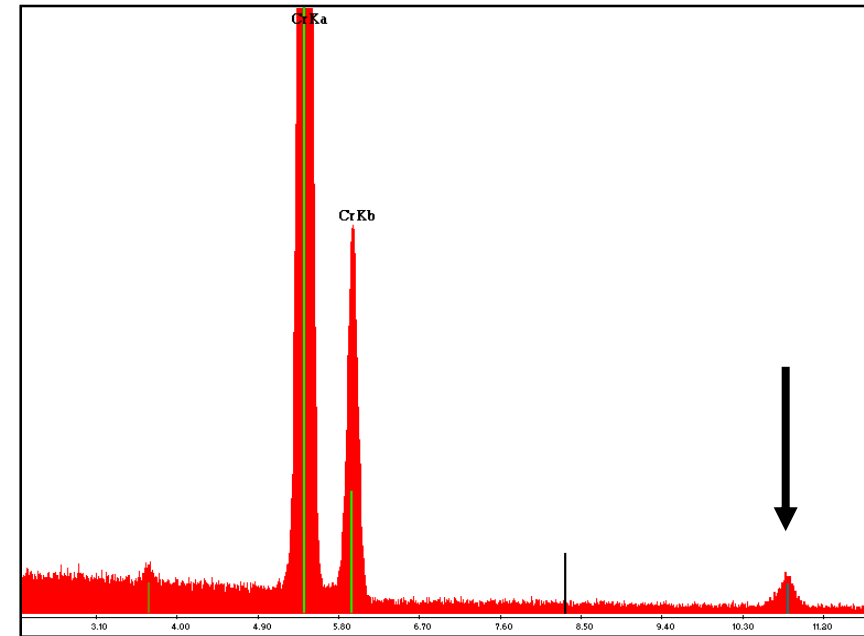


Spectral artefacts - Sum peaks



Spectrum of Aluminium at high count rate showing the Al sum peak at twice the $K\alpha$ energy.

$$\text{Sum peak Al } K\alpha = 2 \times 1.487 \text{ keV} = 2.974 \text{ keV}$$



Spectrum of Chromium at high count rate showing the Cr sum peak at twice the $K\alpha$ energy.

$$\text{Sum peak Cr } K\alpha = 2 \times 5.411 \text{ keV} = 10.822 \text{ keV}$$



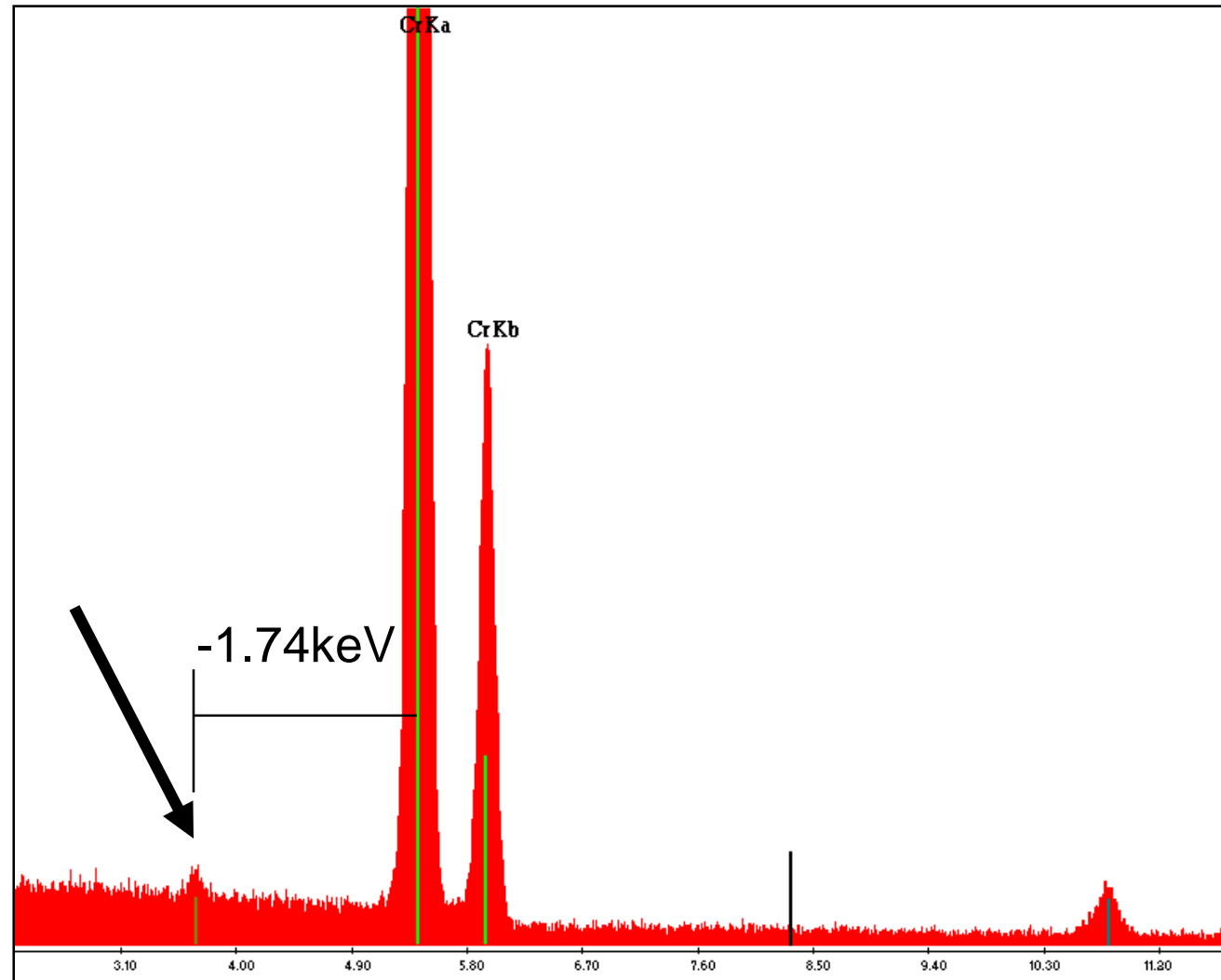
Spectral artefacts - Escape peaks

- Escape peak: result of losing Si K energy in the Si-dead layer of the crystal
- Si K line = 1.74 keV
- Remaining energy is original energy minus Si K energy
- Difficult to identify
- Intensity of the escape peak belongs to the main peak
- Example :
 - Fe escape peak = same position as La $L\alpha$ peak**
 - Cr escape peak = same position as Ca $K\alpha$ peak**



Spectral artefacts - Escape peaks

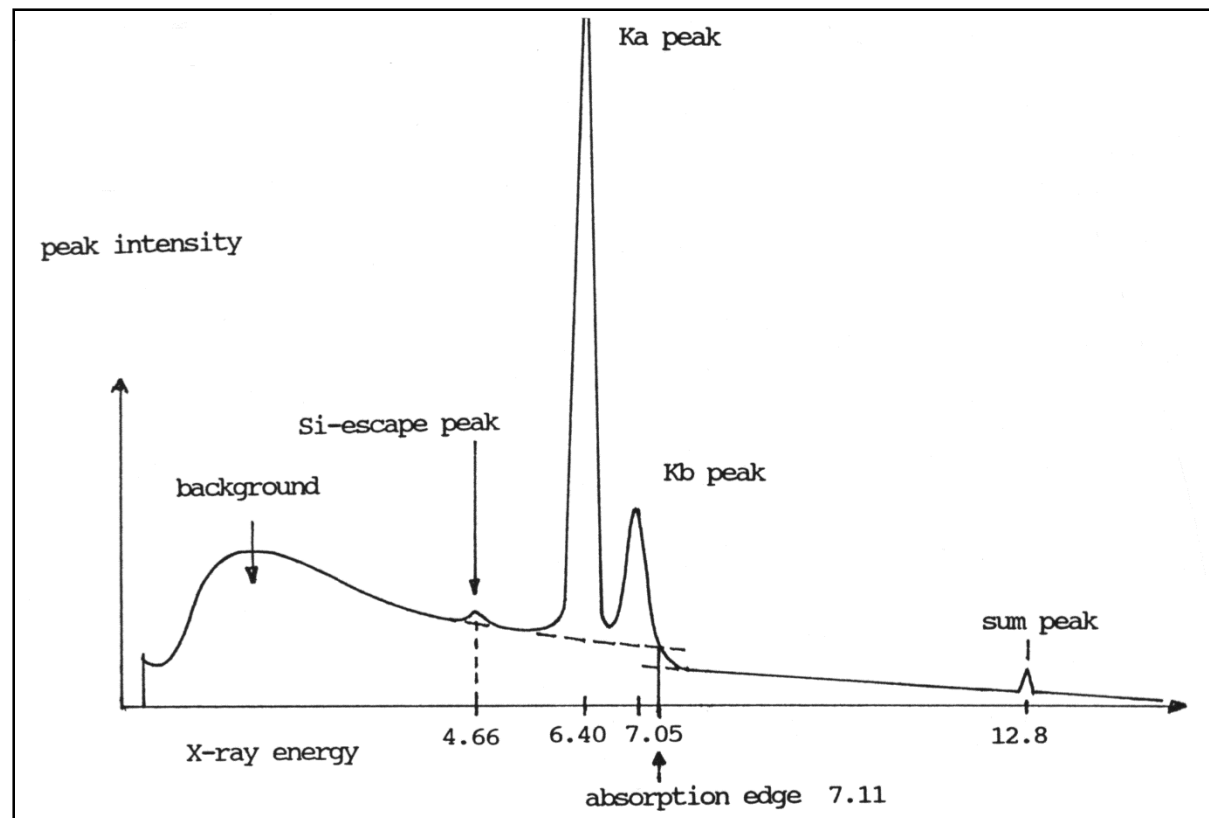
Escape peak of Cr $K\alpha$ = $5.411 - 1.740 = 3.671$ keV at Ca $K\alpha$ energy





Spectral artefacts - overview

Artificial spectrum of Fe showing background shape, escape and sum peaks and the absorption edge



Project WND-POWR.03.02.00-00-1043/16

International interdisciplinary PhD Studies in Materials Science with English as the language of instruction

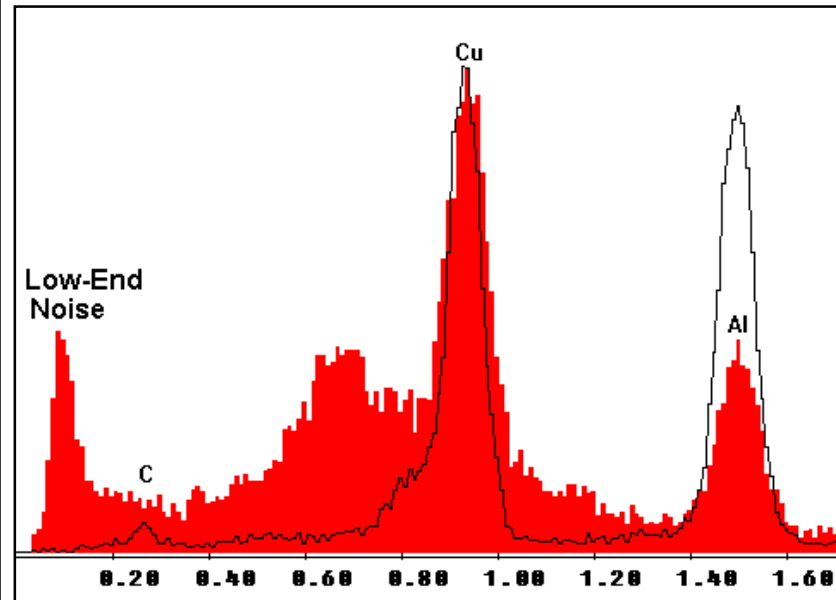
Project co-financed by the European Union within the European Social Funds



Spectral artefacts

Warming of the detector

- As the detector warms the noise peak widens
- All peaks will broaden and may shift in energy
- Also note large incomplete charge collection area to the left of the Cu peak



Project WND-POWR.03.02.00-00-1043/16

International interdisciplinary PhD Studies in Materials Science with English as the language of instruction

Project co-financed by the European Union within the European Social Funds



Summary - Spectral Artifacts

- Many artifacts possible
- Most important ones
 - Peak Overlap
 - Pulse pile-up (sum) peaks
 - Silicon Escape peaks

When performing qualitative analysis, a lot of artefacts can make a contribution, which can lead to false conclusions if not recognised in an early stage!

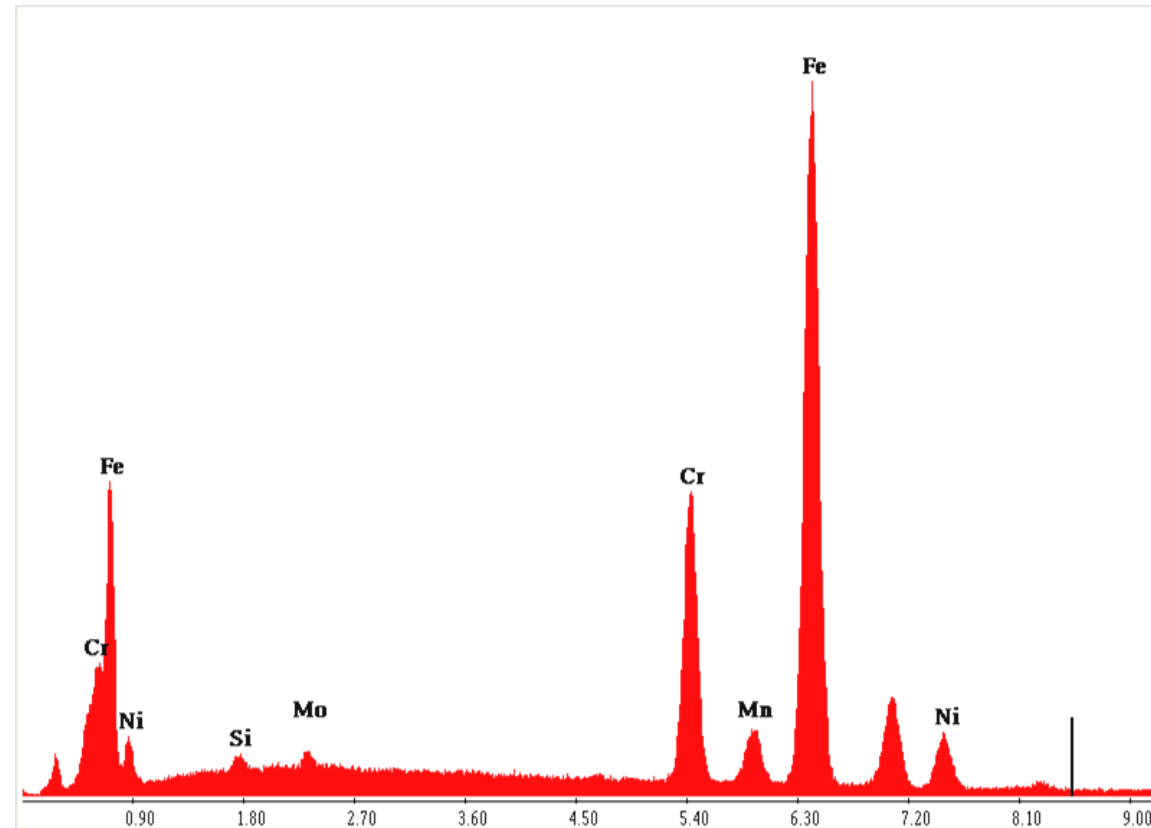


Mode of analysis

- **point analysis**
- **„line-scan”**
- **„mapping”**



Qualitative point analysis



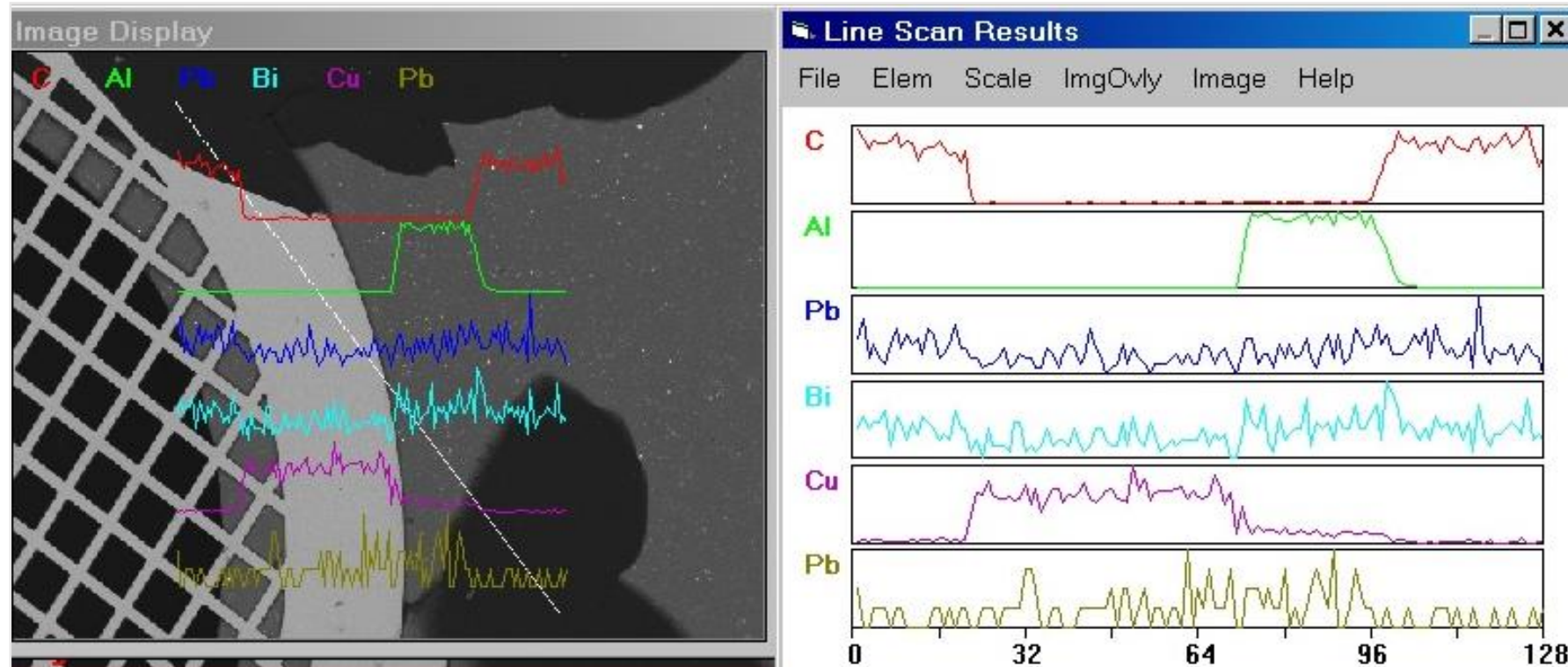
Project WND-POWR.03.02.00-00-1043/16

International interdisciplinary PhD Studies in Materials Science with English as the language of instruction

Project co-financed by the European Union within the European Social Funds

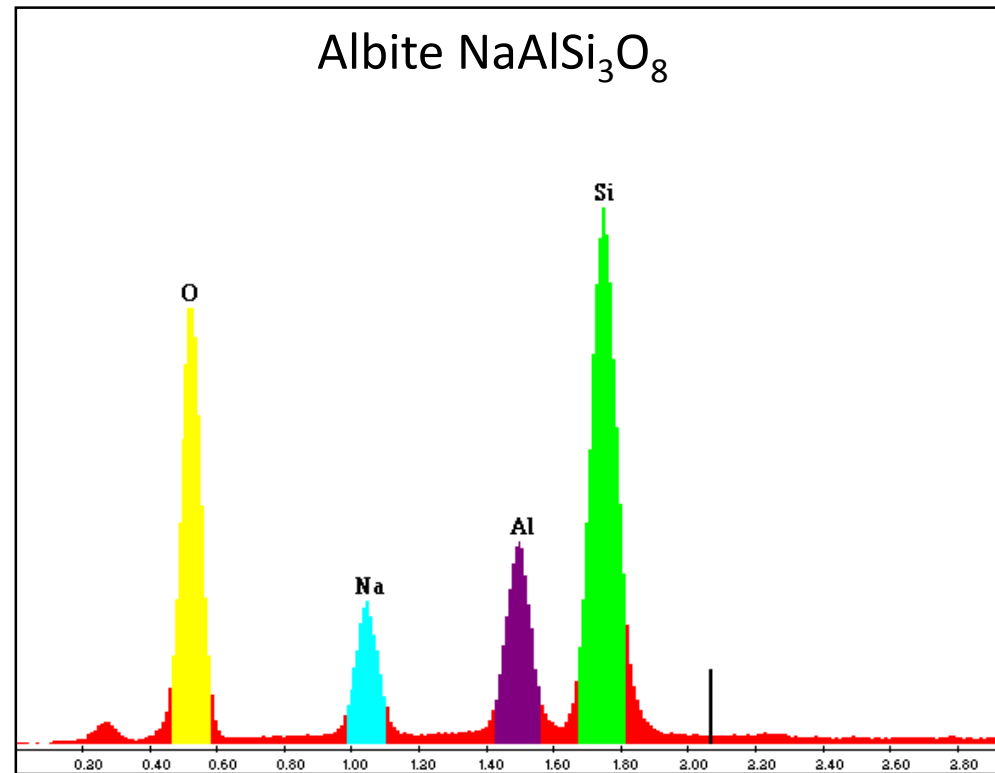


Linescan

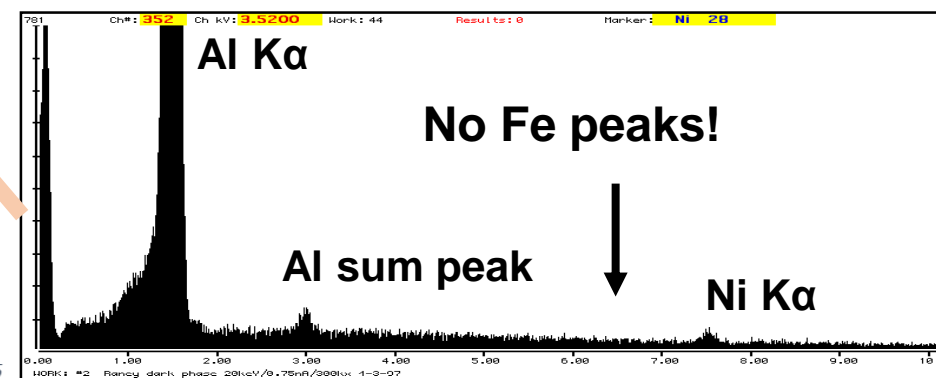
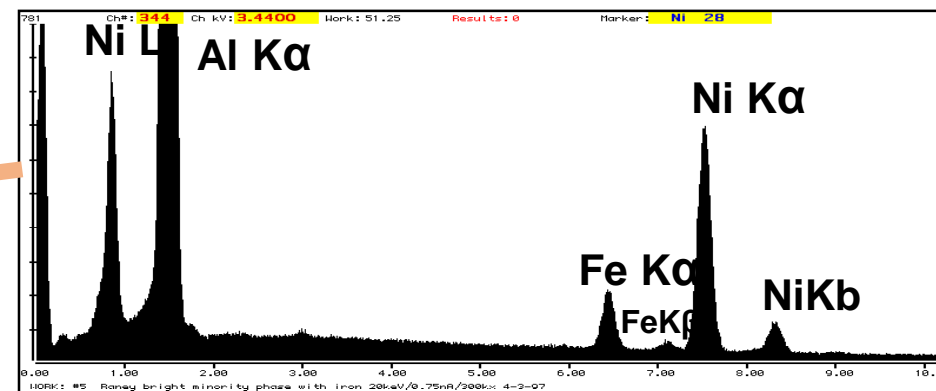
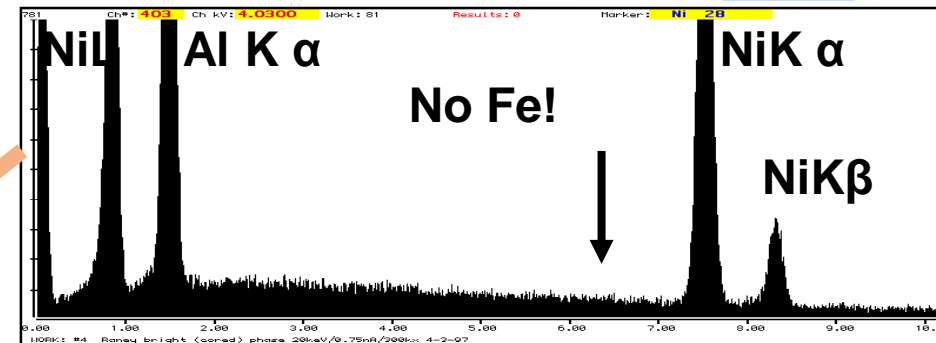
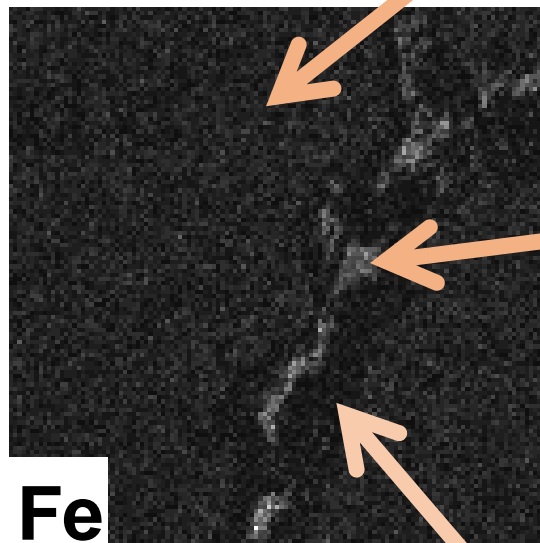




Mapping



The width of the regions is dependant of the spectrum resolution.



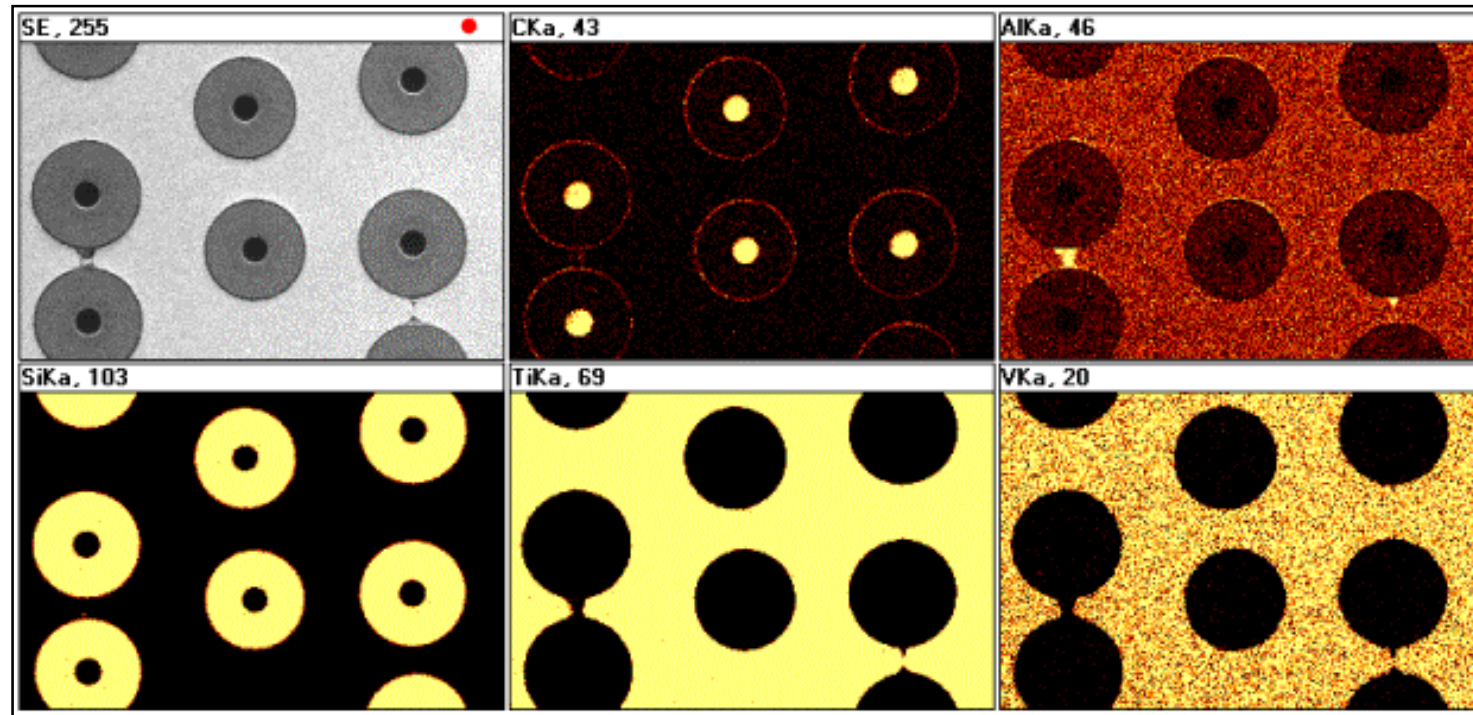
Project WND-POWR.03.02.00-00-1043/16

International interdisciplinary PhD Studies in Materials Science with English as the language of instruction

Project co-financed by the European Union within the European Social Funds



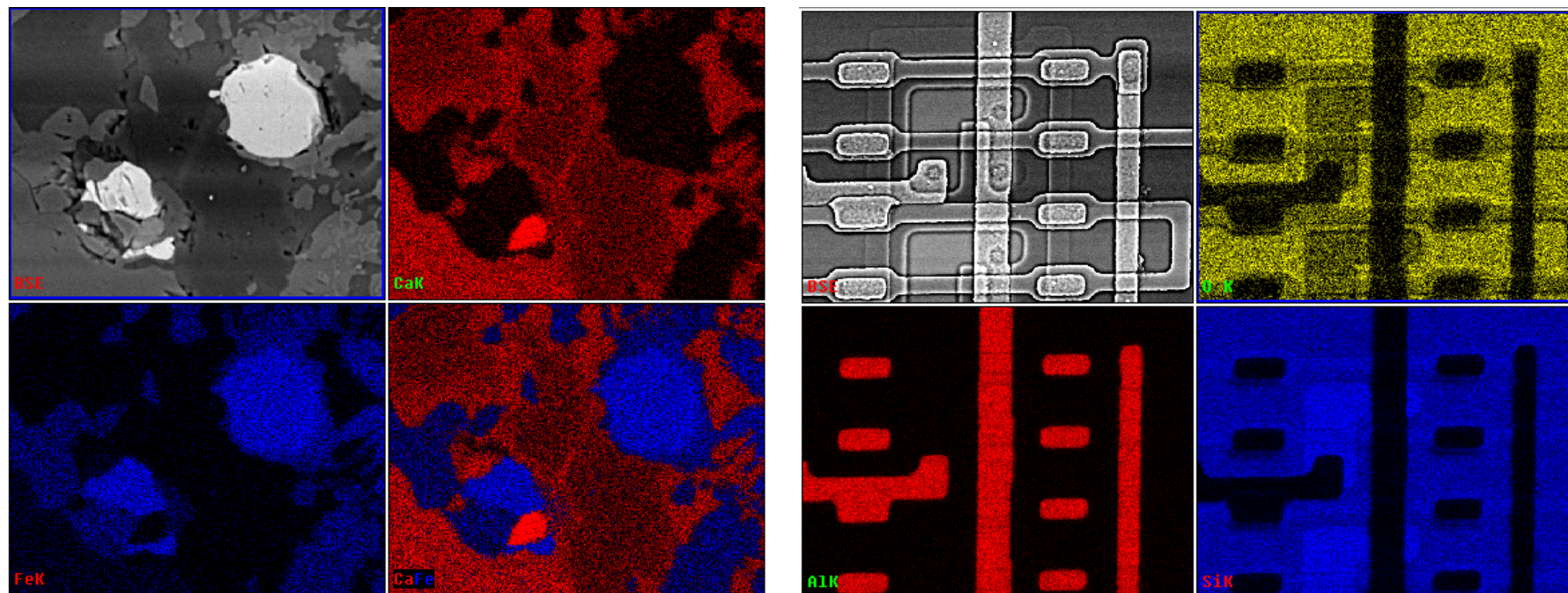
Multi Element Mapping



Composite: TiAlV matrix reinforced with SiC fibres

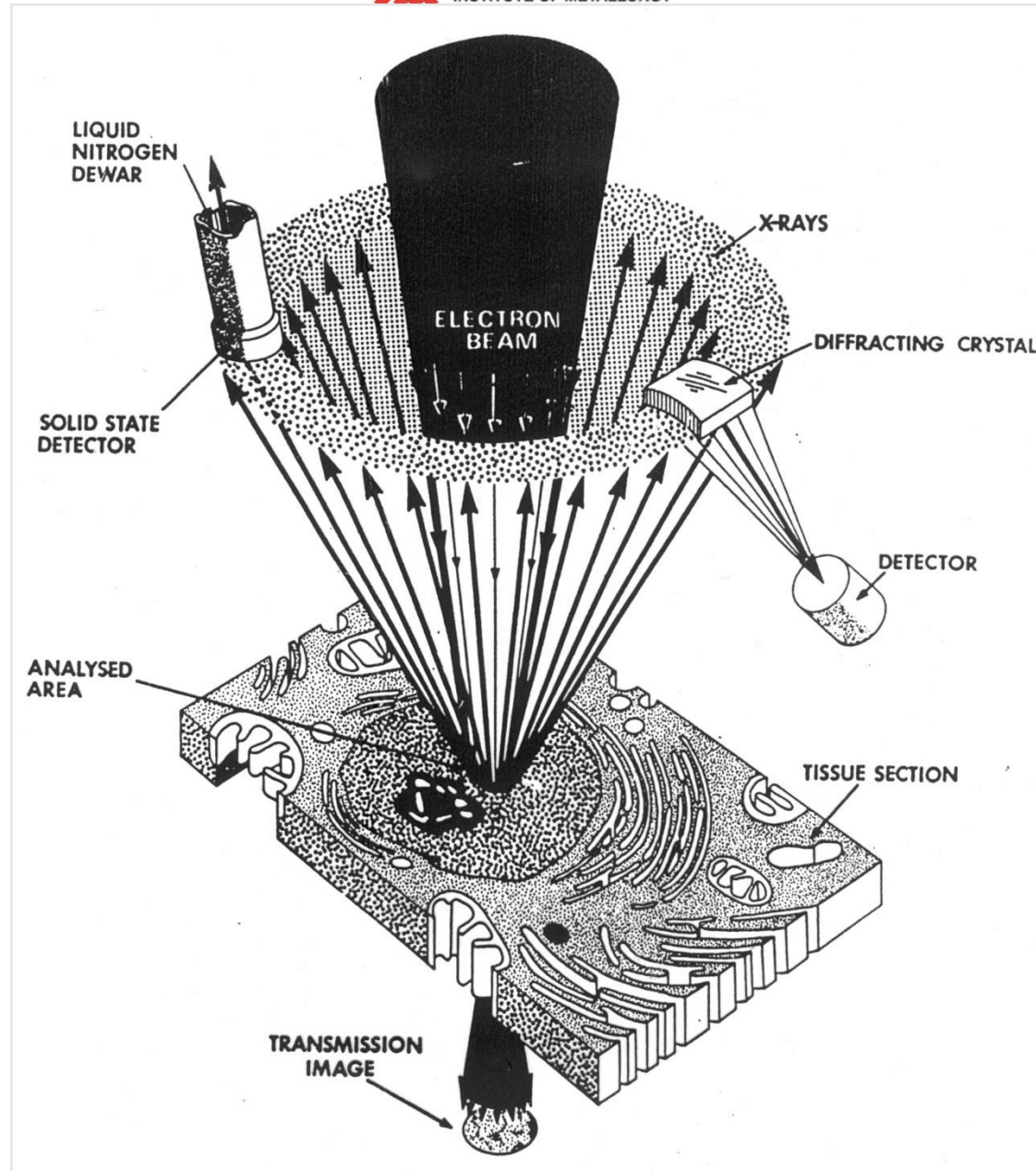


Multi Element Mapping





EDS
(EDXS)
Energy
Dispersive
Spectrometry



WDS
(WDXS)
Wavelength
Dispersive
Spectrometry



WDS - Wavelength Dispersive Spectrometry

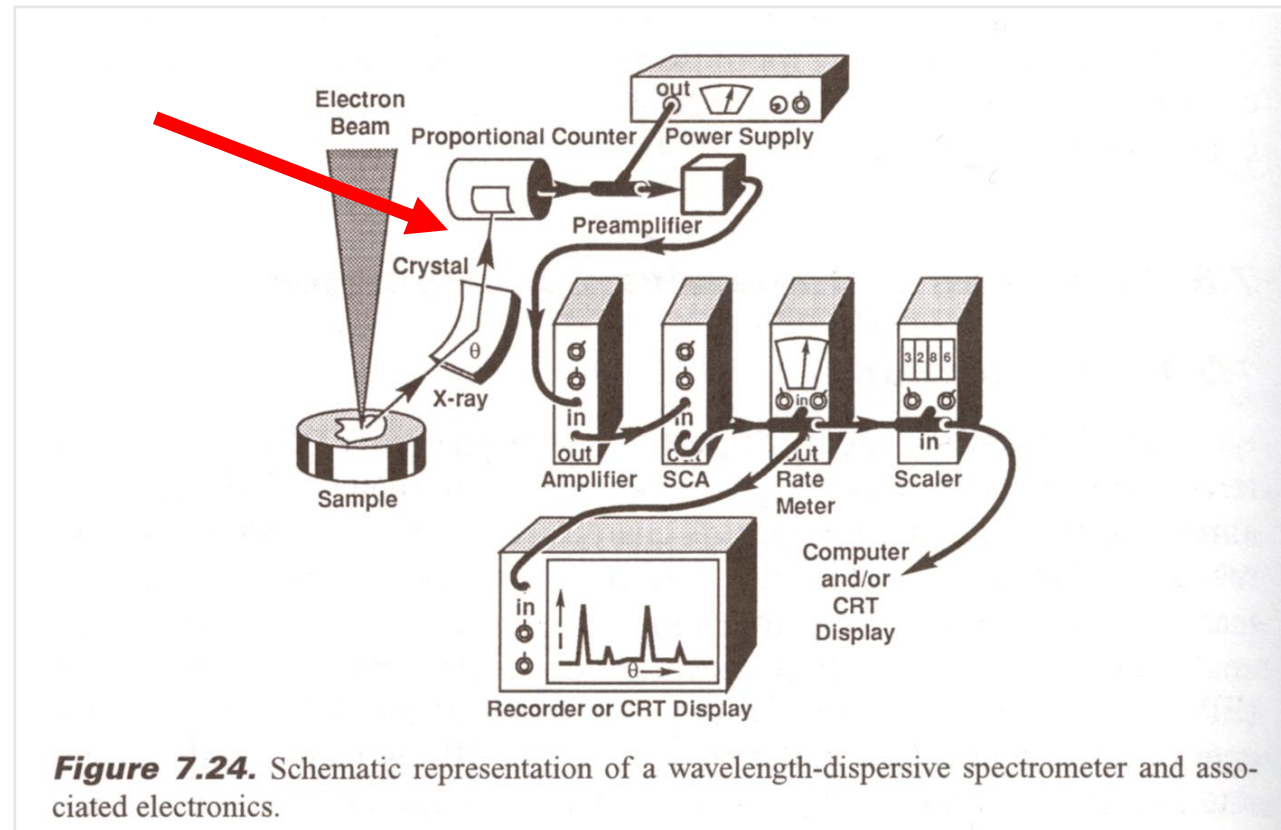
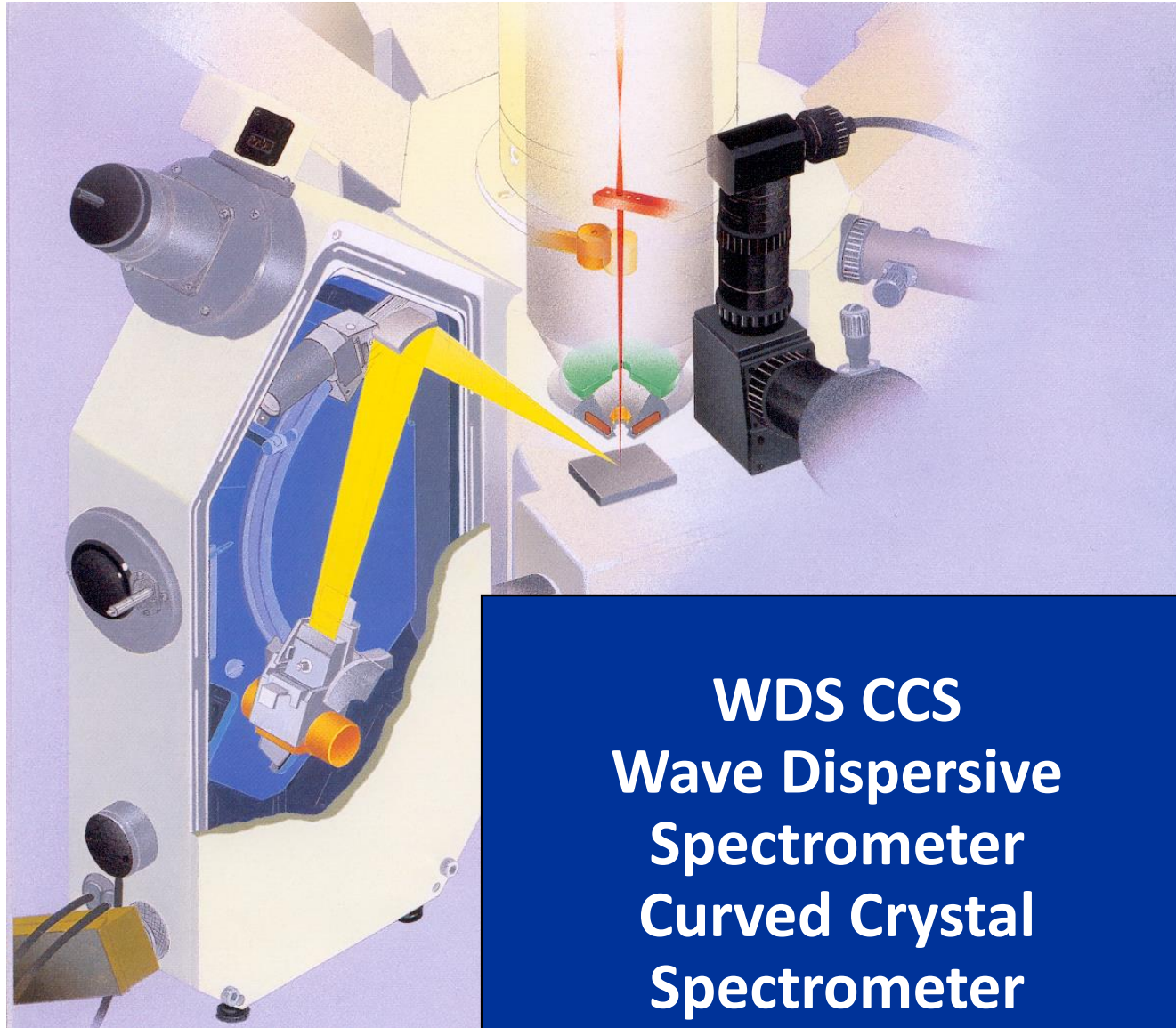


Figure 7.24. Schematic representation of a wavelength-dispersive spectrometer and associated electronics.



Project WND-POWR.03.02.00-00-1043/16

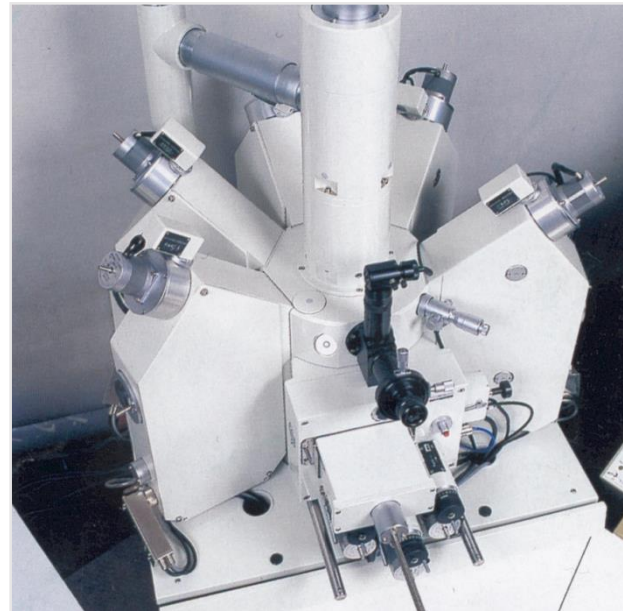
International interdisciplinary PhD Studies in Materials Science with English as the language of instruction

Project co-financed by the European Union within the European Social Funds



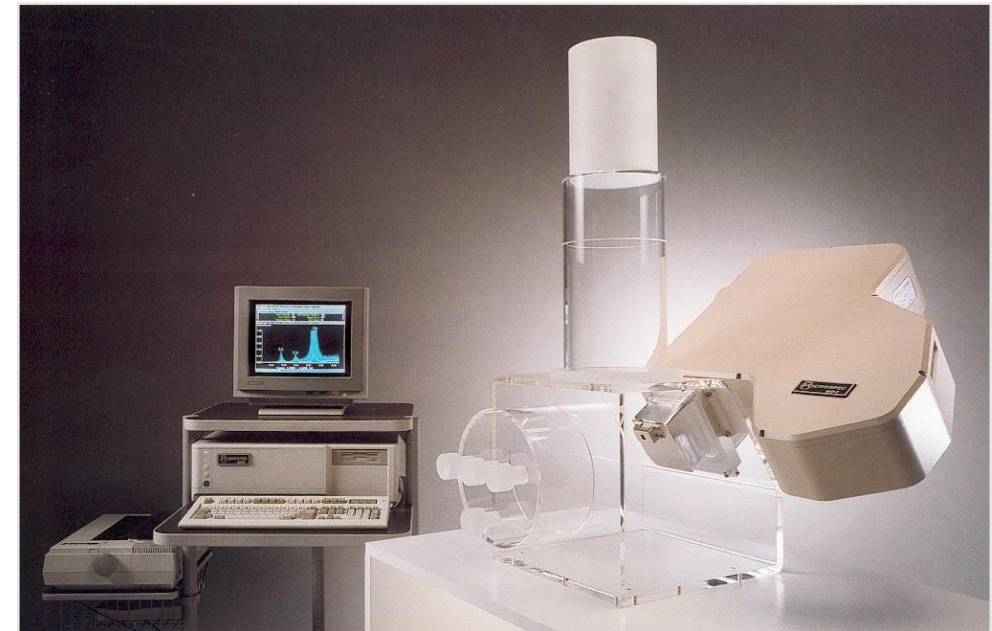
WDS - Wavelength Dispersive Spectrometer (Curved Crystal Spectrometer)

a) 5 spectrometers: „take-off” Angle 62°

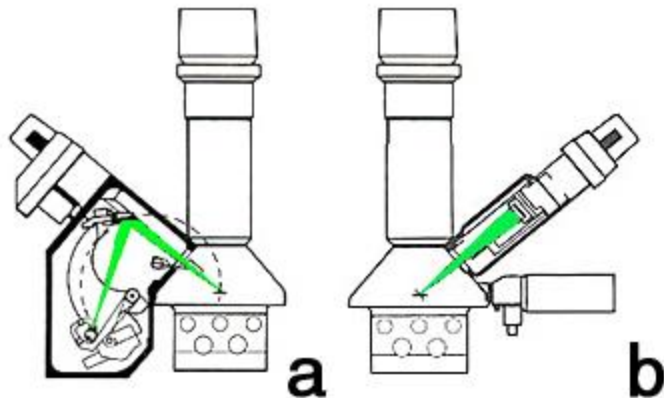


Vertical spectrometer

b) Single spectrometer: „take-off” Angle 45°

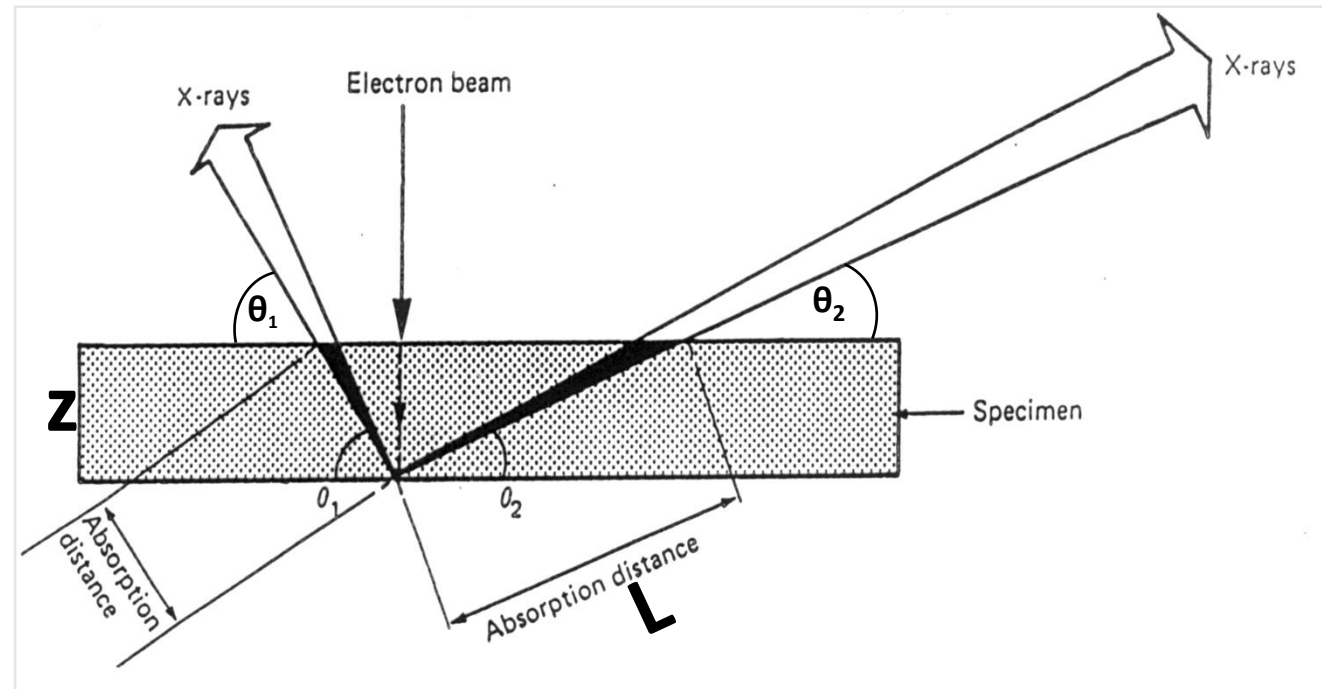


Inclined spectrometer





X-ray absorption



TOA (Take-off angle)



Beer Law

$$\frac{I}{I_0} = e^{-\mu\rho L}$$

$$\frac{I}{I_0} = e^{-\mu\rho z / \sin \theta}$$

$$\mu_M = \sum_{i=1}^n \mu_i w_i$$

where:

μ – mass thickness [cm²/g]

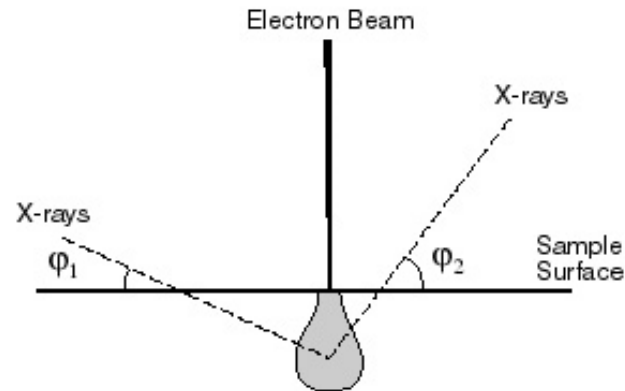
ρ – density [g/cm³]

L – absorption distance

z – thickness

I – X-ray intensity detected

I₀ – X-ray intensity generated





Attenuation of Ni K α (7.472 keV) by 2 μm thickness of the sample 30 wt. % of Ni and 70 wt. % of Fe; density of the sample 7.8 g/cm³

$$\mu_{\text{Fe}} = 380 \text{ cm}^2/\text{g}$$

$$\mu_{\text{Ni}} = 59 \text{ cm}^2/\text{g}$$

$$\mu_{\text{M}} = 0.7 \times 380 + 0.3 \times 59 = 284 \text{ cm}^2/\text{g}$$

$$\frac{I}{I_0} = \exp(-284 \times 7.8 \times 2 \times 10^{-4}) = e^{-0.443} = 0.642$$

Take-off angle: 51.5° $\frac{I}{I_0} = e^{-0.443 / \sin(51.5)} = 0.586$

Take-off angle: 15° $\frac{I}{I_0} = e^{-0.443 / \sin(15)} = 0.181$

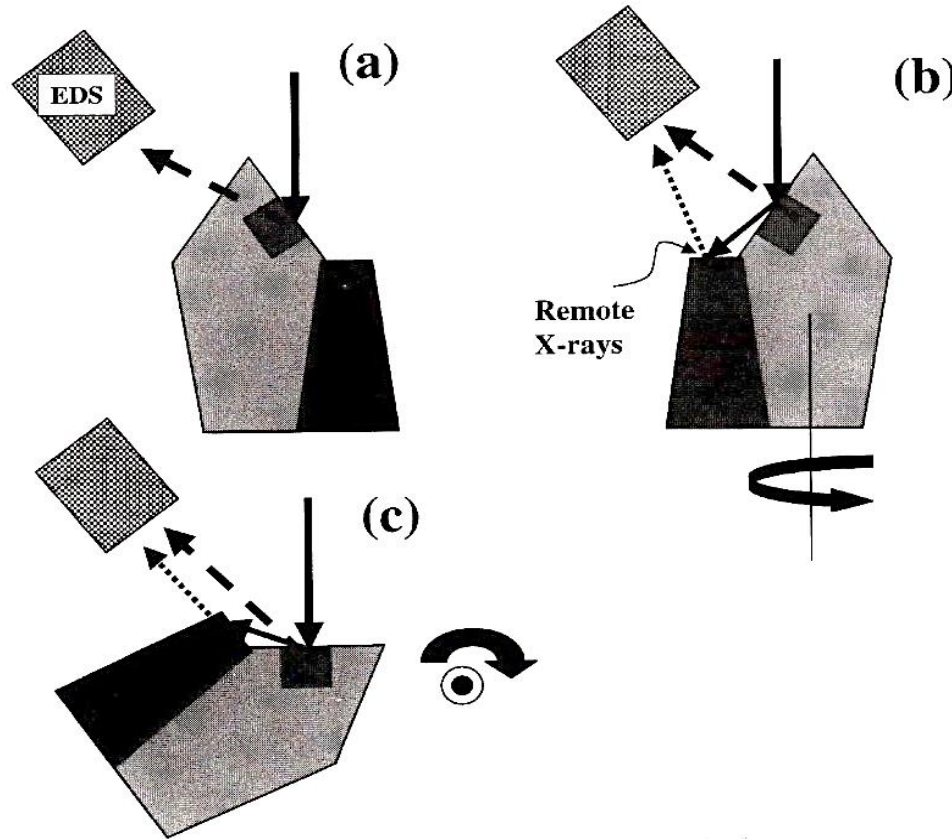
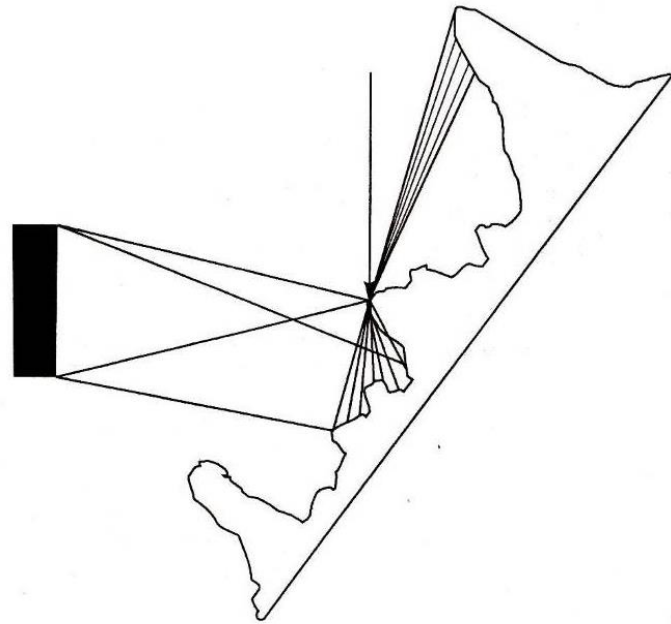
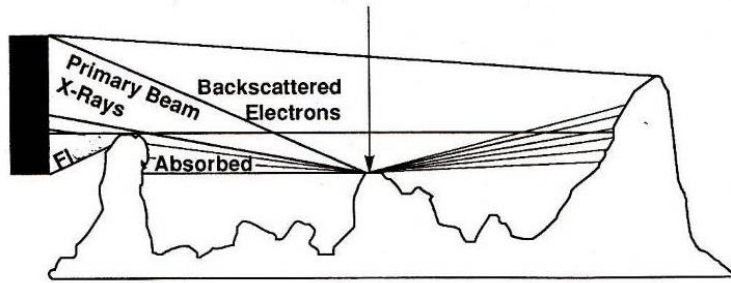


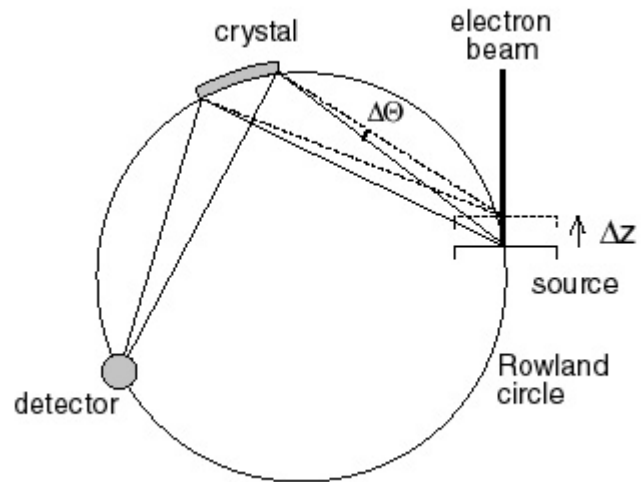
Figure 10.16. Reorientation of a rough specimen to optimize the spectrum quality: (a) Poor orientation relative to the EDS because of a long absorption path, which will selectively diminish low-energy photons. (b) Specimen rotated to bring the feature to face the EDS; the tilt still permits significant remote scattering to contribute to the spectrum. (c) Specimen tilted to bring the feature to the normal beam incidence condition; remote scattering is reduced because backscattering is minimized, but, depending on the exact surroundings, remote contributions to the spectrum are still possible.

Figure 10.15. Schematic illustration of remote scattering effects from rough surfaces. Electron scattering paths are indicated. Fl, Remote fluorescence.

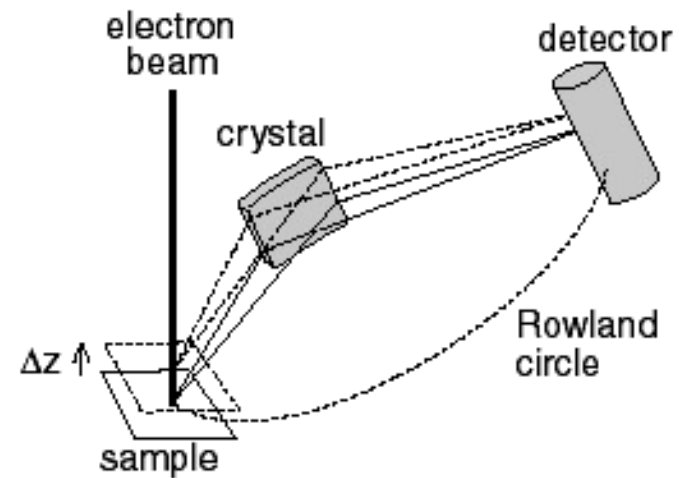


Curved Crystal Spectrometer

Vertical spectrometer

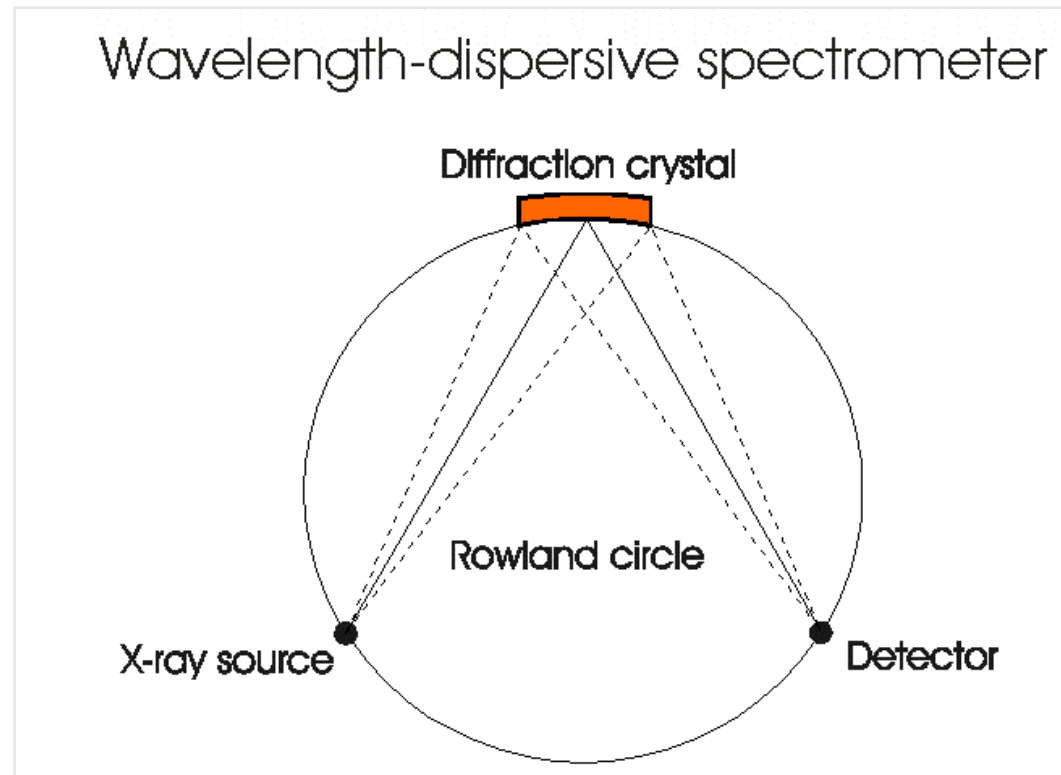


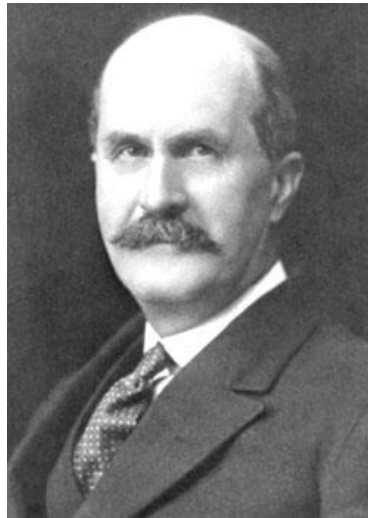
Inclined spectrometer



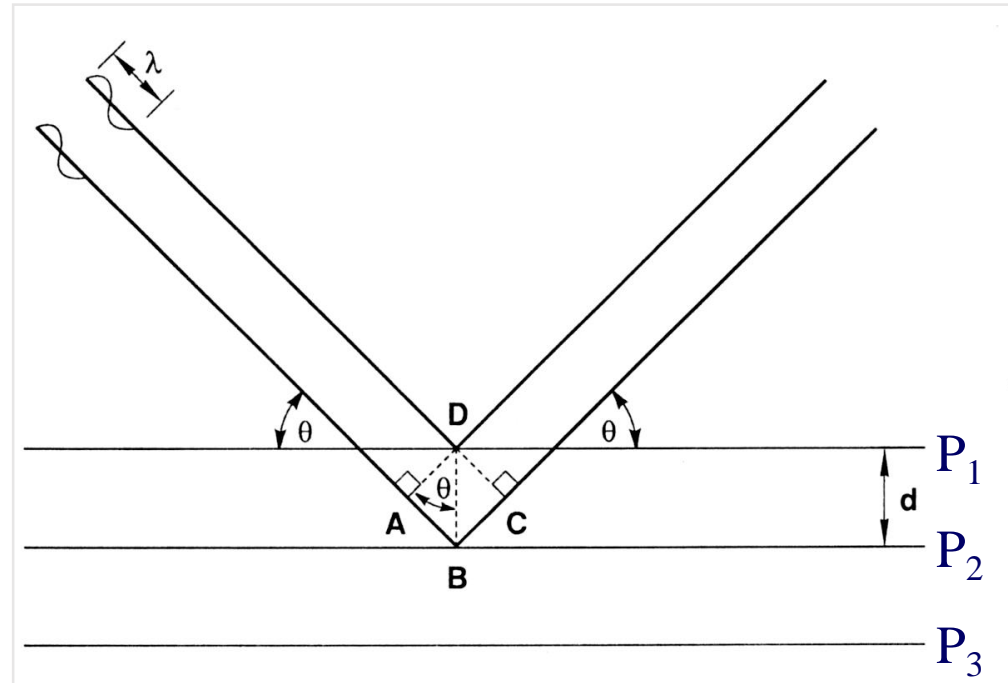


Curved Crystal Spectrometer

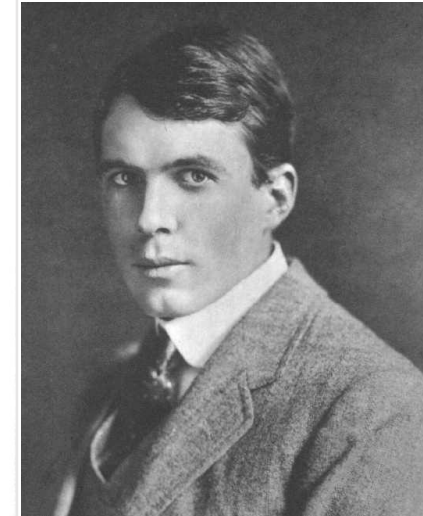




William Henry Bragg



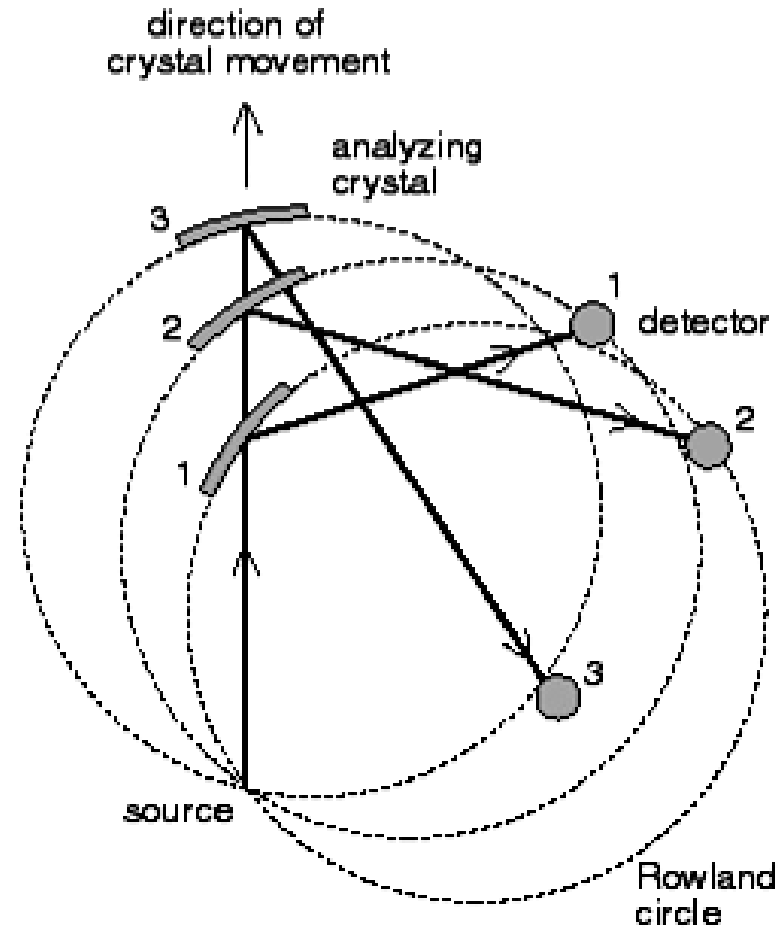
$$n \lambda = 2d \sin \theta$$



William Laurence Bragg

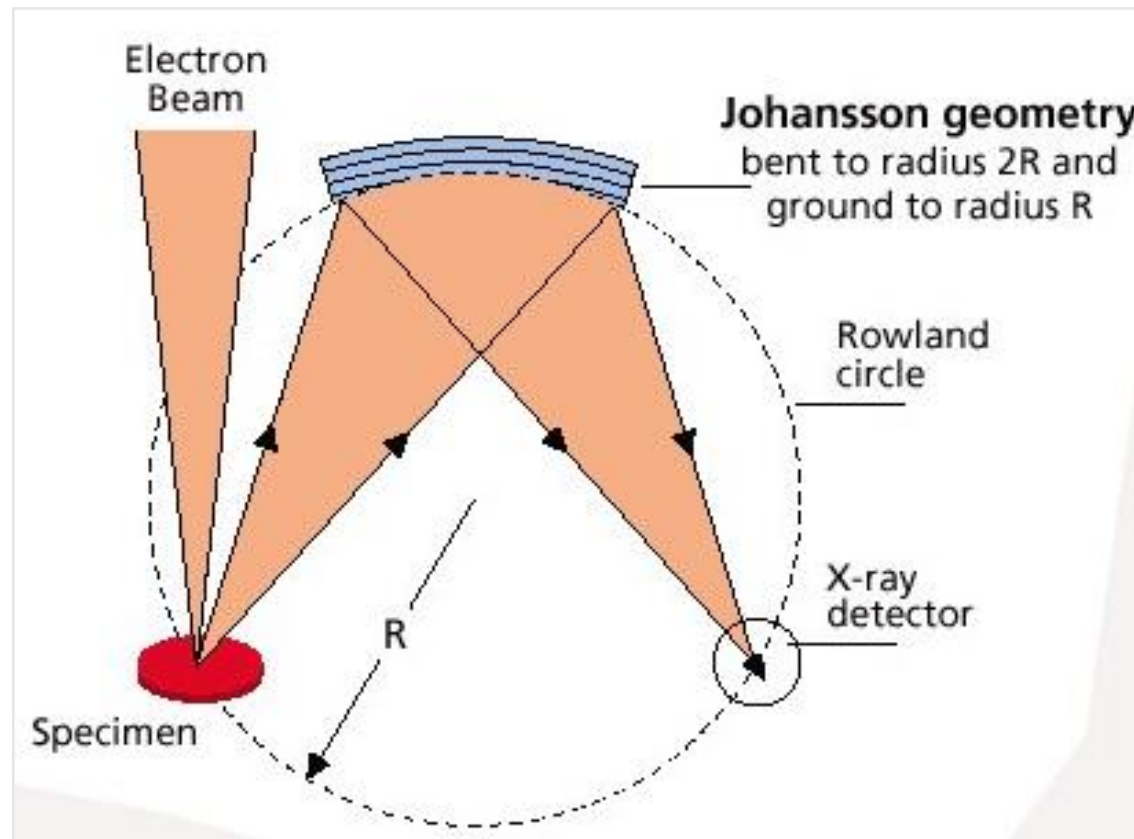


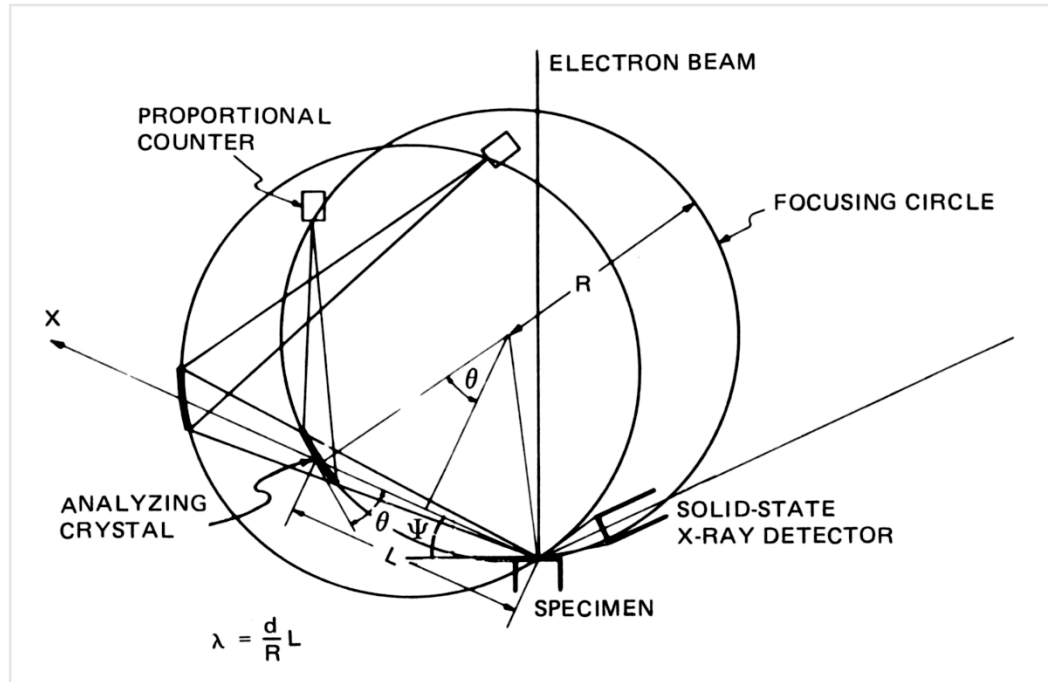
Curved Crystal Spectrometer





Curved Crystal Spectrometer





$$\text{for } n = 1 \quad \lambda = 2d \sin \theta$$

$$\sin \theta = \frac{\lambda}{2d}$$

from geometric relationship:

$$\frac{L}{2} = R \sin \theta$$

$$\text{stąd} \quad \frac{L}{2} = \frac{\lambda}{2d} \rightarrow \lambda = \frac{d}{R} L$$

LiF crystal

$L_{min} = 60.5\text{mm}$, $L_{max} = 254\text{mm}$, Radius $R = 140\text{mm}$

($\lambda = 12.3981/E$ [keV])

$$\lambda_{min} = \frac{d}{R} L_{min} = \frac{4.027/2}{140} \times 60.5 = 0.870 \text{ \AA} \sim 14.3 \text{ keV}$$

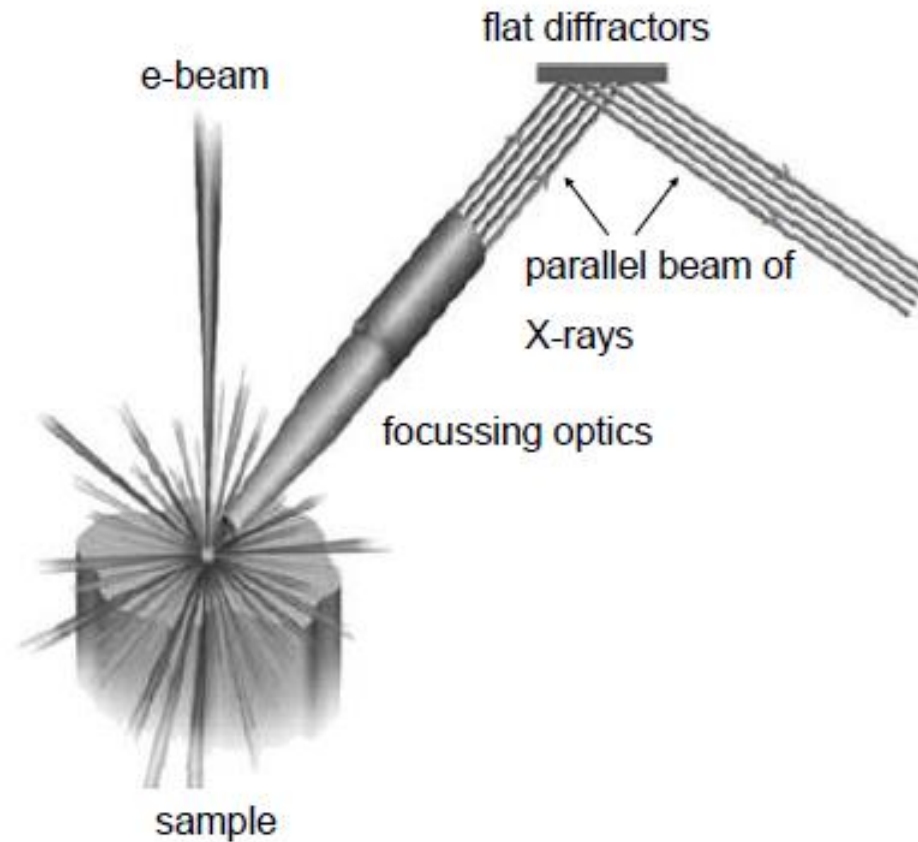
$$\lambda_{max} = \frac{d}{R} L_{max} = 0.014 \times 254 = 3.65 \text{ \AA} \sim 3.4 \text{ keV}$$



Crystal	2d Spacing Å	Element Coverage (K Lines) (L Lines)	eV Range
MoB ₄ C	197	Be, B, C	100 - 360
MoB ₄ C	120	C	220 - 320
CrSc	80	C, N	200 - 420
	80	Ti L (optimized)	400 - 500
WSi	60	O - N Ti - Ga	420 - 1100
TAP	25.75	Na - Si Ga - Rb	1100 - 1700
PET	8.74	Si - S Rb - Mo	1700 - 2400
LiF(200)	4.027	K - Ge	3300 - 10.8KeV
LiF(220)	2.847	V - Y	4700 - 15.3KeV

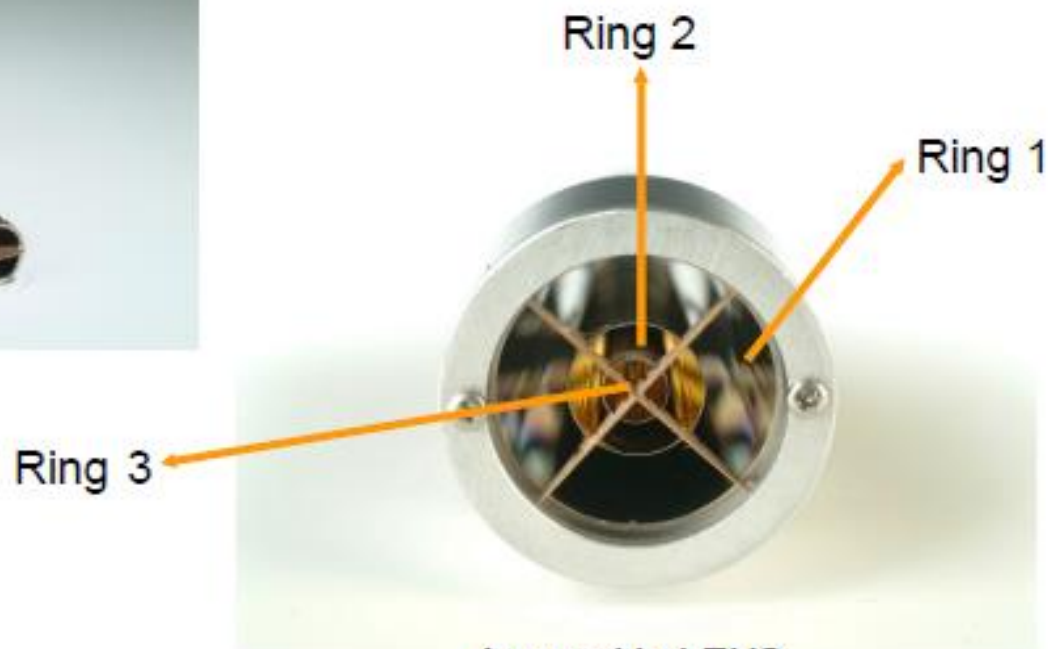


Flat Crystal (Parallel Beam Spectrometer or PBS)





X-Ray Mirrors (High Collection Optics)



As used in LEXS

Ring 1 – < 500 eV

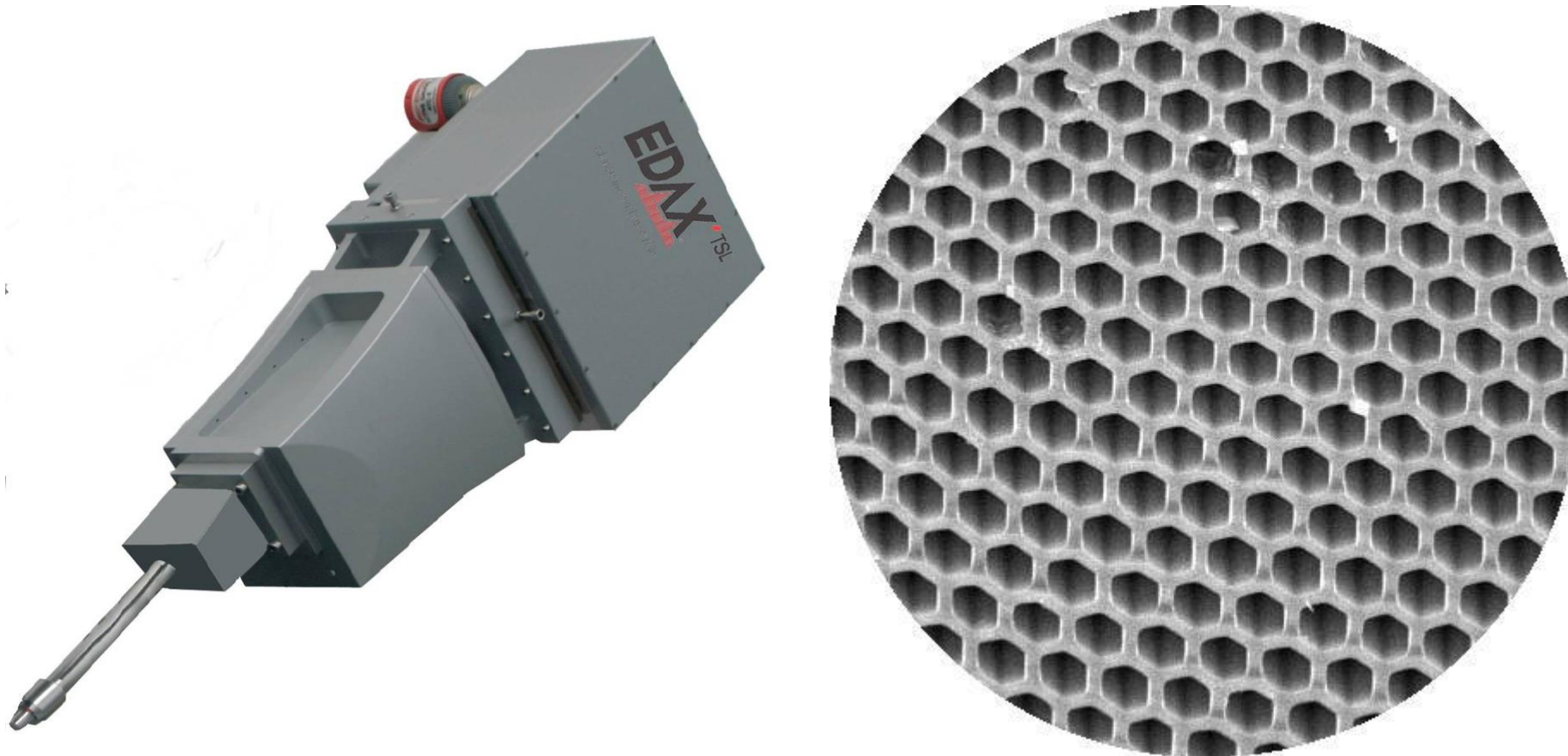
Ring 2 – 500-1500 eV

Ring 3 – 1500-2400eV

Example with concentric mirrors:
200 μm (Be Ka : 0.108 keV)
25 μm (Si Ka : 1.75 keV)



Polycapillary optics



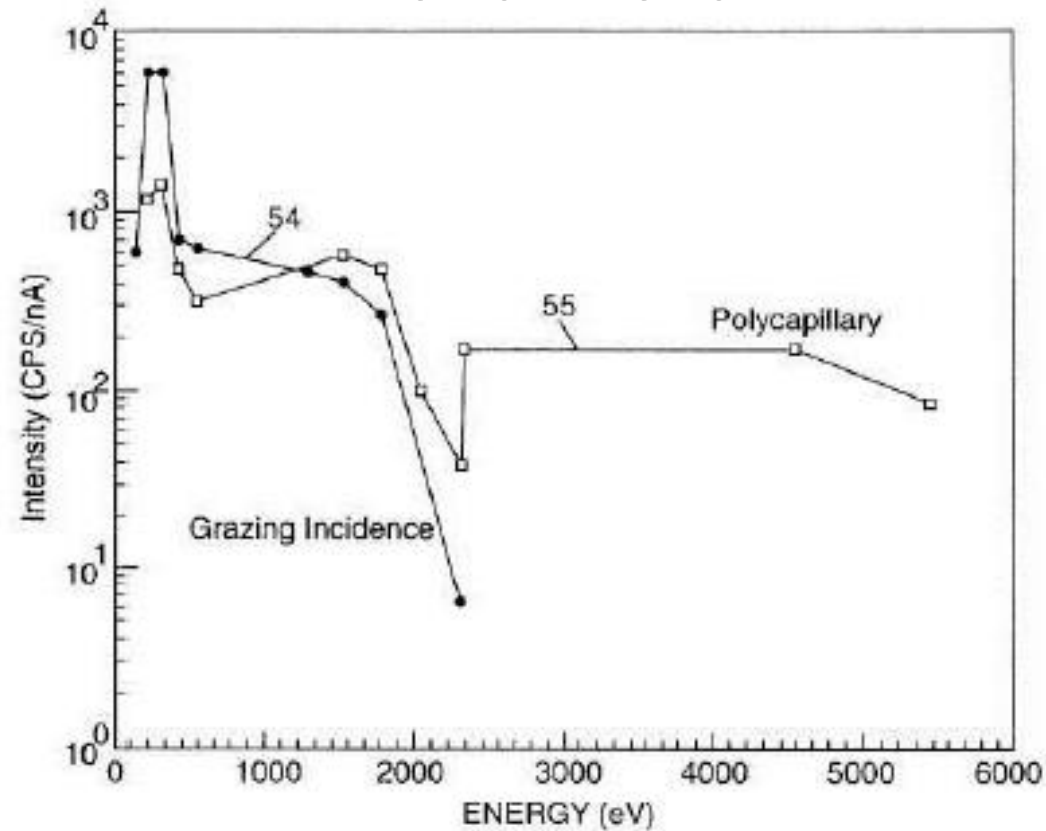
500 000 capillars

Project WND-POWR.03.02.00-00-1043/16

International interdisciplinary PhD Studies in Materials Science with English as the language of instruction

Project co-financed by the European Union within the European Social Funds

High Collection Optics (HCO) versus Polycapillary optics



The concentric mirrors has higher reflection efficiency than the polycapillary optic for lower energies, whereas the polycapillary optic is a more effective optic for higher energies

Project WND-POWR.03.02.00-00-I043/16

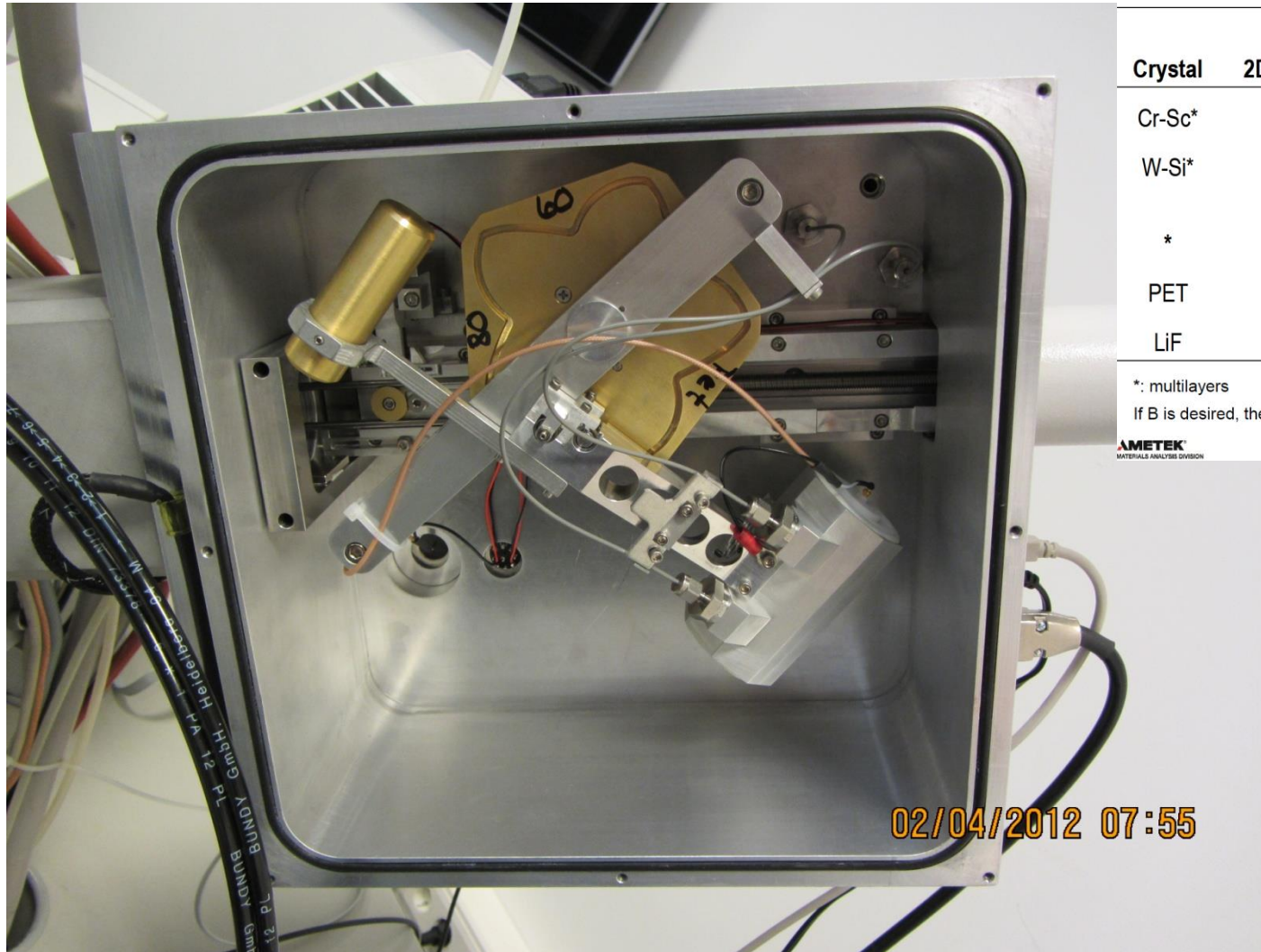
International interdisciplinary PhD Studies in Materials Science with English as the language of instruction

Project co-financed by the European Union within the European Social Funds



PBS for C

Diffractors used in TEXS



Crystal	2D Spacing, A	Element Range	ev Range
Cr-Sc*	80	C,N	185-420
W-Si*	60	O-Mg	420-1100
*	30	Mg-Al	1100-1700
PET	8.74	Si-K	1700-3600
LiF	4.02	Ca-Ge	3600-10000

*: multilayers

If B is desired, the 80 diffractor can be replaced with 100

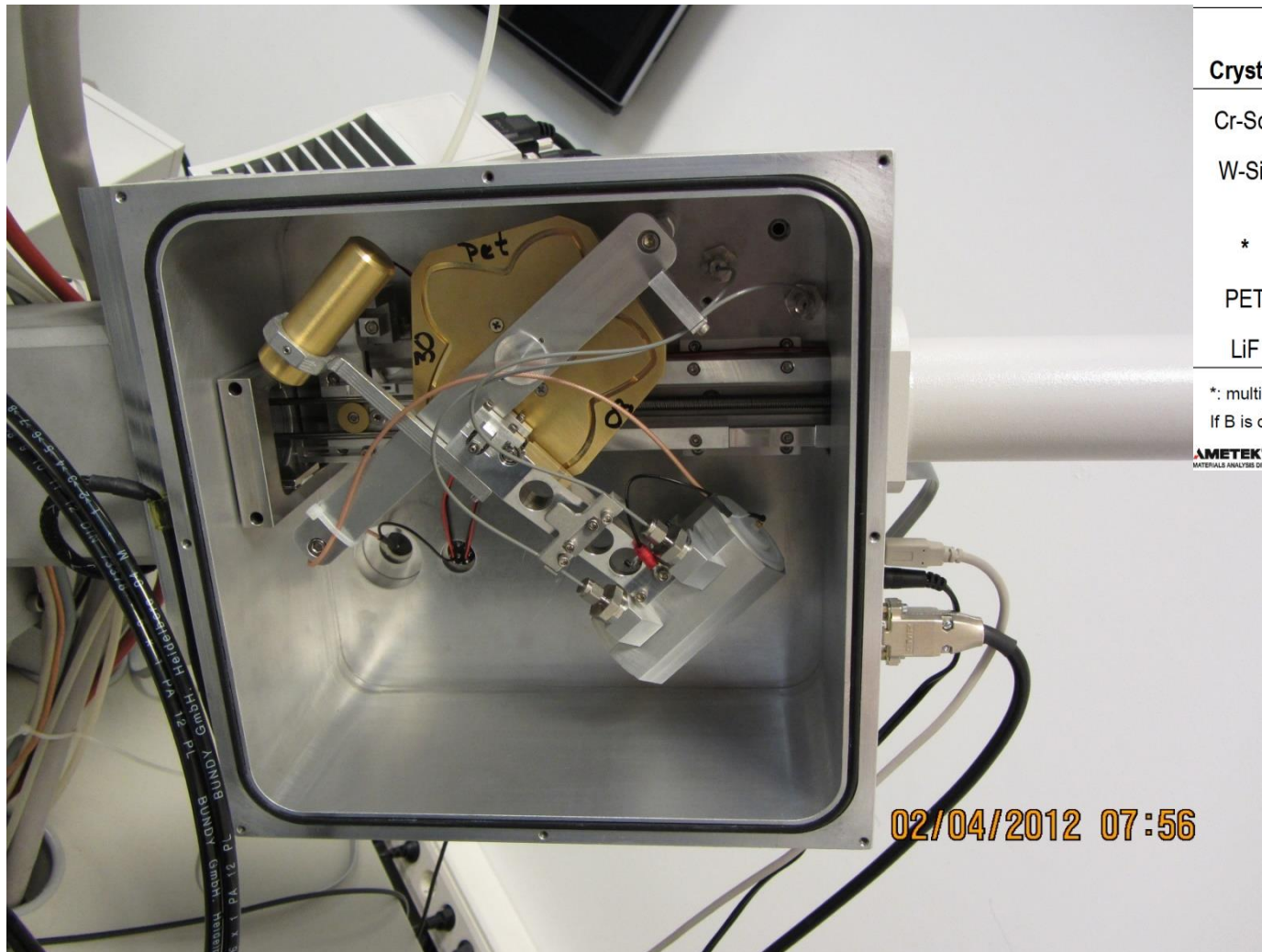
AMETEK
MATERIALS ANALYSIS DIVISION

EDAX
Smart Insight



PBS for Al K α and Cu L α

Diffraction used in TEXS



Crystal	2D Spacing, A	Element Range	ev Range
Cr-Sc*	80	C,N	185-420
W-Si*	60	O-Mg	420-1100
*	30	Mg-Al	1100-1700
PET	8.74	Si-K	1700-3600
LiF	4.02	Ca-Ge	3600-10000

*: multilayers

If B is desired, the 80 diffractor can be replaced with 100


 MATERIALS ANALYSIS DIVISION


 Smart Insight

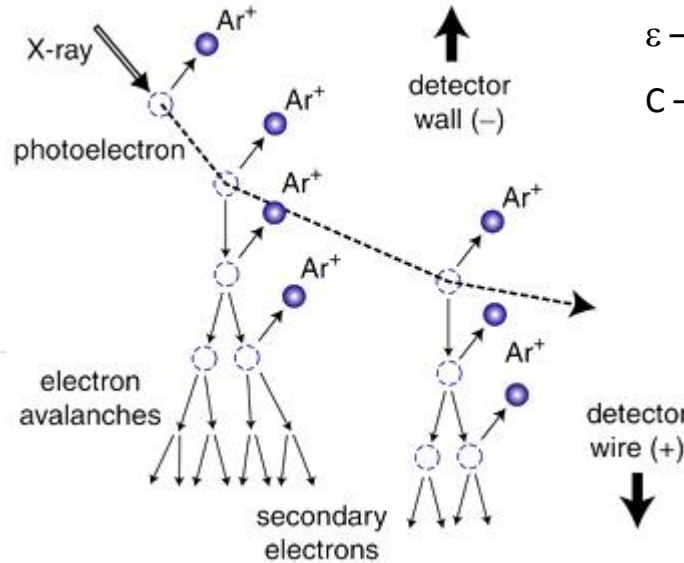
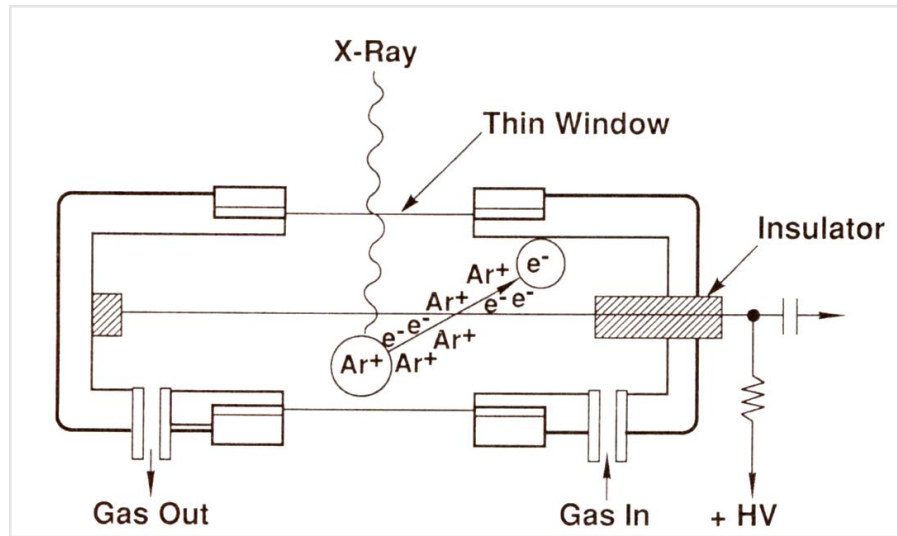
Project WND-POWR.03.02.00-00-1043/16

International interdisciplinary PhD Studies in Materials Science with English as the language of instruction

Project co-financed by the European Union within the European Social Funds



Proportional counter



n – number of carriers, e – electron charge $1.6 \times 10^{-19} \text{C}$
 q – total charge
 E – X-ray energy (eg. Cu $K\alpha$ 8.04 keV)
 ϵ – effective ionization potential $\text{Ar} \rightarrow \text{Ar}^+ e^-$; ca 28 eV
 C – argon permittivity

$$n = \frac{E}{\epsilon}$$

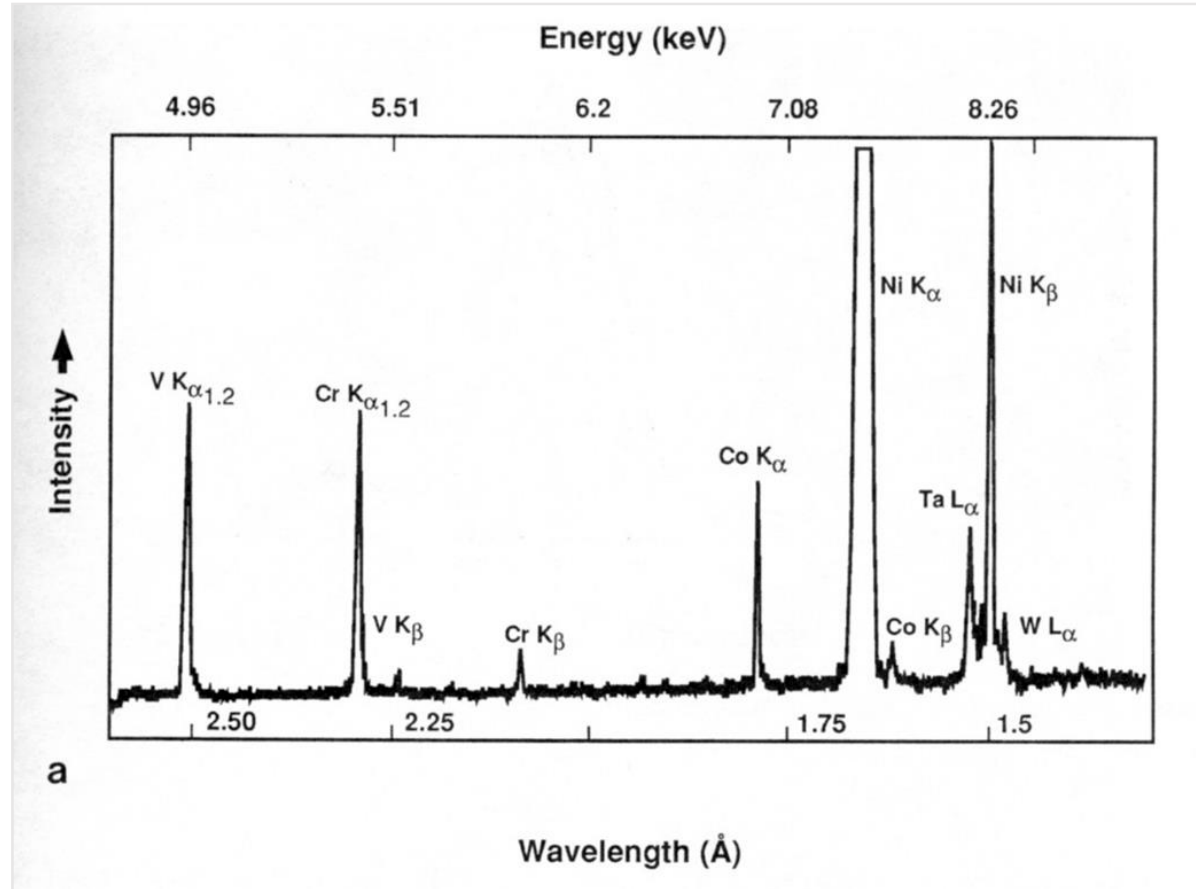
$$q = ne = 287 \times 1.6 \times 10^{-19} \text{C} = 4.6 \times 10^{-17} \text{C}$$

$$V = \frac{q}{C} = \frac{4.6 \times 10^{-17}}{1 \times 10^{-12}} = 46 \mu\text{V}$$

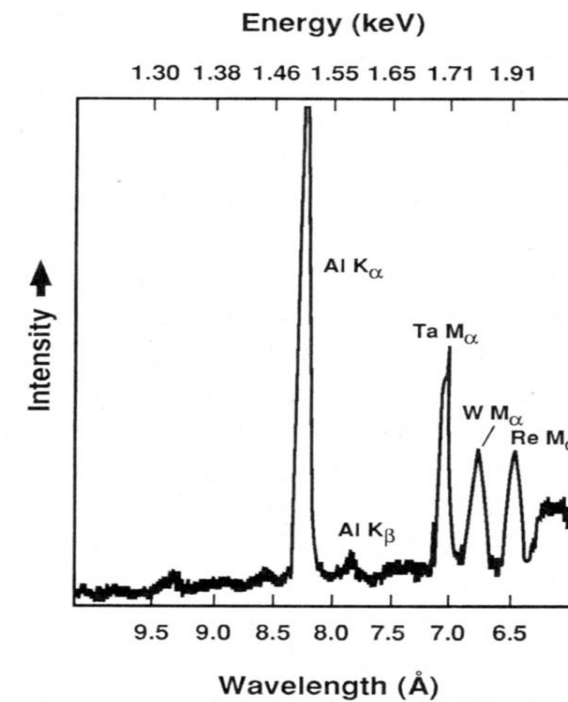
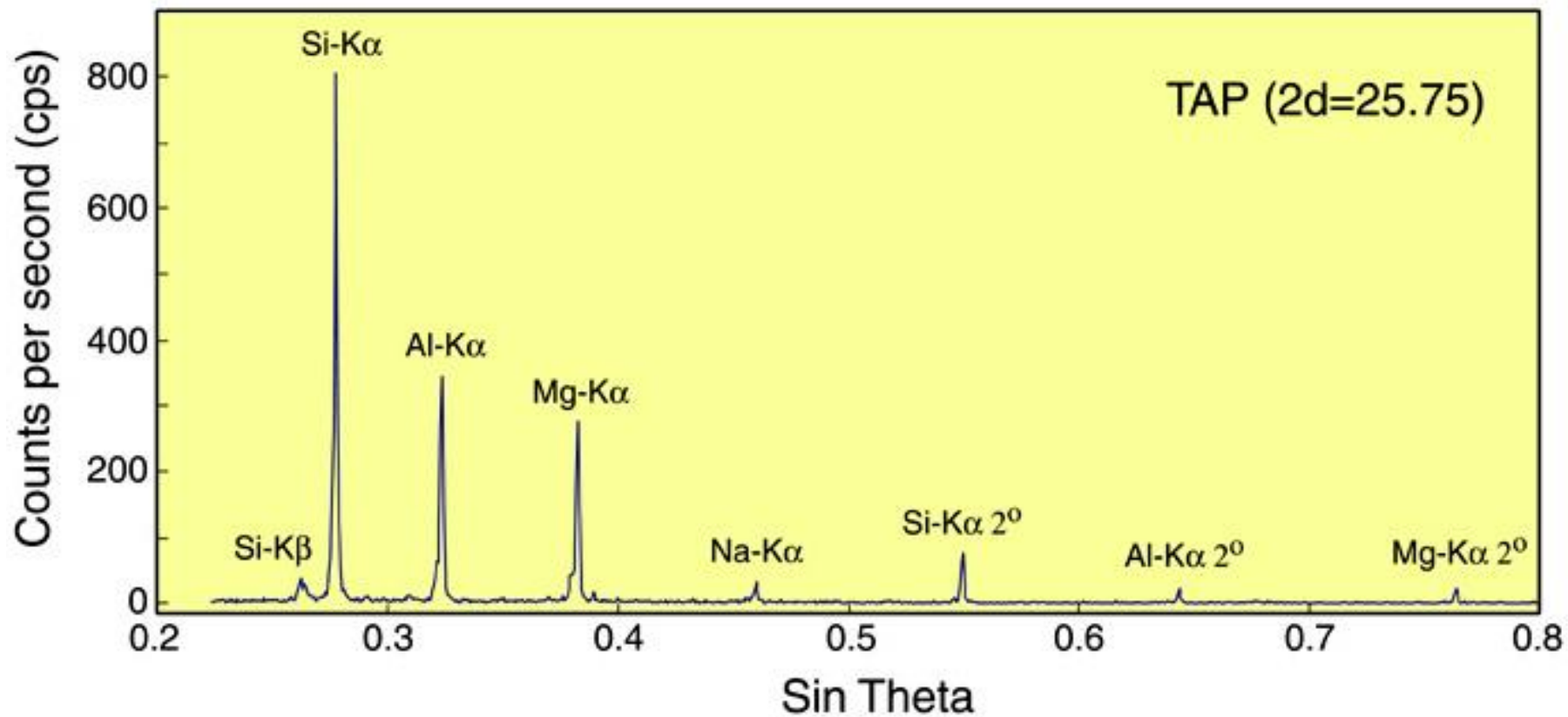


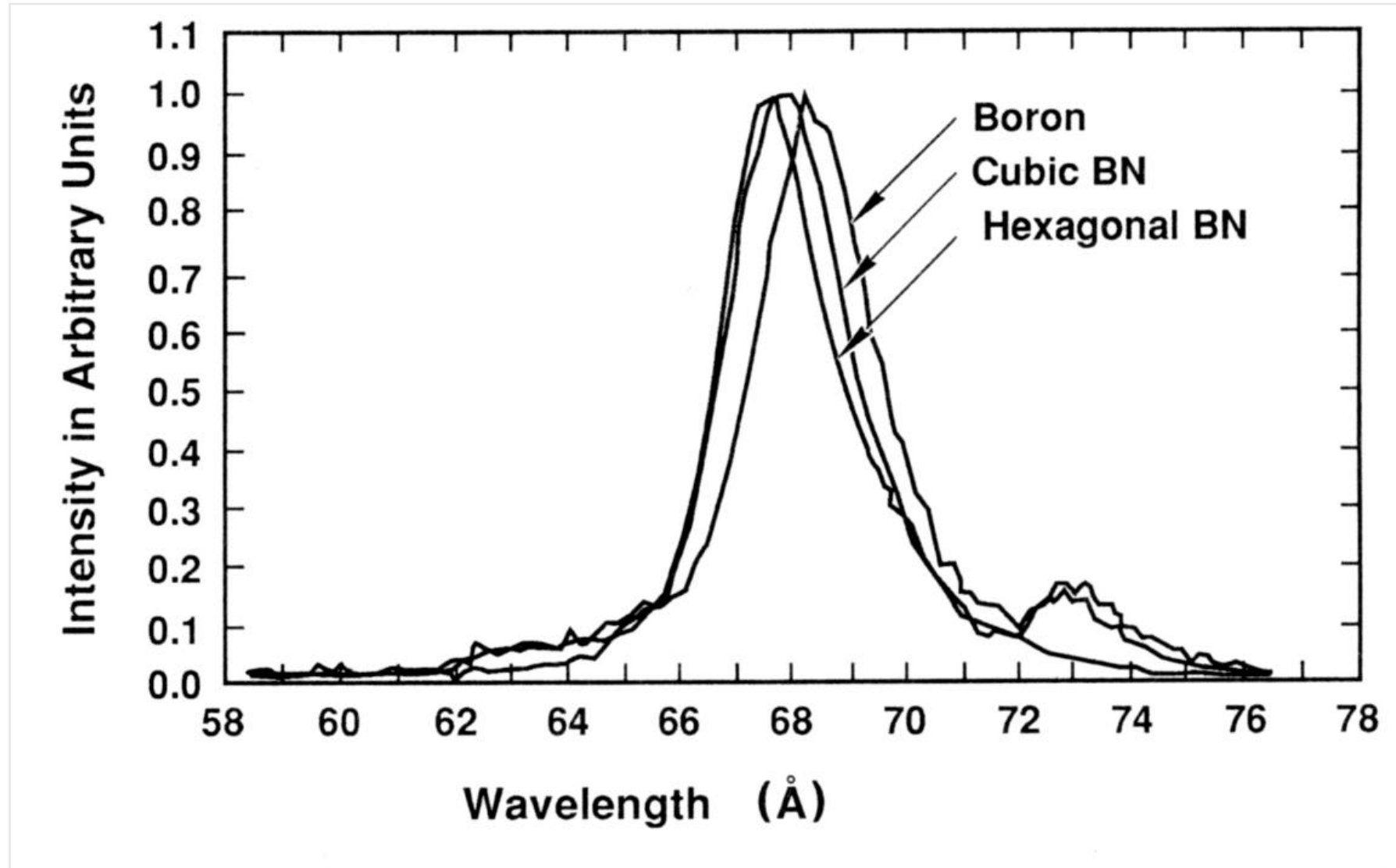


Examples



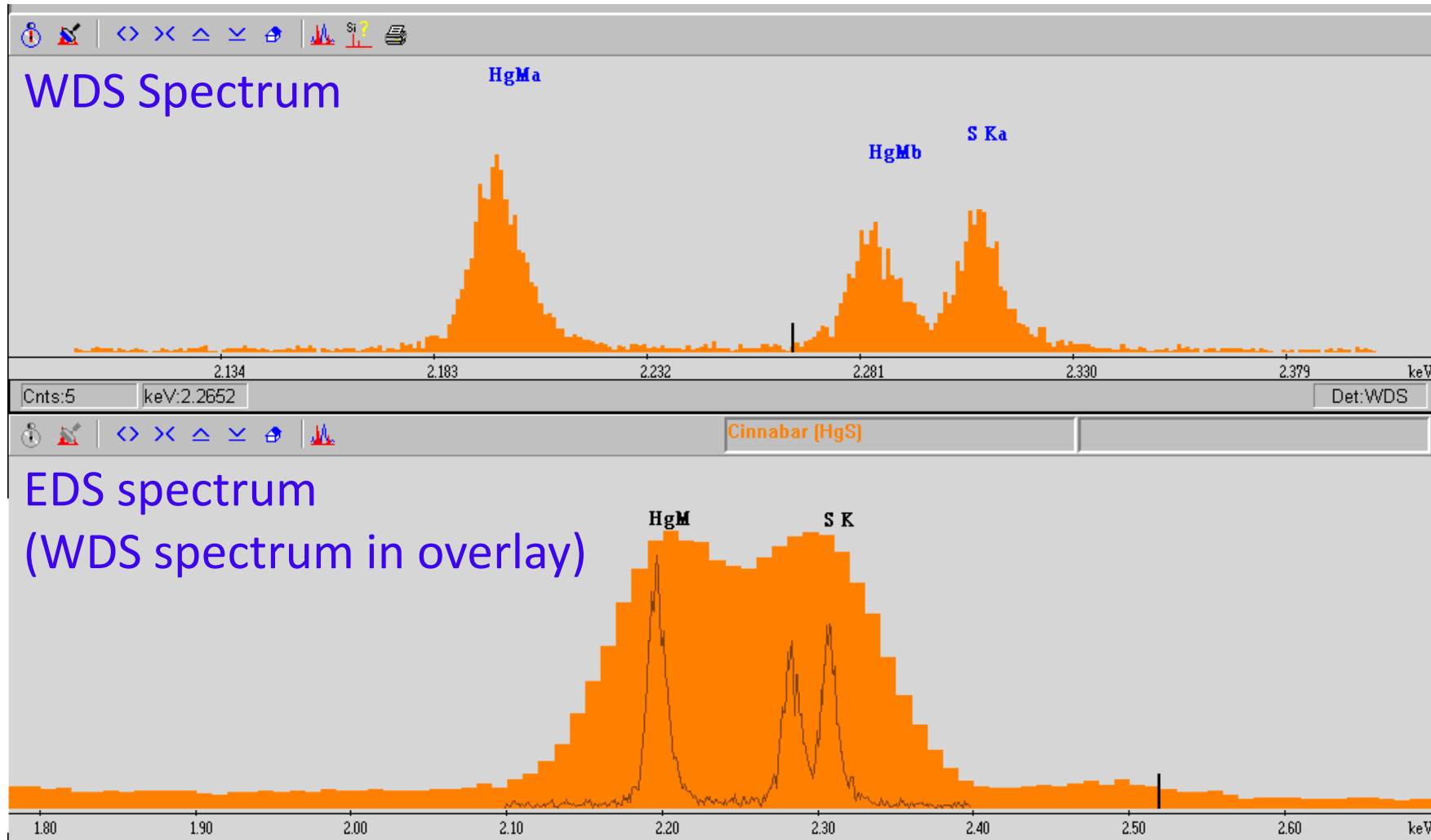
LiF 2d = 4.027 Å







EDS versus WDS - HgS



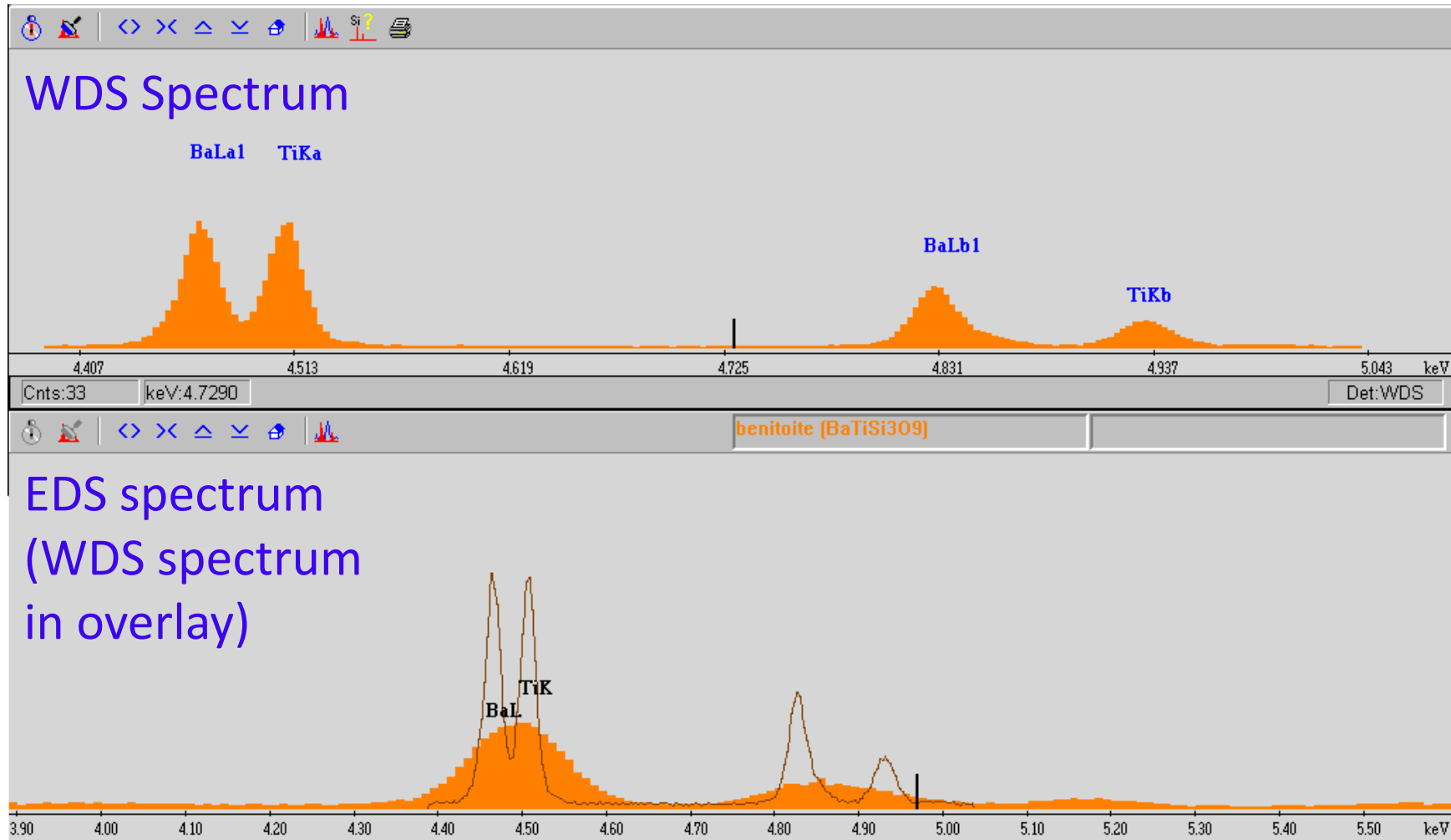
Project WND-POWR.03.02.00-00-1043/16

International interdisciplinary PhD Studies in Materials Science with English as the language of instruction

Project co-financed by the European Union within the European Social Funds



EDS versus WDS - BaTiSi₃O₉





Quantitative analysis

Quantitative analysis is based on a proportionality between the number of atoms i (or concentration C_i) and the number of characteristic X-ray detected

$$**$I_i = \textit{constant} \times C_i$**$$

This proportionality „*constant*” depends however on the sample composition. This is so called „matrix effect”



Concentrations can be calculated by a number of methods:

- **Approximation by k-ratio**
- **Calibration curves**
- **Applying matrix corrections to the k-ratio (ZAF method or Phi-Rho-Z method)**
- **Relying on fundamental parameters (standardless method)**



K- ratio

$$k_i = \frac{I_i}{I_{(i)}} = \frac{\textit{X - ray Intensity Element Sample}}{\textit{X - ray Intensity Pure Element}}$$

The k-ratio can be used to determine an approximate concentration as follows. For an unknown sample: $I_i = \text{constant} \times C_i$ whereas for a pure element: $I_{(i)} = \text{constant} \times 1$ (where the concentrations are by weight)
Thus:

$$C_i \approx \frac{I_i}{I_{(i)}} = k_i$$

Note that this equation is only approximate since the „constant” is not truly constant



Element	True conc. wt%	$k_i \times 100$	% difference
C	0.82	0.17	-80
Cr	4.18	5.18	24
V	1.88	2.08	11
Mn	0.26	0.253	-3
Fe	81.8	80.8	-1

The approximation is very good for iron since the matrix (tool steel) is very similar to pure iron. The calculated carbon concentration is incorrect because the pure carbon matrix is quite different from a small amount of carbon in steel.

Matrix corrections are needed !



ZAF correction

Since the concentration and X-ray intensity are proportional, there is relation between the intensity and the concentration in an unknown sample (labeled u) and a standard (s). The concentration of an element i in an unknown sample is:

$$C_i^{(u)} \approx C_i^{(s)} \frac{I_i^{(u)}}{I_i^{(s)}}$$

The ZAF method can be used to correct the observed X-ray intensities for differences in matrix composition between standard and unknown sample:

$$C_i^{(u)} \approx C_i^{(s)} \frac{I_i^{(u)} F^{(u)}}{I_i^{(s)} F^{(s)}}$$



ZAF correction

The factor F involves the atomic number or Z correction, the absorption correction (A) and the fluorescence correction (F) so that:

$$F = F_Z F_A F_F$$

which is the origin of the name ZAF correction. Thus

$$C_i^{(u)} \approx C_i^{(s)} \frac{I_i^{(u)} (F_Z)_i^{(u)} (F_A)_i^{(u)} (F_F)_i^{(u)}}{I_i^{(s)} (F_Z)_i^{(s)} (F_A)_i^{(s)} (F_F)_i^{(s)}}$$

$$C_i^{(u)} \approx C_i^{(s)} \frac{I_i^{(u)}}{I_i^{(s)}} Z_i A_i F_i$$

Note that Z-, A- and F-corrections are RATIOS of the effect in the unknown sample and the standard. The more similar the standards and the unknown are, the closer the correction will be to 1 and the more accurate the concentration estimate



ZAF correction

The terms Z_i , A_i and F_i are often referred to as the Z-,A- and F-corrections.

Z_i - the atomic number correction, takes care of the difference in backscattering and stopping power

A_i - the absorption correction corrects for the difference in absorption of the X-rays when travelling out of the sample

F_i - the fluorescence correction corrects for the contribution from the X-rays that are not generated by the electron beam but by fluorescence induced by characteristic X-rays of the elements

$$C_i^{(u)} = k_i Z_i A_i F_i$$

The absorption factor, the A factor, is usually the most important one, especially if light elements are present. It corrects for those X-rays that were generated in the sample but absorbed before they were able to leave the surface and be detected. The A factor is a ratio of the absorption behaviour between the standard and the unknown.



Quantitative analysis

Sample steel, 25kV

Element	K-ratio	Z	A	F	WT%
Cr K	0.1927	1.005	1.014	0.831	16.32
Mn K	0.0099	1.021	1.004	0.991	1.01
Fe K	0.7167	1.001	1.045	0.988	74.07
Ni K	0.0735	0.982	1.192	1.000	8.60

Cr too high : total ZAF correction

$$1.005 \times 1.014 \times 0.831 = 0.8468$$

$$\text{Correct Cr contents} = 0.1927 \times 0.8468 \times 100\% = 16.32\%$$



Quantitative analysis

kV : 25.00 Tilt : 0.00 Take-off : 35.00 Tc : 40
Detector Type : SUTW Resolution : 144.00 Lsec : 100

**EDAX ZAF Quantification (Standardless)
Element Normalized**

Element	Wt %	K-Ratio	Z	A	F
SiK	0.54	0.0020	1.1074	0.3348	1.0018
CrK	18.67	0.2157	0.9949	0.9842	1.1798
MnK	0.89	0.0087	0.9784	0.9940	1.0089
FeK	71.60	0.6878	0.9985	0.9512	1.0114
NiK	8.31	0.0710	1.0175	0.8398	1.0000
Total	100.00				

ZAF correction for steel at **25 kV**, including Si

kV : 15.00 Tilt : 0.00 Take-off : 35.00 Tc : 40
Detector Type : SUTW Resolution : 144.00 Lsec : 100

**EDAX ZAF Quantification (Standardless)
Element Normalized**

Element	Wt %	K-Ratio	Z	A	F
SiK	0.59	0.0039	1.1440	0.5716	1.0009
CrK	18.57	0.2099	0.9979	0.9940	1.1394
MnK	1.12	0.0111	0.9796	0.9978	1.0065
FeK	71.09	0.7031	0.9978	0.9826	1.0087
NiK	8.62	0.0823	1.0126	0.9432	1.0000
Total	100.00				

ZAF correction for steel at **15 kV**, including Si

The results are almost equal, so independent of kV used.

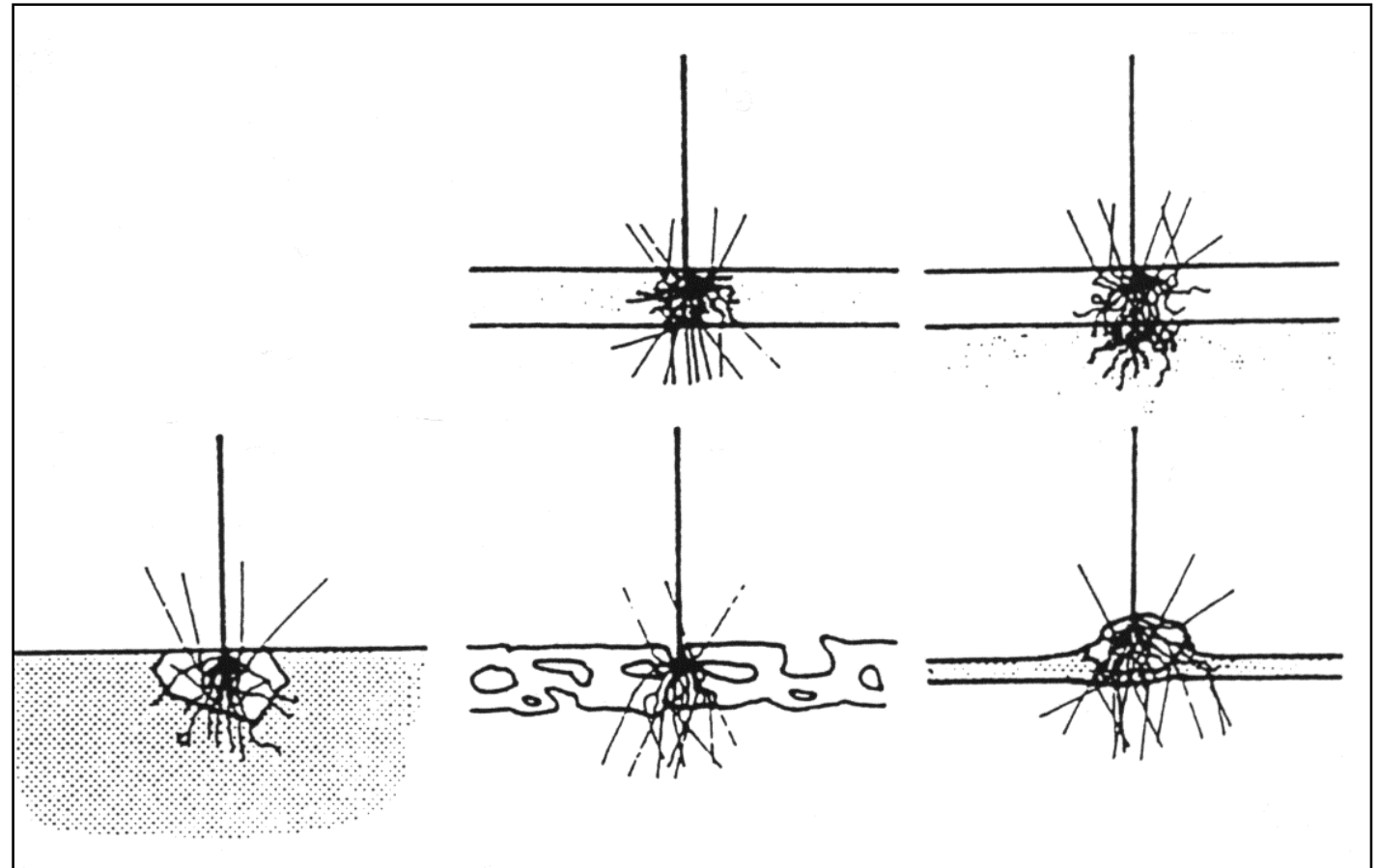
Note the very low value A of the lightest element i.e. silicon. Almost half of the Si X-rays were absorbed by the other (heavier) elements, before they were able to leave the surface.



Quantitative analysis

Several situations where the calculation of the ZAF factors does not apply :

- unsupported thin film
- thin film on substrate
- inclusion or particle
- biological sample
- particle on thin foil





Quantitative analysis - Sources of errors

Situations where the ZAF factors do not apply

- X-ray interaction volume larger than phase size
- Wrong coating (preferable carbon coating)
- Poor statistics (acquisition time/count rate is too low)
- High count rate (dead time is too high)
- Overlapping elements (trace elements)
- Energy calibration errors
- **Improper background subtraction!**
- Irregular specimen surfaces
- Skirt effect (low vacuum SEM/ESEM)



Quantitative analysis

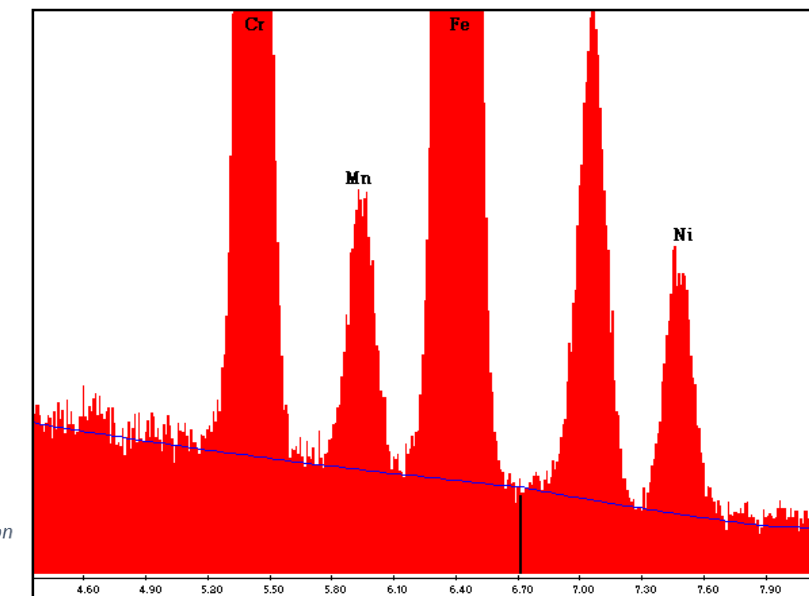
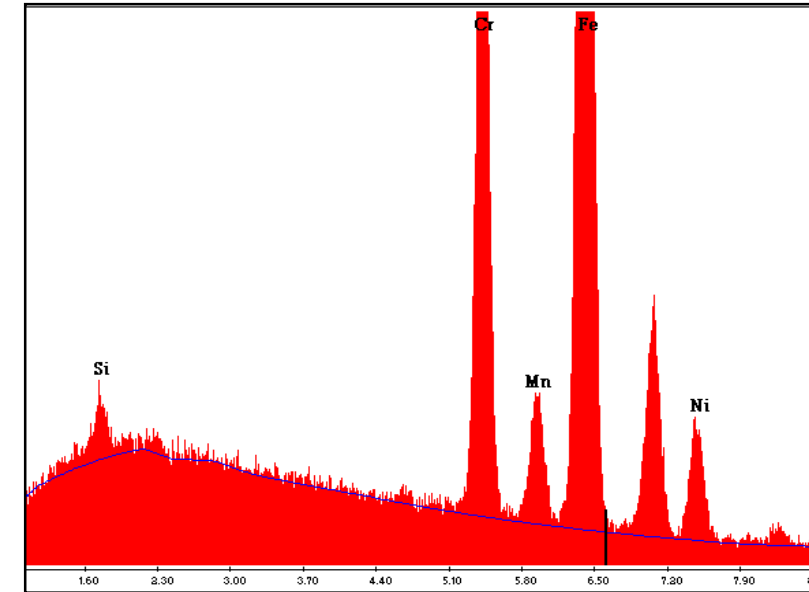
Background subtraction

- Background needs to be removed before quantification
 - Auto or Manual method
- Background shape will affect the quantitative results: normally a very small effect
 - Pay attention to absorption edges
(in glasses and minerals: Si absorption edge)

Two approaches are used in systems today.

One method is to construct automatically a background model on the basis of the known physics plus suitable corrections for the real world. This method of background modelling is fast and lets the user see and pass judgement on the quality of the model.

The other method is manual modelling. In this method the user can make his own background model by making the correct form or make corrections to the background model based on the automatic background points. With the manual background method it is possible to correct for the different absorption edges of a sample.

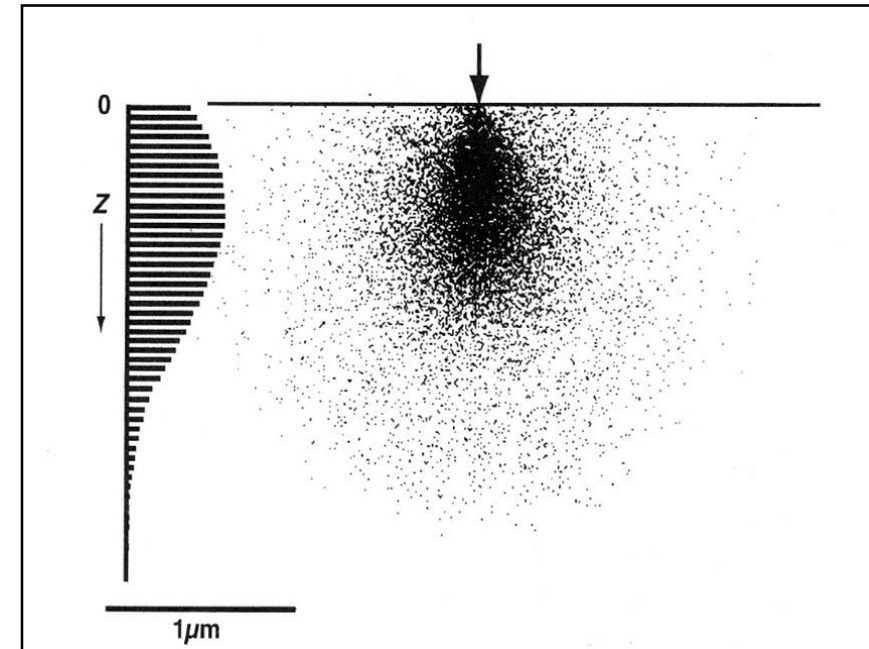




Quantitative analysis – Phi-Rho-Z method

The ZAF method produces reliable results for X-rays lines greater than 1.0 keV. For X-rays softer than 1 keV, the Phi-Rho-Z curve method is probably more accurate. It may also be more accurate for non-conducting samples such as oxides and silicates.

A Phi-Rho-Z curve is an ionisation distribution in which ionisations (Phi) are plotted against mass-depth (Rho-Z).



$\Phi(\rho z)$ programs are based on attempts to describe as accurately as possible the number of ionizations or x-ray photons (ϕ) as a function of the mass depth (ρz) in the specimen. They must be considered the most direct, genuine and straightforward approach to bulk matrix corrections. They also provide the best possible starting base for thin film analysis and in-depth profiling procedures.



Quantitative analysis

ZAF correction of B₄C

kV : 10.00 Tilt : 0.00 Take-off
Detector Type : SUTW, Sapphire Resolu

EDAX **ZAF** Quantification (Standardless)
Element Normalized

Element	Wt %	At %	K-Ratio
B K	83.25	84.66	0.7635
C K	16.75	15.34	0.0208
Total	100.00	100.00	

Phi-Rho-Z correction of B₄C

kV : 10.00 Tilt : 0.00 Take-off
Detector Type : SUTW, Sapphire Resolu

EDAX **PhiRhoZ** Quantification (Standardless)
Element Normalized

Element	Wt %	At %	K-Ratio
B K	76.06	77.92	0.6683
C K	23.94	22.08	0.0230
Total	100.00	100.00	

(80 at % Boron and 20 at % Carbon)

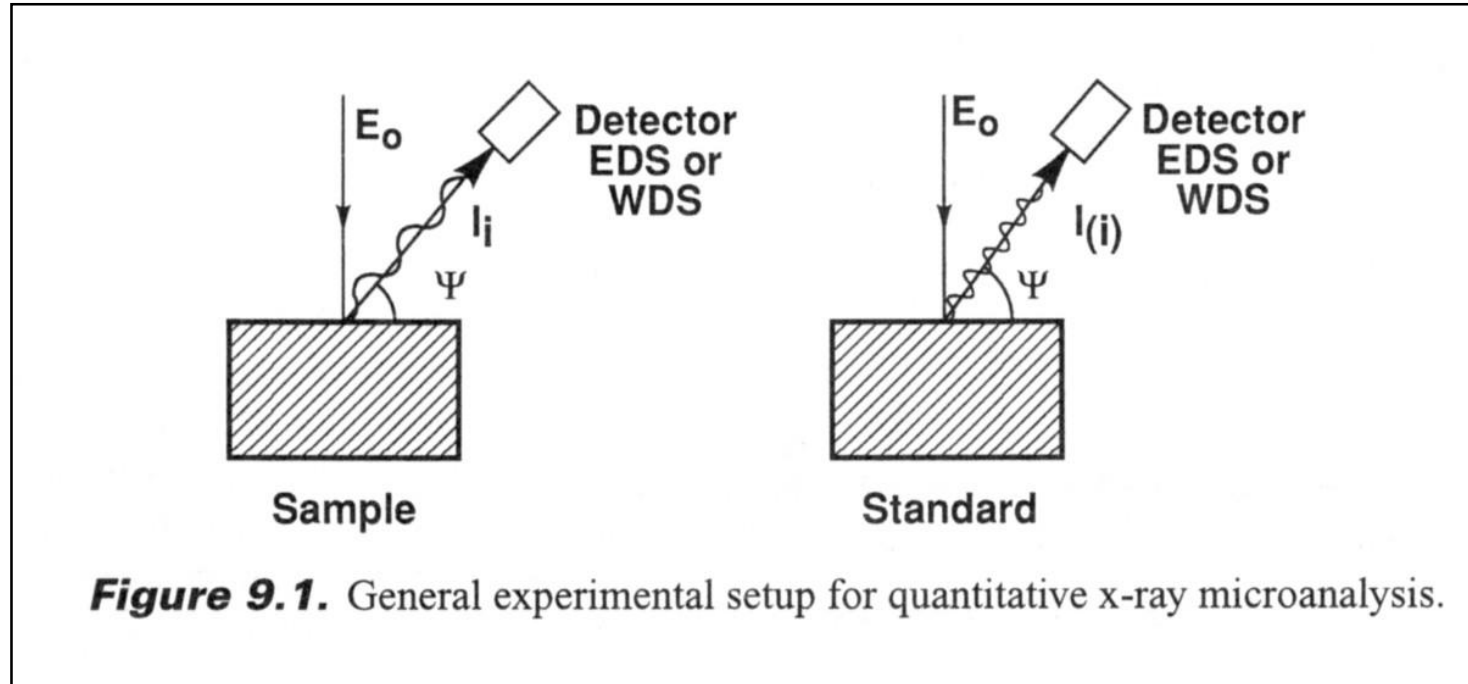


Quantitative analysis – Steps:

1. Define the problem (keV, beam current, analysis time, etc.)
2. Perform a qualitative analysis to determine the elements to be measured
3. Select the necessary sample(s) and appropriate standards
4. Prepare the sample and standards for X-ray analysis
5. Measure the appropriate X-ray intensities for qualitative analysis
 - a. Obtain the X-ray spectrum of the specimen and standards under defined and reproducible conditions
 - b. Process the spectra of the specimen and standards to remove the background
 - c. Process the spectra of the specimen and standards if peaks overlaps occur
6. Develop the X-ray intensity k-ratios using the specimen intensity I_i and the standard intensity $I_{(i)}$ after continuum background is subtracted
7. Perform quantitative matrix corrections to obtain numerical concentrations

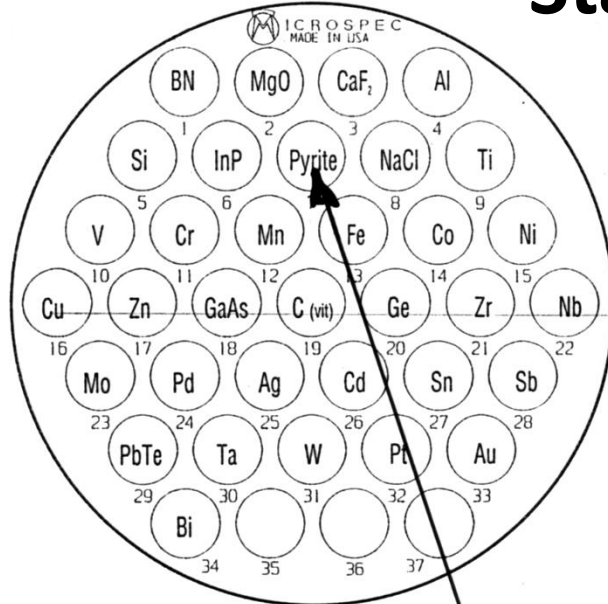


Quantitative analysis – Steps:



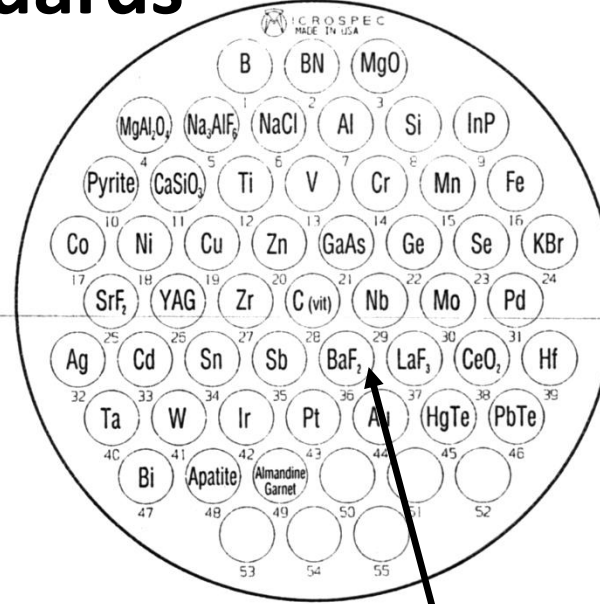


Standards



Universal Set 1
34 Standards, 25mm holder

	wt. % FeS ₂
Fe	46.40
S	53.41
Cu	0.05
Co	0.10
As	0.04



Universal Set 2
49 Standards, 32mm holder

	at. % BaF ₂	wt. % BaF ₂
Ba	33.3	78.33
F	66.7	21.67

Project WND-POWR.03.02.00-00-1043/16

International interdisciplinary PhD Studies in Materials Science with English as the language of instruction

Project co-financed by the European Union within the European Social Funds



The Phi-Rho-Z and ZAF techniques yield quite similar results, within a few percent relative, for analysis of:

- $K\alpha$ lines of atomic number 12 (Mg) and above,**
- when analyses are made at E_0 values between 15 and 30 keV.**

The Phi-Rho-Z correction yields more accurate results for the analysis of:

- light elements (O,N,C,B)**
- low energy (< 1keV) $L\alpha$ lines**
- analyses at 10 keV and below.**



Quantitative standardless analysis

Advantages:

- Results normalised to 100 wt.% (in many cases standardless analysis is the preferred method for its greater speed and ease of use)
- Flexible, kV independent
- Every identified peak will be quantified

Disadvantage:

- Detector efficiency can not be predicted with sufficient accuracy for X-ray lines below 1 keV (small variations in detector parameters – window thickness, Si dead layer etc.) can cause variations in measured intensity

FAST BUT NOT ACCURATE!!!



Quantitative standardless analysis

Since for standardless analysis we have no X-ray standard intensity $I_i^{(s)}$, it can be calculated relying on fundamental parameters:

$$I_{\text{Calculated}}^{(s)} = n \frac{\Omega}{4\Pi} \varepsilon_d \omega p f(\chi) \frac{N_o}{A} R \int_{E_o}^{E_c} \frac{Q(E)}{dE/d(\rho s)} dE$$

where:

N – the number of electrons entering the sample

$\Omega/4\Pi$ – the solid angle

ε_d – the detector efficiency

ω – the X-ray fluorescence yield

p – relative probability of transition involved

$f(\chi)$ – the absorption correction

R – backscatter correction (1- η)

N_o – Avogadro number

A – atomic number

Q – cross-section

E_c – critical ionization energy

E_o – energy of electron beam

The integral represents the cross-section of the ionisation involved

Project WND-POWR.03.02.00-00-I043/16

International interdisciplinary PhD Studies in Materials Science with English as the language of instruction

Project co-financed by the European Union within the European Social Funds



Quantitative analysis – precision

- Chemical analysis results Mg = 2.28 wt.%
- Standardless results: Mg = 2 wt.%
- Full standards method results: Mg = 2.28 wt.%

The best precision can be achieved by use of standards

Quantitative analysis – accuracy

Results (in wt %)	Description	Relative error in %
100 - 20	Main element	2 %
20 - 5	Major element	4 %
5 – 1	Minor element	10 % to 20 %
1 - 0.2	Trace element	50 % (up to 100%)

Example: Pb = 21.13 % +/- 2% of 21.13%

results in 21.13 +/- 0.42 wt %, so between 20.7 wt% and 21.5 wt%



Literature for X-ray Microanalysis

- **Scanning Electron Microscopy and X-Ray Microanalysis (Third Edition), *Joseph Goldstein, Dale Newbury, David Joy, Charles Lyman, Patrick Echlin, Eric Lifshin, Linda Sawyer and Joseph Michael*, Kluwer Academics/Plenum Publishers, 2003;**
- **Electron Microprobe Analysis and Scanning Electron Microscopy in Geology, *S.J.B. Reed*, Cambridge University Press, 1996**
- **Electron Microprobe Analysis, (Second Edition), *S.J.B. Reed*, Cambridge University Press, 1993**
- **Electron Probe Quantification, *K.F.J. Heinrich and D.E. Newbury*, Plenum Press, New York, 1991.**
- **X-Ray Spectrometry in Electron Beam Instruments, *David Williams, Joseph Goldstein and Dale Newbury*, Plenum Press, New York, 1995**
- **Electron Microscopy and Analysis, (Third Edition), *Peter Goodhew, John Humphries, Richard Beanland*, Taylor & Francis, London, 2001.**
- **EDAX Course Proceedings, Tilburg, 2005.**